Efficient System Designs for Single and Multi-User Spatial Modulations

by

©Ibrahim Osama Ibrahim Mahmoud Al-Nahhal

A dissertation submitted to the School of Graduate Studies
in partial fulfillment of the requirements for the degree of

Doctor of Philosophy

Faculty of Engineering and Applied Science
Memorial University of Newfoundland

October 2020

St. John's, Newfoundland

Abstract

Spatial modulation (SM) and quadrature SM (QSM) are promising versions of the single-user multiple-input multiple-output (MIMO) system that overcome the problem of inter-channel-interference which occurs in conventional MIMO systems. Both SM and QSM exploit the index of the activated antenna(s) to carry additional information to enhance the total spectral efficiency of the system transmission. In the detection, the SM and QSM systems jointly detect the index of the activated antenna(s) as well as the transmitted modulation symbol, which is an exhaustive process especially for higher order modulations and large system dimensions. This exhaustive process contradicts the demands of future wireless networks that require low-power consumption and low communication latency.

To fulfill the demand of low-complex decoders at the receiver side for future wireless networks, I propose three different low-complexity decoders for single-user SM and QSM MIMO systems. These algorithms are based on the concept of sphere decoding for the tree-search structure. The first proposed algorithm provides a significant reduction in the decoding complexity with optimal bit error rate (BER) performance. The second proposed algorithm provides an extra reduction in the decoding complexity without sacrificing the optimality of the BER performance. Finally, the third algorithm provides a flexible trade-off between complexity and BER performance to be suitable for most hardware implementations. The proposed algorithms are studied in terms of BER performance and expected decoding complexity for the single-user SM and QSM MIMO systems.

For multi-user SM-MIMO, a low-cost system is proposed using the sparse code multiple access (SCMA) technique. The proposed low-cost SM-SCMA system significantly reduces the required number of transmit antennas with almost no loss in terms of the BER performance and decoding complexity, compared with the conventional SM-SCMA. At the receiver, the message passing algorithm (MPA) is employed to detect the transmitted signals, which suffers from high decoding complexity in practical implementations. To address this issue, three low-complexity decoding algorithms are proposed for the SM-SCMA system. The first algorithm provides the benchmark for the decoding complexity at the expense of the BER performance. The second algorithm slightly increases the decoding complexity with a significant improvement in the BER performance. Finally, the third algorithm provides a near-optimum BER performance with a considerable decoding complexity reduction when compared to the MPA decoder. Moreover, it supports the parallel hardware implementation and strikes a trade-off between decoding complexity and BER performance.

More specifically, the three low-complexity receivers for the single-user SM and QSM MIMO systems are introduced in Chapters 2, 3, 4 and 5. In Chapter 2, the first low-complexity algorithm for single-user QSM-MIMO system is proposed. The second low-complexity algorithm for SM-MIMO system is introduced in Chapter 3, and is analyzed in Chapter 4. The reliable decoder for single-user SM-MIMO system is proposed in Chapter 5. For multi-user SM-SCMA, the low-cost system is proposed in Chapter 6; at the receiver side, the three low-complexity decoders for the SM-SCMA system are proposed and analyzed in Chapter 7.

To my father and mother ...

To my lovely wife and kids ...

To my two sisters and two brothers ...

To my entire family and friends ...

Acknowledgments

Praise be to Allah, the Cherisher and Sustainer of the Worlds. After thanking Almighty "ALLAH" for his blessing and guidance to complete this work, I would like to offer my sincere thanks to my supervisors Prof. Octavia Dobre and Dr. Salama Ikki for their valuable guidance and advice. I would like to express my deep appreciation to Prof. Octavia for her professionalism and personal caring for her students before and after the study; I was lucky to be her student, and I encourage hard-worker graduate students to go through this amazing experience with her. I would like to acknowledge the financial support provided by my supervisors, the Faculty of Engineering and Applied Science, the School of Graduate Studies, and the Natural Science and Engineering Research Council of Canada (NSERC).

I would like to thank my Egyptian university, Al-Azhar University in Cairo, for letting me try this fruitful experience. Since a significant part of my education was in Egypt and my foundations were laid in schools of the Zagazig and Cairo cities, I would like to thank my elementary school teachers, my uncle Hosny who taught me math at secondary and high schools, my B.Sc. professors, and my M.Sc. thesis supervisor Prof. Masoud Alghoniemy who put me on the right path of scientific research and has been still in touch with me.

The final word of acknowledgment is reserved to my parents for their unconditional support, to my two sisters and two brothers for their love, to my friends all over the world, to my sweetheart and lovely wife Israa and our kids for their patience and for motivating me. Finally, I would like to say that "*I am nothing without you all.*"

Co-Authorship Statement

I, Ibrahim Al-Nahhal, hold a principle author status for all the manuscript chapters (Chapters 2 - 7) in this dissertation. However, each manuscript is co-authored by my supervisors and co-researchers, whose contributions have facilitated the development of this work as described below.

- Paper 1 in Chapter 2: I. Al-Nahhal, O. A. Dobre, and S. Ikki, "Quadrature Spatial Modulation Decoding Complexity: Study and Reduction," IEEE Wireless Communications Letters, vol. 6, pp. 378-381, Jun. 2017.
  I was the primary author, with authors 2 and 3 contributing to the idea, its formulation and development, and refinement of the presentation.

- Paper 2 in Chapter 3: I. Al-Nahhal, O. A. Dobre, and S. Ikki, "Low Complexity Decoders for Spatial and Quadrature Spatial Modulations," in Proceeding IEEE Vehicle Technology Conference (VTC-Spring), 2018, pp. 1–5.
  I was the primary author, with authors 2 and 3 contributing to the idea, its formulation and development, and refinement of the presentation.

- Paper 3 in Chapter 4: I. Al-Nahhal, E. Basar, O. A. Dobre, and S. Ikki, "Optimum Low-Complexity Decoder for Spatial Modulation," IEEE Journal on Selected Areas in Communications, vol. 37, no. 9, pp. 2001-2013, Jul. 2019.
  I was the primary author, with authors 2 - 4 contributing to the idea, its formulation

and development, and refinement of the presentation.

- Paper 4 in Chapter 5: I. Al-Nahhal, O. A. Dobre, and S. Ikki, "Reliable Detection for Spatial Modulation Systems," accepted, IEEE Vehicle Technology Conference (VTC-Fall), 2020.

  I was the primary author, with authors 2 and 3 contributing to the idea, its formulation and development, and refinement of the presentation.

- Paper 5 in Chapter 6: I. Al-Nahhal, O. A. Dobre, E. Basar, and S. Ikki, "Low-Cost Uplink Sparse Code Multiple Access for Spatial Modulation," IEEE Transactions Vehicle Technology, vol. 68, no. 9, pp. 9313-9317, Jul. 2019.

  I was the primary author, with authors 2 - 4 contributing to the idea, its formulation and development, and refinement of the presentation.

- Paper 6 in Chapter 7: I. Al-Nahhal, O. A. Dobre, and S. Ikki, "On the Complexity Reduction of Uplink Sparse Code Multiple Access for Spatial Modulation," accepted, IEEE Transactions on Communications, Aug. 2020.

  I was the primary author, with authors 2 and 3 contributing to the idea, its formulation and development, and refinement of the presentation.

_____ _____

Ibrahim Al-Nahhal Date

Table of Contents

List of Tables

List of Figures

List of Abbreviations

AWGN	Additive White Gaussian Noise
b/s/Hz	Bit/Second/Hertz
BER	Bit Error Rate
bpcu	Bits Per Channel Use
BPSK	Binary Phase-Shift-Keying
CDF	Cumulative Distribution Function
CS	Compressive Sensing
CSIR	Channel State Information at the Receiver Side
DA	Data-Aided
DSP	Digital Signal Processor
EBCS	Enhanced Bayesian Compressive Sensing
ED	Euclidean Distance
ExCo	Extra Complexity
FCSD	Fixed-Complexity Sphere Decoder

FES	Fully Expanded Stage
flops	Floating Point Operations
FN	Function Nodes
GSM	Generalized Spatial Modulation
IAS	Inter-Antenna Synchronization
ICI	Inter-Channel Interference
m-M	Minimum-Distance of Maximum-Length
MAP	Maximum a Posteriori Probability
MIMO	Multiple-Input Multiple-Output
ML	Maximum–Likelihood
mmWave	Millimeter-Wave
MPA	Message Passing Algorithm
MSUD	Modified Successive User Detection
NoM	Number of Misses
NOMA	Non-Orthogonal Multiple Access
ORE	Orthogonal Resource Element
PAM	Pulse Amplitude Modulation
pdf	Probability Density Function
PEP	Pairwise Error Probability

PSK	Phase Shift Keying
QAM	Quadrature Amplitude Modulation
QSM	Quadrature Spatial Modulation
RC	Reduced-Complexity
RF	Radio Frequency
RGSM	Rotational Generalized Spatial Modulation
S/P	Serial-to-Parallel
SCMA	Sparse Code Multiple Access
SD	sphere Decoder
SE	Spectral Efficiency
SES	Single Expanded Stage
SM	Spatial Modulation
SNR	Signal-to-Noise Ratio
SUD	Successive User Detection
UBCR	Upper Bound of the Complexity Reduction
VLC	Visible Light Communication
VN	Variable Nodes
VN	Visited Node

Chapter 1

Introduction

1.1 Background

In 1874, Guglielmo Marconi, the father of radio frequency (RF) signals, was born in Italy. At an early age, he was influenced by Heinrich Hertz who tried to transmit the electromagnetic waves through the air. Following numerous unsuccessful attempts, Marconi was finally able to send a wireless signal across the Atlantic in 1901, drawing the world's attention to a groundbreaking field of technology. The site of Marconi's experiment is still a venue for tourists at the Signal Hill in St. John's, Newfoundland, and continues to be a witness to one of the remarkable inventions for humanity. About three years after Marconi's experiment, specifically in 1904, John Fleming invented the thermionic diode which has become an essential component in wireless devices. Marconi and Fleming never knew that they were about to forever change the face of the world. Since then, numerous universities, research labs and industrial companies have dedicated resources to improve the wireless communication systems.

Currently, wireless technology is an essential part of life. People rely heavily on technology for most of their daily life, such as forecasting the weather, following the news all

over the world, communicating with each other, controlling houses and industrial processes remotely, etc. Recently, there has been a significant pressure on scientists and engineers to add more advanced and robust elements to the wireless systems to accommodate relentlessly increasing demands. One such promising element is the multiple-input multiple-output (MIMO) system.

1.2 MIMO Systems

The MIMO communication system was proposed in 1970 as a multi-channel digital transmission system for wired communication systems [1]. In 1993, the MIMO system was proposed for wireless communications as a multiplexing scheme that can increase the overall system data rate. This can be achieved by dividing the higher data rate into several low-data rate signals and transmitting them from multiple antennas. At that time, the application of MIMO was limited since the size of antennas was relatively large, and the building of a wireless system equipped with multiple antennas was infeasible. In the last two decades and after the revolution of antenna manufacturing, MIMO has received the utmost attention from both academia and industry [2]. Since then, MIMO has became a key technology for wireless communication systems that require high data rates/spectral efficiency transmission [3].

The downside of increasing the spectral efficiency and data rate using MIMO systems is an increase in the implementation cost and decoding complexity. This is due to the following reasons:

1. Presence of inter-channel interference (ICI) because all transmit antennas are required to be activated at the same time, which degrades the performance.

2. Need for inter-antenna synchronization (IAS).

3. Presence of multiple RF chains, which increases the overall cost of the system.

4. High decoding complexity when the optimum decoders are employed to decode the transmitted signals.

The above drawbacks of MIMO systems limit their application for several wireless communication systems. The single antenna system avoids the drawbacks of the MIMO system at the expense of reduced spectral efficiency, absent multiplexing gain, less served users, etc. Therefore, a novel wireless technology that lies in between the single antenna and MIMO has been launched in recent years, namely spatial modulation (SM).

1.3 Single-User Spatial Modulation

SM is a promising technique that has been recently proposed to overcome the MIMO drawbacks for possible application to the next wireless generations [4]-[7]. SM is a type of MIMO system that exploits the index of the transmit antennas to deliver an extra part of the input bit-stream, in addition to transmitting the modulated signal. This can be achieved by activating only one transmit antenna at a time, and then sending the modulated signal from it. Therefore, the SM-MIMO system utilizes the uniqueness and randomness of the wireless channel to deliver additional information. Upon implementing this brilliant idea, the SM system completely eliminates the ICI and does not require IAS since only one RF chain is used at a time. Besides, the SM system has a lower implementation cost compared to the traditional MIMO system, and it provides a better spectral efficiency compared to the traditional single antenna system.

1.3.1 SM Functionality

The SM-MIMO system activates only one antenna at a time to avoid the drawbacks of multiple antennas systems [8]. Fig. 1.1 shows the tridimensional constellation diagram of the SM-MIMO system for four transmit antennas and four modulation symbols. Assume that the current input bit-stream is 1110; the first two bits (i.e., 11) activate the 4-th antenna, while the rest of the transmitter antennas radiate no power. The modulated symbol corresponding to the second two bits (i.e., 10) is now ready to be transmitted from the 4-th antenna. It is worth noting that both the real and imaginary parts of the modulated symbol are transmitted from the same active antenna (i.e., the 4-th antenna in this example).

Fig. 1.2 shows the bit-steam mapping in the SM-MIMO system for the same example mentioned above. As seen from this figure, a single RF chain is used at the transmitter and is received by all receiver antennas. Therefore, no ICI occurs during the transmission. At the receiver side, the signal is detected by performing all possible combinations between the transmit antennas and modulated symbols, which is referred to as maximum-likelihood (ML) decoding.

1.3.2 The QSM-MIMO System

As previously mentioned, the SM-MIMO system overcomes the traditional MIMO problems. On the other hand, the traditional MIMO provides a better spectral efficiency compared to the SM-MIMO systems. Quadrature SM (QSM) is a promising variant of the SM-MIMO system, which employs the in-phase and quadrature dimensions to improve the spectral efficiency of the conventional SM [9]. In other words, the real and imaginary components of the modulated symbol are transmitted from two different antennas. At the receiver side, the optimum ML detector jointly estimates the two active transmit antenna indices conveying the in-phase and quadrature pulse amplitude modulation (PAM) as well as the PAM symbols.

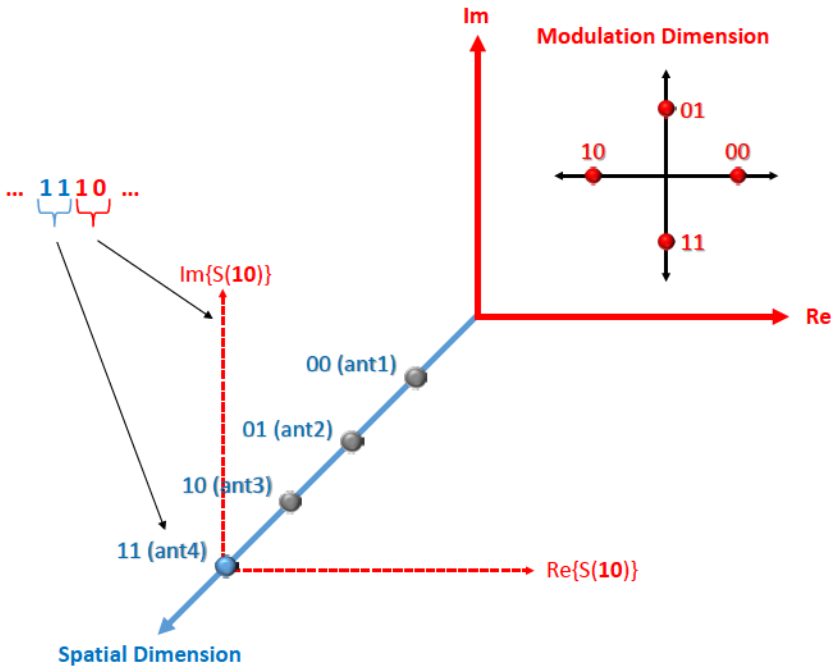

Fig. 1.1: Tridimensional constellation diagram of the SM-MIMO system for 4 transmit antennas and 4 modulation symbols.

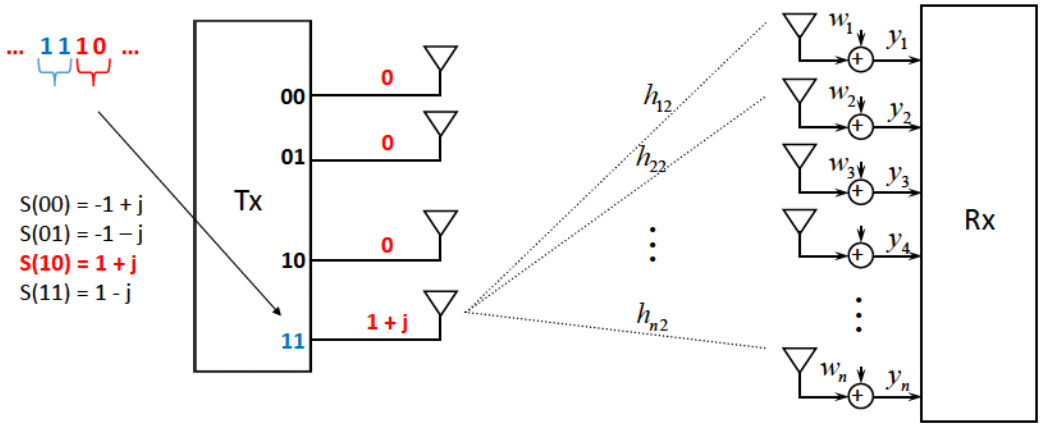

Fig. 1.2: Example of input bit-stream mapping in the SM-MIMO system for 4 transmit antennas and 4 modulation symbols.

Fig. 1.3 depicts an example of the tridimensional constellation diagram of the QSM-MIMO system for four transmit antennas and four modulation symbols. As shown in this figure, the real part of the modulated symbol is transmitted from the 4-th antenna, while the imaginary part of the modulated symbol is delivered from the 2-nd antenna. Thus, the total number of transmitted bits at a time using QSM is 6, whereas the SM transmits only 4 bits at a time.

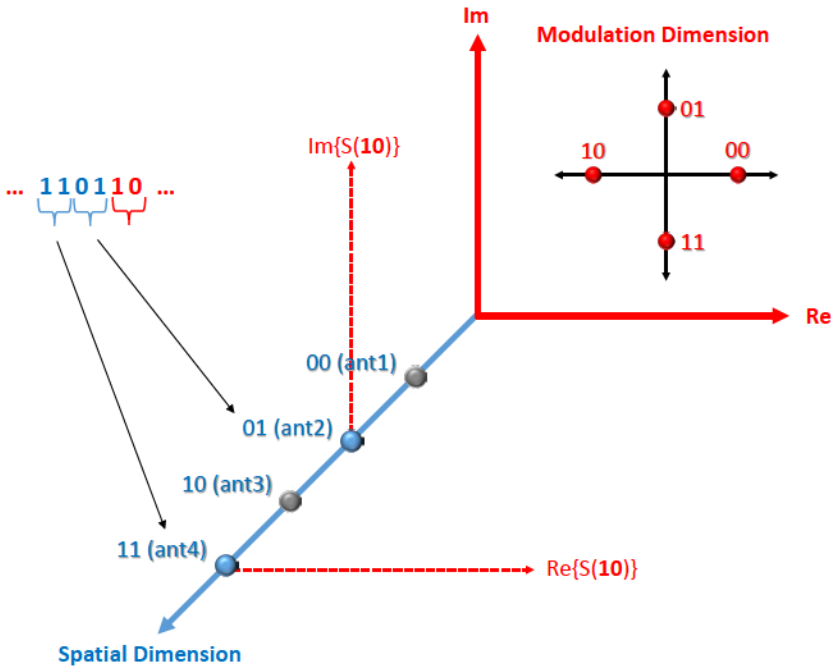

Fig. 1.3: Tridimensional constellation diagram of the QSM-MIMO system for 4 transmit antennas and 4 modulation symbols.

1.4 Multi-User SM

In practice, the wireless communication systems include multiple users that can share the medium and access it based on a specific access technique. Non-orthogonal multiple access (NOMA) has been recognized as a promising technique for future wireless networks, and has received remarkable attention in recent years [10]. NOMA can be classified mainly as power-domain and code-domain. The power and code orthogonality constraints are relaxed

for multiple-user access to improve the spectral efficiency and increase the number of served users.

In this thesis, sparse code multiple access (SCMA) code-domain NOMA is considered, which was initially proposed in [11] and [12]. In the SCMA scheme that is shown in Fig. 1.4, a unique multidimensional codebook is assigned to each user to share the medium with the other users. The SCMA codebooks are sparse (i.e., contain zeros) and carefully designed to provide a good performance. The sparsity property of the SCMA codebooks enables the application of the iterative message passing algorithm (MPA) to provide near ML BER performance with complexity lower than the ML. The MPA is an iterative algorithm that maximizes the posteriori probability of each user's codeword. Since the complexity of the MPA is still high for practical implementations, reducing the decoding complexity is a point of utmost interest in this context.

1.4.1 SCMA Functionality

Herein, an illustrative example is discussed to explain the concept of SCMA using six users, as seen in Fig. 1.5. Assume that each user has a codebook containing four codewords, i.e., each user can send two bits at a time. The users' codewords consist of four subcarriers. It is worth noting that all users' codebooks are designed to allow only three users to share a subcarrier, as shown in Fig. 1.5. Moreover, the number of non-zero elements for each codeword is fixed (e.g., two in this example).

Suppose that the six users need to transmit the following two bits per user in its order: 01, 00, 11, 00, 10, 01. Thus, the second codeword that corresponds to 01 in the first user's codebook will be transmitted, and so on for the rest of the users. Now, the composite transmitted signal of the six users is represented by a complex vector which consists of four elements. Each element of the composite transmitted vector comes from three different users.

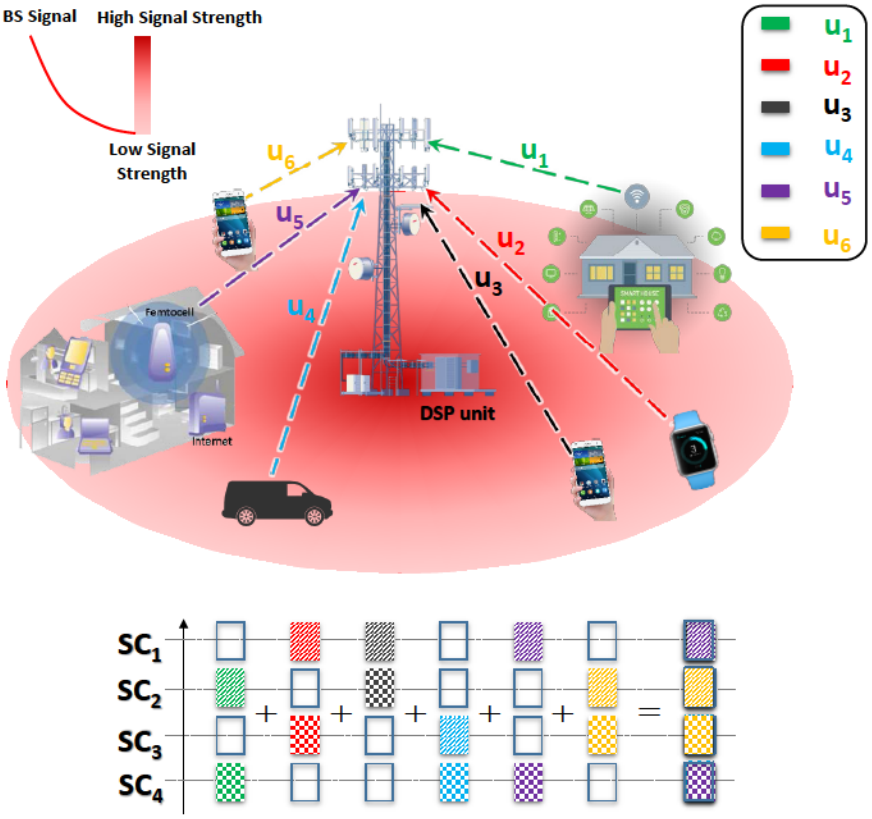

Fig. 1.4: Basic concept of SCMA technique for 6 users and 4 subcarriers.

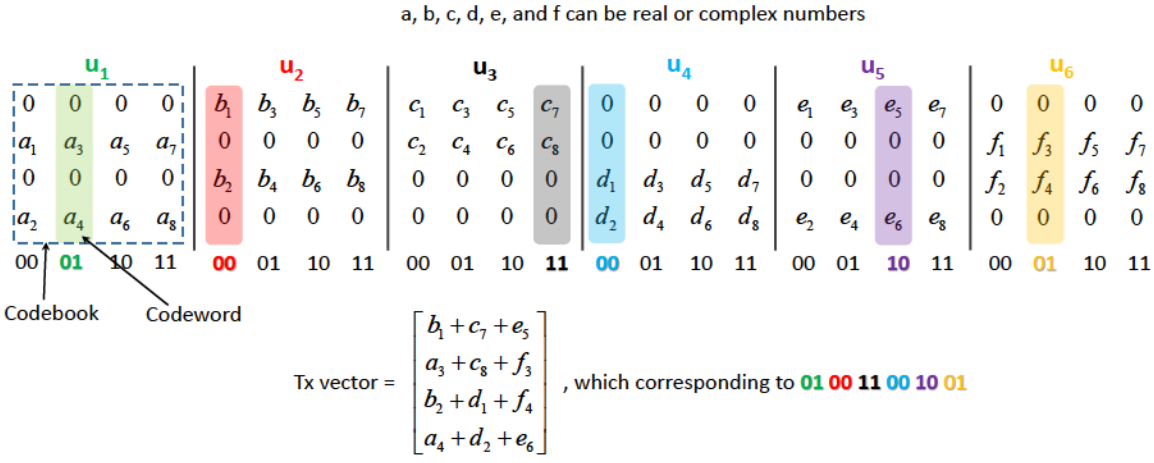

Fig. 1.5: Example of SCMA technique for 6 users and 4 subcarriers.

At the receiver, the decoder utilizes MPA to detect the transmitted codeword for each user, given that the codebooks for all six users are known at the receiver side. The MPA iteratively maximizes the posteriori probability of each user's codeword, and estimates a solution that corresponds to the maximum a posteriori probability.

1.4.2 The SM-SCMA System

With the increased need for high spectral efficiency transmission, the conventional MIMO assisted by the SCMA scheme becomes infeasible due to its complexity. Besides, the MIMO-SCMA system suffers from the same problems as the traditional MIMO systems, such as ICI and IAS. Recently, the multi-user SM has been assisted by SCMA (SM-SCMA) to provide a high spectral efficiency transmission and overcome the traditional MIMO-SCMA problems [13], [14]. In an SM-SCMA system, part of the input bit-stream activates only one transmit antenna, while the rest selects the user codeword to be transmitted from that active antenna. Thus, no ICI occurs and there is no need for IAS, which would be otherwise required for MIMO-SCMA. Unfortunately, the high number of required transmit antennas in SM-SCMA and the high complexity of the MPA implementation renders it unsuitable for many hardware implementations.

1.5 Potential Applications of SM to Emerging Communication Systems

- Millimeter-wave (mmWave) communication is a promising wireless communication system that accommodates increasingly high data rates and spectral efficiency services [15], [16]. However, it suffers from high propagation loss since it works in high-frequency bands. One of the proposed solutions to tackle this problem is to apply

beamforming technology with a large number of antennas to compensate for the introduced propagation loss. Unfortunately, the use of a massive number of antennas (i.e., a large number of RF chains) increases the cost of the transceiver, which limits the practical implementation. Besides hybrid pre-coding, currently considered to reduce the number of RF chains in massive MIMO systems, SM-MIMO system is a promising candidate for the mmWave communication systems that uses a limited number of RF chains. The SM-MIMO system for mmWave systems is studied in some recent research works [17]-[21].

- Visible light communication (VLC) is a recent and favorable technology, which attracts RF-free working environments, such as airports, hospitals, etc. [22], [23]. Usually, most of the places are equipped with a large number of LEDs, which makes MIMO feasible for integration with the VLC technology. Therefore, the SM-MIMO system is also an auspicious candidate for VLC technology, which is studied in recent research works [24]-[29].

- The SCMA system is a code-domain NOMA that progressively suffers from high decoding complexity as the number of served users increases. Moreover, the design of the user's codebook becomes an issue when the spectral efficiency increases. SM is consequently a propitious candidate when it comes to increasing the spectral efficiency without changing the user's codebook while at the same time maintaining an affordable decoding complexity [13], [14].

1.6 Motivation and Outline

Motivation

Efficient system design is an important issue in future generations of wireless communication systems [30], [31]. An example is the design of low-complexity receivers: these not only decrease the communication system latency but also reduce the receiver power consumption, which leads to increased battery lifetime.

Based on the aforementioned discussions regarding the single and multi-user SM system, the following research problems are investigated in this thesis:

- Efficient receivers are proposed, which reduce the decoding complexity of the ML for the single-user SM and QSM systems. These efficient receivers reduce the decoding complexity without sacrificing the BER performance.
- A full assessment of these efficient receivers is performed to evaluate their behavior.
- A complete analysis of the expected decoding complexity of the efficient receivers is provided.
- A reliable decoder is proposed to fit a wide range of practical applications with specific requirements for both operation and hardware implementation.
- An efficient transmitter for multi-user SM-MIMO assisted by SCMA is proposed. This efficient transmitter should overcome the high number of required antennas for the existing SM-SCMA system.
- The efficient transmitter of the SM-SCMA should take into consideration the decoding complexity and BER performance, compared to the existing SM-SCMA system.
- Efficient receivers should also be considered for the multi-user SM-SCMA system.

These receivers should provide a considerable reduction in the decoding complexity with an acceptable BER performance.

Thesis organization

The rest of this dissertation is organized as follows: Chapter 2 proposes a low-complexity decoding algorithm for single-user square QSM-MIMO. Chapter 3 proposes a low-complexity algorithm for general QSM and SM single-user MIMO system. Chapter 4 provides further investigations of the algorithm proposed in Chapter 3 in terms of expected decoding complexity and behavior of the algorithm for perfect and imperfect channel state information at the receiver side. Chapter 5 proposes a reliable decoder for single-user SM-MIMO systems. A low-cost multi-user SM-MIMO system is subsequently proposed in Chapter 6 with the aid of the SCMA technique. Low-complexity decoders for the SM-SCMA system are proposed in Chapter 7. Finally, the thesis is concluded in Chapter 8.

1.7 Contributions

Motivated by the previous discussion, I have identified and investigated the following research points in both single-user and multi-user SM-MIMO systems:

1. I have designed a low-complexity decoder for a single-user square QSM system [32]. This algorithm guarantees the optimal ML BER performance with a significant reduction in the decoding complexity, compared to the ML and other conventional algorithms. Moreover, the expected decoding complexity of the proposed algorithm is derived.

2. I have proposed a low-complexity decoder for single-user general SM and QSM MIMO systems [33]. The proposed algorithm significantly reduces the decoding

complexity without sacrificing the optimality of the ML BER performance.

3. I have investigated the behavior of the proposed algorithm mentioned in the second point from the decoding complexity perspective [34]. The expected decoding complexity of the proposed algorithm has been derived in the presence of perfect and imperfect channel state information at the receiver. The optimality of the proposed algorithm is mathematically proven. Furthermore, different simulation scenarios with different spectral efficiencies have been provided to confirm the findings.

4. I have designed a reliable decoding algorithm that can either reduce the decoding complexity with optimal ML BER performance or provide a flexible trade-off between the BER and complexity for a single-user SM-MIMO system[35]. The BER and expected complexity analysis have been derived and confirmed with simulations.

5. I have proposed an efficient transmitter for the multi-user SM-SCMA system [36]. The complete formulations of the transmitter and receiver for the novel system have been provided. The complexity analysis of the proposed SM-SCMA system has been studied. The proposed system significantly reduces the number of transmit antennas required to deliver the same spectral efficiency as the existing system, at the expense of a slight increase in the decoding complexity and negligible deterioration in the BER performance.

6. I have proposed three low-complexity decoding algorithms for the multi-user SM-SCMA system [37]. The first algorithm can be considered a benchmark for the decoding complexity at the expense of the BER performance, which is still acceptable for some practical applications. The second algorithm improves the BER performance of the first algorithm with the added cost of a minimal increase in the decoding complexity. The third algorithm not only provides the optimal BER performance with a significant reduction in the decoding complexity, but also ensures a flexible

trade-off between the BER and complexity. These algorithms suit a wide range of practical applications with specific requirements for both operation and hardware implementation. The mathematical formulation, complexity analysis, and simulation results are provided to support these findings.

References

[1] A. Kaye and D. George, “Transmission of multiplexed PAM signals over multiple channel and diversity systems," *IEEE Transactions on Communication Technology*, vol. 18, no. 5, pp. 520-526, Oct. 1970.

[2] J. Mietzner, R. Schober, L. Lampe, W. H. Gerstacker, and P. A. Hoher, “Multiple–antenna techniques for wireless communications – A comprehensive literature survey”, *IEEE Commun. Surveys Tuts.*, vol. 11, no. 2, pp. 87–105, 2nd quarter 2009.

[3] M. A. Albreem, M. Juntti, and S. Shahabuddin, “Massive MIMO Detection Techniques: A Survey,” *IEEE Commun. Surveys Tuts.*, vol. 21, no. 4, pp. 3109-3132, 4th quarter 2019.

[4] M. D. Renzo, H. Haas, and P. M. Grant, “Spatial modulation for multiple-antenna wireless systems: A survey,” *IEEE Commun. Mag.*, vol. 49, no. 12, pp. 182-191, Dec. 2011.

[5] M. Renzo, H. Haas, A. Ghrayeb, S. Sugiura, and L. Hanzo, “Spatial modulation for generalized MIMO: Challenges, opportunities and implementation,” *Proc. IEEE*, vol. 102, no. 1, pp. 56–103, Jan. 2014.

[6] T. Mao, Q. Wang, Z. Wang, and S. Chen, “Novel index modulation techniques: A survey,” *IEEE Commun. Surveys Tuts.*, vol. 21, no. 1, pp. 315-348, 1st quarter 2019.

[7] M. Wen et al., "A survey on spatial modulation in emerging wireless systems: Research progresses and applications," *IEEE J. Sel. Areas Commun.*, vol. 37, no. 9, pp. 1949-1972, Sep. 2019.

[8] R. Mesleh, H. Haas, S. Sinanovic, C. W. Ahn, and S. Yun, "Spatial modulation," *IEEE Trans. Veh. Technol.*, vol. 57, no. 4, pp. 2228–2241, July 2008.

[9] R. Mesleh, S. S. Ikki, and H. M. Aggoune, "Quadrature spatial modulation," *IEEE Trans. Veh. Technol.*, vol. 64, pp. 2738–2742, Jun. 2015.

[10] W. Shin, M. Vaezi, B. Lee, D. J. Love, J. Lee, and H. V. Poor, "Non-orthogonal multiple access in multi-cell networks: Theory, performance, and practical challenges," *IEEE Commun. Mag.*, vol. 55, no. 10, pp. 176–183, Oct. 2017.

[11] H. Nikopour and H. Baligh, "Sparse code multiple access," in *Proc. IEEE Int. Symposium on Personal Indoor and Mobile Radio Commun. (PIMRC)*, Sep. 2013, pp. 332–336.

[12] M. Taherzadeh, H. Nikopour, A. Bayesteh, and H. Baligh, "SCMA codebook design," in *Proc. IEEE Veh. Technol. Conf. (VTC Fall)*, Sep. 2014, pp. 1–5.

[13] Y. Liu, L. L. Yang, and L. Hanzo, "Spatial modulation aided sparse code division multiple access," *IEEE Trans. Wireless Commun.*, vol. 17, no. 3, pp. 1474–1487, Mar. 2018.

[14] Z. Pan, J. Luo, J. Lei, L. Wen, and C. Tang, "Uplink spatial modulation SCMA system," *IEEE Commun. Lett.,* vol. 23, no. 1, pp. 184-187, Jan. 2019.

[15] S. Rangan, T. S. Rappaport, and E. Erkip, "Millimeter-wave cellular wireless networks: Potentials and challenges," *Proc. IEEE*, vol. 102, no. 3, pp. 366–385, Mar. 2014.

[16] W. Wu, N. Zhang, N. Cheng, Y. Tang, K. Aldubaikhy, and X. Shen, "Beef up mmWave dense cellular networks with D2D-assisted cooperative edge caching," *IEEE Trans. Veh. Technol.*, vol. 68, no. 4, pp. 3890-3904, Apr. 2019.

[17] N. Ishikawa, R. Rajashekar, S. Sugiura, and L. Hanzo, "Generalized spatial modulation-based reduced-RF-chain millimeter-wave communications," *IEEE Trans. Veh. Technol.*, vol. 66, no. 1, pp. 879–883, Jan. 2017.

[18] P. Liu and A. Springer, "Space shift keying for LOS communication at mmWave frequencies," *IEEE Wireless Commun. Lett.,* vol. 4, no. 2, pp. 121–124, Apr. 2015.

[19] P. Liu, M. D. Renzo, and A. Springer, "Line-of-sight spatial modulation for indoor mmWave communication at 60 GHz," *IEEE Trans. Wireless Commun.*, vol. 15, no. 11, pp. 7373–7389, Nov. 2016.

[20] P. Liu, J. Blumenstein, N. S. Perovi, M. D. Renzo, and A. Springer, "Performance of generalized spatial modulation MIMO over measured 60GHz indoor channels," *IEEE Trans. Commun.*, vol. 66, no. 1, pp. 133– 148, Jan. 2018.

[21] A. Younis, N. Abuzgaia, R. Mesleh, and H. Haas, "Quadrature spatial modulation for 5G outdoor millimeterwave communications: Capacity analysis," *IEEE Trans. Wireless Commun.*, vol. 16, no. 5, pp. 2882–2890, May 2017.

[22] D. Karunatilaka, F. Zafar, V. Kalavally, and R. Parthiban, "LED based indoor visible light communications: State of the art," *IEEE Commun. Surveys Tuts.*, vol. 17, no. 3, pp. 1649–1678, Third Quarter 2015.

[23] W. O. Popoola, "Impact of VLC on light emission quality of white LEDs," *J. Lightw. Technol.*, vol. 34, no. 10, pp. 2526–2532, May 2016.

[24] C. R. Kumar and R. K. Jeyachitra, "Power efficient generalized spatial modulation MIMO for indoor visible light communications," *IEEE Photon. Technol. Lett.*, vol. 29, no. 11, pp. 921–924, Jun. 2017.

[25] W. O. Popoola and H. Haas, "Demonstration of the merit and limitation of generalised space shift keying for indoor visible light communications," *J. Lightw. Technol.*, vol. 32, no. 10, pp. 1960–1965, May 2014.

[26] K. Xu, H. Yu, and Y. Zhu, "Channel-adapted spatial modulation for massive MIMO visible light communications," *IEEE Photon. Technol. Lett.*, vol. 28, no. 23, pp. 2693–2696, Dec. 2016.

[27] T. Wang, F. Yang, L. Cheng, and J. Song, "Spectral-efficient generalized spatial modulation based hybrid dimming scheme with LACO-OFDM in VLC," *IEEE Access*, vol. 6, pp. 41 153–41 162, 2018.

[28] J. Wang, J. Zhu, S. Lin, and J. Wang, "Adaptive spatial modulation based visible light communications: SER analysis and optimization," *IEEE Photon. J.*, vol. 10, no. 3, pp. 1–14, Jun. 2018.

[29] A. Yesilkaya, E. Basar, F. Miramirkhani, E. Panayirci, M. Uysal, and H. Haas, "Optical MIMO-OFDM with generalized LED index modulation," *IEEE Trans. Commun.*, vol. 65, no. 8, pp. 3429–3441, Aug. 2017.

[30] J. G. Andrews, S. Buzzi, W. Choi, S. V. Hanly, A. Lozano, A. C. Soong, and J. C. Zhang, "What will 5g be?" *IEEE J. Sel. Areas Commun.*, vol. 32, pp. 1065–1082, Jun. 2014.

[31] P. Yang, M. Di Renzo, Y. Xiao, S. Li, and L. Hanzo, "Design guidelines for spatial modulation," *IEEE Commun. Surveys Tuts.*, vol. 17, pp. 6–26, 1st Quart. 2015.

[32] I. Al-Nahhal, O. A. Dobre, and S. Ikki, "Quadrature spatial modulation decoding complexity: Study and reduction," *IEEE Wireless Commun. Lett.,* vol. 6, pp. 378-381, Jun. 2017.

[33] I. Al-Nahhal, O. A. Dobre, and S. Ikki, "Low complexity decoders for spatial and quadrature spatial modulations," in *Proc. IEEE Veh. Technol. Conf. (VTC-Spring)*, 2018, pp. 1–5.

[34] I. Al-Nahhal, E. Basar, O. A. Dobre, and S. Ikki, "Optimum low-complexity decoder for spatial modulation," *IEEE J. Sel. Areas Commun.*, vol. 37, no. 9, pp. 2001-2013, Jul. 2019.

[35] I. Al-Nahhal, O. A. Dobre, and S. Ikki, "Reliable detection for spatial modulation systems," arXiv preprint arXiv:2006.05084.

[36] I. Al-Nahhal, O. A. Dobre, E. Basar, and S. Ikki, "Low-cost uplink sparse code multiple access for spatial modulation," *IEEE Trans. Veh. Technol.*, vol. 68, no. 9, pp. 9313-9317, Jul. 2019.

[37] I. Al-Nahhal, O. A. Dobre, and S. Ikki, "On the complexity reduction of uplink sparse code multiple access for spatial modulation," accepted, *IEEE Trans. Commun., Aug. 2020. doi: 10.1109/TCOMM.2020.3018184.*

Chapter 2

Quadrature Spatial Modulation Decoding Complexity: Study and Reduction

2.1 Abstract

This chapter presents the computational complexity reduction of the maximum likelihood-quadrature spatial modulation (QSM-ML) decoder as compared with the conventional SM-ML. Furthermore, a novel reduced-complexity (RC) sphere decoder algorithm, especially designed for QSM decoders, is proposed. It is shown that the QSM-RC algorithm achieves the optimum QSM-ML bit error ratio performance. Using Monte Carlo simulations and mathematical analysis, at the same spectral efficiency and with notable superior performance, it is shown that the QSM-ML and QSM-RC decoders provide at least 50% and up to 96% reduction in the number of visited nodes, respectively, compared to the SM-ML decoder.

2.2 Introduction

Low complexity represents an important requirement for the next generation of wireless systems [1]. In practical applications, reducing the computational complexity of algorithms or systems is of utmost importance, while maintaining the performance within acceptable limits.

Quadrature spatial modulation (QSM) is a promising technique [2], which employs the in-phase and quadrature dimensions to improve the throughput of the conventional SM [3]. At the receive-side, the optimum maximum likelihood (ML) detector [2] jointly estimates the two active transmit antenna indices conveying the in-phase and quadrature pulse amplitude modulations (PAMs) as well as the PAMs. The detection process requires a high running cost.

Recently, low-complexity decoding algorithms have been proposed for SM [4]-[6], and surveyed in [7]. In [4], [5], the sphere decoder (SD) [8] is applied to SM by employing a pruned radius (threshold) which depends on the number of receive antennas and noise variance. Estimation of the noise variance can be done either based on pilots/preamble or blindly [9]. The former leads to a loss of spectral efficiency, while the accuracy in the latter case depends on the data length. Furthermore, the noise variance estimation is required when the channel environment changes. In [6], a low-complexity algorithm has been proposed for SM. However, the algorithm requires an exhaustive pre-processing step to calculate the pseudo inverse of the channel matrix entries; additionally, the optimum bit error rate (BER) performance is not attained. In [10], the issue of the exhaustive pre-processing required in [6] is overcome by exploiting the sparsity property of large-scale QSM and the minimum mean square equalization. However, this does not hold for low/moderate-scale QSM systems. Furthermore, the algorithm in [10] requires estimation of the noise variance and does not provide the optimum BER performance.

In previous work [2], [10], the authors have not noticed that the QSM not only improves the conventional SM BER performance, but it also reduces the decoding complexity.

In this chapter, the contribution is twofold:

1) The QSM-ML decoding complexity is studied: it is shown that the QSM-ML reduces the complexity of the SM-ML decoder by at least half, at the same spectral efficiency.

2) A novel low-complexity SD algorithm is proposed for QSM systems; the proposed algorithm provides: a) the optimum ML BER performance; b) simple radius which requires neither estimation of the noise variance nor exhaustive pre-processing; and c) more reduction in the complexity when compared with the existing algorithms, if they are directly applied to QSM.

Analytical results are obtained for the complexity of the algorithms, and are confirmed with the Monte Carlo simulation.

2.3 The QSM System Model

Consider an $N_r \times N_t$ MIMO system, which employs QSM [2], with N_t and N_r as the number of transmit and receive antennas, respectively. The complex-valued transmitted symbol $s_t = s_t^{\Re} + \jmath s_t^{\Im}$ is divided into two real-valued PAMs, $s_t^{\Re}$ and $s_t^{\Im}$, where $s_t \in \{s_1, \cdots, s_{M_{\text{QSM}}}\}$, with M_{QSM} as the modulation order of the corresponding quadrature amplitude modulation (QAM). The transmitted symbol is delivered through an $N_r \times N_t$ flat fading channel, $\mathbf{H} \in \mathbb{C}^{N_r \times N_t}$. The noisy received vector, $\mathbf{y} \in \mathbb{C}^{N_r \times 1}$, is expressed as

$$\mathbf{y} = \mathbf{h}_{n_t^{\Re}} s_t^{\Re} + \jmath \mathbf{h}_{n_t^{\Im}} s_t^{\Im} + \mathbf{w}, \tag{2.1}$$

where $\mathbf{h}_{\mathbf{n_t^{\Re}}}$ and $\mathbf{h}_{n_t^{\Im}}$ denote the transmitted $n^{\Re}$-th and $n^{\Im}$-th columns of $\mathbf{H}$, respectively, and $\mathbf{w} \in \mathbb{C}^{N_r \times 1}$ is the additive white Gaussian noise (AWGN), $\mathbf{w} \sim \mathcal{CN}(0, \sigma^2)$. Note that, in this chapter, the subscripts t, $\Re$ and $\Im$ represent the actual transmitted, real and imaginary,

receptively.

Assuming that the channel state information is known at the QSM receiver, the optimal ML detector jointly estimates the two active transmit antenna indices, $\hat{n}_t^{\Re}$ and $\hat{n}_t^{\Im}$, as well as the corresponding real-valued PAMs, $\hat{s}_t^{\Re}$ and $\hat{s}_t^{\Im}$

$$\left[\hat{n}_t^{\Re}, \hat{n}_t^{\Im}, \hat{s}_t^{\Re}, \hat{s}_t^{\Im}\right] = \underset{n^{\Re}, n^{\Im}, s^{\Re}, s^{\Im}}{\arg\min} \left\| \mathbf{y} - \left(\mathbf{h}_{n^{\Re}} s^{\Re} + \jmath \mathbf{h}_{n^{\Im}} s^{\Im}\right) \right\|_F^2, \tag{2.2}$$

where $\|.\|_F$ denotes the Frobenius norm. Even though (2.2) is optimum, it requires intensive computations due to the exhaustive search of the ML detector.

2.4 The QSM-ML Decoder Complexity

In this section, I prove the reduction in decoding complexity of the QSM-ML over the conventional SM-ML at the same spectral efficiency. Note that the complexity in this chapter is defined as the average number of visited nodes (VNs) necessary to find the solution [4].

Consider a spectral efficiency of η (bit/sec/Hz). In SM, the spectral efficiency is given by $\eta_{\text{SM}} = \log_2(N_t M_{\text{SM}})$ [3], where M_{SM} is the SM modulation order. As discussed in [4], [5], the SM-ML detection can be converted into a tree-search structure with the total number of nodes equal to $M_{\text{SM}} N_t N_r$. Since the ML procedure visits all nodes, the complexity of the SM-ML detection is $C_{\text{SM-ML}} = M_{\text{SM}} N_t N_r$.

Turning to QSM, the spectral efficiency is given by $\eta_{\text{QSM}} = \log_2(N_t^2 M_{\text{QSM}})$ [2], where M_{QSM} is the QSM modulation order. Hence, the condition of achieving the same spectral efficiency for SM and QSM is $M_{\text{QSM}} = M_{\text{SM}}/N_t$.

The QSM-ML detection operation is divided into two independent SM-ML tree-searches; the first and second tree-searches are for the in-phase and quadrature PAM, respectively. The in-phase and quadrature PAMs are drawn from $\sqrt{M_{\text{QSM}}}$ real-valued numbers. Thus, the complexity of the QSM-ML decoder is provided by both in-phase and quadrature tree-search

complexities, and is expressed as $C_{\text{QSM-ML}}=2\sqrt{M_{\text{QSM}}}N_tN_r$.

Therefore, the complexity reduction ratio between the QSM-ML and the SM-ML, $\mathcal{R}_{\text{QSM-ML}}$, is given by

$$\mathcal{R}_{\text{QSM-ML}} = \frac{C_{\text{SM-ML}} - C_{\text{QSM-ML}}}{C_{\text{SM-ML}}} = 1 - \frac{2}{\sqrt{M_{\text{SM}}N_t}}. \tag{2.3}$$

For example, when $M_{\text{SM}} = 4$ and $N_t = 4$ ($\eta_{\text{SM}} = 4$), the reduction ratio is $\mathcal{R}_{\text{QSM-ML}} = 50\%$. It can be easily noticed that $\mathcal{R}_{\text{QSM-ML}}$ increases as $M_{\text{SM}}N_t$ increases.

2.5 Reduced-Complexity QSM Algorithm

The proposed reduced-complexity QSM (QSM-RC) algorithm is based on SD [8], and employs the tree-search structure shown in Fig. 2.1. The figure shows an example of QSM-RC decoder for $\eta = 4$ bit/sec/Hz, $N_r = 3$, $N_t = 2$ and $M_{\text{QSM}} = 4$. As seen, the QSM-RC decoding procedure is divided into two tree-searches denoted by $\Omega \in \{\Re, \Im\}$, with the tree-search level as $i \in \{1, \cdots, N_r\}$. For a given Ω, the tree-search branch, $j \in \{1, \cdots, N_t\sqrt{M_{\text{QSM}}}\}$, is formed from a combination of the transmit antenna index $n \in \{1, \cdots, N_t\}$ and the transmitted PAM symbol $s \in \{1, \cdots, \sqrt{M_{\text{QSM}}}\}$.

For a given Ω, the QSM-RC performs an ML search only on paths that lead to nodes with Euclidean distance (ED) less than or equal to a specific sphere pruned radius ρ^2_Ω. The ED at level i and branch j is denoted by $d^\Omega_{i,j}$ and is given as $d^\Omega_{i,j} = \left|y^\Omega_i - (h_{i,n}s)^\Omega_j\right|^2$, where $|.|$ is the modulus operation, $y^\Omega_i \in \{y^\Omega_1, \cdots, y^\Omega_{N_r}\}$ is the i-th complex-valued element of the vector $\mathbf{y}^{\mathbf{\Omega}}$ and $h_{i,n}$ is the element (i, n) of the matrix $\mathbf{H}$. Note that, in a given branch j, the accumulated ED at any node is the sum of the preceding EDs.

For a given Ω, the QSM-RC algorithm is summarized in Algorithm 2.1 and explained as follows:

Step 1: Calculate the EDs at the first level ($i = 1$), then order them ascendingly to obtain

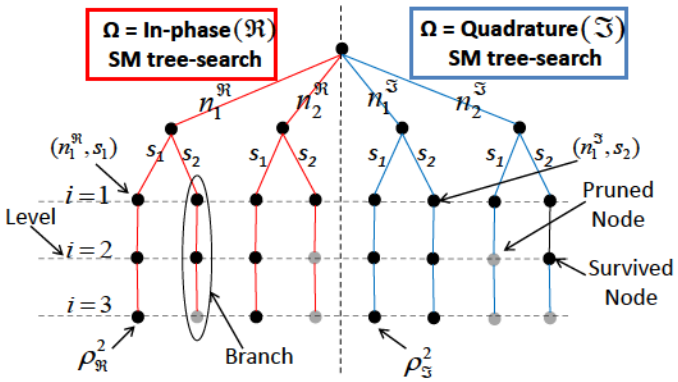

Fig. 2.1: The tree-search structure for the QSM-RC decoder for $\eta = 4$ bit/sec/Hz, $N_r = 3$, $N_t = 2$ and $M_{\text{QSM}} = 4$.

$$\left[e^{\Omega}_{1,1} \ \cdots \ e^{\Omega}_{1,N_t\sqrt{M_{\text{QSM}}}} \right] = \text{sort}\left(\left[d^{\Omega}_{1,1} \ \cdots \ d^{\Omega}_{1,N_t\sqrt{M_{\text{QSM}}}} \right] \right), \tag{2.4}$$

where sort(.) is the ascending order function. Note that the calculations of the EDs of the first level are common to other algorithms. Thus, this step is not considered to be an additional step.

Step 2: Visit all nodes of the first branch ($j = 1$) which starts with $e^{\Omega}_{1,1}$, to obtain the accumulated ED of the first branch.

Step 3: Assign the value of the accumulated ED, calculated in step 2, to be the initial value of ρ^2_{Ω}

$$\rho^2_{\Omega} = \sum_{i=1}^{N_r} e^{\Omega}_{i,1}. \tag{2.5}$$

Step 4: Sequentially visit the tree-search branches in the order of the sorted EDs in (2.4), as long as the accumulated ED of that branch is still inside the sphere.

Step 5: Update ρ^2_{Ω} whenever the algorithm finds any branch accumulated ED smaller than the current value.

Step 6: Estimate n^{Ω}_t and s^{Ω}_t using

$$\left[\hat{n}_t^{\Omega}, \hat{s}_t^{\Omega}\right] = \underset{n^{\Omega}, s^{\Omega}}{\arg\min} \left\{ \left\| \mathbf{y}^{\Omega} - (\mathbf{h}_n s)_j^{\Omega} \right\|_F^2 \leq \rho_{\Omega}^2 \right\}. \tag{2.6}$$

Note that (2.5) provides a complete branch inside the sphere at the beginning of the decoding process, and then the QSM-RC algorithm discards visiting the next tree-search branches based on the value of (2.5). Thus, the optimal solution will not be missed. In other words, the discarded branches can not provide the optimal solution because they already have EDs greater than the EDs of the visited branches, which guarantees the optimum ML BER performance for the QSM-RC algorithm.

2.6 Complexity analysis of the QSM-RC

The number of VNs of the QSM-RC algorithm equal to $\zeta = \zeta^{\Re} + \zeta^{\Im}$, where $\zeta^{\Re}$ and $\zeta^{\Im}$ represent the complexities of the in-phase and quadrature tree-search, respectively. For a given Ω, the number of VNs is given by

$$\zeta^{\Omega} = N_r + \sum_{j=2}^{N_t\sqrt{M_{\text{QSM}}}} \left[\mathcal{P}_{1,j}^{(\text{sort})} \left(\sum_{i=1}^{N_r} \mathcal{P}_{i,j}^{(\text{inside})} \right) \right], \tag{2.7}$$

where the first term of the right hand side represents the number of VNs which is required for calculating the pruned radius in (2.5), $\mathcal{P}_{1,j}^{(\text{sort})}$ denotes the probability of sorting node $(1, j)$, and $\mathcal{P}_{i,j}^{(\text{inside})}$ denotes the probability of having a node (i,j) inside the sphere. As long as $\mathcal{P}_{1,j}^{(\text{sort})}$ and $\mathcal{P}_{i,j}^{(\text{inside})}$ are independent random variables, the second term of the right hand side represents the number of VNs in the branches from $j = 2$ to $N_t\sqrt{M_{\text{QSM}}}$, with each branch having N_r nodes.

Hence, as shown in Appendix, the number of VNs of the QSM-RC algorithm for a given Ω is

Algorithm 2.1 QSM-RC pseudo-code

- **Sort** $\left\{d_{1,j}^{\Omega}\right\}$ to obtain $\left\{e_{1,j}^{\Omega}\right\}$ as in (2.4).
- **Compute** ρ_{Ω}^{2} as in (2.5).

1: $for\ \ j=2:\ \ N_t\sqrt{M_{\text{QSM}}}$
2: **Initiate** the accumulated ED $D_j^{\Omega}=0$.
3: $for\ \ i=1:\ \ N_r$
4: **Compute** the Euclidean distance $d_{i,j}^{\Omega}=\left|y_i^{\Omega}-(h_{i,n}s)_j^{\Omega}\right|^2$
5: **Set** $D_j^{\Omega}=D_j^{\Omega}+d_{i,j}^{\Omega}$.
6: $if\ \ D_j^{\Omega}\geq\rho_{\Omega}^{2}$
7: **Go to** line 1.
8: end
9: end
10: **Update** ρ_{Ω}^{2} (if accumulated ED $D_j^{\Omega}<\rho_{\Omega}^{2}$) .
11: end

- **Estimate** n_t^{Ω} and s_t^{Ω} as in (2.6).
- **Repeat** the same procedures for the other Ω.

$$C_{\text{QSM-RC}}^{\Omega}=\begin{cases}\zeta^{\Omega}+\left(N_t\sqrt{M_{\text{QSM}}}-1\right) & \zeta^{\Omega}\leq\left(N_t\sqrt{M_{\text{QSM}}}-1\right)\\ \zeta^{\Omega} & \text{otherwise}\end{cases}. \tag{2.8}$$

Thus, the total number of VNs for the QSM-RC algorithm is $C_{\text{QSM-RC}}=C_{\text{QSM-RC}}^{\Re}+C_{\text{QSM-RC}}^{\Im}$, and the complexity reduction ratio between the QSM-ML and SM-ML is

$$\mathcal{R}_{\text{QSM-RC}}=\frac{C_{\text{SM-ML}}-C_{\text{QSM-RC}}}{C_{\text{SM-ML}}}. \tag{2.9}$$

It is worth mentioning that the lowest number of VNs that can be reached is when the algorithm visits no node inside the tree-search. In this case, the total number of visited nodes is limited to the number of VNs used in steps 1 and 3, which is

$$C_{\text{min}}^{\Omega}=N_r+N_t\sqrt{M_{\text{QSM}}}-1. \tag{2.10}$$

Therefore, the theoretical upper bound of the complexity reduction (UBCR) ratio $\mathcal{R}_{\text{UBCR}}$, is given by

$$\mathcal{R}_{\text{UBCR}} = 1 - \frac{2(N_r + N_t\sqrt{M_{\text{QSM}}} - 1)}{M_{\text{SM}} N_t N_r}. \tag{2.11}$$

2.7 Numerical results

In this section, I assess the complexity reduction of the proposed QSM-RC as well as the QSM-ML, in comparing with the conventional SM-ML. The effect of sorting in (2.4) will be demonstrated, and I refer to the unsorted version of the QSM-RC as QSM-URC. The algorithm proposed for the SM-SD in [4] will be applied for the QSM for comparison purpose; this is referred to QSM-SD and uses the same parameters as in [4]. The UBCR in (2.11) is what all the algorithms try to achieve. The presented results are obtained by running Monte-Carlo simulations over 10^6 Rayleigh flat fading channel realizations. Note that simulations confirm the analytical results in (2.3) and Section 2.6.

In Fig. 2.2, the complexity reduction ratio of different QSM decoders is studied in case of $N_r = 4$ for $\eta = 6$ bit/sec/Hz and $M_{\text{QSM}} = 4$ ($M_{\text{SM}} = 16$). It can be seen that the QSM-RC algorithm has the best reduction ratio; it requires only 22 dB signal-to-noise ratio (SNR) to approach the UBCR which is 92%. At 22 dB SNR, the QSM-URC has a complexity reduction ratio of 85%, which shows 7% gain obtained from the sorting step in the QSM-RC algorithm. Fig. 2.3 shows the number of VNs required for different QSM decoders versus N_t at SNR = 10 dB and $N_r = 8$ using different spectral efficiencies. The QSM-ML requires a smaller number of VNs than SM-ML, and the QSM-RC has the least number of VNs. Fig. 2.3 shows that the proposed QSM-RC is valid for $N_t \leq N_r$ and $N_t \geq N_r$.

Fig. 2.4 shows the BER performance of different QSM decoders versus SNR for $\eta = 8$ bit/sec/Hz, $M_{\text{SM}} = 64$ and $N_r = 4$. The QSM-RC and QSM-URC provide the optimum

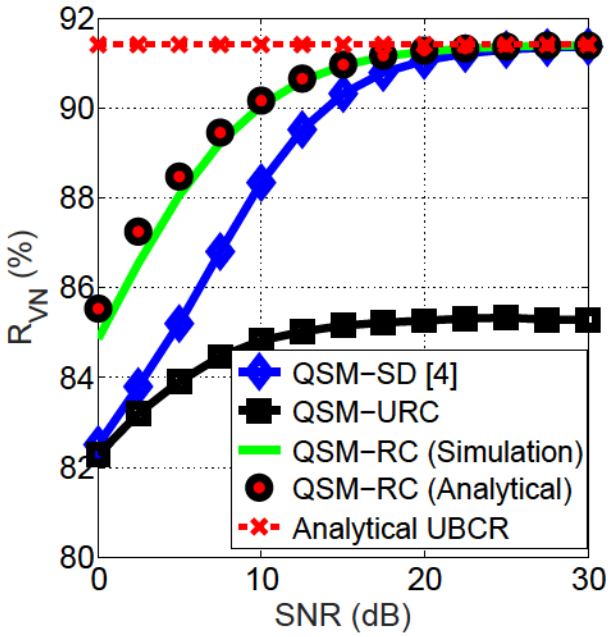

Fig. 2.2: Complexity reduction comparison of different QSM decoders for $M_{\text{QSM}} = 4$, $\eta = 6$ bit/sec/Hz, $N_t = 4$ and $N_r = 4$.

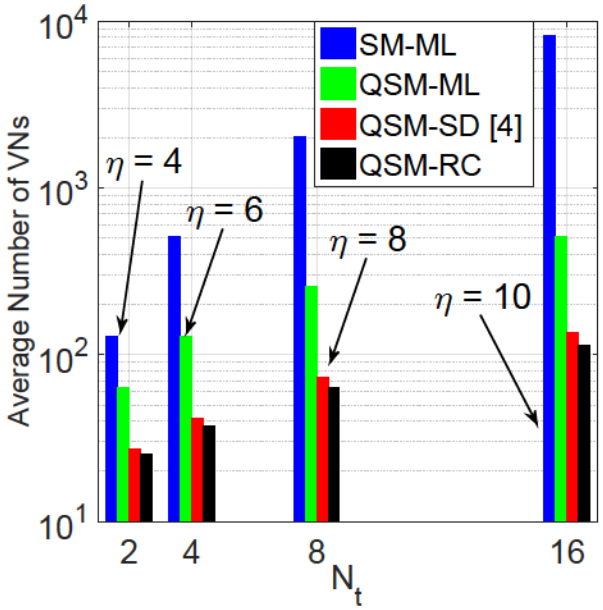

Fig. 2.3: Number of VNs comparison of different QSM decoders for $M_{\text{QSM}} = 4$, SNR $= 10$ dB and $N_r = 8$.

BER performances of the QSM-ML due to (2.5), while the QSM-SD [4] deteriorates at high SNR due to the dependency of its pruned radius on the noise variance which becomes small. In this case, the QSM-SD [4] visits fewer nodes than what are required to obtain the optimum performance. Fig. 2.5 shows that the QSM-ML complexity reduction ratio is 87% for all SNR values, while 20 dB SNR is enough to allow the QSM-RC reach 96%. Note that, from Fig. 2.2 and 2.5, the complexity reduction increases as the M_{SM} increases, which agrees with (2.11).

It is seen from these figures that the QSM-ML system reduces the decoding complexity of the SM-ML beside its superiority in BER performance. However, the QSM-ML decoding process is still exhaustive. The QSM-RC algorithm provides a significant reduction in the complexity without any loss in BER performance.

2.8 Conclusion

This chapter provides a mathematical proof of the reduction in complexity for the QSM-ML decoder when compared with the SM-ML at the same spectral efficiency, by at least 50% of the number of visited nodes. Moreover, a novel reduced-complexity algorithm designed for QSM is proposed. Unlike the QSM-RC algorithm, the existing SD algorithms in the literature have some obstacles if directly applied to QSM. The QSM-RC provides the optimal ML BER performance by assigning at least one tree-search branch inside the sphere, and provides reduction up to 96% in the number of visited nodes.

2.9 APPENDIX: Proof of (2.8)

To find $\mathcal{P}_{1,j}^{(\text{sort})}$ and $\mathcal{P}_{i,j}^{(\text{inside})}$ in (2.7), consider $u_{i,j}^{\Omega} = y_i^{\Omega} - (h_{i,n}s)_j^{\Omega}$ and $y_i^{\Omega} = (h_{i,n}s)_t^{\Omega} + w_i^{\Omega}$, where $(h_{i,n}s)_t^{\Omega}$ is the actual transmitted combination element consisting of the transmitted

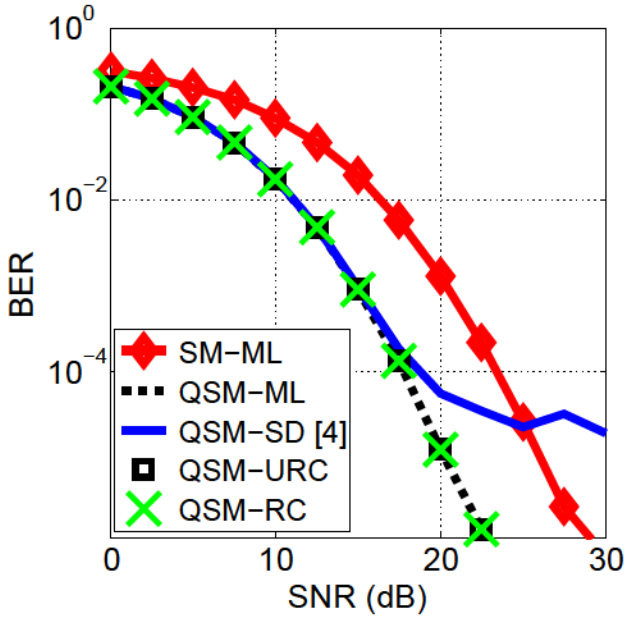

Fig. 2.4: BER-performance comparison of different QSM decoders for $\eta = 8$ bit/sec/Hz, $N_r = 4$, $N_t = 4$, $M_{\text{SM}} = 64$ and $M_{\text{QSM}} = 16$.

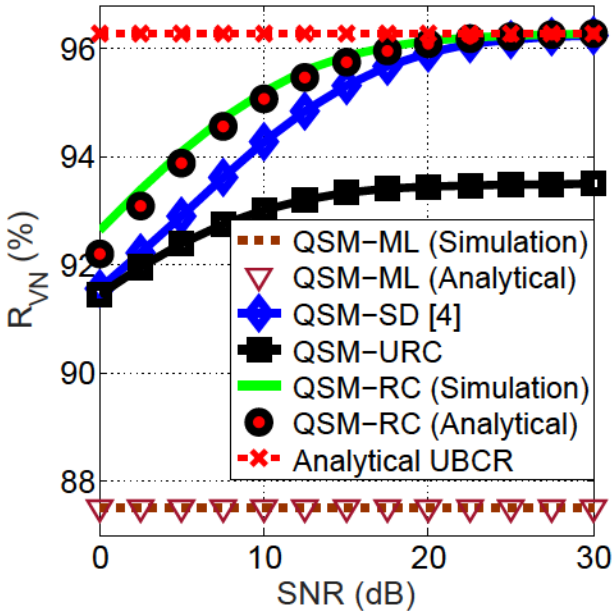

Fig. 2.5: Complexity reduction comparison of different QSM decoders for $\eta = 8$ bit/sec/Hz, $N_r = 4$, $N_t = 4$, $M_{\text{SM}} = 64$ and $M_{\text{QSM}} = 16$.

PAM symbol s_t^{Ω} using antenna with index n_t, and w_i^{Ω} is i-th noise element of the $\mathbf{w}$ in (2.1). Thus, (2.6) can be re-written as,

$$\left[\hat{n}_t^{\Omega}, \hat{s}_t^{\Omega}\right] = \arg\min_{j} \left\{ \sum_{i=1}^{N_r} \left| u_{i,j}^{\Omega} \right|^2 \leq \rho_{\Omega}^2 \right\}. \tag{2.12}$$

Note that the distribution of the accumulated ED for any level i, $\sum_{k=1}^{i} \left| u_{k,j}^{\Omega} \right|^2 = \frac{\sigma^2}{2} \Psi_{i,j}$, with $\Psi_{i,j}^{\Omega} = \sum_{k=1}^{i} (u_{k,j}^{\Omega}/(\sigma/\sqrt{2}))^2$, is a non-central chi-squared distribution with i degrees of freedom [4], [11]. Consequently, the cumulative distribution function F(.) of the random variable $\Psi_{i,j}^{\Omega}$ is [12, (Ch. 2)]

$$\Pr\left(\Psi_{i,j}^{\Omega} \leq \psi^2 \left| s_t^{\Omega}, n_t, \mathbf{H}, \sigma^2 \right.\right) = \mathrm{F}\left(\left(\frac{\psi}{\sigma/\sqrt{2}} \right)^2, i, \frac{\sum_{k=1}^{i} \left| (h_{k,n} s)_t^{\Omega} - (h_{k,n} s)_j^{\Omega} \right|^2}{\sigma^2/2} \right). \tag{2.13}$$

The closed form expression of (2.13) for odd degrees of freedom, i, is not available. However the solution can be evaluated numerically. For even degrees of freedom, i, the solution of (2.13) is expressed in terms of the generalized Marcum's Q-function as [12, (2.1-124)].

Since sorting probability $\mathcal{P}_{1,j}^{(\mathrm{sort})}$ in (2.7) can be expressed as

$$\mathcal{P}_{1,j}^{(\mathrm{sort})} = \Pr\left(\min\left\{ e_{1,j}^{\Omega}, e_{1,j+1}^{\Omega}, \cdots, e_{1,N_t\sqrt{M_{\mathrm{QSM}}}}^{\Omega} \right\} \geq e_{1,j}^{\Omega} \right), \tag{2.14}$$

the solution of (2.14) is given as [13, (p. 325)]:

$$\mathcal{P}_{1,j}^{(\mathrm{sort})} = 1 - \prod_{n=j}^{N_t\sqrt{M_{\mathrm{QSM}}}} \left(1 - \Pr\left(e_{1,n}^{\Omega} < e_{1,j}^{\Omega} \right) \right), \tag{2.15}$$

where the term $\Pr\left(e_{1,n}^{\Omega} < e_{1,j}^{\Omega}\right)$ is given in (2.13) with $i = 1$.

Now, I can directly calculate the probability of having a node (i, j) at level i inside the sphere given a radius ρ_{Ω} as

$$\mathcal{P}_{i,j}^{(\text{inside})} = \Pr\left(\Psi_{i,j}^{\Omega} \leq \left(\frac{\rho_{\Omega}^2}{\sigma^2/2}\right) \left| s_t^{\Omega}, n_t, \mathbf{H}, \sigma^2 \right.\right), \tag{2.16}$$

where (2.16) is evaluated from (2.13).

From (2.7), (2.15) and (2.16), the derived complexity assumes that, initially, the algorithm knows if the node is outside or inside the sphere. However, this assumption is inaccurate and a correction factor is required to consider the initial VNs. In other words, the number of VNs can not be less than (2.10). To account for this, the number of VNs in (2.7) is modified as in (2.8), where $\left(N_t\sqrt{M_{\text{QSM}}} - 1\right)$ is the initial number of VNs.

References

[1] J. G. Andrews, S. Buzzi, W. Choi, S. V. Hanly, A. Lozano, A. C. Soong, and J. C. Zhang, "What will 5g be?" *IEEE J. Sel. Areas Commun.*, vol. 32, pp. 1065–1082, Jun. 2014.

[2] R. Mesleh, S. S. Ikki, and H. M. Aggoune, "Quadrature spatial modulation," *IEEE Trans. Veh. Technol.*, vol. 64, pp. 2738–2742, Jun. 2015.

[3] R. Y. Mesleh, H. Haas, S. Sinanovic, C. W. Ahn, and S. Yun, "Spatial modulation," *IEEE Trans. Veh. Technol.*, vol. 57, pp. 2228–2241, Jul. 2008.

[4] A. Younis, R. Mesleh, H. Haas, and P. M. Grant, "Reduced complexity sphere decoder for spatial modulation detection receivers," in *Proc. IEEE GLOBECOM*, 2010, pp. 1–5.

[5] A. Younis, S. Sinanovic, M. Di Renzo, R. Mesleh, and H. Haas, "Generalised sphere decoding for spatial modulation," *IEEE Trans. Commun.*, vol. 61, pp. 2805–2815, Jul. 2013.

[6] Q. Tang, Y. Xiao, P. Yang, Q. Yu, and S. Li, "A new low-complexity near-ml detection algorithm for spatial modulation," *IEEE Wireless Commun. Lett.*, vol. 2, pp. 90–93, Feb. 2013.

[7] P. Yang, M. Di Renzo, Y. Xiao, S. Li, and L. Hanzo, "Design guidelines for spatial modulation," *IEEE Commun. Surveys Tuts*., vol. 17, pp. 6–26, 1st Quart. 2015.

[8] E. Viterbo and J. Boutros, "A universal lattice code decoder for fading channels," *IEEE Trans. Inf. Theory*, vol. 45, pp. 1639–1642, Jul. 1999.

[9] F. Bellili, R. Meftehi, S. Affes, and A. Stéphenne, "Maximum likelihood snr estimation of linearly-modulated signals over time-varying flat-fading simo channels," *IEEE Trans. Signal Process.*, vol. 63, pp. 441–456, Jan. 2015.

[10] L. Xiao, P. Yang, S. Fan, S. Li, L. Song, and Y. Xiao, "Low-complexity signal detection for large-scale quadrature spatial modulation systems," *IEEE Commun. Letters*, vol. 20, pp. 2173-2176, Nov. 2016.

[11] B. Hassibi and H. Vikalo, "On the sphere-decoding algorithm I. Expected complexity," *IEEE Trans. Signal Process.*, vol. 53, pp. 2806–2818, Aug. 2005.

[12] J. Proakis, *Digital Communications Systems Engineering*, 4th ed. McGraw-Hill, 2000.

[13] A. Leon-Garcia, *Probability, Statistics, and Random Processes for Electrical Engineering*, 3rd ed. Pearson/Prentice Hall Upper Saddle River, NJ, 2008.

Chapter 3

Low Complexity Decoders for Spatial and Quadrature Spatial Modulations

3.1 Abstract

In spatial modulation (SM) and SM (QSM), the maximum–likelihood (ML) decoder provides the optimum solution with high decoding complexity at the receiver side. This chapter presents a novel low-complexity algorithm for decoding the SM and QSM symbols, referred to as the min-max algorithm. This is an intelligent searching algorithm, particularly designed for the tree-search of the SM and QSM decoders. The proposed algorithm expands the minimum Euclidean distance (ED) by adding a single node at each step, without considering the order of the branches. The expanding process stops if the minimum ED occurs at the end of a fully expanded branch. It is shown that the proposed algorithm achieves the optimum ML bit error rate performance with a significant reduction in the decoding complexity comparing with SM-ML and QSM-ML, as well as other existing sphere decoding algorithms. Simulations and mathematical analysis are provided to assess the decoding performance and complexity of the proposed algorithm.

3.2 Introduction

Low-complexity represents a vital requirement for the next generation of wireless technologies [1]. In real-time applications, at acceptable limits of performance, having a low-complexity detection is of utmost importance.

Spatial modulation (SM) overcomes the inter-channel interference problem of multiple-input multiple-output (MIMO) by activating only one transmit antenna for every time instance [2]. Transmitted data determines the active antenna, as well as the symbol to be transmitted from the antenna. Quadrature spatial modulation (QSM) is an evolved version [3] of SM, which utilizes the in-phase and quadrature dimensions in order to enhance the throughput of the conventional SM. At the receiver, the optimum maximum likelihood (ML) detector [2], [3] jointly estimates the active transmit antenna indices and symbols. The detection procedure has a high running cost, especially for real-time applications.

Recently, low-complexity detection algorithms have been proposed for SM [4]-[6] and QSM [7], [8]. In [4], [5], the sphere decoder (SD) [9] is applied to the SM system, and provides the optimum bit error rate (BER) performance. However, it requires knowledge of the noise variance [10]. In [6], [7], low-complexity decoders are proposed for SM and large-scale QSM, respectively. However, the proposed decoders have not achieved the optimum BER. Furthermore, the latter requires knowledge of the noise variance. In [8], a reduced-complexity algorithm is proposed for QSM, which provides the ML BER performance and does not depend on the noise variance. However, more reduction in the decoding complexity can be still achieved.

In this chapter, I propose a low-complexity decoder for both SM and QSM systems, referred to as the min-max (m-M) algorithm. The main idea of the proposed algorithm is to perform a single expansion to the minimum Euclidean distance (ED) over all tree-search branches, until the minimum ED occurs at the end of a fully expanded (maximum length)

branch. The algorithm provides a significant reduction in complexity in terms of the number of visited nodes when compared with conventional algorithms in the literature, as well as the optimum BER performance.

3.3 SM and QSM System Models

Assume I have an $N_r \times N_t$ MIMO system, where N_t and N_r represent the number of transmit and receive antennas, respectively. The complex-valued symbol x_t is transmitted through an $N_r \times N_t$ flat fading channel, $\mathbf{H} \in \mathbb{C}^{N_r \times N_t}$, and the received signal is also affected by additive white Gaussian noise (AWGN) with zero-mean and variance σ_n^2, $\mathbf{w} \sim \mathcal{CN}(0, \sigma_n^2)$. The spectral efficiency, η is the information rate delivered from the transmitter to the receiver for a given bandwidth. The received vector $\mathbf{y} \in \mathbb{C}^{N_r \times 1}$ depends on the system, i.e., SM or QSM.

3.3.1 Spatial Modulation

In the SM system, a symbol is transmitted from only one active antenna at each time instance. The antenna and transmitted symbol are chosen according to the input data. In this case, the target spectral efficiency, η_{SM}, is delivered by using two symbols: the spatial symbol and the constellation symbol. The former represents the index of the active antenna during transmission, while the latter is drawn from the M-ary quadrature amplitude modulation (M-QAM). Consequently, $\eta_{\text{SM}} = \log_2(N_t) + \log_2(M_{\text{SM}}) = \log_2(N_t M_{\text{SM}})$, where M_{SM} is the modulation order of the SM system. In other words, the number of combinations, Λ, between the N_t columns of $\mathbf{H}$ (spatial symbols) and M_{SM} symbols (constellation symbols) is $\Lambda = 2^{\eta_{\text{SM}}} = N_t M_{\text{SM}}$, leading to a spectral efficiency of η_{SM} bit/second/Hertz (b/s/Hz).

The noisy received vector, $\mathbf{y}_{\text{SM}}$, for the SM system can be expressed as

$$\mathbf{y}_{\text{SM}} = \mathbf{h}_{n_t} x_{\text{SM}_t} + \mathbf{w} = \chi_{\text{SM}_t} + \mathbf{w}, \tag{3.1}$$

where $\mathbf{h}_{n_t}$ denotes the n_t-th column of $\mathbf{H}$, which means that the antenna of index $n_t \in \{1, \cdots, N_t\}$ is activated, $x_{\text{SM}_t} \in \{x_1, \cdots, x_{M_{\text{SM}}}\}$ is the transmitted symbol, and $\chi_{\text{SM}_t} = \mathbf{h}_{n_t} x_{\text{SM}_t} \in \{\chi_1, \cdots, \chi_\Lambda\}$ is the transmitted combination of the spatial and constellation symbols. Note that the subscript t represents the transmitted symbol/index.

At the receiver, the target is to estimate the transmitted combination χ_{SM_t}. Assuming that the channel state information is perfectly known at the SM receiver, the optimal ML detector jointly estimates the transmitted combination $\tilde{\chi}^{(\text{ML})}_{\text{SM}_t}$ by employing an exhaustive search over all possible combinations as

$$\tilde{\chi}^{(\text{ML})}_{\text{SM}_t} = \underset{\chi_{\text{SM}} = \chi_1, \cdots, \chi_\Lambda}{\arg\min} \left\| \mathbf{y}_{\text{SM}} - \chi_{\text{SM}} \right\|_F^2, \tag{3.2}$$

where $\|.\|_F$ denotes the Frobenius norm.

3.3.2 Quadrature Spatial Modulation

The QSM system splits the complex-valued transmitted symbol $x_{\text{QSM}_t} = x^{\Re}_{\text{QSM}_t} + \jmath x^{\Im}_{\text{QSM}_t}$ into its in-phase and quadrature components, $x^{\Re}_{\text{QSM}_t}$ and $x^{\Im}_{\text{QSM}_t}$, and exploits the orthogonality property between these dimensions to independently deliver them to the receive-side. It should be noted that each component is transmitted as in SM, and can have a different channel environment. The noisy received vector, $\mathbf{y}_{\text{QSM}} \in \mathbb{C}^{N_r \times 1}$, is expressed as

$$\mathbf{y}_{\text{QSM}} = \mathbf{h}_{n_t^{\Re}} x^{\Re}_{\text{QSM}_t} + \jmath \mathbf{h}_{n_t^{\Im}} x^{\Im}_{\text{QSM}_t} + \mathbf{w} = \chi^{\Re}_{\text{QSM}_t} + \chi^{\Im}_{\text{QSM}_t} + \mathbf{w}, \tag{3.3}$$

where $x_{\text{QSM}_t} \in \{x_1, \cdots, x_{M_{\text{QSM}}}\}$, with M_{QSM} as the modulation order, and $\mathbf{h}_{\mathbf{n_t^{\Re}}}$ and $\mathbf{h}_{n_t^{\Im}}$ denote the $n_t^{\Re}$-th and $n_t^{\Im}$-th columns of $\mathbf{H}$, respectively. In square QSM, the constellation

symbols for the real and imaginary components are drawn from $\sqrt{M_{\text{QSM}}}$ real-valued numbers and transmitted from the same number of transmit antennas, N_t. Thus, the QSM spectral efficiency is $\eta_{\text{QSM}} = 2\left(\log_2\left(N_t\right) + \log_2\left(\sqrt{M_{\text{QSM}}}\right)\right) = \log_2\left(N_t^2 M_{\text{QSM}}\right)$.

Consequently, the ML decoder in (3.2) becomes

$$\tilde{\chi}_{\text{QSM}_t}^{\Re\,(\text{ML})}, \tilde{\chi}_{\text{QSM}_t}^{\Im\,(\text{ML})} = \underset{\chi_{\text{QSM}_t}^{\Re}, \chi_{\text{QSM}_t}^{\Im}}{\arg\min} \left\| \text{y} - \left(\chi_{\text{QSM}}^{\Re} + \jmath \chi_{\text{QSM}}^{\Im}\right) \right\|_F^2, \tag{3.4}$$

where $\chi_{\text{QSM}_t}^{\Re}$ and $\chi_{\text{QSM}_t}^{\Im} \in \{\chi_1, \cdots, \chi_\Lambda\}$ represent the two transmitted combinations, and $\Lambda = N_t\sqrt{M_{\text{QSM}}}$.

3.3.3 The Tree-Search Structure Concept

Equations (3.2) and (3.4) can be solved by employing the tree-search structure [4], [5], [8]. Fig. 3.1 provides an example of how the tree-search is constructed for the SM decoders. Consider I have a 3×2 MIMO system with binary phase-shift-keying (BPSK). The spectral efficiency in this case is $\eta_{\text{SM}} = 4$ b/s/Hz with the total number of combinations, $\Lambda = 4$. Each combination with index $j \in \{1, 2, 3, 4\}$ can be represented as a branch with length N_r. The ML algorithm visits all nodes for all branches to declare the estimated combination (with index j) which corresponds to the minimum ED at the last level. In SD [9], the algorithm discards some nodes based on a pre-determined threshold, in order to save complexity in the decoding process. Note that the QSM tree-search consists of two independent SM-like tree-searches: one for the in-phase and one for the quadrature component.

3.4 Proposed m-M Low-Complexity Algorithm

In this section, I propose a low-complexity decoding algorithm for SM and QSM based on a smart way of finding the ML solution inside the tree-search, which is referred to as the m-M

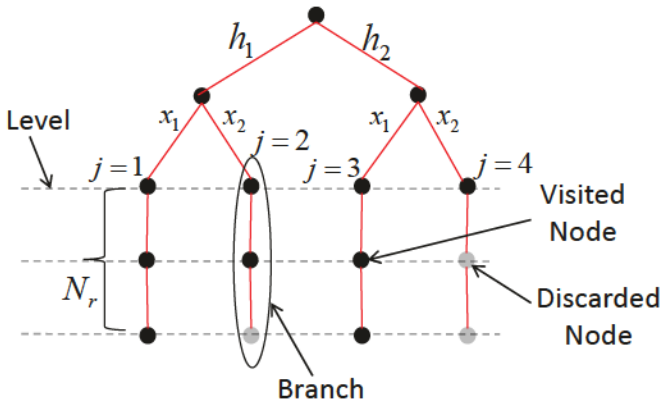

Fig. 3.1: The tree-search structure for the SM-SD algorithm for $\eta_{SM} = 4$ b/s/Hz, $N_r = 3$, $N_t = 2$ and $M_{\text{SM}} = 2$.

algorithm. Unlike the existing SD algorithms, the proposed m-M algorithm is not restricted to perform a full expansion for a specific branch before moving to the next one. It avoids visiting the unnecessary nodes by making a single expansion to the minimum ED across all branches. Further, it stops if and only if at least one branch is fully expanded and ends with the minimum ED.

To formulate it mathematically, let $\mathbf{v} \in \mathbb{R}^{\Lambda \times 1} = [v_1 \quad \cdots \quad v_\Lambda]$ represent the vector of visited nodes for each branch. It should be noted that the value v_j, $j = 1, \cdots, \Lambda$, represents the number of visited nodes (i.e., levels) for the j-th branch. Assume that $\mathbf{d} \in \mathbb{R}^{\Lambda \times 1} = [d_{v_1,1} \quad \cdots \quad d_{v_\Lambda,\Lambda}]$ is the ED vector for each expanded branch, with

$$d_{v_j,j} = \sum_{k=1}^{v_j} |y_k - \chi_{k,j}|^2 , \tag{3.5}$$

where $d_{v_j,j}$ is the ED of the j-th branch at level v_j and $|.|$ is the modulus operation.

The proposed m-M algorithm is summarized in Algorithm 3.1 and explained as follows:

Step 1: Initialize $\mathbf{v}$ by the all-ones vector and $\mathbf{d}$ by calculating the EDs at the first level $\left(\mathbf{d} = [d_{1,1} \quad \cdots \quad d_{1,\Lambda}]\right)$, where the elements of $\mathbf{d}$ are calculated from (3.5). In case of QSM, the m-M algorithm is applied to the two tree-searches corresponding to the two components, at the same time. Note that the calculation at the EDs of the first level is

necessary for both ML and SD algorithms. Thus, this step introduces no extra complexity for the proposed m-M algorithm.

Step 2: Find the index, j_{min}, which corresponds to the minimum element value of vector $\mathbf{d}$

$$j_{min} = \underset{j=1,\cdots,\Lambda}{\arg\min}\{\mathbf{d}\}\,, \tag{3.6}$$

where $\min\{\mathbf{d}\}$ finds the minimum element of vector $\mathbf{d}$.

Step 3: Increment the value of the j_{min}-th element of vector $\mathbf{v}$ by one

$$v_{j_{min}} \rightarrow v_{j_{min}} + 1. \tag{3.7}$$

It should be noted that the maximum value of $v_{j_{min}}$ is N_r. In this case, I define $\{\mathbf{j}_{max}\}$ as the set of indices whose values reached N_r, as

$$\{\mathbf{j}_{max}\} = \arg\{v_j | v_j = N_r\,,\, j = 1, \cdots, \Lambda\}\,. \tag{3.8}$$

Step 4: Update the j_{min}-th element of vector $\mathbf{d}$ according to the updated value of $v_{j_{min}}$ using (3.5). In other words, I expand the j_{min}-th tree-search branch by one node.

Step 5: Find j_{min} from (3.6) as in **Step 2**, then check whether the updated j_{min} belongs to $\{\mathbf{j}_{max}\}$ or not. If not, repeat **Step 2** to **Step 5**. Otherwise, go to **Step 6**. Note that this step guarantees the optimality of the solution, as it will be discussed in Section 3.6.

Step 6: Estimate the transmitted combination, $\tilde{\chi}_t^{(\text{m-M})}$

$$\tilde{\chi}_t^{(\text{m-M})} = \arg\min\{\mathbf{d}\,(\{\mathbf{j}_{max}\})\}\,, \tag{3.9}$$

where $\mathbf{d}\,(\{\mathbf{j}_{max}\})$ represents the elements of $\mathbf{d}$ whose indices belong to the set $\{\mathbf{j}_{max}\}$.

It should be noted that the name of "min-max" comes from **Step 6**, which estimates the

Algorithm 3.1 The proposed m-M algorithm pseudo-code.

- **Initialize** $\mathbf{v} = \begin{bmatrix} 1 & 1 & \cdots & 1 \end{bmatrix}$, $j_{max} = 0$.
- **Compute** $\mathbf{d} = \begin{bmatrix} d_{1,1} & d_{1,2} & \cdots & d_{1,\Lambda} \end{bmatrix}$ as in (3.5).
- **Reserve** an empty vector $\mathbf{j}_{max} = [.]$ as a buffer.

1: **for** $n = 1 : N_r\Lambda$ **do**
2: **Find** the index $j_{min} = \underset{j=1,\cdots,\Lambda}{\arg\min}\{\mathbf{d}\}$.
3: **if** $\mathbf{j}_{max}$ is NOT empty
4: **if** $j_{min} \in \mathbf{j}_{max}$
5: **go to** line 13.
6: **else**
7: **go to** line 10.
8: **end if**
9: **end if**
10: **Set** $v_{j_{min}} \rightarrow v_{j_{min}} + 1$, then **Update** $\mathbf{v}$.
11: **Update** the j_{min}-th element of $\mathbf{d}$ based on (3.5).
12: **Update** $\mathbf{j}_{max}$ based on (3.8).
13: **end for**

- **Estimate** $\tilde{\chi}_t^{(\text{m-M})}$ from (3.9).

transmitted combination by finding the index of the minimum ED of the fully expanded (maximum length) branches.

3.5 Complexity Analysis

Here, the number of visited nodes is considered to be the decoding complexity indicator. Thus, the complexity of the ML and m-M algorithms can be calculated from summing up the elements of the visited nodes vector, $\mathbf{v}$, at the end of the algorithm. In other words, the decoding complexity $C = \text{sum}\{\mathbf{v}\}$, where $\text{sum}\{\cdot\}$ is the summation of all elements of vector $\mathbf{v}$.

For the SM-ML decoders, the algorithm expands all nodes for all branches with length N_r. Thus, the value of the elements of vector $\mathbf{v}$ is N_r at the end of the algorithm, and the

decoding complexity for SM-ML, $C_{\text{SM}}^{\text{ML}}$, is

$$C_{\text{SM}}^{\text{ML}} = \text{sum}\left\{\mathbf{v}\right\} = N_r \Lambda = N_r N_t M_{\text{SM}}. \tag{3.10}$$

In case of square QSM-ML, the total decoding complexity for both tree-searches $C_{\text{QSM}}^{\text{ML}}$, is

$$C_{\text{QSM}}^{\text{ML}} = 2 \times \text{sum}\left\{\mathbf{v}\right\} = 2N_r \Lambda = 2N_r N_t \sqrt{M_{\text{QSM}}}. \tag{3.11}$$

Therefore, the complexity reduction ratio between the SM-ML and m-M algorithm, $\mathcal{R}_{\text{SM}}$, is given by

$$\mathcal{R}_{\text{SM}} = \frac{C_{\text{SM}}^{\text{ML}} - C_{\text{SM}}^{\text{m-M}}}{C_{\text{SM}}^{ML}} = 1 - \frac{\text{sum}\left\{\mathbf{v}_{\text{SM}_{\text{m-M}}}\right\}}{N_r N_t M_{\text{SM}}}, \tag{3.12}$$

where $\mathbf{v}_{\text{SM}_{\text{m-M}}}$ is the visited nodes vector of the m-M algorithm for the SM system. Furthermore, the total complexity reduction ratio between the QSM-ML and m-M algorithm, $\mathcal{R}_{\text{QSM}}$, is given by

$$\mathcal{R}_{\text{QSM}} = \frac{C_{\text{QSM}}^{\text{ML}} - C_{\text{QSM}}^{\text{m-M}}}{C_{\text{QSM}}^{\text{ML}}} = 1 - \frac{\text{sum}\left\{\mathbf{v}_{\text{QSM}_{\text{m-M}}}^{\Re}\right\} + \text{sum}\left\{\mathbf{v}_{\text{QSM}_{\text{m-M}}}^{\Im}\right\}}{2N_r N_t \sqrt{M_{\text{QSM}}}}, \tag{3.13}$$

where $\mathbf{v}_{\text{QSM}_{\text{m-M}}}^{\Re}$ and $\mathbf{v}_{\text{QSM}_{\text{m-M}}}^{\Im}$ are the visited tree-search nodes vectors of the m-M algorithm for the two QSM tree-searches.

In the best scenario, the m-M algorithm expands only one branch which ends with the minimum ED. Consequently, the total number of visited nodes is limited to N_r nodes for the fully expanded branch, as well as $\Lambda - 1$ nodes at the first tree-search level. Thus, $C_{min}^{\text{SM}} = N_r + N_t M_{\text{SM}} - 1$ and $C_{min}^{\text{QSM}} = 2\left(N_r + N_t \sqrt{M_{\text{QSM}}} - 1\right)$, where C_{min}^{SM} and C_{min}^{QSM} denote the minimum decoding complexity that can be achieved for the SM and QSM, respectively. Therefore, the theoretical upper bound of the complexity reduction (UBCR) ratio for the SM and QSM is $\mathcal{R}_{\text{UBCR}}^{\text{SM}}$ and $\mathcal{R}_{\text{UBCR}}^{\text{QSM}}$, respectively, and can be calculated by

plugging C_{min}^{SM} and C_{min}^{QSM} into (3.12) and (3.13), respectively, as

$$\mathcal{R}_{\text{UBCR}}^{\text{SM}} = 1 - \frac{(N_r + N_t M_{\text{SM}} - 1)}{N_r N_t M_{\text{SM}}}, \tag{3.14}$$

and

$$\mathcal{R}_{\text{UBCR}}^{\text{QSM}} = 1 - \frac{(N_r + N_t \sqrt{M_{\text{QSM}}} - 1)}{N_r N_t \sqrt{M_{\text{QSM}}}}. \tag{3.15}$$

3.6 Union Bound Error Probability Analysis

In this section, I prove the optimality of the proposed m-M algorithm performance. Although the exact expression of the SM and QSM BER is not derived because of its difficult analysis, the union bound provides a tight expression to the simulation analysis [11].

The general expression of the union bound for SM [2] and QSM [3] is

$$P_{b,\Omega} = \frac{1}{(\eta_\Omega)\, 2^{\eta_\Omega}} \sum_{k=1}^{2^{\eta_\Omega}} \sum_{l=1}^{2^{\eta_\Omega}} \delta_{k,l} \mathbb{E}\left\{ \mathbb{P}\text{r}_{\Omega}^{\text{(m-M)}} \left(\chi_k \rightarrow \tilde{\chi}_l \right) \right\}, \tag{3.16}$$

where $P_{b,\Omega}$ is the union bound probability, $\Omega \in \{\text{SM}, \text{QSM}\}$, $\mathbb{P}\text{r}_{\Omega}^{\text{(m-M)}} \left(\chi_k \rightarrow \tilde{\chi}_l \right)$ denotes the pairwise error probability (PEP) of the proposed m-M algorithm, $\mathbb{E}\{\cdot\}$ is the expected value operation, and $\delta_{k,l}$ represents the number of bit errors which corresponds to the instant PEP event.

In order to evaluate $\mathbb{P}\text{r}_{\Omega}^{\text{(m-M)}} \left(\chi_k \rightarrow \tilde{\chi}_l \right)$, let us assume two sets: ψ_V, which is defined as the set of visited nodes and ψ_D, which is the set of discarded nodes by the m-M algorithm. Thus, PEP can be formulated as [5]

$$\mathbb{P}\text{r}_{\Omega}^{\text{(m-M)}} \left(\chi_k \rightarrow \tilde{\chi}_l \right) = \mathbb{P}\text{r}\left(\tilde{\chi}_{min} \neq \chi_t | \tilde{\chi}_{min} \in \psi_V \right) + \mathbb{P}\text{r}\left(\tilde{\chi}_{min} \in \psi_D \right), \tag{3.17}$$

where $\tilde{\chi}_{min}$ is the estimated minimum ED of the m-M algorithm. It should be noted that $\tilde{\chi}_{min}$ is considered to be the output of the proposed algorithm. The two probabilistic terms on the right-hand side of (3.17) are mutually exclusive because $\tilde{\chi}_{min}$ can not belong to ψ_V and ψ_D in the same time.

Furthermore, the probabilities $\Pr(\tilde{\chi}_{min} \neq \chi_t)$ and $\Pr(\tilde{\chi}_{min} \in \psi_V)$ are independent, and consequently, (3.17) can be re-written as

$$\Pr_{\Omega}^{(\text{m-M})}(\chi_k \to \tilde{\chi}_l) = \Pr(\tilde{\chi}_{min} \neq \chi_t) + \Pr(\tilde{\chi}_{min} \in \psi_D), \tag{3.18}$$

where $\Pr(\tilde{\chi}_{min} \in \psi_V) + \Pr(\tilde{\chi}_{min} \in \psi_D) = 1$.

From **Step 5** of the proposed algorithm, as presented in Section 3.4, the minimum ED (optimal solution) is not missed because the algorithm stops if the estimated minimum ED, $\tilde{\chi}_{min}$, occurs at the end of a fully expanded branch and no other node has a smaller ED. In other words, the discarded/saved nodes result from stopping the expansion of a specific branch because there is another node, in another branch, which has a smaller ED value. Thus, the saving comes from the branches which are not fully expanded.

Since the EDs inside branches are accumulated (i.e., the new value is added to the previous one), it is impossible to have a lower ED value in ψ_D than in ψ_V. Consequently, $\Pr(\tilde{\chi}_{min} \in \psi_D) = 0$ and $\Pr(\tilde{\chi}_{min} \in \psi_V) = 1$. Thus, (3.18) becomes

$$\Pr_{\Omega}^{(\text{m-M})}(\chi_k \to \tilde{\chi}_l) = \Pr(\tilde{\chi}_{min} \neq \chi_t). \tag{3.19}$$

It should be noted that the right-hand side of (3.19) is the ML PEP event which can be found in [2], [5] and [3] for the SM and QSM, respectively. Thus, the proposed algorithm provides the same union bound error probability as the ML decoder. Having the same union bound error probability does not necessarily guarantee having the same BER performance as the ML. However, $\Pr(\tilde{\chi}_{min} \in \psi_D) = 0$ means that the m-M algorithm will not miss the ML

solution. Thus, the proposed algorithm guarantees having the same BER ML performance.

3.7 Numerical results

In this section, I evaluate the reduction in the decoding complexity of the proposed m-M algorithm, when compared with the ML and SD low-complexity algorithms presented in [5] and [8] for the SM and QSM decoders, respectively. The threshold value required by the algorithm in [5] is optimized to obtain the ML BER performance, according to [5, Eq. (37)]. I consider two spectral efficiencies, $\eta = 6$ b/s/Hz and $\eta = 10$ b/s/Hz, using 8×4 16-QAM for SM (4-QAM for QSM) and 16×16 64-QAM for SM (4-QAM for QSM), respectively. The presented results are achieved by running Monte-Carlo simulations over 10^5 Rayleigh flat fading channel realizations.

In Figs. 3.2 and 3.3, the mean value of the complexity reduction ratio in (3.12) and (3.13) is shown. It can be seen that the proposed algorithm requires around 22.5 and 20 dB signal-to-noise ratio (SNR) to approach the UBCRs for the SM and QSM, respectively. At these specific values of the SNR, for $\eta = 6$ b/s/Hz, the proposed m-M algorithm provides an average reduction in the decoding complexity ratio of 86% and 76.5% for the SM and QSM, respectively. The complexity reduction ratio increases as η increases, which agrees with (3.12) and (3.13). For example, by increasing η to 10 b/s/Hz, the average complexity reduction ratio increases by 7.5% and 14% for the SM and QSM, respectively.

For the comparison purpose, Figs. 3.4 and 3.5 show the gain in terms of the number of saved nodes, obtained from using the proposed m-M algorithm over those in [5] and [8], for both SM and QSM. Note that the gain means the difference in the decoding complexities of the proposed m-M algorithm and the other algorithms. As a general observation, the gain achieved by using the proposed algorithm over [5] is greater than the one over [8]. Furthermore, the gain increases as η increases, and exceeds 10^3 and 10^2 at low SNR and

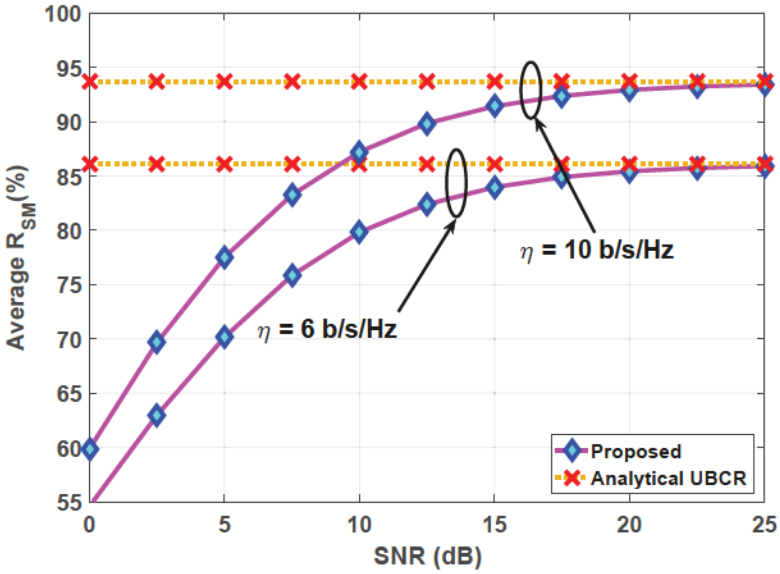

Fig. 3.2: Reduction in complexity between the SM-ML and proposed m-M algorithms for $\eta = 6$ b/s/Hz and $\eta = 10$ b/s/Hz.

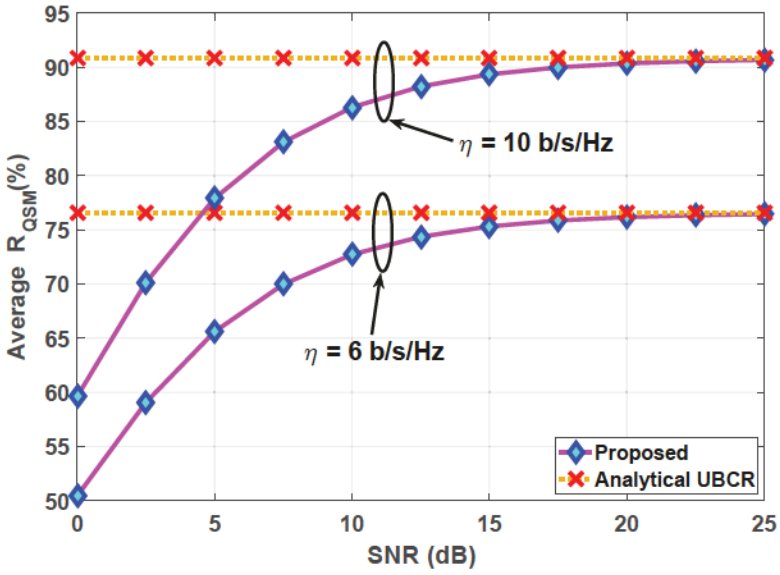

Fig. 3.3: Reduction in complexity between the QSM-ML and proposed m-M algorithms for $\eta = 6$ b/s/Hz and $\eta = 10$ b/s/Hz.

$\eta = 10$ b/s/Hz for the SM and QSM, respectively.

The BER performance of different SM decoders versus SNR is shown in Fig. 3.6. It can be seen that the proposed m-M algorithm, as well as those in [5] and [8], provide the optimum BER performance of the SM-ML decoder. As QSM consists of two independent SM decoders, the proposed m-M algorithm provides the optimum BER performance for QSM as well; results are omitted due to the space consideration.

It is seen from these figures that the proposed m-M algorithm reduces the decoding complexity of the SM-ML and QSM-ML without loss in the BER performance.

3.8 Conclusion

This chapter provides a novel low-complexity decoding algorithm for SM and QSM, referred to as the m-M algorithm. The proposed algorithm provides a significant reduction in the decoding complexity over the existing SD algorithms by employing a single expansion to the minimum ED across branches, until the minimum ED is reached to the end of a fully expanded branch. When compared with the ML decoder, the proposed m-M algorithm provides the same BER performance with saving in the number of visited nodes up to 93.6% and 90.8% in case of SM and QSM, respectively.

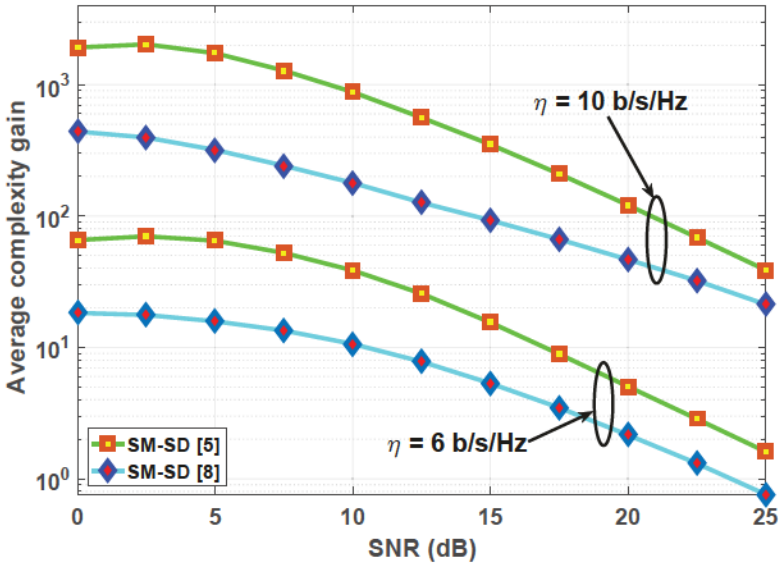

Fig. 3.4: Complexity gain when using the proposed m-M over the SM-SD algorithms in [5] and [8], for $\eta = 6$ b/s/Hz and $\eta = 10$ b/s/Hz.

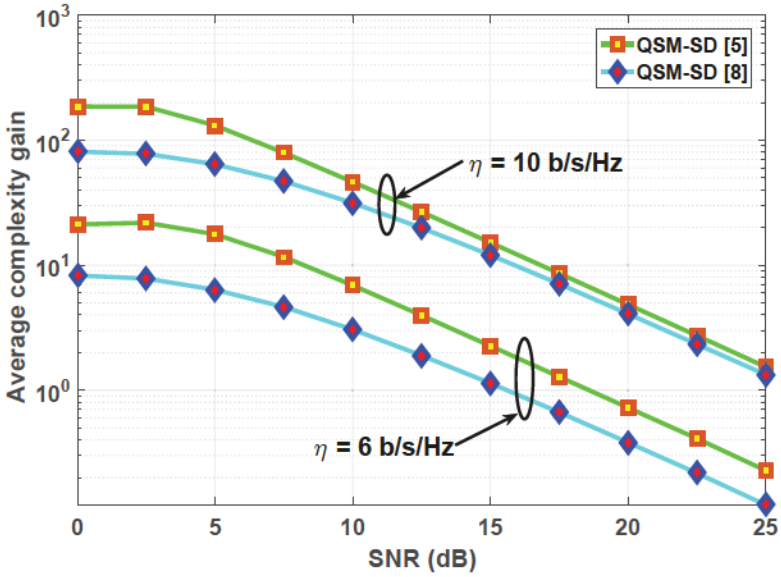

Fig. 3.5: Complexity gain when using the proposed m-M over the QSM-SD algorithms in [5] and [8], for $\eta = 6$ b/s/Hz and $\eta = 10$ b/s/Hz.

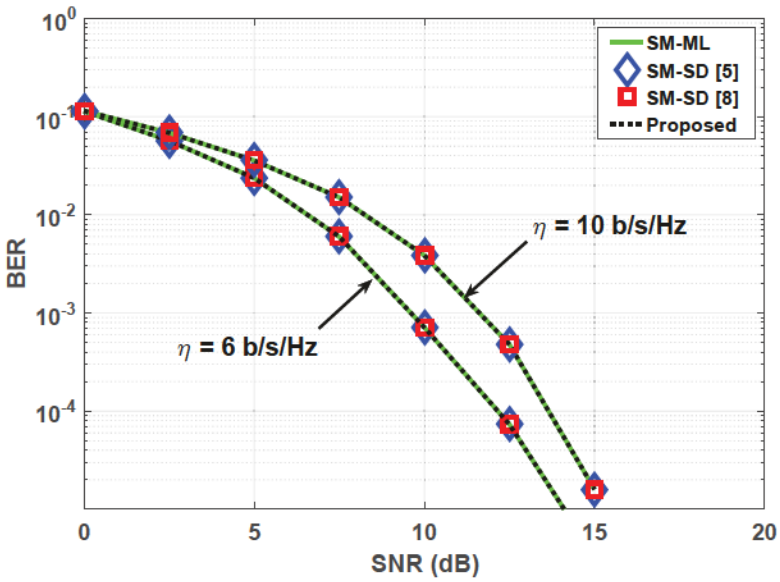

Fig. 3.6: BER performance comparison of different SM decoders for $\eta = 6$ b/s/Hz and $\eta = 10$ b/s/Hz.

References

[1] J. G. Andrews, S. Buzzi, W. Choi, S. V. Hanly, A. Lozano, A. C. Soong, and J. C. Zhang, "What will 5g be?," *IEEE J. Sel. Areas Commun.*, vol. 32, pp. 1065–1082, Jun. 2014.

[2] R. Y. Mesleh, H. Haas, S. Sinanovic, C. W. Ahn, and S. Yun, "Spatial modulation," *IEEE Trans. Veh. Technol.*, vol. 57, pp. 2228–2241, Jul. 2008.

[3] R. Mesleh, S. S. Ikki, and H. M. Aggoune, "Quadrature spatial modulation," *IEEE Trans. Veh. Technol.*, vol. 64, pp. 2738–2742, Jun. 2015.

[4] A. Younis, R. Mesleh, H. Haas, and P. M. Grant, "Reduced complexity sphere decoder for spatial modulation detection receivers," in *Proc. IEEE GLOBECOM*, 2010, pp. 1–5.

[5] A. Younis, S. Sinanovic, M. Di Renzo, R. Mesleh, and H. Haas, "Generalised sphere decoding for spatial modulation," *IEEE Trans. Commun.*, vol. 61, pp. 2805–2815, Jul. 2013.

[6] Q. Tang, Y. Xiao, P. Yang, Q. Yu, and S. Li, "A new low-complexity near-ml detection algorithm for spatial modulation," *IEEE Wireless Commun. Lett.*, vol. 2, pp. 90–93, Feb. 2013.

[7] L. Xiao, P. Yang, S. Fan, S. Li, L. Song, and Y. Xiao, "Low-complexity signal detection for large-scale quadrature spatial modulation systems," *IEEE Commun. Lett.*, vol. 20, pp. 2173-2176, Nov. 2016.

[8] I. Al-Nahhal, O. A. Dobre, and S. Ikki, "Quadrature spatial modulation decoding complexity: Study and reduction," *IEEE Wireless Commun. Lett.*, vol. 6, pp. 378-381, Jun. 2017.

[9] E. Viterbo and J. Boutros, "A universal lattice code decoder for fading channels," *IEEE Trans. Inf. Theory*, vol. 45, pp. 1639–1642, Jul. 1999.

[10] F. Bellili, R. Meftehi, S. Affes, and A. Stéphenne, "Maximum likelihood snr estimation of linearly-modulated signals over time-varying flat-fading simo channels," *IEEE Trans. Signal Process.*, vol. 63, pp. 441–456, Jan. 2015.

[11] J. Proakis, *Digital Communications Systems Engineering*, 4th ed. New York, NY, USA: McGraw-Hill, 2000.

Chapter 4

Optimum Low-Complexity Decoder for Spatial Modulation

4.1 Abstract

In this chapter, a novel low-complexity detection algorithm for spatial modulation (SM), referred to as the minimum-distance of maximum-length (m-M) algorithm, is proposed and analyzed. The proposed m-M algorithm is a smart searching method that is applied for the SM tree-search decoders. The behavior of the m-M algorithm is studied for three different scenarios: i) perfect channel state information at the receiver side (CSIR), ii) imperfect CSIR of a fixed channel estimation error variance, and iii) imperfect CSIR of a variable channel estimation error variance. Moreover, the complexity of the m-M algorithm is considered as a random variable, which is carefully analyzed for all scenarios, using probabilistic tools. Based on a combination of the sphere decoder (SD) and ordering concepts, the m-M algorithm guarantees to find the maximum-likelihood (ML) solution with a significant reduction in the decoding complexity compared to SM-ML and existing SM-SD algorithms; it can reduce the complexity up to 94% and 85% in the perfect CSIR and the worst scenario

of imperfect CSIR, respectively, compared to the SM-ML decoder. Monte Carlo simulation results are provided to support our findings as well as the derived analytical complexity reduction expressions.

4.2 Introduction

Multiple-input multiple-output (MIMO) systems, which is an integral part of modern wireless communication standards, activate all transmit antennas to increase the spectral efficiency and/or improve the bit-error-ratio (BER) performance [2]. On the other hand, activating all transmit antennas at the same time not only creates a strong inter-channel interference (ICI) but also requires multiple radio frequency chains. A promising technique called spatial modulation (SM) has been studied in recent years [3]-[5] to overcome these problems in next-generation systems. In SM [6]-[9], only one transmit antenna is activated during the transmission burst, where the active transmit antenna is chosen out of all transmit antennas according to a part of the input bit-stream. The active antenna transmits a phase shift keying (PSK) or quadrature amplitude modulation (QAM) symbol, through a wireless medium, based on the rest of the input bit-stream. At the receiver side, all receive antennas receive the delivered signal and forward it to the digital signal processor (DSP) unit for decoding. The maximum-likelihood (ML) detector is utilized to decode the received signal by attempting all possible combinations of the QAM/PSK symbols and the transmit antennas, where this process depends on the number of transmit antennas, receive antennas, and modulation order. Consequently, the ML algorithm is classified to be costly from the decoding complexity point of view, particularly for increasing number of transmit/receive antennas and constellation points.

Low-latency communications and energy-efficient transmission techniques are among the next generation (5G) requirements [10]; one solution to achieve this is the design of

low-complexity decoding algorithms for the SM system. Recently, low-complexity decoding algorithms have been proposed for the SM system in [11]-[17], and surveyed in [18]. In [11]-[13], the sphere decoding (SD) concept of [19], [20] is exploited to provide a low-complexity detection at the BER level of the brute-force ML detector. The authors of [11]-[13] have provided a threshold (pruned radius for the SD) that depends on the number of receive antennas, noise variance, and a predetermined constant, which changes for each different MIMO system. The noise variance estimation process is an exhaustive step required for every change in the channel environment; it can be achieved either blindly or using data-aided (DA) techniques like preamble/pilots [21]-[22] transmission. In [14], the authors have proposed an algorithm that provides a trade-off between the BER performance and decoding complexity for the SM decoders. This algorithm requires an exhaustive pre-processing step to calculate the pseudo-inverse of the channel matrix columns. This step is mitigated in [15] by considering a sparse channel of a large-scale MIMO system. However, the problem of noise variance dependency still exists in [15]. Furthermore, the ML BER performance has not been achieved in [14] and [15]. The authors of [16] have provided a low-complexity algorithm with the ML BER performance for the quadrature SM (QSM) decoders by treating the QSM symbol as two independent SM symbols. The reduction in the decoding complexity comes from the ordering concept, with no dependency on the noise variance. However, further reduction in the decoding complexity can be attained. The authors in [17] have proposed an algorithm with near-ML performance, which reduces the computational complexity of the SM decoders based on modified beam search and ordering concepts, by splitting the tree-search into sub-trees. It should be noted that the algorithms in [11]-[17] consider perfect knowledge of the channel state information at the receiver side (CSIR), and no study is presented in the case of imperfect CSIR.

In this chapter, I propose a low-complexity algorithm for the SM decoders, referred to as the *minimum-distance of maximum-length* (m-M) algorithm. Based on the tree-search

concept, the m-M algorithm performs only one expansion to the minimum Euclidean distance (ED) across all tree-search branches until the minimum ED occurs at the end of a fully expanded branch. The proposed m-M algorithm provides a significant reduction in the decoding complexity with the ML BER performance, and requires no knowledge of the noise variance. I provide a complete study of our proposed algorithm in the case of perfect and imperfect CSIR. In case of imperfect CSIR, I consider two scenarios for the fixed and variable variance of the error in the channel estimation, respectively. In addition, I derive tight probabilistic expressions for the expected decoding complexity of the m-M algorithm for all scenarios.

The rest of the chapter[1] is organized as follows: In Section 4.3, the system model of the SM transmitter and receiver is summarized. In Section 4.4, the proposed m-M algorithm is introduced. In Section 4.5, tight analytical expressions of the m-M algorithm decoding complexity are derived for perfect and imperfect CSIR. In Section 4.6, the optimality of the m-M algorithm is discussed. The numerical results and conclusion are provided in Sections 4.7 and 4.8, respectively.

4.3 System Model

4.3.1 SM Modulator

Consider the implementation of an SM scheme for $N_r \times N_t$ MIMO system, where N_t and N_r denote the number of transmit and receive antennas, respectively. The incoming bit-stream is divided into two groups: the first group of $\log_2(N_t)$ bits selects the transmit antenna that will

[1]Notations: Boldface uppercase and lowercase letters represent matrices and vectors, respectively. $\mathcal{CN}$ stands for a complex-valued normally distributed random variable. $\|.\|$ denotes the Euclidean norm. $|.|$ returns the absolute value of an element. $.^{\Re}$ and $.^{\Im}$ denote the real and imaginary components, respectively. $\mathbb{E}\{.\}$ denotes the expectation operation. $\mathbb{P}\mathrm{r}(.)$ is the probability of an event. $f_{.}(.)$ denotes the probability density function (pdf) of a random variable. sum $\{.\}$ returns the summation of all elements values of a vector. $k!$ stands for the factorial operation of an integer k.

be activated, while the second group of $\log_2(M)$ bits selects the QAM/PSK symbol that will be delivered from that antenna, where M denotes the order of the QAM/PSK constellation. Therefore, the number of bits delivered in every time instance by the SM system is

$$\eta = \log_2(N_t) + \log_2(M), \tag{4.1}$$

where η denotes the spectral efficiency in bits per channel use (bpcu). The active antenna transmits $s_t \in \{s_1, \ldots, s_M\}$ through a Rayleigh fading path between the transmit antenna and all N_r receive antennas, where s_t is the transmitted QAM/PSK symbol. This path represents the transmit channel, $\mathbf{h}_t \sim \mathcal{CN}(0,1)$, which is drawn from the full channel matrix, $\mathbf{H} \in \mathbb{C}^{N_r \times N_t}$.

Assume that the data symbol s_t is transmitted over $\mathbf{h}_t$ to form the transmitted SM symbol combination, $\mathbf{x}_t \in \{\mathbf{x}_1, \ldots, \mathbf{x}_{MN_t}\}$, where $\mathbf{x}_t = \mathbf{h}_t s_t$. It should be noted that the transmitted combination is drawn from MN_t different possible combinations, which result from combining M QAM/PSK symbols with N_t transmit antennas. Due to the additive white Gaussian noise (AWGN), the SM symbol is received as

$$\mathbf{y} = \mathbf{x}_t + \mathbf{w}, \tag{4.2}$$

where $\mathbf{y} \in \mathbb{C}^{N_r \times 1}$ denotes the noisy received vector and $\mathbf{w} \in \mathbb{C}^{N_r \times 1}$ is the AWGN vector with entries having zero-mean and variance σ_n^2 (i.e., $\mathbf{w} \sim \mathcal{CN}(0, \sigma_n^2)$). Note that QAM is considered in this chapter.

4.3.2 SM-ML Demodulation

At the receiver side, the DSP unit utilizes the ML detection algorithm to estimate the transmitted combination. The ML algorithm attempts all possible combinations to find the one that provides the minimum ED with the received signal vector [7], which corresponds to

the index of

$$\hat{j}_{\mathrm{ML}} = \underset{j=1,\cdots,MN_t}{\arg\min} \|\mathbf{y} - \mathbf{x}_j\|^2 = \underset{j=1,\cdots,MN_t}{\arg\min} \sum_{n=1}^{N_r} |y_n - x_{n,j}|^2 , \tag{4.3}$$

where $\hat{j}_{\mathrm{ML}}$ is the index of the estimated combination using the ML detection algorithm, y_n is the n-th element of $\mathbf{y}$, and $x_{n,j}$ is the n-th element of the j-th combination.

It should be noted that estimating the transmitted combination can be achieved using a graphical approach, named *tree-search* method. Fig. 4.1 illustrates the tree-search concept for the SM demodulation with $M = 2$, $N_t = 2$, and $N_r = 3$. In the SM tree-search method, each possible combination of $\mathbf{x}_j$ in (4.3) is represented by a tree-search branch whose length is N_r tree-search nodes (or levels). Each node is an accumulation of the previous EDs in the same branch, which can be represented as

$$d_{i,j} = \sum_{n=1}^{i} |y_n - x_{n,j}|^2 , \qquad i = 1, \ldots, N_r, \tag{4.4}$$

where $d_{i,j}$ is the node metric at the i-th level of the j-th branch. Hence, (4.3) can be rewritten as

$$\hat{j}_{\mathrm{ML}} = \underset{j=1,\ldots,MN_t}{\arg\min} \{d_{N_r,j}\} . \tag{4.5}$$

Thus, the ML solution for the estimated transmitted combination is denoted by $\hat{\mathbf{x}}_{\mathrm{ML}}$ and given as

$$\hat{\mathbf{x}}_{\mathrm{ML}} = \mathbf{x}_{\hat{j}_{\mathrm{ML}}} . \tag{4.6}$$

The total number of nodes for the SM tree-search is MN_tN_r, which is 12 in the example of Fig. 4.1. To estimate the transmitted combination using the ML detection algorithm, the DSP unit exhaustively visits all nodes, which can be problematic for increasing values of M,

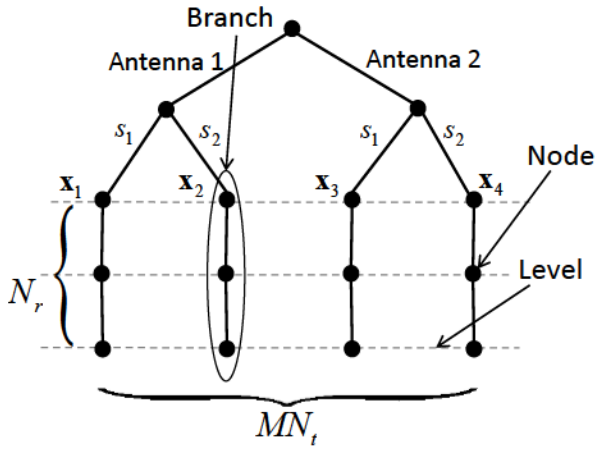

Fig. 4.1: SM tree-search decoder for $M = 2$, $N_t = 2$, and $N_r = 3$ with four branches.

N_t and N_r. Thus, reducing the decoding complexity has paramount importance for real-time applications.

4.4 Minimum-Distance of Maximum-Length Algorithm

Unlike the existent SD algorithms in the literature, the proposed m-M algorithm performs only one node expansion at a time; the expanded node is chosen to be of minimum ED across all branches. The proposed algorithm jumps from one branch to another according to where the minimum ED is, and stops if the minimum ED occurs at the end of a fully expanded branch (i.e., maximum length).

For mathematical formulation, assume that $\mathbf{v} = [v_1 \dots v_{MN_t}] \in \mathbb{R}^{1\times MN_t}$ denote the vector of visited nodes, where v_j takes integer values from 1 up to N_r and represents the number of nodes already visited of the j-th branch for $j = 1, \dots, MN_t$. Also, let $\mathbf{d} = \left[d_{v_1,1} \dots d_{v_{MN_t},MN_t}\right] \in \mathbb{R}^{1\times MN_t}$ denote the ED vector, where $d_{v_j,j}$ is given by (4.4) by setting $i = v_j$ (i.e., $d_{v_j,j} = \sum_{n=1}^{v_j} |y_n - x_{n,j}|^2$, where $d_{v_j,j}$ represents the ED (node metric) of the v_j-th level for the j-th branch).

Algorithm 4.1 summarizes the proposed m-M algorithm that is explained as follows:

Step 1: Initialize all elements of $\mathbf{v}$ to unity (i.e., $v_j = 1\ \forall j$), and then calculate each element of the vector $\mathbf{d}$ from (4.4) accordingly. It should be noted that the elements of $\mathbf{d}$ in this step represent the first ED of all branches (i.e., $\mathbf{d} = [d_{1,1} \dots d_{1,MN_t}]$).

Step 2: Determine the argument of the minimum element of $\mathbf{d}$ as

$$j_{\min} = \underset{j=1,\dots,MN_t}{\arg\min} \{d_{v_j,j}\}. \tag{4.7}$$

Step 3: Increase the $j_{\min}$-th element of $\mathbf{v}$ by one

$$v_{j_{\min}} \rightarrow v_{j_{\min}} + 1. \tag{4.8}$$

Note that this step ensures that the algorithm makes a single expansion to the minimum ED, which leads to the increase of the corresponding element of the vector $\mathbf{v}$ by one. The maximum value of $v_j\ \forall j$ that can be reached is N_r; therefore, I can define $\mathbf{j}_{\max}$ as the set of indices whose values reached N_r, as

$$\mathbf{j}_{\max} = \text{find}\left(\mathbf{v} = N_r\right), \tag{4.9}$$

where $\text{find}\left(\mathbf{v} = N_r\right)$ returns the indices of the elements of $\mathbf{v}$ that are equal to N_r. At the beginning, $\mathbf{j}_{\max}$ is buffered as an empty set, and is updated when at least one branch is fully expanded.

Step 4: Update the $j_{\min}$-th element of $\mathbf{d}$ by calculating the new $d_{v_{j_{\min}},j_{\min}}$ from (4.4) based on $v_{j_{\min}}$ calculated from **Step 3**.

Step 5: Find the new $j_{\min}$ from (4.7) as in **Step 2**, and then check whether the following condition is true or not:

$$j_{\min} \in \mathbf{j}_{\max}. \tag{4.10}$$

If $j_{\min} \notin \mathbf{j}_{\max}$, then go back to **Step 2**. Otherwise, find the index of the estimated transmitted

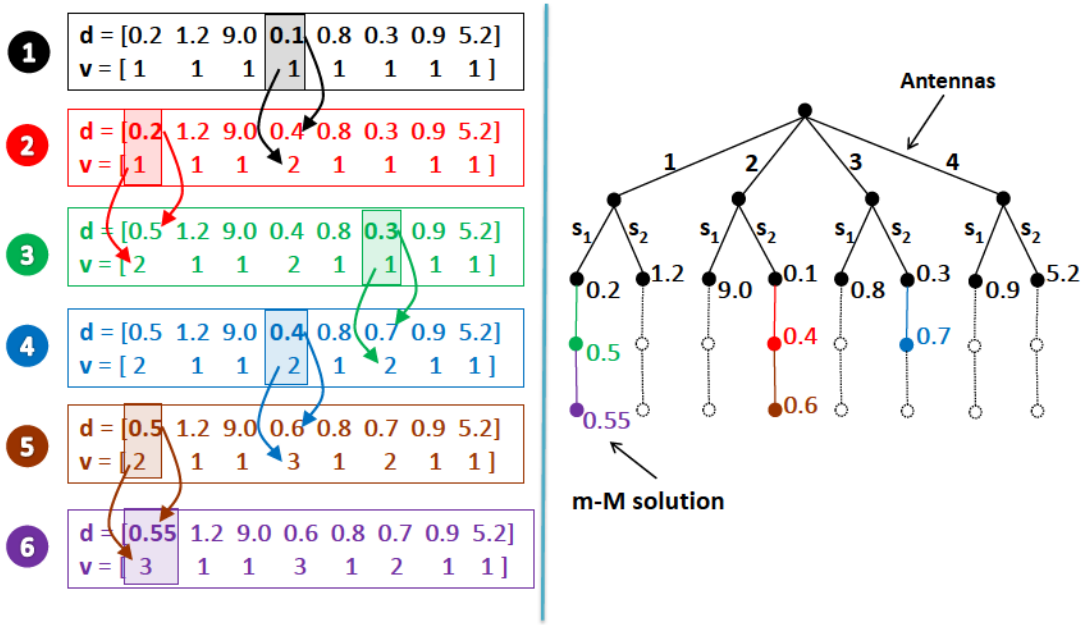

Fig. 4.2: A numerical example for the m-M algorithm (3×4 SM-MIMO system and $M = 2$).

combination as

$$\hat{j}_{\text{m-M}} = \underset{j \in \mathbf{j}_{\max}}{\arg\min} \{d_{v_j,j}\}, \tag{4.11}$$

where $\hat{j}_{\text{m-M}}$ denotes the index of the estimated transmitted combination from the m-M algorithm. Note that in case of $v_j = N_r \ \forall j$ in (4.11), the ML version in (4.5) is obtained. The estimated transmitted combination from m-M algorithm, $\hat{\mathbf{x}}_{\text{m-M}}$, is

$$\hat{\mathbf{x}}_{\text{m-M}} = \mathbf{x}_{\hat{j}_{\text{m-M}}}. \tag{4.12}$$

Note that the condition in (4.10) is called the optimality condition, and guarantees that the ML solution will not be missed before stopping the m-M algorithm (i.e., $\hat{\mathbf{x}}_{\text{m-M}} = \hat{\mathbf{x}}_{\text{ML}}$).

Fig. 4.2 illustrates a numerical example for the proposed m-M algorithm. Consider a 3×4 MIMO system with $M = 2$. Thus, I have 8 branches with 3 nodes/levels length. First, the m-M algorithm initializes $\mathbf{v}$ by all-ones, and calculates the the first ED of each branch. The m-M algorithm finds the minimum ED of $\mathbf{d}$, which is 0.1 in our example. This ED

Algorithm 4.1 Pseudo-code of the proposed m-M algorithm.

- **Initialize** $\mathbf{v} = [1\ 1\ \ldots\ 1] \in \mathbb{R}^{1\times MN_t}$, $j_{\max} = 0$.
- **Compute** the elements of $\mathbf{d} = [d_{1,1} \ldots d_{1,MN_t}]$, where $d_{1,j} = |y_1 - x_{1,j}|^2$ and $j = 1, \ldots, MN_t$.
- **Reserve** an empty vector $\mathbf{j}_{\max} = [.]$ as a buffer.

1: **while** $n \leq N_r MN_t$ **do**
2: **Find** the index $j_{\min} = \underset{j=1,\ldots,MN_t}{\arg\min} \{d_{v_j,j}\}$.
3: **if** $\mathbf{j}_{\max}$ is NOT empty
4: **if** $j_{\min} \in \mathbf{j}_{\max}$
5: **go to** line 14.
6: **else**
7: **go to** line 10.
8: **end if**
9: **end if**
10: **Set** $v_{j_{\min}} \rightarrow v_{j_{\min}} + 1$, then **Update** $\mathbf{v}$.
11: **Update** the $j_{\min}$-th element of $\mathbf{d}$ as:

$$d_{v_{j_{\min}},j_{\min}} \rightarrow d_{v_{j_{\min}},j_{\min}} + \left| y_{v_{j_{\min}}} - x_{v_{j_{\min}},j_{\min}} \right|^2.$$

12: **Update** $\mathbf{j}_{\max}$ based on $\mathbf{j}_{\max} = \text{find}\,(\mathbf{v} = N_r)$.
13: **Set** $n \rightarrow n + 1$.
14: **end while**

- **Estimate** $\hat{\mathbf{x}}_{\text{m-M}}$ from $\hat{\mathbf{x}}_{\text{m-M}} = \mathbf{x}_{j_{\min}}$.

corresponds to the 4-th branch ($j_{\min} = 4$); thus, the m-M algorithm expands this node after increasing the 4-th element of $\mathbf{v}$ by one (i.e., $v_{j_{\min}} = v_4 = 2$ and $d_{2,4} = 0.4$). In the second iteration, the m-M algorithm finds the new minimum ED in $\mathbf{d}$ (i.e., 0.2), which is placed in the first branch ($j_{\min} = 1$). Then, the first element of $\mathbf{v}$ is updated to be 2 and the first element of $\mathbf{d}$ is updated accordingly (i.e., $v_1 = 2$ and $d_{2,1} = 0.5$). The algorithm jumps from one branch to another according to the location of the minimum ED across all branches, as illustrated in iterations 3, 4, and 5. Note that the m-M algorithm detects one element of $\mathbf{v}$ reaches N_r (i.e., full expansion for that branch) from iteration 5, which is the 4-th branch. According to (4.10), the algorithm has to check if the new minimum ED comes at a fully expanded branch or not before deciding to stop. In our example, the algorithm will not stop

at iteration 5 because there is a minimum ED at the first branch (i.e., 0.5). Therefore, the algorithm makes a single expansion to the first branch after updating the first element of $\mathbf{v}$ (i.e., $v_1 = 3$ and $d_{3,1} = 0.55$); and then, it checks the place of the minimum ED once more. In this example, the iteration 6 shows that the minimum ED (i.e., 0.55) comes at the end of a fully expanded branch, which corresponds to the first branch (i.e., $\hat{j}_{\text{m-M}} = 1$). Thus, the m-M algorithm stops and declares that the estimated transmitted combination is the first one (i.e., the first symbol was transmitted from the first antenna).

4.5 Complexity Analysis

In this chapter, I consider the number of visited nodes inside the tree-search as the complexity indicator. Since $\mathbf{v}$ represents the visited nodes for each branch, the summation of its elements at the final iteration gives the total complexity of the m-M algorithm in terms of the number of visited nodes. Consider the complexity of the m-M algorithm denoted by $C_{\text{m-M}} = \text{sum}\left\{\mathbf{v}^{\text{f}}\right\}$, where $\mathbf{v}^{\text{f}}$ is the vector $\mathbf{v}$ at the final iteration. Since the elements of $\mathbf{v}^{\text{f}}$ are random variables (r.v.'s), $C_{\text{m-M}}$ is an r.v. as well. In this section, I provide a tight expression for the expected complexity of the proposed m-M algorithm in the case of perfect CSIR, as well as imperfect CSIR.

The average complexity of the m-M algorithm $C_{\text{m-M}}$ can be expressed as

$$C_{\text{m-M}} = \mathbb{E}\left\{\text{sum}\left\{\mathbf{v}^{\text{f}}\right\}\right\}. \tag{4.13}$$

Although the m-M algorithm is a breadth-first search algorithm, its expected complexity is equivalent to that of a depth-first SD algorithm with pruned radius, $R_{\text{m-M}}$, equal to the minimum ED of vector $\mathbf{d}$ at the final iteration (i.e., 0.55 in the example illustrated in Fig. 4.2). Therefore, $R_{\text{m-M}}$ can be written as

$$R_{\text{m-M}} = d_{N_r,\hat{j}_{\text{m-M}}} = \sum_{n=1}^{N_r} \left| y_n - x_{n,\hat{j}_{\text{m-M}}} \right|^2 = \left\| \mathbf{y} - \hat{\mathbf{x}}_{\text{m-M}} \right\|^2, \tag{4.14}$$

where $\hat{j}_{\text{m-M}}$ given from (4.11) and $\hat{\mathbf{x}}_{\text{m-M}}$ are given in (4.7) and (4.12), respectively. For simplicity, I consider $\hat{\mathbf{x}}_{\text{m-M}} \rightarrow \mathbf{x}_t$; this assumption most likely holds particularly in high signal-to-noise ratio (SNR) ($\hat{\mathbf{x}}_{\text{m-M}} = \hat{\mathbf{x}}_{\text{ML}}$ since the m-M algorithm guarantees the ML solution). Thus, substituting (4.2) and this assumption in (4.14) yields

$$R_{\text{m-M}} = \left\| \mathbf{w} \right\|^2. \tag{4.15}$$

It should be noted that the pruned radius in (4.14) is considered the optimum threshold that can be used in the SD-based algorithms. Since the decoding complexity of the proposed m-M algorithm is equivalent to that of a depth-first algorithm using the optimum pruned radius in (4.14), the proposed algorithm provides a better complexity than the optimum BER algorithms in the literature.

Now, I can write $C_{\text{m-M}}$ in (4.13) as [11], [16]

$$C_{\text{m-M}} \approx MN_t + \sum_{j=1}^{MN_t} \sum_{i=1}^{N_r} \mathbb{P}\text{r}\left(d_{i,j} \leq R_{\text{m-M}} \left| \mathbf{x}_t, \mathbf{H}, \sigma_n^2, R_{\text{m-M}} \right. \right). \tag{4.16}$$

It is worth noting that (4.16) is the generic form of the expected complexity, and its closed-form solution depends on the algorithm itself. Note that (4.16) finds the probability of $d_{i,j}$ being visited when the SD radius is $R_{\text{m-M}}$ (the node is considered to be visited if $d_{i,j} \leq R_{\text{m-M}}$ and vice versa). Ideally, $\mathbb{P}\text{r}\left(d_{i,j} \leq R_{\text{m-M}} \right)$ under the conditions previously given should be zero or one. The correction factor MN_t in (4.16) is needed since the $\mathbb{P}\text{r}\left(d_{i,j} \leq R_{\text{m-M}} \right)$ misses almost MN_t nodes at the final iteration.

4.5.1 Perfect Channel State Information at the Receiver

To find the closed form expression of the right-hand-side of (4.16), the conditional probability distribution of $d_{i,j}$ should be determined first. From (4.2) and (4.4), I can rewrite (4.4) in terms of the real and imaginary components as

$$d_{i,j} = \sum_{n=1}^{i} \left| \left(w_n^{\Re} + x_{n,t}^{\Re} - x_{n,j}^{\Re} \right) + \jmath \left(w_n^{\Im} + x_{n,t}^{\Im} - x_{n,j}^{\Im} \right) \right|^2 = \sum_{n=1}^{i} \left(\mathcal{R}_n^2 + \mathcal{I}_n^2 \right), \tag{4.17}$$

where $\mathcal{R}_n = w_n^{\Re} + x_{n,t}^{\Re} - x_{n,j}^{\Re}$ and $\mathcal{I}_n = w_n^{\Im} + x_{n,t}^{\Im} - x_{n,j}^{\Im}$ are Gaussian distributed with variances $\sigma_n^2/2$, and means $\left(x_{n,t}^{\Re} - x_{n,j}^{\Re} \right)$ and $\left(x_{n,t}^{\Im} - x_{n,j}^{\Im} \right)$, respectively. Consequently, $d_{i,j}$ is a non-central chi-squared r.v. with $2i$ degrees of freedom and non-centrality parameter $\gamma_{i,j}^2$ given by [23, (Ch. 2)]

$$\gamma_{i,j}^2 = \sum_{n=1}^{i} \left[\left(x_{n,t}^{\Re} - x_{n,j}^{\Re} \right)^2 + \left(x_{n,t}^{\Im} - x_{n,j}^{\Im} \right)^2 \right]. \tag{4.18}$$

The probability distribution function (pdf) of $d_{i,j}$ for $d_{i,j} \geq 0$ is calculated as [23, (Ch. 2)]

$$f_{d_{i,j}}(d_{i,j}) = \frac{1}{\sigma_n^2} \left(\frac{d_{i,j}}{\gamma_{i,j}^2} \right)^{(i-1)/2} \exp\left(-\frac{\gamma_{i,j}^2 + d_{i,j}}{\sigma_n^2} \right) I_{i-1}\left(\frac{\sqrt{d_{i,j}\, \gamma_{i,j}^2}}{\sigma_n^2/2} \right), \tag{4.19}$$

where $I_{i-1}(\centerdot)$ is the first kind modified Bessel function of order $(i-1)$. Since $d_{i,j}$ has an even degrees of freedom, the closed form expression of the cumulative distribution function (CDF) for (4.19) is given as [23, (Ch. 2)]

$$\Pr\left(d_{i,j} \leq R_{\text{m-M}} \left| \mathbf{x}_t, \mathbf{H}, \sigma_n^2, R_{\text{m-M}} \right. \right) = 1 - Q_i\left(\frac{\gamma_{i,j}}{\sigma_n/\sqrt{2}}, \frac{\sqrt{R_{\text{m-M}}}}{\sigma_n/\sqrt{2}} \right), \tag{4.20}$$

where $Q_i(\centerdot, \centerdot)$ denotes the generalized Marcum function of order i.

To remove the dependency of (4.20) on the instantaneous value of $R_{\text{m-M}}$, an expectation over the pdf of $R_{\text{m-M}}$ should be calculated. (4.15) can be written in terms of its real and imaginary components as

$$R_{\text{m-M}} = \sum_{n=1}^{N_r} \left[\left(w_n^{\Re} \right)^2 + \left(w_n^{\Im} \right)^2 \right]. \tag{4.21}$$

Therefore, $R_{\text{m-M}}$ is a central chi-square r.v. with $2N_r$ degrees of freedom and its pdf, $f_{R_{\text{m-M}}}(R_{\text{m-M}})$, is [23, (Ch. 2)]

$$f_{R_{\text{m-M}}}(R_{\text{m-M}}) = \frac{(R_{\text{m-M}})^{N_r-1}}{\sigma_n^{2N_r}\,(N_r-1)!} \exp\left(\frac{-R_{\text{m-M}}}{\sigma_n^2} \right). \tag{4.22}$$

From (4.20) and (4.22), the expected value of (4.20) over the pdf of $R_{\text{m-M}}$ can be written as

$$\Pr\left(d_{i,j} \leq R_{\text{m-M}} \left| \mathbf{x}_t, \mathbf{H}, \sigma_n^2 \right. \right) = \int_0^{\infty} \left[1 - Q_i \left(\frac{\gamma_{i,j}}{\sigma_n/\sqrt{2}}, \frac{\sqrt{R_{\text{m-M}}}}{\sigma_n/\sqrt{2}} \right) \right] f_{R_{\text{m-M}}}(R_{\text{m-M}}) \;\; \mathrm{d}R_{\text{m-M}}. \tag{4.23}$$

The closed form solution of the integration in (4.23) can be found in [24], and then, the complexity in (4.16) is expressed as

$$C_{\text{m-M}} \approx MN_t + \sum_{j=1}^{MN_t} \sum_{i=1}^{N_r} \left[1 - \left[1 - \frac{\exp\left(-\gamma_{i,j}^2/\sigma_n^2\right)}{2^{N_r}} \right.\right.$$

$$\left.\left. \times \left[\Phi_1 \left(N_r, 1, 1; \frac{1}{2}, \frac{\gamma_{i,j}^2}{2\sigma_n^2} \right) - \sum_{k=1}^{i-1} \frac{(N_r)_k}{2^k\, k!}\, {}_1F_1 \left(N_r + k; k+1; \frac{\gamma_{i,j}^2}{2\sigma_n^2} \right) \right] \right] \right], \tag{4.24}$$

where $(N_r)_k$ denotes the Pochhammer symbol, Φ_1 is the Humbert hypergeometric function of the first kind, and ${}_1F_1$ denotes the Kummer hypergeometric function [25].

4.5.2 Imperfect Channel State Information at the Receiver

In this subsection, the complexity of the proposed m-M algorithm in (4.16) is assessed in the presence of imperfect CSIR. To the best of the authors' knowledge, in case of imperfect CSIR, the expected complexity is not analyzed in the literature. Assume that there is an error between the estimated channel coefficient at the receiver side and the actual channel coefficient, which is denoted by $\mathbf{e} \sim \mathcal{CN}(0, \sigma_e^2)$, where σ_e^2 is the variance of the error in the channel estimation. Thus, the estimated channel entry becomes $\hat{\mathbf{h}} = \mathbf{h} + \mathbf{e}$ and the combination element in (4.4) becomes $x_{n,j} + \hat{e}_{n,j}$, where $\hat{e}_{n,j} = e_n s_j$, with s_j as the QAM symbol in j-th combination with energy of $|s_j|^2$ and e_n as the n-th element of vector $\mathbf{e}$. In this case, for least square solution of (4.4), $\hat{\mathbf{h}} \sim \mathcal{CN}(0, 1 + \sigma_e^2)$ depends on $\mathbf{h}$ with a correlation coefficient of $\rho = 1/\sqrt{1+\sigma_e^2}$ [26]-[27], [28, (p. 282)]; the conditional variance of the elements of the noisy received vector, ζ_j^2, is given by [27], [29]

$$\zeta_j^2 = \mathrm{Var}\left(y|\hat{\mathbf{h}}\right) = \sigma_n^2 + \left(1-\rho^2\right)|s_j|^2. \tag{4.25}$$

It should be noted that the σ_e^2 may be considered as fixed or variable when SNR changes. In theory, the error in channel estimation decreases as the SNR increases [30], [31]; therefore, I can consider $\sigma_e^2 = 1/\mathrm{snr}$ in case of variable σ_e^2 where snr denotes the signal-to-noise ratio in linear scale (i.e., SNR = $10\log_{10}(\mathrm{snr})$).

$d_{i,j}$ in (4.17) in the case of imperfect-CSIR is denoted by $\hat{d}_{i,j}$ and given as

$$\hat{d}_{i,j} = \sum_{n=1}^{i} \left| \left(w_n^{\Re} - \hat{e}_{n,j}^{\Re} + x_{n,t}^{\Re} - x_{n,j}^{\Re}\right) + \jmath\left(w_n^{\Im} - \hat{e}_{n,j}^{\Im} + x_{n,t}^{\Im} - x_{n,j}^{\Im}\right)\right|^2 = \sum_{n=1}^{i}\left(\hat{\mathcal{R}}_n^2 + \hat{\mathcal{I}}_n^2\right), \tag{4.26}$$

where $\hat{\mathcal{R}}_n = w_n^{\Re} - \hat{e}_{n,j}^{\Re} + x_{n,t}^{\Re} - x_{n,j}^{\Re}$ and $\hat{\mathcal{I}}_n = w_n^{\Im} - \hat{e}_{n,j}^{\Im} + x_{n,t}^{\Im} - x_{n,j}^{\Im}$ are Gaussian distributed with variances $\zeta_j^2/2$, and means $\left(x_{n,t}^{\Re} - x_{n,j}^{\Re}\right)$ and $\left(x_{n,t}^{\Im} - x_{n,j}^{\Im}\right)$, respectively. Consequently,

$\hat{d}_{i,j}$ is a non-central chi-squared r.v. with $2i$ degrees of freedom and non-centrality parameter $\gamma_{i,j}^2$ given by (4.18), and its pdf for $\hat{d}_{i,j} \geq 0$ becomes [23, (Ch. 2)]

$$f_{\hat{d}_{i,j}}(\hat{d}_{i,j}) = \frac{1}{\zeta_j^2}\left(\frac{\hat{d}_{i,j}}{\gamma_{i,j}^2}\right)^{(i-1)/2} \exp\left(-\frac{\gamma_{i,j}^2 + \hat{d}_{i,j}}{\zeta_j^2}\right) I_{i-1}\left(\frac{\sqrt{\hat{d}_{i,j}\,\gamma_{i,j}^2}}{\zeta_j^2/2}\right). \tag{4.27}$$

Therefore, (4.20) becomes

$$\Pr\left(\hat{d}_{i,j} \leq \hat{R}_{\text{m-M}} \,\middle|\, \mathbf{x}_t, \mathbf{H}, \sigma_n^2, \sigma_e^2, \hat{R}_{\text{m-M}}\right) = 1 - Q_i\left(\frac{\gamma_{i,j}}{\zeta_j/\sqrt{2}}, \frac{\sqrt{\hat{R}_{\text{m-M}}}}{\zeta_j/\sqrt{2}}\right), \tag{4.28}$$

where $\hat{R}_{\text{m-M}}$ denotes the threshold of the m-M algorithm in the case of imperfect CSIR. It should be noted that for the case of imperfect CSIR, the threshold in (4.21) becomes

$$\hat{R}_{\text{m-M}} = \sum_{n=1}^{N_r}\left[\left(w_n^{\Re} - \hat{e}_{n,t}^{\Re}\right)^2 + \left(w_n^{\Im} - \hat{e}_{n,t}^{\Im}\right)^2\right], \tag{4.29}$$

where $\left(w_n^{\Re} - \hat{e}_{n,t}^{\Re}\right)$ and $\left(w_n^{\Im} - \hat{e}_{n,t}^{\Im}\right)$ are Gaussian distributed with zero-mean and variance of $\zeta_t^2/2$, where

$$\zeta_t^2 = \sigma_n^2 + \left(1 - \rho^2\right)|s_t|^2, \tag{4.30}$$

with s_t as the transmitted QAM symbol with energy $|s_t|^2$.

Consequently, $\hat{R}_{\text{m-M}} \geq 0$ is a central chi-squared distributed r.v. with $2N_r$ degrees of freedom and its pdf is given by [23, (Ch. 2)]

$$f_{\hat{R}_{\text{m-M}}}(\hat{R}_{\text{m-M}}) = \frac{\left(\hat{R}_{\text{m-M}}\right)^{N_r-1}}{\zeta_t^{2N_r}\,(N_r-1)!}\exp\left(\frac{-\hat{R}_{\text{m-M}}}{\zeta_t^2}\right). \tag{4.31}$$

From (4.28) and (4.31), the expected value of (4.28) over the pdf of $\hat{R}_{\text{m-M}}$ can be written

as

$$\mathbb{P}\mathrm{r}\left(\hat{d}_{i,j} \leq \hat{R}_{\text{m-M}} \left| \mathbf{x}_t, \mathbf{H}, \sigma_n^2, \sigma_e^2 \right.\right) = \int_0^{\infty} \left[1 - Q_i\left(\frac{\gamma_{i,j}}{\zeta_j/\sqrt{2}}, \frac{\sqrt{\hat{R}_{\text{m-M}}}}{\zeta_j/\sqrt{2}}\right)\right] f_{\hat{R}_{\text{m-M}}}(\hat{R}_{\text{m-M}}) \ \mathrm{d}\hat{R}_{\text{m-M}}. \tag{4.32}$$

The closed form of the integration in (4.32) can be found in [24], and then, the complexity in (4.16) is obtained as

$$\hat{C}_{\text{m-M}} \approx MN_t + \sum_{j=1}^{MN_t} \sum_{i=1}^{N_r} \left[1 - \left[1 - \frac{\zeta_j^{2N_r} \exp\left(-\gamma_{i,j}^2/\zeta_j^2\right)}{\left(\zeta_j^2 + \zeta_t^2\right)^{N_r}} \left[\Phi_1\left(N_r, 1, 1; \frac{\zeta_t^2}{\zeta_j^2 + \zeta_t^2}, \frac{\gamma_{i,j}^2 \zeta_t^2}{\zeta_j^2\left(\zeta_j^2 + \zeta_t^2\right)}\right)\right.\right.\right.$$

$$\left.\left.\left. - \sum_{k=1}^{i-1} \frac{(N_r)_k}{k!} {}_1F_1\left(N_r + k; k+1; \frac{\gamma_{i,j}^2 \zeta_t^2}{\zeta_j^2\left(\zeta_j^2 + \zeta_t^2\right)}\right)\right]\right]\right]. \tag{4.33}$$

4.6 Optimality of BER Performance

In this section, I discuss the BER performance optimality of the proposed m-M algorithm based on the condition in (4.10). The effect of omitting this condition on the proposed m-M algorithm is also studied. I define an indicator for the BER performance optimality as the number of times the proposed m-M algorithm misses the ML solution, referred to as the number of misses (NoM). In other words, the BER of the m-M algorithm will be the same as the ML BER if the NoM equals zero and vice versa. It should be noted that NoM is an r.v. that depends on the SNR and σ_e^2.

Let us invoke the general expression of the union bound error probability of SM-ML detector as [6], [27]

$$P_b = \frac{1}{(\eta)\, 2^{\eta}} \sum_{k=1}^{2^{\eta}} \sum_{l=1}^{2^{\eta}} \delta_{k,l} \mathbb{E}\left\{ \mathbb{P}\mathrm{r}^{(\mathrm{ML})}\left(\mathbf{x}_k \rightarrow \tilde{\mathbf{x}}_l\right) \right\}, \tag{4.34}$$

where P_b is the union bound probability, $\mathbb{P}\mathrm{r}^{(\mathrm{ML})}\left(\mathbf{x}_k \rightarrow \tilde{\mathbf{x}}_l\right)$ stands for the pairwise error probability (PEP) of the proposed SM-ML decoder, $\delta_{k,l}$ represents the number of bit errors which corresponds to the instant PEP event, and the spectral efficiency η is given from (4.1). Let us consider that $\Delta^{\text{m-M}}$ is the NoM between the m-M algorithm solution and the ML solution. Now, the PEP of the m-M algorithm is denoted by $\mathbb{P}\mathrm{r}^{(\text{m-M})}\left(\mathbf{x}_k \rightarrow \tilde{\mathbf{x}}_l\right)$ and given as [13]

$$\mathbb{P}\mathrm{r}^{(\text{m-M})}\left(\mathbf{x}_k \rightarrow \tilde{\mathbf{x}}_l\right) = \mathbb{P}\mathrm{r}^{(\mathrm{ML})}\left(\mathbf{x}_k \rightarrow \tilde{\mathbf{x}}_l\right) + \mathbb{P}\mathrm{r}\left(\Delta^{\text{m-M}} \neq 0\right). \tag{4.35}$$

According to (4.10), if the m-M algorithm detects a minimum ED at the end of fully expanded branch, this means that no further expansion will happen in the current minimum ED (the branch length can not be $N_r + 1$) and the current minimum ED is a global minimum across all other branches. Therefore, the ML solution will not be missed (i.e., $\mathbb{P}\mathrm{r}\left(\Delta^{\text{m-M}} \neq 0\right) = 0$) and the union bound error probability of the proposed m-M algorithm is exactly the same as (4.34).

To study the effect of removing the optimality condition in (4.10), consider an m-M algorithm without this condition, referred to as the m-Mw algorithm. It should be noted that the m-Mw algorithm is not a stand-alone algorithm, and it is mentioned here to discuss the optimality condition in (4.10) for the proposed m-M algorithm. The m-Mw algorithm stops and declares the solution whenever only one branch is fully expanded. In such a case, the NoM takes a non-zero value and $\mathbb{P}\mathrm{r}\left(\Delta^{\text{m-Mw}} \neq 0\right) \neq 0$. Fig. 4.3 shows the average NoM versus SNR; 10^4 Rayleigh flat fading channel realizations are run for each SNR value, for 8×8 SM-MIMO using 8-QAM. As we can see, the NoM reduces as SNR increases and σ_e^2 decreases. For instance, the m-Mw algorithm misses 2020, 564 and 20 ML solution out of

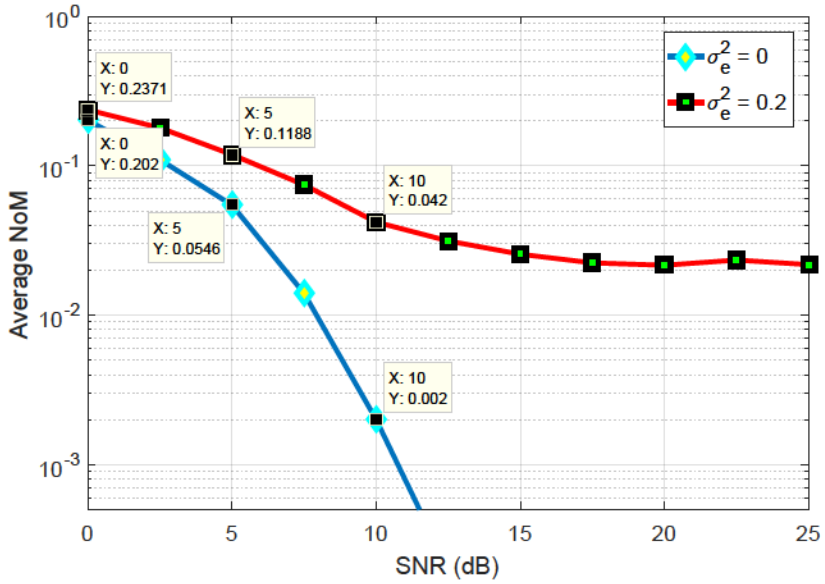

Fig. 4.3: Average number of NoM of the m-Mw algorithm for 8×8 SM-MIMO and 8-QAM.

10^4 runs at SNR of 0, 5 and 10 dB, respectively, in case of perfect CSIR; for imperfect CSIR with $\sigma_e^2 = 0.2$, the NoM for the m-Mw algorithm is 2371, 1188 and 420 out of 10^4 runs at SNR of 0, 5 and 10 dB, respectively.

Hence, the condition in (4.10) ensures that the minimum ED which comes at the end of a fully expanded branch is a global minimum across all branches; thus, the ML solution is achieved. Additionally, omitting the condition in (4.10) leads to a significant BER deterioration when compared with the ML performance.

4.7 Numerical Results and Discussions

In this section, I evaluate the behavior of the proposed m-M algorithm in terms of BER and decoding complexity. In addition, comparisons between the m-M algorithm and SM-SD algorithms in the literature are presented. Since the m-M algorithm provides the optimal BER performance, I consider the SM-SD algorithms (such as given in [13] and [16]) in comparisons. Three scenarios are considered: a) perfect CSIR ($\sigma_e^2 = 0$), b) imperfect CSIR

with fixed σ_e^2 ($\sigma_e^2 = 0.1$ and 0.2), and c) imperfect CSIR with variable σ_e^2 ($\sigma_e^2 = 1/\text{snr}$). Two spectral efficiency values are considered: $\eta = 6$ bpcu using 8-QAM for $N_r \times 8$ SM-MIMO system, and $\eta = 8$ bpcu using 16-QAM for $N_r \times 16$ SM-MIMO system. The value of N_r for both cases describes the type of the system. In the case of determined SM-MIMO system, $N_r = N_t$ (i.e., $N_r = 8$ and 16 for $\eta = 6$ and 8, respectively). For under-determined SM-MIMO system, $N_r < N_t$ (e.g., $N_r = 6$ and 12 for $\eta = 6$ and 8, respectively). Finally, I have an over-determined SM-MIMO system if $N_r > N_t$ (e.g., $N_r = 10$ and 20 for $\eta = 6$ and 8, respectively). Monte Carlo simulations are used to obtain the presented results for all scenarios by running at least 5×10^5 Rayleigh flat fading channel realizations.

4.7.1 BER Comparison

In this subsection, the BER performance of the SM-ML, SM-SD [13], SM-SD [16], and proposed m-M algorithms are compared with respect to SNR. Figs. 4.4, 4.5 and 4.6 show the BER performance of different SM decoders for determined, under-determined, and over-determined SM-MIMO systems, respectively. The left sub-plots in all three figures present $\eta = 6$ bpcu, while the right ones show $\eta = 8$ bpcu. As observed from these figures, the two SM-SD algorithms in [13] and [16], as well as the proposed m-M algorithm provide the same SM-ML BER for all values of σ_e^2 (i.e., 0, 0.1, 0.2, and 1/snr). As expected, the best BER is obtained when $\sigma_e^2 = 0$, while the BER degrades for increasing values of σ_e^2. Unlike the BER obtained from having $\sigma_e^2 = 1/\text{snr}$, an error floor occurs in the case of $\sigma_e^2 = 0.1$ and 0.2 even in high SNR due to the fixed values of σ_e^2. The error floor is mitigated as N_r increases. For instance, the error floor of the $\sigma_e^2 = 0.1$ curve in Fig. 4.5(b) can not be reduced to 5×10^{-4} when $N_r = 12$; when $N_r = 16$ in Fig. 4.4(b) for the $\sigma_e^2 = 0.1$ curve, the error floor occurs at 10^{-4}; however, it further reduces to 10^{-5} when $N_r = 20$ in Fig. 4.6(b) for the $\sigma_e^2 = 0.1$ curve.

It can be seen from these figures that there is no preference in BER between the proposed

m-M algorithm and the other SM-SD algorithms in [13] and [16]. For all presented scenarios, the low-complexity algorithms (the m-M algorithm, and SM-SD algorithms in [13] and [16]) provide the same BER as the SM-ML detection. It is worth noting that in practice, the channel estimation accuracy improves as the SNR increases (i.e., $\sigma_e^2 = 1/\text{snr}$), and the ML BER performance can be still reasonable, as seen from Figs. 4.4, 4.5 and 4.6.

4.7.2 Analytical Complexity Assessment

In this subsection, I evaluate the accuracy of the analytical expressions for the expected decoding complexity of the m-M algorithm given in (4.24) and (4.33). As mentioned before, the number of visited nodes (VNs) is used as a measure for the decoding complexity of all algorithms in this chapter. Figs. 4.7, 4.8 and 4.9 present the comparison results between the analytical expressions and computer simulation results of the determined, under-determined and over-determined SM-MIMO systems, respectively, for $\eta = 6$ and 8 bpcu. In all figures, the analytical expression for $\sigma_e^2 = 0$ is given from (4.24), while the analytical expression for $\sigma_e^2 = 0.1$, 0.2 and $(1/\text{snr})$ is given from (4.33). From these figures, I observe that the analytical expressions in (4.24) and (4.33) match the computer simulation results after SNR values of 5 dB, while some mismatches occur at low SNR values.

It should be noted that the mismatch between the analytical expressions and simulation results at low SNR values comes from the assumptions of $\hat{\mathbf{x}}_{\text{m-M}} \rightarrow \mathbf{x}_t$ in (4.15). At low SNR, the ML solution (the same as $\hat{\mathbf{x}}_{\text{m-M}}$) misses the true solution, $\mathbf{x}_t$, which means that $\|\mathbf{y} - \mathbf{x}_t\|_F^2 > \|\mathbf{y} - \hat{\mathbf{x}}_{\text{m-M}}\|_F^2$. In other words, the threshold $R_{\text{m-M}}$ in (4.15) used for the analytical expressions will be greater than the actual threshold in (4.14), which leads to the count of more nodes than the reality. By increasing the SNR, the ML solution most probably estimates the true solution; the assumption of $\hat{\mathbf{x}}_{\text{m-M}} \rightarrow \mathbf{x}_t$ becomes more reliable. In the case of $\sigma_e^2 = 1/\text{snr}$, σ_e^2 becomes very high at low SNR values (e.g., $\sigma_e^2 = 1$ at zero SNR) which dramatically affects the accuracy of (4.33).

As it can be seen from these figures, the derived analytical expressions in (4.24) and (4.33) accurately describe the decoding complexity of the proposed m-M algorithm in both perfect and imperfect CSIR especially at high SNR values for determined, under-determined, and over-determined SM-MIMO systems.

4.7.3 Complexity Comparison

In this subsection, I compare the complexity of the proposed m-M algorithm with the optimal BER performance SM-SD algorithms ([13] and [16]). It should be noted that the threshold of the SM-SD algorithm in [13] is optimized to provide the optimal BER. The comparison goal is to determine the decoding complexity reduction ratio between the desired and SM-ML algorithms, which is given as

$$C_{\mathrm{R}} = \frac{MN_tN_r - C_{\Lambda}}{MN_tN_r} = 1 - \frac{C_{\Lambda}}{MN_tN_r}, \tag{4.36}$$

where C_{R} denotes the complexity reduction ratio, MN_tN_r is the decoding complexity of the ML detector, and C_{Λ} denotes the decoding complexity of the target algorithm with $\Lambda \in$ {m-M, SM-SD [13], SM-SD [16]}. The minimum number of nodes that can be visited by any algorithm is a one fully expanded branch (i.e., N_r nodes) in addition to the nodes of the first row in the tree-search (i.e., $MN_t - 1$ nodes). Thus, I can define the maximum reduction in the decoding complexity ratio that can be achieved by any algorithm, $C_{\mathrm{R}}^{\max}$, as

$$C_{\mathrm{R}}^{\max} = 1 - \frac{N_r + MN_t - 1}{MN_tN_r}. \tag{4.37}$$

Figs. 4.10, 4.11 and 4.12 show the complexity reduction ratio in (4.36) versus different values of SNR for determined, under-determined, and over-determined SM-MIMO systems, respectively. Each figure contains four sub-figures which represent all scenarios of σ_e^2 (i.e., 0, 0.1, 0.2, and $1/\mathrm{snr}$), while each sub-figure presents the two available spectral efficiencies,

$\eta = 6$ and 8 bpcu. According to (4.37), $C_{\mathrm{R}}^{\max} = 86.1\%$ and 93.4% in Fig. 4.10 for $\eta = 6$ and 8 bpcu, respectively; $C_{\mathrm{R}}^{\max} = 82\%$ and 91.3% in Fig. 4.11 for $\eta = 6$ and 8 bpcu, respectively; and $C_{\mathrm{R}}^{\max} = 88.6\%$ and 94.6% in Fig. 4.12 for $\eta = 6$ and 8 bpcu, respectively.

In the case of $\sigma_e^2 = 0$ and $1/\mathrm{snr}$, the proposed m-M algorithm provides the best reduction in the decoding complexity ratio over the SM-SD [13] and SM-SD [16] algorithms. The m-M algorithm as well as the other two algorithms reach to $C_{\mathrm{R}}^{\max}$ at high SNR. It should be noted that when η increases, the decoding complexity ratio increases for all algorithms. In the case of fixed σ_e^2 (i.e., 0.1 and 0.2), no algorithm reaches $C_{\mathrm{R}}^{\max}$. However, the proposed m-M algorithm provides the best reduction in the decoding complexity ratio for all values of SNR. Also, as σ_e^2 increases, the reduction in complexity gain of the m-M algorithm over the other two algorithm increases.

As it can be seen from these figures, the proposed m-M algorithm provides a better complexity reduction ratio in the low SNR in the case of perfect CSIR and variable σ_e^2. Moreover, it has the superiority over the existing SM-SD algorithms for all values of SNR in the case of imperfect CSIR with fixed σ_e^2. In addition, the m-M algorithm is more robust to the increase of σ_e^2 than the existing SM-SD algorithms.

4.7.4 Complexity Reduction Sensitivity

I have noticed from Figs. 4.10, 4.11 and 4.12 that the reduction in the decoding complexity ratio for the m-M algorithm increases as the SM-MIMO dimensions (M, N_t, and N_r) increase. However, I need to determine which dimension affects more the complexity reduction ratio. In this subsection, I assess the reduction in the complexity ratio versus only one SM-MIMO dimension.

In Fig. 4.13, the decoding complexity reduction ratio of the m-M algorithm is assessed versus the QAM order, M, for the 16×16 SM-MIMO system. It can be seen that the complexity reduction ratio slightly increases as M increases. For example, for $\sigma_e^2 = 0.2$, the

complexity reduction ratio increases from 76% to 78.5% at $M = 8$ and 128, respectively. Thus, the complexity reduction ratio of the proposed m-M algorithm is sensitive to the slightly change of M.

In Fig. 4.14, I evaluate the decoding complexity reduction ratio of the m-M algorithm versus N_t at $N_r = M = 16$. It can be noticed that the increase of the decoding complexity reduction is negligible in comparison with the case of variable N_t. Consequently, the change of N_t has almost no effect on the decoding complexity ratio of the m-M algorithm.

The decoding complexity reduction is evaluated versus different values of N_r in Fig. 4.15 for $N_t = M = 16$. I can see from this figure that the complexity reduction ratio increases from 68% at $N_r = 4$ to 90% at $N_r = 128$ for $\sigma_e^2 = 0$, and from 64% at $N_r = 4$ to 82% at $N_r = 128$ for $\sigma_e^2 = 0.2$. Thus, the decoding complexity of the m-M algorithm increases logarithmically as N_r increases.

Finally, I can see from these figures that the decoding complexity reduction ratio of the m-M algorithm is sensitive to the change of N_r, while is nonsensitive to the changes of N_t or M.

4.7.5 Discussions

As seen from our comprehensive comparisons, the proposed m-M algorithm provides significant reduction in the decoding complexity basically without BER performance loss. For SM systems, compressive sensing (CS)-based algorithms have been recently proposed in [32]-[34] to provide sub-optimal BER performance with a reduction in the decoding complexity. These CS-based algorithms exploit the sparsity of the SM signals to provide low-complexity detection at the expense of BER deterioration. Normally, the CS-based algorithms are suitable for over-determined SM-MIMO systems (i.e., $N_r > N_t$) to reduce the BER performance gap versus the ML solution. The authors of [34] have proposed an enhanced Bayesian CS (EBCS) algorithm to provide low-complexity detection with near ML

BER performance. The minimum decoding complexity of the EBCS algorithm in [34] can be achieved at high SNR, which is about $\mathcal{O}(N_r N_t^2)+\mathcal{O}(N_r N_t)+\mathcal{O}(N_t)+\mathcal{O}(N_r)$ floating point operations (flops). Since the ML decoder costs $9MN_rN_t$ flops, the maximum complexity reduction that can be achieved from [34] when compared with the ML decoder in high SNR is 87.2% and 88.1% for 12×8 SM-MIMO with 8-QAM and 20×16 SM-MIMO with 16-QAM, respectively. As shown in Fig. 4.12-(a) and (4.37), the proposed m-M algorithm provides 88.6% and 94.6% complexity reduction after 15 dB for 12×8 SM-MIMO with 8-QAM and 20×16 SM-MIMO with 16-QAM, respectively. Thus, the proposed algorithm has a higher complexity reduction without any BER performance loss when compared with the ML decoder.

Another recent low-complexity algorithm that provides a near-ML BER performance is proposed in [17] by dividing the tree-search into N_t subtrees with $2N_r$ levels (for the real-form representation of (4.3)) and M branches. The transmit and receive antennas are ordered to reach the solution faster. In the first subtree, the algorithm visits a different number of nodes in each level, $K = [k_1\ k_2\ \ldots k_{2N_r}]$, where k_i represents the number of best nodes that should be kept in the i-th level and expanded in the next level. The minimum ED at the final level is used as a pruned radius for scanning the next $N_t - 1$ subtrees by applying the SD concept in [11]. In high SNR, the minimum decoding complexity of the algorithm in [17] is $(\sum_{i=1}^{2N_r} k_i) + M(N_t - 1)$ visited nodes plus the cost of Eq. (5) in [17]. As discussed in (4.37), the proposed m-M algorithm can visit only $(2N_r + MN_t - 1)$ nodes to achieve the optimum BER performance. For instance, for a 4×4 SM-MIMO system with 64-QAM and $K = [64\ 26\ 26\ 8\ 8\ 2\ 2\ 1]$ as mentioned in [17], the minimum decoding complexity of [17] in high SNR is 329 visited nodes plus the cost of Eq. (5) in [17], while our proposed algorithm visits only 263 nodes to achieve the optimum BER performance in high SNR (almost high SNR is after 15 dB, as shown in Figs. 4.10, 4.11 and 4.12). Thus, the m-M algorithm provides a lower decoding complexity than the algorithm in [17] without

losing the optimality of BER performance.

For high rate SM transmissions, one of the suggested solutions is to use a high value of N_t. Two systems are proposed to provide high rate transmission using smaller N_t; 1) generalized SM (GSM) which activates more than one transmit antenna at a time [35], and 2) quadrature SM (QSM) which delivers the symbols using the in-phase and quadrature dimensions [36]. At the receiver side, the GSM and QSM systems have a similar tree-search structure to the SM, and hence, the proposed m-M algorithm can be applied in a straightforward manner.

4.8 Conclusion

This chapter has proposed a novel low-complexity decoding algorithm for SM-MIMO systems, referred to as the m-M algorithm. The m-M algorithm provides a significant reduction in the decoding complexity in terms of the number of nodes which are visited during the algorithm run. The proposed algorithm guarantees achieving the ML solution by employing a single expansion to the minimum ED across all tree-search branches, and stopping if this minimum ED occurs at the end of a fully expanded tree-search branch. Furthermore, tight expressions for the expected decoding complexity of the m-M algorithm have been derived. The proposed algorithm and analytical expressions have been assessed in three different scenarios: perfect CSIR, as well as imperfect CSIR with a fixed and a variable channel estimation error variances, respectively. All scenarios have been investigated for different types of SM-MIMO systems including determined, under-determined, and over-determined systems. The numerical results have shown that the proposed algorithm provides the best reduction in the decoding complexity over existing optimal SM-SD algorithms. The future work may focus on the development of the soft-decoding version of the m-M algorithm.

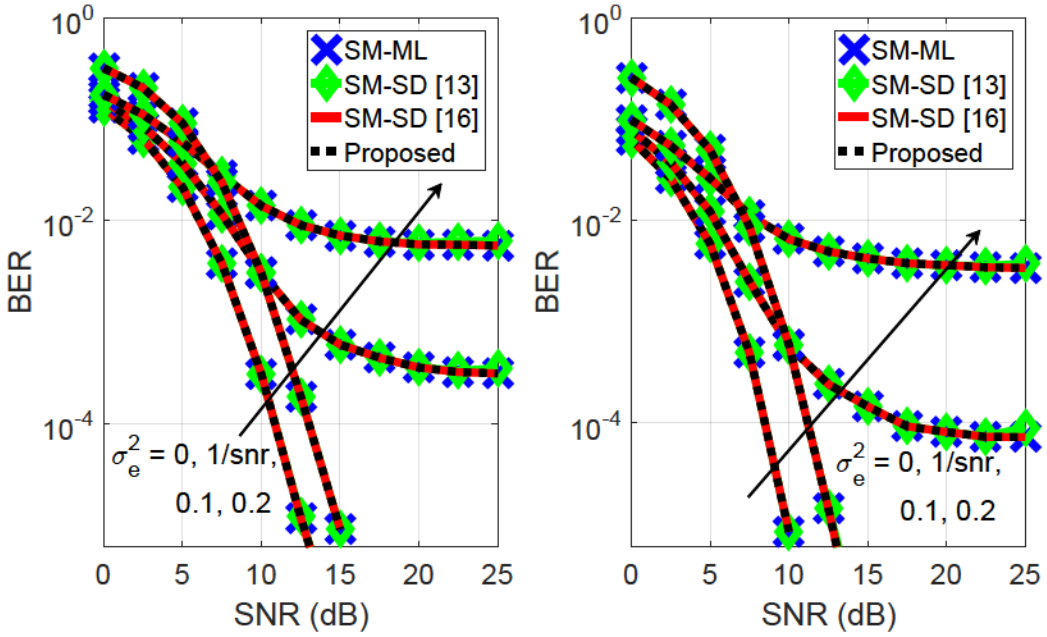

(a) 8-QAM for 8 × 8 SM-MIMO. (b) 16-QAM for 16 × 16 SM-MIMO.

Fig. 4.4: BER comparison of determined SM-MIMO system for different decoders.

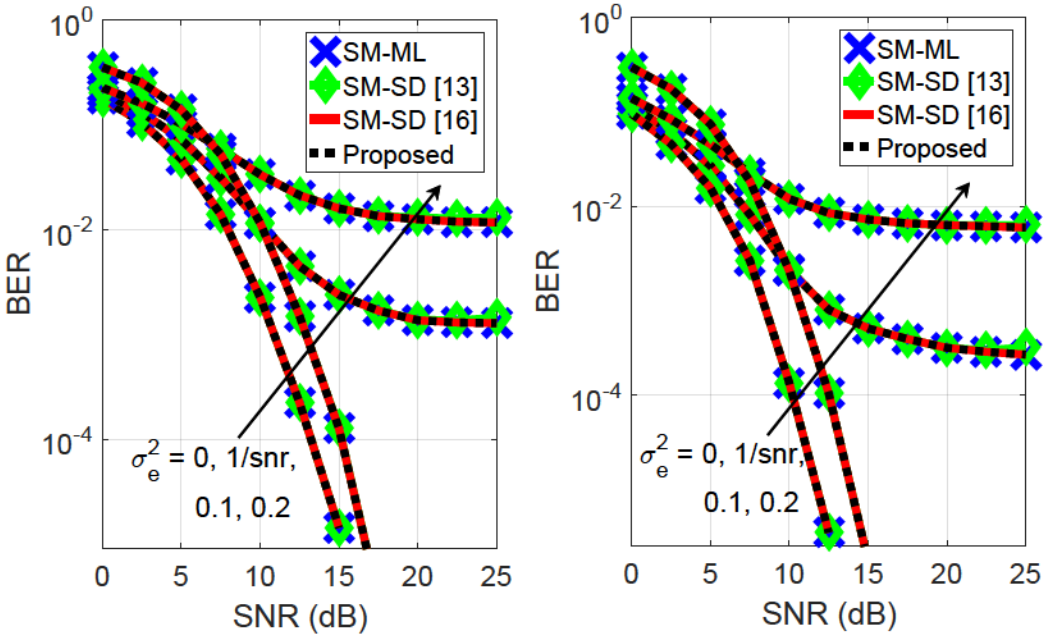

(a) 8-QAM for 6 × 8 SM-MIMO. (b) 16-QAM for 12 × 16 SM-MIMO.

Fig. 4.5: BER comparison of under-determined SM-MIMO system for different decoders.

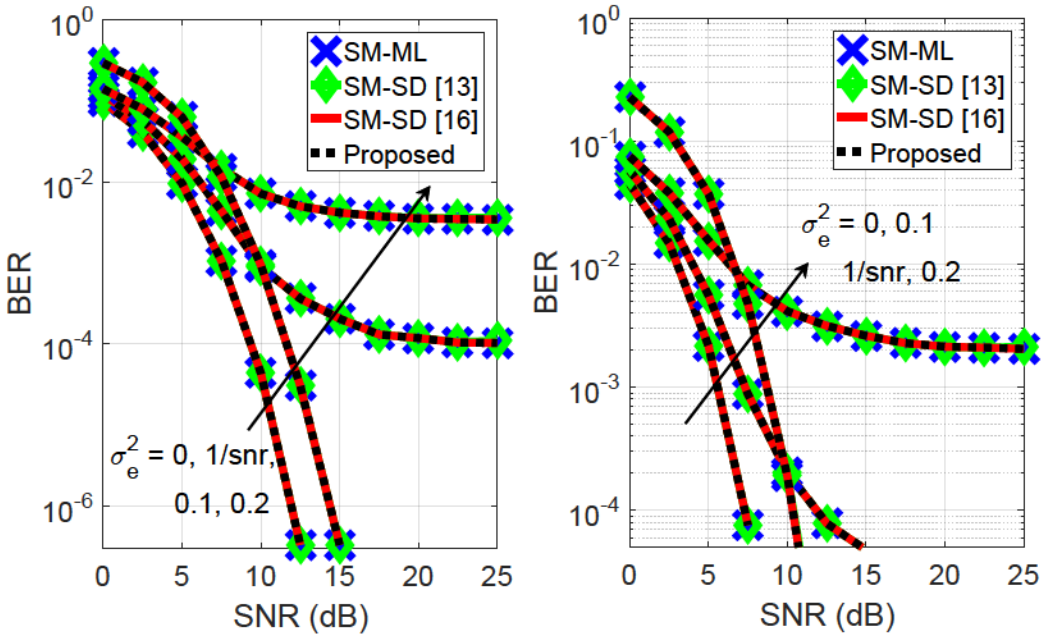

(a) 8-QAM for 10×8 SM-MIMO. (b) 16-QAM for 20×16 SM-MIMO.

Fig. 4.6: BER comparison of over-determined SM-MIMO system for different decoders.

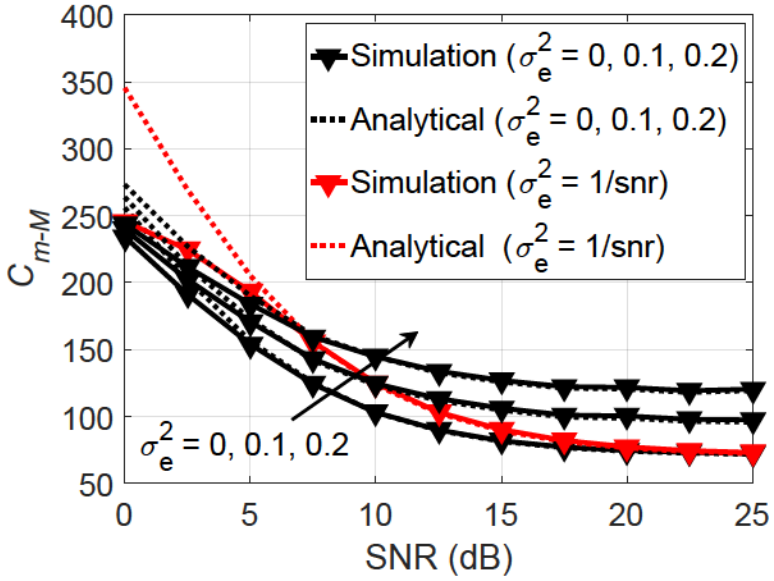

(a) 8-QAM for 8×8 SM-MIMO.

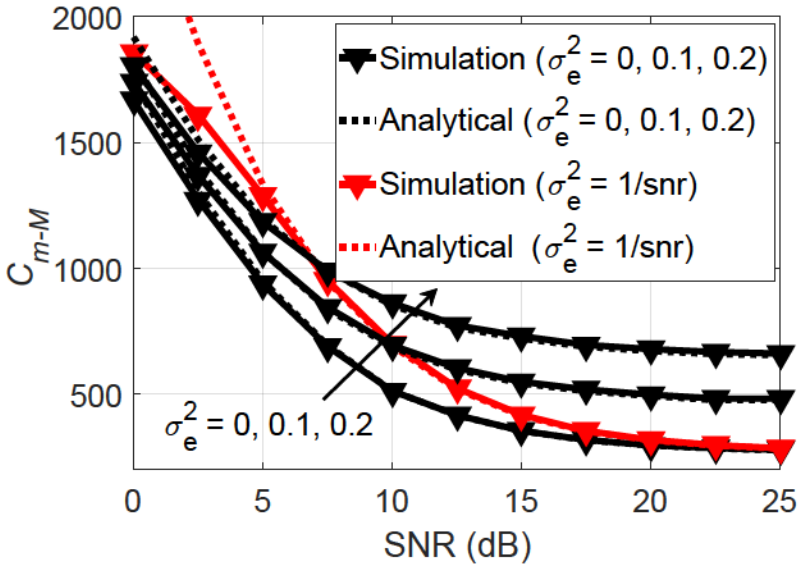

(b) 16-QAM for 16×16 SM-MIMO.

Fig. 4.7: Complexity of determined SM-MIMO system for the proposed m-M algorithm.

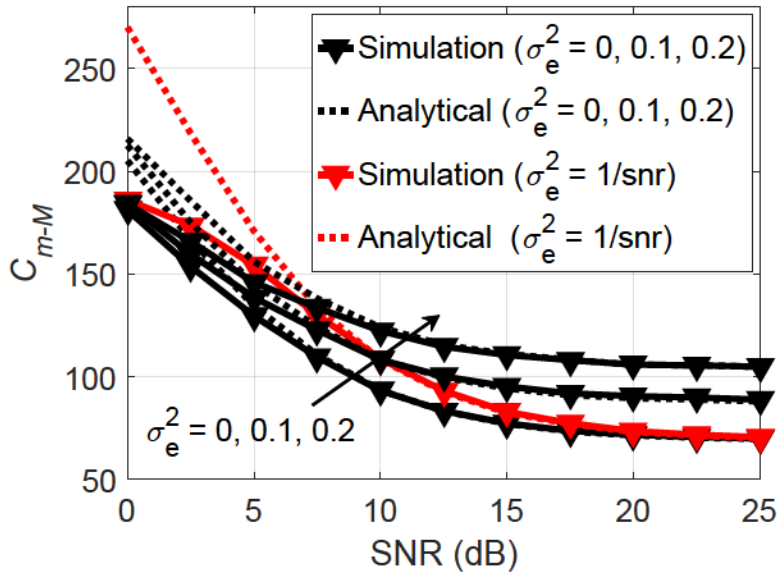

(a) 8-QAM for 6×8 SM-MIMO.

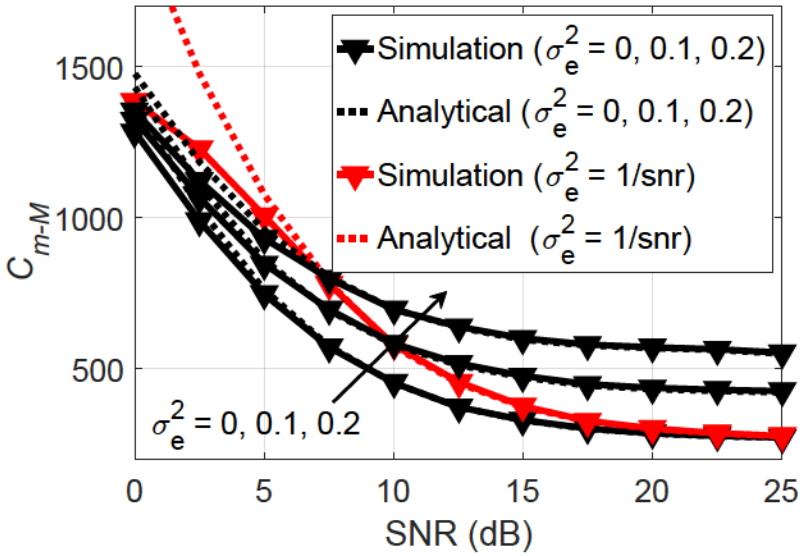

(b) 16-QAM for 12×16 SM-MIMO.

Fig. 4.8: Complexity of under-determined SM-MIMO system for the proposed m-M algorithm.

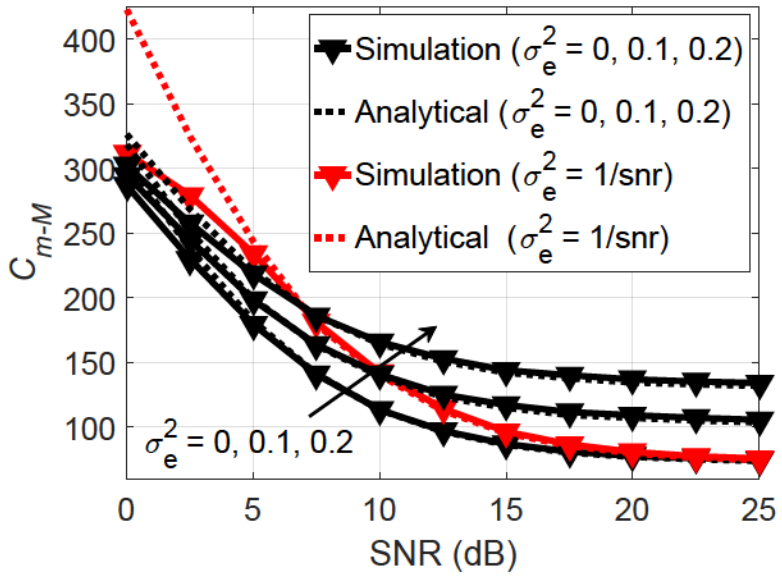

(a) 8-QAM for 10×8 SM-MIMO.

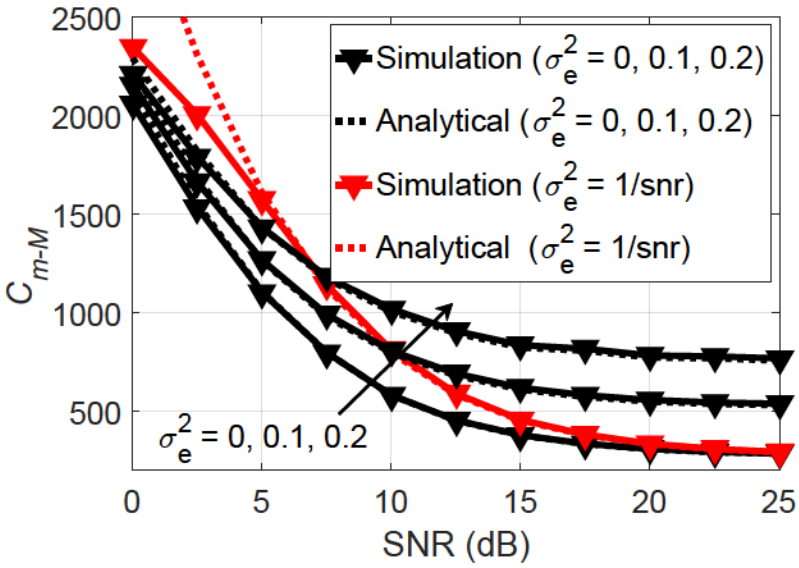

(b) 16-QAM for 20×16 SM-MIMO.

Fig. 4.9: Complexity of over-determined SM-MIMO system for the proposed m-M algorithm.

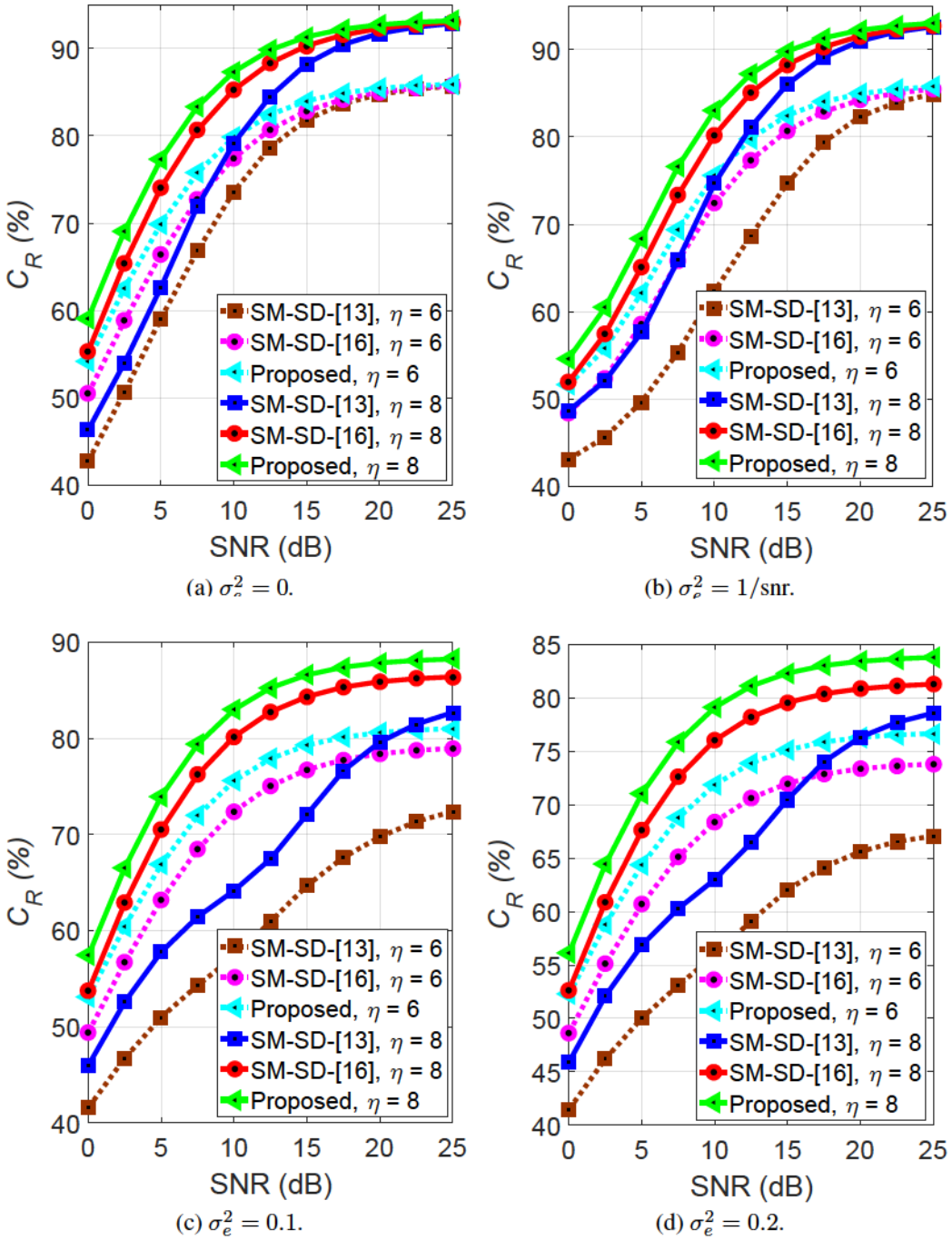

(a) $\sigma_e^2 = 0$. (b) $\sigma_e^2 = 1/\text{snr}$.

(c) $\sigma_e^2 = 0.1$. (d) $\sigma_e^2 = 0.2$.

Fig. 4.10: Complexity reduction comparison of determined SM-MIMO system for different decoders.

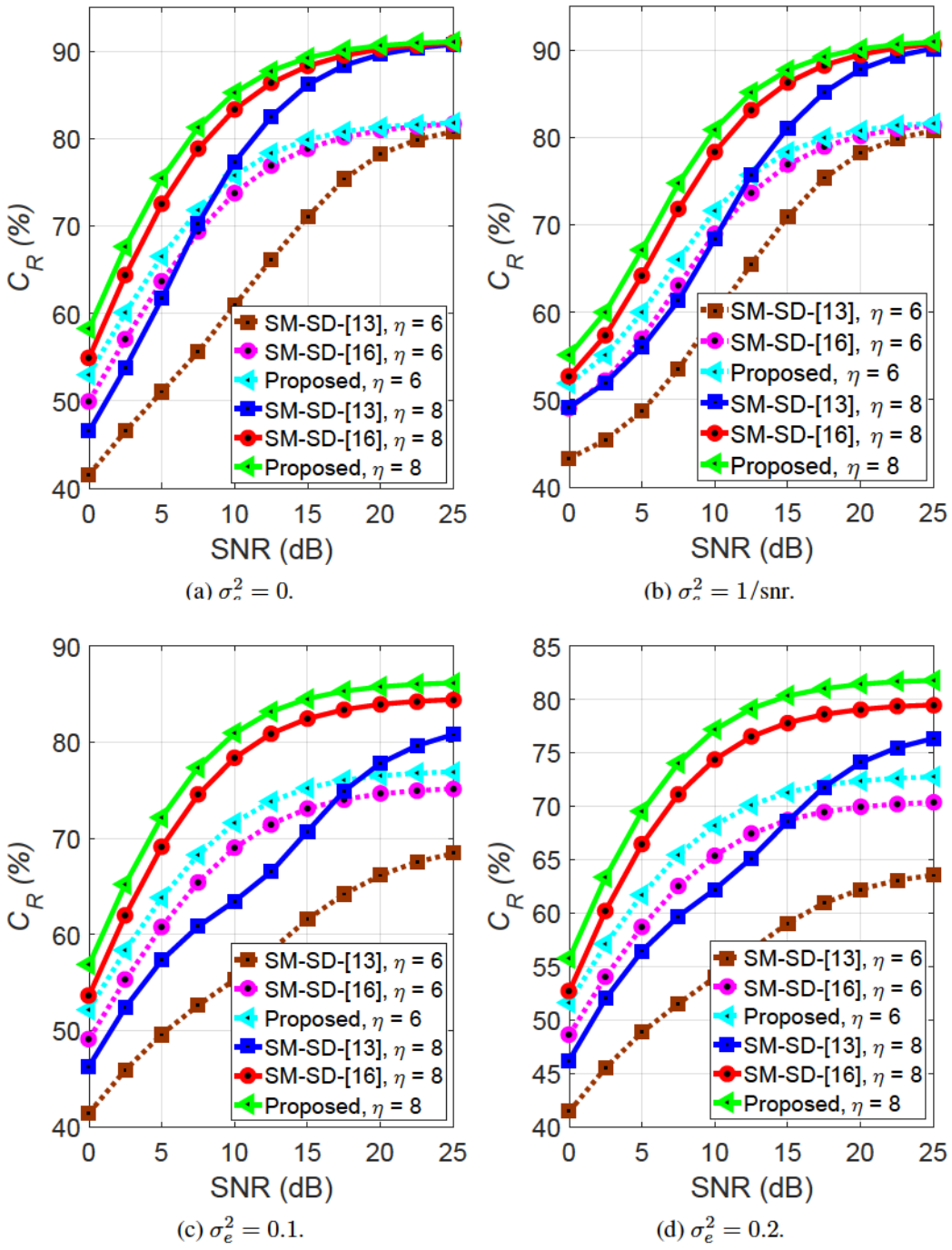

(a) $\sigma_e^2 = 0$. (b) $\sigma_e^2 = 1/\text{snr}$.

(c) $\sigma_e^2 = 0.1$. (d) $\sigma_e^2 = 0.2$.

Fig. 4.11: Complexity reduction comparison of under-determined SM-MIMO system for different decoders.

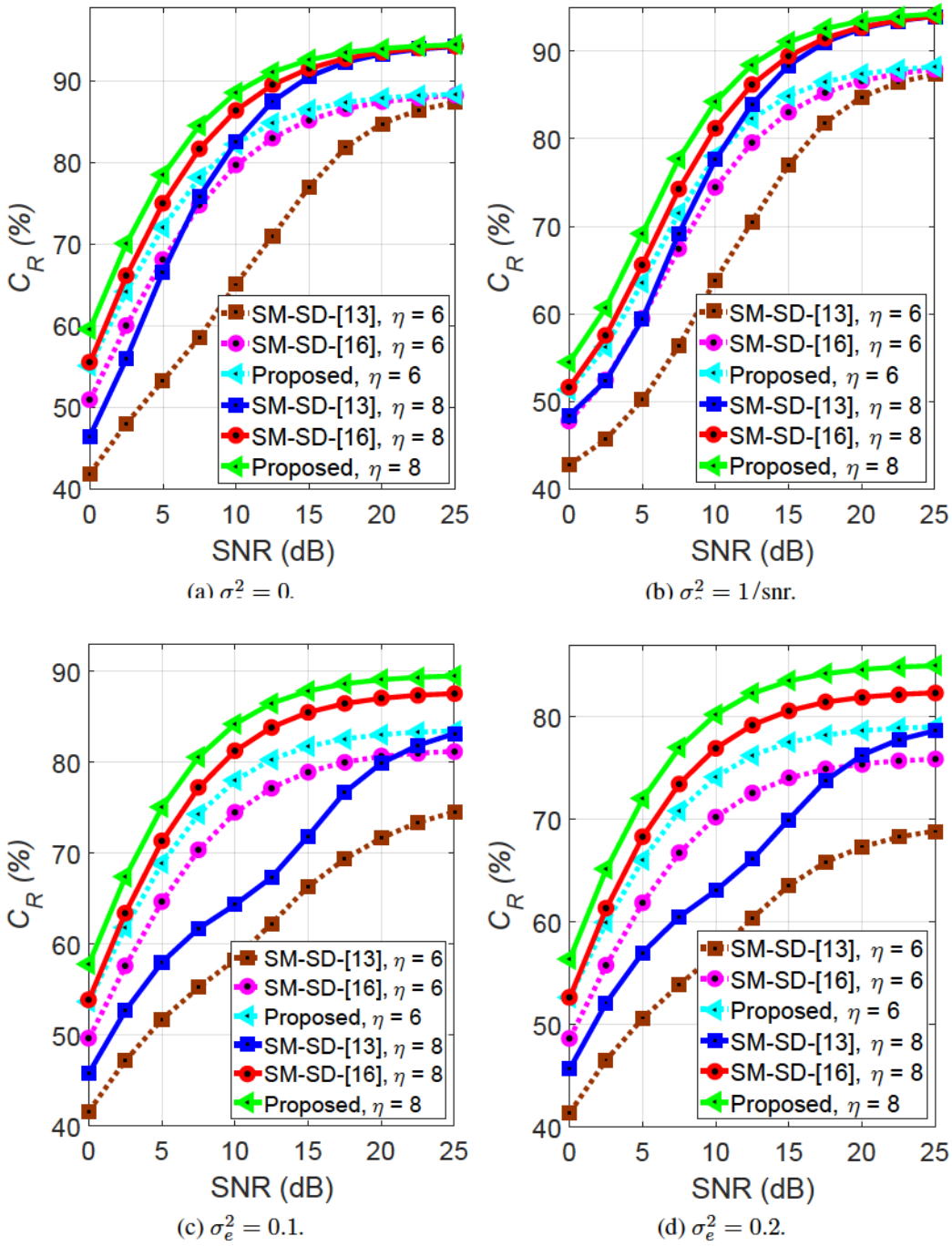

(a) $\sigma_e^2 = 0$. (b) $\sigma_e^2 = 1/\text{snr}$.

(c) $\sigma_e^2 = 0.1$. (d) $\sigma_e^2 = 0.2$.

Fig. 4.12: Complexity reduction comparison of over-determined SM-MIMO system for different decoders.

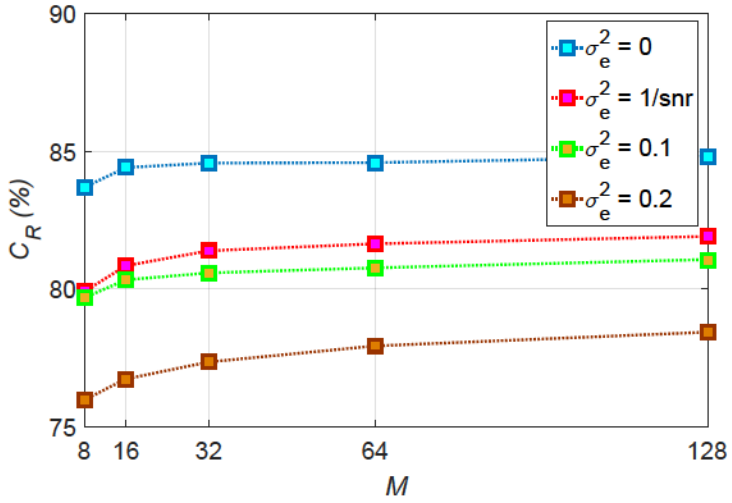

Fig. 4.13: Complexity reduction of the proposed m-M algorithm for $N_t = N_r = 16$ and variable M.

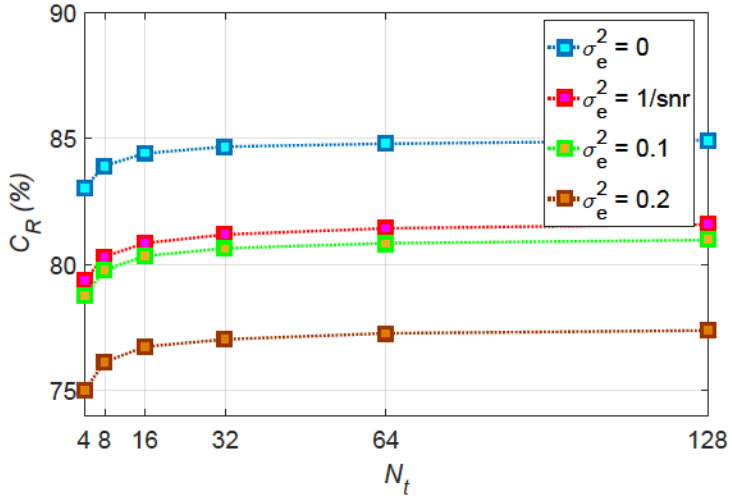

Fig. 4.14: Complexity reduction of the proposed m-M algorithm for $M = N_r = 16$ and variable N_t.

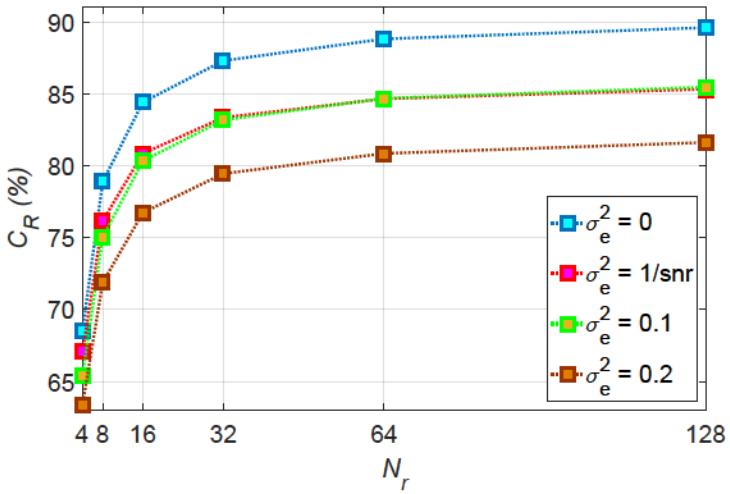

Fig. 4.15: Complexity reduction of the proposed m-M algorithm for $N_t = M = 16$ and variable N_r.

References

[1] I. Al-Nahhal, O. A. Dobre, and S. Ikki, "Low complexity decoders for spatial and quadrature spatial modulations," in *Proc. IEEE Veh. Technol. Conf. (VTC-Spring)*, 2018, pp. 1–5.

[2] E. Telatar, "Capacity of multi-antenna Gaussian channels," *European Trans. Telecommun.*, vol. 10, no. 6, pp. 585–595, Nov.-Dec. 1999.

[3] C.-X. Wang et al., "Cellular architecture and key technologies for 5G wireless communication networks," *IEEE Commun. Mag.*, vol. 52, no. 2, pp. 122–130, Feb. 2014.

[4] M. Renzo, H. Haas, A. Ghrayeb, S. Sugiura, and L. Hanzo, "Spatial modulation for generalized MIMO: Challenges, opportunities and implementation," *Proc. IEEE*, vol. 102, no. 1, pp. 56–103, Jan. 2014.

[5] E. Basar, "Index modulation techniques for 5G wireless networks," *IEEE Commun. Mag.*, vol. 54, no. 7, pp. 168–175, Jul. 2016.

[6] R. Mesleh, H. Haas, S. Sinanovic, C. W. Ahn, and S. Yun, "Spatial modulation," *IEEE Trans. Veh. Technol.*, vol. 57, no. 4, pp. 2228–2241, July 2008.

[7] J. Jeganathan, A. Ghrayeb, and L. Szczecinski, "Spatial modulation: Optimal detection and performance analysis," *IEEE Commun. Lett.*, vol. 12, no. 8, pp. 545–547, Aug. 2008.

[8] E. Basar, Ü. Aygölü, E. Panayırcı, and H. V. Poor, "Space-time block coded spatial modulation," *IEEE Trans. Commun.*, vol. 59, no. 3, pp. 823–832, Mar. 2011.

[9] M. Di Renzo, H. Haas, and P. M. Grant, "Spatial modulation for multiple-antenna wireless systems: A survey," *IEEE Commun. Mag.*, vol. 49, no. 12, pp. 182–191, Dec. 2011.

[10] J. G. Andrews, S. Buzzi, W. Choi, S. V. Hanly, A. Lozano, A. C. Soong, and J. C. Zhang, "What will 5G be?" *IEEE J. Sel. Areas Commun.*, vol. 32, no. 6, pp. 1065–1082, Jun. 2014.

[11] A. Younis, R. Mesleh, H. Haas, and P. M. Grant, "Reduced complexity sphere decoder for spatial modulation detection receivers," in *Proc. IEEE GLOBECOM*, 2010, pp. 1–5.

[12] A. Younis, M. Di Renzo, R. Mesleh, and H. Haas, "Sphere decoding for spatial modulation," in *Proc. 2011 IEEE Int. Conf. Commun.*, pp. 1–6.

[13] A. Younis, S. Sinanovic, M. Di Renzo, R. Mesleh, and H. Haas, "Generalised sphere decoding for spatial modulation," *IEEE Trans. Commun.*, vol. 61, no. 7, pp. 2805–2815, July 2013.

[14] Q. Tang, Y. Xiao, P. Yang, Q. Yu, and S. Li, "A new low-complexity near-ml detection algorithm for spatial modulation," *IEEE Wireless Commun. Lett.*, vol. 2, no. 1, pp. 90–93, Feb. 2013.

[15] L. Xiao, P. Yang, S. Fan, S. Li, L. Song, and Y. Xiao, "Low-complexity signal detection for large-scale quadrature spatial modulation systems," *IEEE Commun. Lett.*, vol. 20, pp. 2173-2176, Nov. 2016.

[16] I. Al-Nahhal, O. A. Dobre, and S. Ikki, "Quadrature spatial modulation decoding complexity: Study and reduction," *IEEE Wireless Commun. Lett.*, vol. 6, pp. 378-381, Jun. 2017.

[17] X. Zhang, Y. Zhang, C. Liu, and H. Jia, "Low-complexity detection algorithms for spatial modulation MIMO systems," *Hindawi Journal of Electrical and Computer Engineering*, doi:10.1155/2018/4034625, 2018.

[18] P. Yang, M. Di Renzo, Y. Xiao, S. Li, and L. Hanzo, "Design guidelines for spatial modulation," *IEEE Commun. Surveys Tuts.*, vol. 17, pp. 6–26, 1st Quart. 2015.

[19] E. Viterbo and J. Boutros, "A universal lattice code decoder for fading channels," *IEEE Trans. Inf. Theory*, vol. 45, no. 5, pp. 1639–1642, Jul. 1999.

[20] B. Hassibi and H. Vikalo, "On the sphere-decoding algorithm I. Expected complexity," *IEEE Trans. Signal Process.*, vol. 53, no. 8, pp. 2806–2818, Aug. 2005.

[21] A. Das and B. D. Rao, "SNR and noise variance estimation for MIMO systems," *IEEE Trans. Signal Process.*, vol. 60, no. 8, pp. 3929–3941, Aug. 2012.

[22] F. Bellili, R. Meftehi, S. Affes, and A. Stéphenne, "Maximum likelihood snr estimation of linearly-modulated signals over time-varying flat-fading simo channels," *IEEE Trans. Signal Process.*, vol. 63, no. 2, pp. 441–456, Jan. 2015.

[23] J. Proakis, *Digital Communications Systems Engineering*, 4th ed. McGraw-Hill, New Yourk, 2000.

[24] P. C. Sofotasios, S. Muhaidat, G. K. Karagiannidis, and B. S. Sharif, "Solutions to integrals involving the Marcum Q-function and applications," *IEEE Signal Process. Lett.*, vol. 22, no. 10, pp. 1752–1756, Oct. 2015.

[25] Y. A. Brychkov, *Handbook of Special Functions: Derivatives, Integrals, Series and other Formulas*, CRC, Florida, USA, 2008.

[26] J. Wu and C. Xiao, "Optimal diversity combining based on linear estimation of Rician fading channels," *IEEE Trans. Commun.*, vol. 56, no. 10, pp. 1612–1615, Oct. 2008.

[27] E. Basar, Ü. Aygölü, E. Panayırcı, and H. V. Poor, "Performance of spatial modulation in the presence of channel estimation errors," *IEEE Commun. Lett.*, vol. 16, no. 2, pp. 176–179, Feb. 2012.

[28] A. Leon-Garcia, *Probability, Statistics, and Random Processes for Electrical Engineering*, 3rd ed. Pearson/Prentice Hall Upper Saddle River, NJ, 2008.

[29] V. Tarokh, A. Naguib, N. Seshadri, and A. Calderbank, "Space-time codes for high data rate wireless communication: performance criteria in the presence of channel estimation errors, mobility, and multiple paths," *IEEE Trans. Commun.*, vol. 47, no. 2, pp. 199–207, Feb. 1999.

[30] M. Biguesh and A. B. Gershman, "MIMO channel estimation: Optimal training and tradeoffs between estimation techniques," in *Proc. ICC*, Paris, France, June 2004, vol. 5, pp. 2658-2662.

[31] M. Biguesh, and A. B. Gershman, "Training based MIMO channel estimation: A study of estimator tradeoffs and optimal training signals," *IEEE Trans. Signal Process.*, vol. 54, pp. 884-893, Mar. 2006.

[32] W. Liu, N. Wang, M. Jin, and H. Xu, "Denoising detection for the generalized spatial modulation system using sparse property," *IEEE Commun. Lett.*, vol. 18, no. 1, pp. 22–25, Jan. 2014.

[33] L. Xiao et al., "Compressive sensing assisted spatial multiplexing aided spatial modulation," *IEEE Trans. Wireless Commun.*, vol. 17, no. 2, pp. 794–807, Feb. 2018.

[34] C. Wang, P. Cheng, Z. Chen, J. A. Zhang, Y. Xiao, and L. Gui, "Near ML low-complexity detection for generalized spatial modulation," *IEEE Commun. Lett.*, vol. 20, no. 3, pp. 618–621, Mar. 2016.

[35] A. Younis, N. Serafimovski, R. Mesleh, and H. Haas, "Generalised spatial modulation," in *Proc. Forty Fourth Asilomar Conf. Signals, Syst., Comput. (ASILOMAR)*, Nov. 2010, pp. 1498–1502.

[36] R. Mesleh, S. S. Ikki, and H. M. Aggoune, "Quadrature spatial modulation," *IEEE Trans. Veh. Technol.*, vol. 64, no. 6, pp. 2738–2742, Jun. 2015.

Chapter 5

Reliable Detection for Spatial Modulation Systems

5.1 Abstract

Spatial modulation (SM) is a promising multiple-input multiple-output system used to increase spectral efficiency. The maximum likelihood (ML) decoder jointly detects the transmitted SM symbol, which is of high complexity. In this chapter, a novel reliable sphere decoder (RSD) algorithm based on tree-search is proposed for the SM system. The basic idea of the proposed RSD algorithm is to reduce the size of the tree-search, and then, a smart searching method inside the reduced tree-search is performed to find the solution. The proposed RSD algorithm provides a significant reduction in decoding complexity compared to the ML decoder and existent decoders as well. Moreover, the RSD algorithm provides a flexible trade-off between the bit error rate (BER) performance and decoding complexity, so as to be reliable for a wide range of practical hardware implementations. The BER performance and decoding complexity analysis for the RSD algorithm are studied, and Monte Carlo simulations are then provided to demonstrate the findings.

5.2 Introduction

Spatial modulation (SM) is a promising technique [1] that has been recently applied to many of the emerging technologies [2], [3]. It overcomes the inter-channel interference (ICI) problem that exists in multiple-input multiple-output (MIMO) systems. The SM system completely eliminates the ICI by delivering a phase-shift-keying (PSK) or quadrature amplitude modulation (QAM) symbol from only one transmit antenna at a time. A part of the input bit-stream determines an active transmit antenna, while the rest determines the PSK/QAM symbol to be delivered from the activated antenna [4], [5]. At the receiver, the maximum-likelihood (ML) decoder is applied to obtain the optimum bit error rate (BER) at the expense of the decoding complexity [6].

Several low-complexity decoding algorithms have been recently proposed in [7]-[12] to reduce the high decoding complexity of the ML decoder. In [7] and [8], the sphere decoder (SD) concept is utilized to reduce the decoding complexity without sacrificing the optimum BER performance. A low-complexity decoding algorithm has been proposed in [9] and extended in [10] by exploiting a smart searching algorithm in the tree-search to obtain the optimum BER performance. The authors in [11] and [12] proposed low-complexity decoders by sacrificing the optimality of the BER performance. The existing SD algorithms suffer from a lack of reliability when it comes to fitting the practical hardware implementation requirements. In other words, the existing algorithms do not provide a suitable trade-off between the BER performance and decoding complexity.

This chapter proposes a novel and reliable SD (RSD) algorithm that provides an advantageous arrangement between the BER performance and decoding complexity. Besides, the proposed RSD algorithm can achieve the optimum BER performance with a significant reduction in the decoding complexity compared to the ML decoder and the existing algorithms as well. The analytical BER analysis and expected decoding complexity of the proposed

algorithm are provided and confirmed through Monte Carlo simulations.

5.3 System Model

Consider an $N_r \times N_t$ SM-MIMO system, where N_r and N_t represent the number of transmit and receive antennas, respectively. SM delivers $\log_2(N_t M)$ bit per channel use, where M is the modulation order of the QAM constellation. The input bit-stream is split into two groups: the first $\log_2(N_t)$ bits select the active antenna, while the second $\log_2(M)$ bits determine the QAM symbol to be transmitted, $s_t \in \{s_1, \cdots, s_M\}$. The SM transmitted message, $\boldsymbol{x}_t$, is equal to $\boldsymbol{h}_t s_t$, where $\boldsymbol{h}_t$ is a vector of the Rayleigh fading channel coefficients with entries distributed as $\mathcal{CN}(0,1)$ and drawn from the channel matrix, $\boldsymbol{H} \in \mathbb{C}^{N_r \times N_t}$. The received signal is

$$\boldsymbol{y} = \boldsymbol{x}_t + \boldsymbol{g}, \tag{5.1}$$

where $\boldsymbol{g} \sim \mathcal{CN}(0, \sigma_g^2)$ is the vector of additive white Gaussian noise (AWGN) samples.

At the receiver side, the ML decoder estimates the transmitted SM message, $\hat{\boldsymbol{x}}_{\text{ML}}$, as [6]

$$\hat{\boldsymbol{x}}_{\text{ML}} = \underset{\boldsymbol{x}_j | j=1,\cdots,MN_t}{\arg\min} \|\boldsymbol{y} - \boldsymbol{x}_j\|^2 = \underset{\boldsymbol{x}_j | j=1,\cdots,MN_t}{\arg\min} \sum_{i=1}^{N_r} |y_i - x_{i,j}|^2. \tag{5.2}$$

The tree-search structure [8], [10] can be used to represent (5.2). The tree-search is a two-dimensional structure with a size of $N_r \times MN_t$; the tree-search width represents the MN_t possibilities of the SM message called branches, while its depth represents the N_r levels of each possibility of the SM message. Fig. 5.1 shows a tree-search example of the ML decoder for $M = 2$, $N_t = 4$, and $N_r = 6$. The accumulated distance metric vector of the i-th level, $\boldsymbol{v}(i) \in \mathbb{R}^{1 \times MN_t}$, is

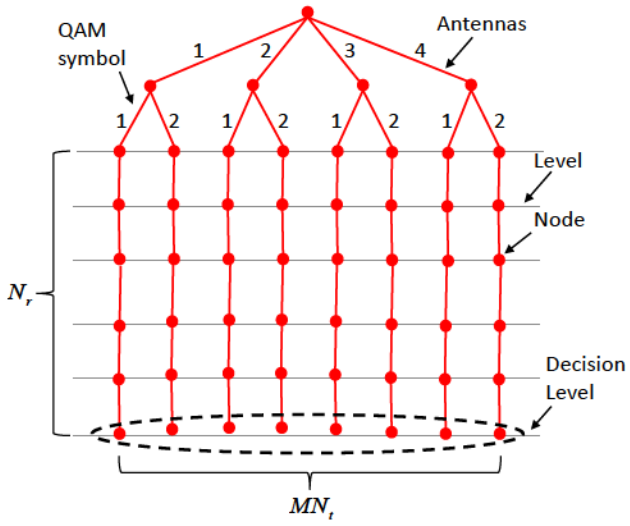

Fig. 5.1: Tree-search of SM-MIMO for $M = 2$, $N_t = 4$, and $N_r = 6$.

$$\boldsymbol{v}(i) = \left[\sum_{n=1}^{i} |y_n - x_{n,1}|^2 \cdots \sum_{n=1}^{i} |y_n - x_{n,MN_t}|^2 \right]. \tag{5.3}$$

Typically, the last level of the tree-search is called the *decision level*. The ML decoder estimates $\hat{\boldsymbol{x}}_{\text{ML}}$ that corresponds to the minimum node in $\boldsymbol{v}(N_r)$ (i.e., at the decision level when $i = N_r$ in (5.3)).

In this chapter, the decoding complexity is defined as the total number of nodes that should be visited in the tree-search to estimate the transmitted SM message. Since the ML decoder visits all nodes in the tree-search, its decoding complexity is $\Psi^{\text{ML}} = MN_tN_r$. The complexity of the ML decoder consequently becomes largely excessive, especially for higher SM-MIMO dimensions and/or QAM sizes. Several works in the literature have been proposed to reduce the ML complexity, which are based on tree-search and SD concepts. However, further complexity reduction can still be achieved, as well as progress towards its reliability to fit a wide range of hardware implementation.

5.4 The Proposed RSD Algorithm

The proposed RSD algorithm firstly reduces the size of the tree-search, and then performs a smart searching method to reach the solution. Let us define ψ_{col} as the number of branches/SM message possibilities that most likely contains the optimum solution. The RSD algorithm performs its searching for the solution inside these ψ_{col} branches and stops at the ψ_{row}-th level, where $1 \leq \psi_{\text{row}} \leq N_r$ is the maximum number of levels that can be visited by the RSD algorithm (i.e., the decision level at ψ_{row}). It is worth noting that the flexibility trade-off between the BER performance and complexity provided by the RSD algorithm comes from changing the value of ψ_{row} within the range of 1 and N_r.

The steps of searching for the solution of the RSD algorithm inside the reduced tree-search are as follows:

Step 1: Expand all nodes of the first level, i.e., $\boldsymbol{v}(1)$ in (5.3).

Step 2: Appropriately choose the smallest ψ_{col} nodes that come from ***Step 1***. It should be noted that the RSD algorithm searches for the solution inside the branches that correspond to the smallest ψ_{col} nodes. Consequently, the RSD algorithm reduces the decoding complexity by at least $(MN_t - \psi_{\text{col}})\psi_{\text{row}}$ nodes. The vector of distance metric nodes in (5.3) yields

$$\boldsymbol{v}(i) = \begin{bmatrix} v(i,1) & \cdots & v(i,j) & \cdots & v(i,\psi_{\text{col}}) \end{bmatrix}, \tag{5.4}$$

where $v(i,j)$ is the j-th node of level i, and given by

$$v(i,j) = \sum_{n=1}^{i} |y_n - x_{n,j}|^2 . \tag{5.5}$$

Step 3: Perform a single expansion to the minimum node in (5.4).

Step 4: Check if the expanded node from ***Step 3*** still has a minimum value among the rest of ψ_{col} nodes or not. If yes, perform another single expansion to that node. If no, find the new minimum node and expand it once.

Algorithm 5.1 The proposed RSD algorithm pseudo-code.

- **Input** $\boldsymbol{H}$, M, and N_t;
- **Compute** $\boldsymbol{v}(1)$ in (5.3);
- **Choose** ψ_{col} empirically, based on M and N_t to most likely include the optimum BER performance;
- **Store** the branches indices that corresponding to the smallest ψ_{col} node of $\boldsymbol{v}(1)$ into $\Xi_{\psi_{\text{col}}}$;
- **Choose** ψ_{row} based on the system requirements from the BER and complexity points of views;
- **Define** $\text{Len}(j)$ as the length of the j-th branch and initiate it with one for $\forall j$;

1: ***While*** $n < \psi_{\textit{row}}\psi_{\textit{col}}$ ***do***
2: **Find** j_{min} that solves $\underset{\substack{j \in \Xi_{\psi_{\text{col}}} \\ i_{\text{min}} \in \{1, \cdots, \psi_{\text{row}}\}}}{\arg\min} \{\boldsymbol{v}(i_{\text{min}})\}$;
3: **Update** i_{min} as the level that corresponding to j_{min};
4: ***if*** $\text{Len}(j_{\text{min}}) == \psi_{\text{row}}$
5: **break** and end the algorithm;
6: ***else***
7: **Expand** $v(i_{\text{min}}, j_{\text{min}}) \leftarrow v(i_{\text{min}} + 1, j_{\text{min}})$;
8: **Update** $\boldsymbol{v}(i_{\text{min}})$ based on $v(i_{\text{min}}, j_{\text{min}})$;
9: ***end if***
10: **Set** $n \leftarrow n + 1$;
11: ***end While***

- **Output** $\hat{\boldsymbol{x}}_{\text{RSD}} = \underset{j \in \Xi_{\psi_{\text{col}}}}{\arg\min} \{\boldsymbol{v}(\psi_{\text{row}})\}$.

Step 5: Repeat ***Step 3*** and ***Step 4*** until the RSD algorithm obtains the minimum node at a branch with a length of ψ_{row}.

Step 6: Find the index corresponding to the node that comes from ***Step 5***, and declare it as the solution of the RSD algorithm. The estimated SM message using the RSD algorithm, $\hat{\boldsymbol{x}}_{\text{RSD}}$, can be given as

$$\hat{\boldsymbol{x}}_{\text{RSD}} = \underset{\boldsymbol{x}_j | j \in \Xi_{\psi_{\text{col}}}}{\arg\min} \sum_{i=1}^{\psi_{\text{row}}} |y_i - x_{i,j}|^2 = \underset{j \in \Xi_{\psi_{\text{col}}}}{\arg\min} \{\boldsymbol{v}(\psi_{\text{row}})\}, \tag{5.6}$$

where $\Xi_{\psi_{\text{col}}}$ denotes the set of branch indices that corresponds to the smallest ψ_{col} metric node values of $\boldsymbol{v}(1)$ (i.e., the first level at $i = 1$ in (5.3)). The RSD algorithm is summarized in Algorithm 5.1.

5.5 Theoretical Analysis

The RSD algorithm provides the optimum BER performance with a significant reduction in the decoding complexity. In addition, by changing the value of ψ_{row}, a flexible trade-off between the BER performance and decoding complexity can be obtained to fit a wide range of hardware implementation. In this section, the BER performance and expected complexity are considered random variables, and their approximate expressions are derived using the probability theory.

5.5.1 BER Upper Bound Analysis

The general expression for the upper bound of the ML BER for SM is [6], [13]

$$\text{BER}^{\text{ML}} \leq \sum_{j=1}^{MN_t} \sum_{\hat{j}=1}^{MN_t} \frac{\delta(\boldsymbol{x}_j, \hat{\boldsymbol{x}}_{\hat{j}}) \mathbb{E}\left\{\mathbb{P}\text{r}^{\text{ML}}\left(\boldsymbol{x}_j \rightarrow \hat{\boldsymbol{x}}_{\hat{j}}\right)\right\}}{MN_t \log_2(MN_t)}, \tag{5.7}$$

where $\mathbb{P}\text{r}^{\text{ML}}(\boldsymbol{x}_j \rightarrow \hat{\boldsymbol{x}}_{\hat{j}})$ is the pairwise error probability (PEP) of the ML algorithm, $\mathbb{P}\text{r}(.)$ denotes the probability of an event, $\mathbb{E}\{\cdot\}$ represents the expectation operation, and $\delta(\boldsymbol{x}_j, \hat{\boldsymbol{x}}_{\hat{j}})$ denotes the Hamming distance which measures the number of bits in error between $\boldsymbol{x}_j$ and $\hat{\boldsymbol{x}}_{\hat{j}}$.

Since the RSD algorithm performs the search inside a portion of the tree-search with a

size of $\psi_{\text{row}} \times \psi_{\text{col}}$, the optimal solution may not be included in that portion of the tree-search. Thus, the PEP in (5.7) for the RSD algorithm can be written as

$$\mathbb{P}\text{r}^{\text{RSD}}\left(\boldsymbol{x}_j \to \hat{\boldsymbol{x}}_{\hat{j}}\right) = \mathbb{P}\text{r}\left(\hat{\boldsymbol{x}}_{\text{opt}} \neq \boldsymbol{x}_t | \hat{\boldsymbol{x}}_{\text{opt}} \in \Xi_{\psi_{\text{col}}}\right) + \mathbb{P}\text{r}\left(\hat{\boldsymbol{x}}_{\text{opt}} \notin \Xi_{\psi_{\text{col}}}\right), \tag{5.8}$$

where $\hat{\boldsymbol{x}}_{\text{opt}}$ is the optimal solution. The conditional probability in (5.8) contains two independent events. The expected value of (5.8) can consequently be written as

$$\mathbb{E}\left\{\mathbb{P}\text{r}^{\text{RSD}}\left(\boldsymbol{x}_j \to \hat{\boldsymbol{x}}_{\hat{j}}\right)\right\} = \underbrace{\mathbb{E}\left\{\mathbb{P}\text{r}\left(\hat{\boldsymbol{x}}_{\text{opt}} \neq \boldsymbol{x}_t\right)\right\}}_{\text{Term 1}} + \underbrace{\mathbb{E}\left\{\mathbb{P}\text{r}\left(\hat{\boldsymbol{x}}_{\text{opt}} \notin \Xi_{\psi_{\text{col}}}\right)\right\}}_{\text{Term 2}}. \tag{5.9}$$

Term 1 in (5.9) can be written as in [6], [13]

$$\mathbb{E}\left\{\mathbb{P}\text{r}\left(\hat{\boldsymbol{x}}_{\text{opt}} \neq \boldsymbol{x}_t\right)\right\} = \mu_{j,\hat{j}}^{\psi_{\text{row}}} \sum_{k=0}^{\psi_{\text{row}}-1} \binom{\psi_{\text{row}} - 1 + k}{k} \left(1 - \mu_{j,\hat{j}}\right)^k, \tag{5.10}$$

with

$$\mu_{j,\hat{j}} = 0.5\left(1 - \sqrt{\frac{\sigma_{j,\hat{j}}^2}{1 + \sigma_{j,\hat{j}}^2}}\right), \quad \sigma_{j,\hat{j}}^2 = \frac{\rho(|s(j)|^2 + |s(\hat{j})|^2)}{4}, \tag{5.11}$$

where ρ is the average signal to noise ratio (SNR), and $s(j)$ is the QAM symbol of the j-th SM transmitted message. Hence, for the RSD algorithm, (5.7) can be written as

$$\text{BER}^{\text{RSD}} \leq \sum_{j=1}^{\psi_{\text{col}}} \sum_{\hat{j}=1}^{\psi_{\text{col}}} \frac{\delta(\boldsymbol{x}_j, \hat{\boldsymbol{x}}_{\hat{j}})}{MN_t \log_2(MN_t)}$$

$$\times \left[\left[\mu_{j,\hat{j}}^{\psi_{\text{row}}} \sum_{k=0}^{\psi_{\text{row}}-1} \binom{\psi_{\text{row}} - 1 + k}{k} \left(1 - \mu_{j,\hat{j}}\right)^k\right] + \mathbb{E}\left\{\mathbb{P}\text{r}\left(\hat{\boldsymbol{x}}_{\text{opt}} \notin \Xi_{\psi_{\text{col}}}\right)\right\}\right]. \tag{5.12}$$

Based on (5.12), the RSD algorithm provides a near optimum BER performance when Term 2 in (5.9) approaches zero (i.e., $\mathbb{P}\mathrm{r}(\hat{\boldsymbol{x}}_{\text{opt}} \notin \Xi_{\psi_{\text{col}}}) \approx 0$); this can be achieved by properly choosing ψ_{col}. In this chapter, ψ_{col} is empirically chosen such that $\mathbb{P}\mathrm{r}(\hat{\boldsymbol{x}}_{\text{opt}} \notin \Xi_{\psi_{\text{col}}}) \approx 0$.

5.5.2 Expected Complexity Analysis

In this chapter, the complexity of the RSD algorithm is measured by the number of visited nodes in the tree-search needed to estimate the solution. In general, the complexity of the SD algorithms is a random variable. The general approximation for the expected SD complexity is [10]

$$\Psi^{\text{SD}} \approx MN_t + \sum_{j=1}^{MN_t} \sum_{i=1}^{N_r} \mathbb{P}\mathrm{r}\left(v(i,j) \leq \zeta \,\middle|\, \boldsymbol{x}_t, \mathbf{H}, \sigma_g^2, \zeta\right), \tag{5.13}$$

where Ψ^{SD} is the expected complexity of an SD algorithm and ζ is the pruned radius (i.e., threshold) of that algorithm. It should be noted that (5.13) represents the general expression and its solution depends on the algorithm itself.

To find the conditional probability in (5.13) for the RSD algorithm, the distributions of $v(i,j)$ and ζ should be defined. From (5.5), $v(i,j)$ has a non-central chi-square distribution with $2i$ degrees of freedom. Thus, the closed-form of the conditional probability in (5.13) is [14, (Ch. 2)]

$$\mathbb{P}\mathrm{r}\left(v(i,j) \leq \zeta \,\middle|\, \boldsymbol{x}_t, \mathbf{H}, \sigma_g^2, \zeta\right) = 1 - Q_i\left(\frac{\sqrt{2\gamma_{i,j}^2}}{\sigma_g}, \frac{\sqrt{2\zeta}}{\sigma_g}\right), \tag{5.14}$$

where $\gamma_{i,j}^2 = \sum_{n=1}^{i} |x_{n,t} - x_{n,j}|^2$, $x_{n,j}$ is the n-th element of the j-th SM transmitted message, and $Q_i(\centerdot, \centerdot)$ is the Marcum Q-function.

To remove the dependency of (5.14) on ζ, the expectation operation should be applied for (5.14) over the distribution of ζ. For simplicity, let us assume that the RSD algorithm

most likely reaches the optimum solution. Thus, the pruned radius can be given from $\zeta = \sum_{i=1}^{\psi_{\text{row}}} |g_i|^2$, where g_i denotes the i-th element of the AWGN vector in (5.1). It is worth noting that this simplified assumption of ζ is especially for high SNR. The distribution of ζ is a central chi-square with $2\psi_{\text{row}}$ degrees of freedom and its probability density function, $f_\zeta(\zeta)$, is [14, (Ch. 2)]

$$f_\zeta(\zeta) = \frac{(\zeta)^{\psi_{\text{row}}-1}}{\sigma_g^{2\psi_{\text{row}}}\,(\psi_{\text{row}}-1)!} \exp\left(\frac{-\zeta}{\sigma_g^2}\right). \tag{5.15}$$

Hence, (5.14) yields

$$\Pr\left(v(i,j) \le \zeta \,\middle|\, \boldsymbol{x}_t, \mathbf{H}, \sigma_g^2\right) = 1 - \int_0^\infty Q_i\left(\frac{\sqrt{2\gamma_{i,j}^2}}{\sigma_g}, \frac{\sqrt{2\zeta}}{\sigma_g}\right) \mathrm{d}\zeta. \tag{5.16}$$

The closed-form expression of (5.16) can be given as [15]

$$\Pr\left(v(i,j) \le \zeta \,\middle|\, \boldsymbol{x}_t, \mathbf{H}, \sigma_g^2\right) = 2^i \exp\left(\frac{-\gamma_{i,j}^2}{\sigma_g^2}\right) \sum_{n=0}^{\psi_{\text{row}}-1} \frac{(i)_n}{2^n\, n!}\, {}_1F_1\left(n+i; i; \frac{\gamma_{i,j}^2}{2\sigma_g^2}\right), \tag{5.17}$$

where $(i)_n$ represents the Pochhammer symbol and ${}_1F_1$ is the Kummer hypergeometric function. Since the RSD algorithm searches for the solution inside a reduced tree-search with a size of $\psi_{\text{row}} \times \psi_{\text{col}}$, the approximation of the expected complexity in (5.13) becomes

$$\Psi^{\text{RSD}} \approx \psi_{\text{col}} + \sum_{j=1}^{\psi_{\text{col}}} \sum_{i=1}^{\psi_{\text{row}}} 2^i \exp\left(\frac{-\gamma_{i,j}^2}{\sigma_g^2}\right) \sum_{n=0}^{\psi_{\text{row}}-1} \frac{(i)_n}{2^n\, n!}\, {}_1F_1\left(n+i; i; \frac{\gamma_{i,j}^2}{2\sigma_g^2}\right), \tag{5.18}$$

where Ψ^{RSD} is the expected complexity of the RSD algorithm.

Alternatively, (5.16) can be numerically calculated using the Gauss–Laguerre quadrature [16]. Thus, (5.13) becomes

$$\Psi^{\text{RSD}} \approx \psi_{\text{col}}\left(\psi_{\text{row}}+1\right) - \frac{1}{(\psi_{\text{row}}-1)!}\sum_{j=1}^{\psi_{\text{col}}}\sum_{i=1}^{\psi_{\text{row}}}\sum_{k=1}^{\beta} w_k \left(z_k\right)^{(\psi_{\text{row}}-1)} Q_k\left(\frac{\sqrt{2\gamma_{i,j}^2}}{\sigma_g}, \sqrt{2z_k}\right), \tag{5.19}$$

where w_k and z_k are given values based on the order β, which is given from [16, (Table 25.9)]. Note that (5.19) provides a value close to that in (5.18) with considerably lower execution time.

5.6 Simulation Results

In this section, the BER and decoding complexity of the proposed RSD algorithm are assessed and compared with optimum algorithms in literature, such as [7], [8], and [10]. Two SM-MIMO systems are considered; 16-QAM for 8×8 and 16×16 SM-MIMO, respectively. As mentioned before, ψ_{col} is empirically chosen to provide the optimum BER performance (i.e., $\mathbb{P}\text{r}(\hat{\boldsymbol{x}}_{\text{opt}} \notin \Xi_{\psi_{\text{col}}}) \approx 0$ in (5.12)) at $\psi_{\text{row}} = N_r$, where $\psi_{\text{col}} = 70$ and 180 for the first and second SM-MIMO systems, respectively. The proposed RSD algorithm is denoted by RSD-(ψ_{row},ψ_{col}) to show the values of ψ_{row} and ψ_{col}. Monte Carlo simulations are used to obtain the results by running at least 10^6 Rayleigh flat fading channel realizations. The channel state information at the receiver is assumed to be perfectly known.

5.6.1 Assessment of Expected Complexity for the RSD Algorithm

The expression in (5.19) is evaluated for the two considered SM-MIMO systems using $\beta = 7$. The expected complexity coming from (5.19) provides almost identical results to (5.18), however, with added speed. The corresponding w_k and z_k at $\beta = 7$ are given in [16, (Table 25.9)].

Figures 5.2 and 5.3 depict the average number of visited nodes of the RSD algorithm

for 16-QAM with 8×8 SM-MIMO and 16-QAM with 16×16 SM-MIMO, respectively. By decreasing ψ_{row}, the size of the tree-search decreases and the complexity decreases correspondingly, as shown in the figures. It is also notable that the RSD algorithm requires less complexity to find the solution as the SNR increases. As seen from these figures, the theoretical analysis in (5.19) (or in (5.18)) provides a tight expression for simulation results, for different values of ψ_{row}. Note that (5.19) perfectly matches the simulation results in the higher SNR, which verifies the feasibility of the pruned radius simplification assumption mentioned in Section 5.5.2.

5.6.2 Comparisons with Literature Algorithms

In this subsection, the BER and complexity are compared with those of the literature algorithms (e.g., [7], [8], and [10]). The complexity comparison is assessed by calculating the complexity reduction ratio which is defined as

$$\Psi^{\Omega}_{\text{Reduction}} = \frac{MN_tN_r - \Psi^{\Omega}}{MN_tN_r} = 1 - \frac{\Psi^{\Omega}}{MN_tN_r}, \tag{5.20}$$

where $\Psi^{\Omega}_{\text{Reduction}}$ is the complexity reduction ratio for the $\Omega \in \{\text{RSD, SD-[7], SD-[8], SD-[10]}\}$ algorithm.

Figures 5.4 and 5.5 show the BER performance of the RSD algorithm compared to the optimum algorithms, for 16-QAM with 8×8 SM-MIMO and 16-QAM with 16×16 SM-MIMO, respectively. As shown from these figures, the RSD-(8,70) and RSD-(16,180) provide the same BER as the ML BER performance for 16-QAM with 8×8 SM-MIMO and 16-QAM with 16×16 SM-MIMO, respectively. It should be noted that the SD-[7] and SD-[8] algorithms provide the same BER performance as the ML and SD-[10] algorithms, and their results are omitted for the visibility of figures. Based on the reliable design of the RSD algorithm, sub-optimal BER performances can be obtained by varying the value of

ψ_{row}. The BER analysis in (5.12) is confirmed via simulation results.

Figures 5.6 and 5.7 depict the complexity reduction ratio of all algorithms for 16-QAM with 8×8 SM-MIMO and 16-QAM with 16×16 SM-MIMO, respectively. As seen from these figures, the RSD algorithm provides the best reduction in complexity compared to all existing algorithms. It also offers reliable decoding complexities that vary from 72% to 92% for 16-QAM with 8×8 SM-MIMO and from 68% to 95% for 16-QAM with 16×16 SM-MIMO. This reliability in the decoding can fit a wide range of practical application requirements.

5.7 Conclusion

This chapter proposes a novel reliable algorithm to decode SM transmitted messages. The BER performance and complexity of the proposed algorithm are theoretically derived. The proposed algorithm provides a significant reduction in the decoding complexity (e.g., up to 95%) compared to ML, without sacrificing the BER performance. A flexible trade-off between the BER performance and complexity is presented to demonstrate the reliability of the proposed algorithm.

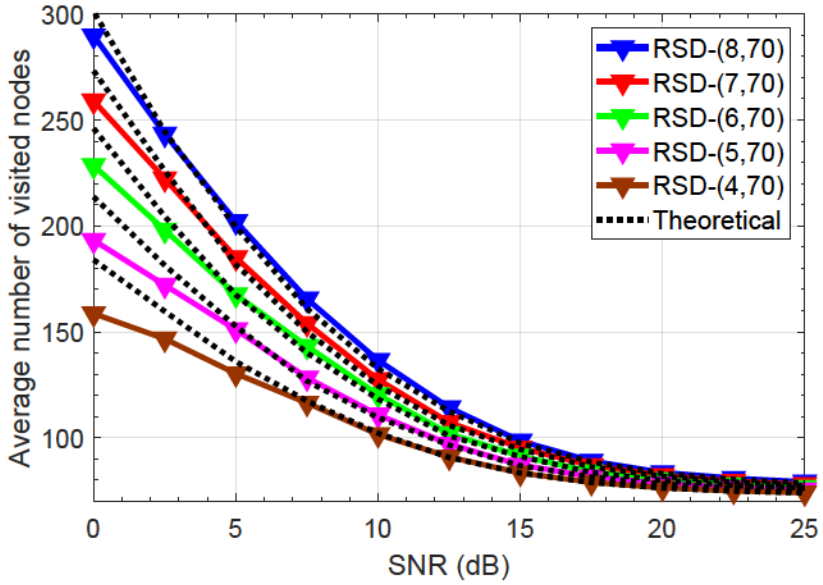

Fig. 5.2: Average number of visited nodes of the proposed RSD algorithm for 16-QAM and 8×8 SM-MIMO system.

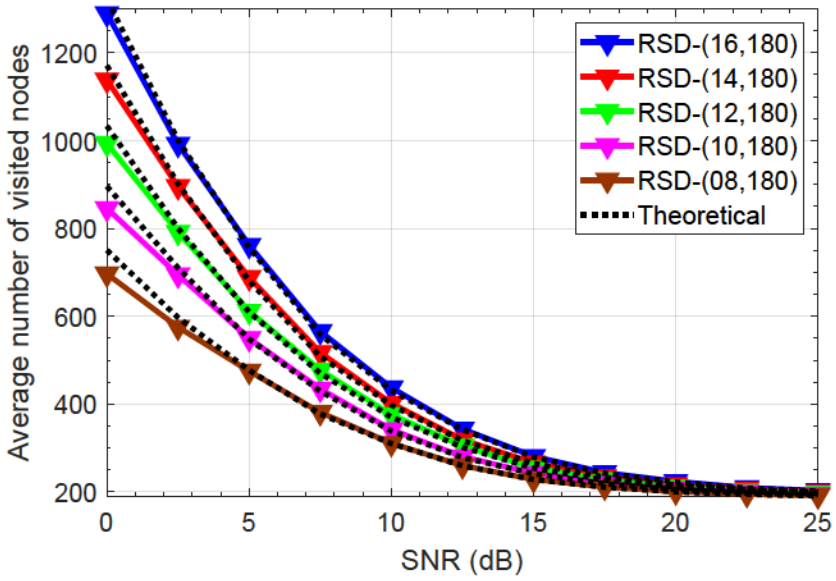

Fig. 5.3: Average number of visited nodes of the proposed RSD algorithm for 16-QAM and 16×16 SM-MIMO system.

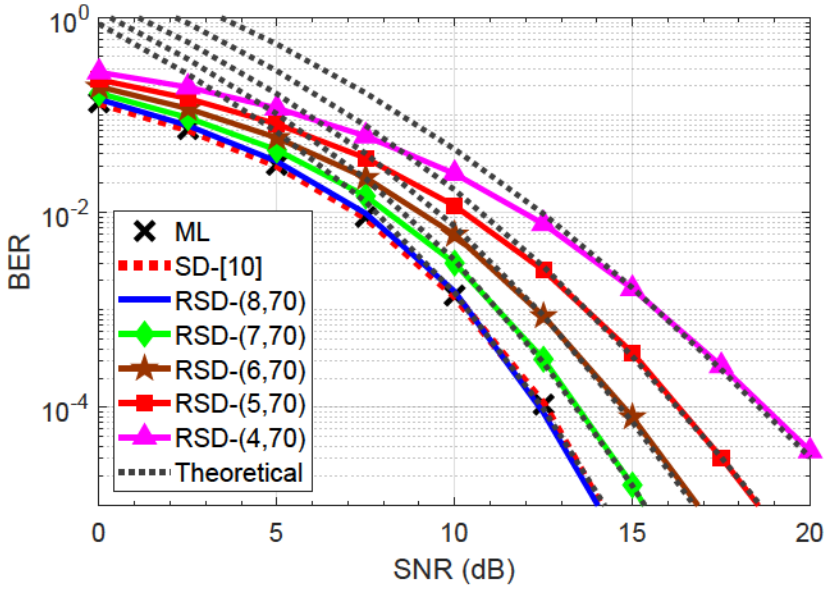

Fig. 5.4: BER comparison for the 16-QAM and 8×8 SM-MIMO system.

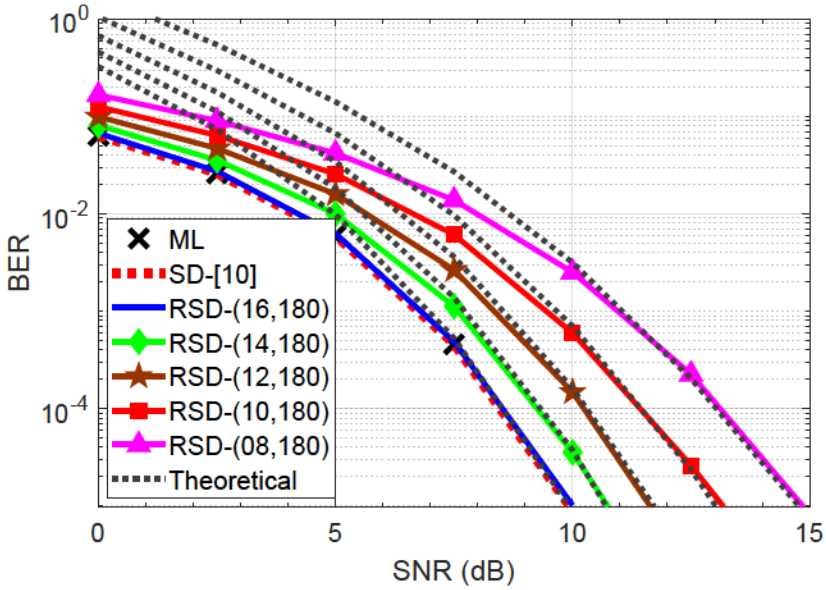

Fig. 5.5: BER comparison for the 16-QAM and 16×16 SM-MIMO system.

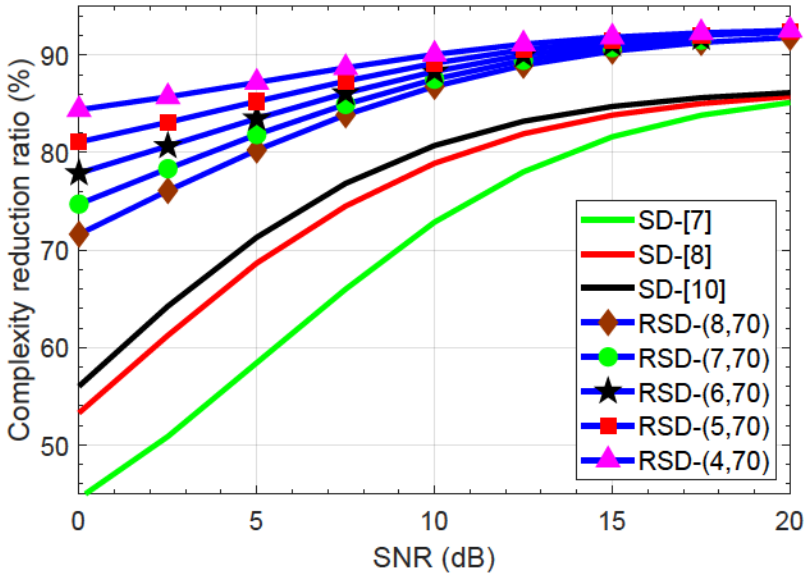

Fig. 5.6: Complexity reduction comparison for the 16-QAM and 8×8 SM-MIMO system.

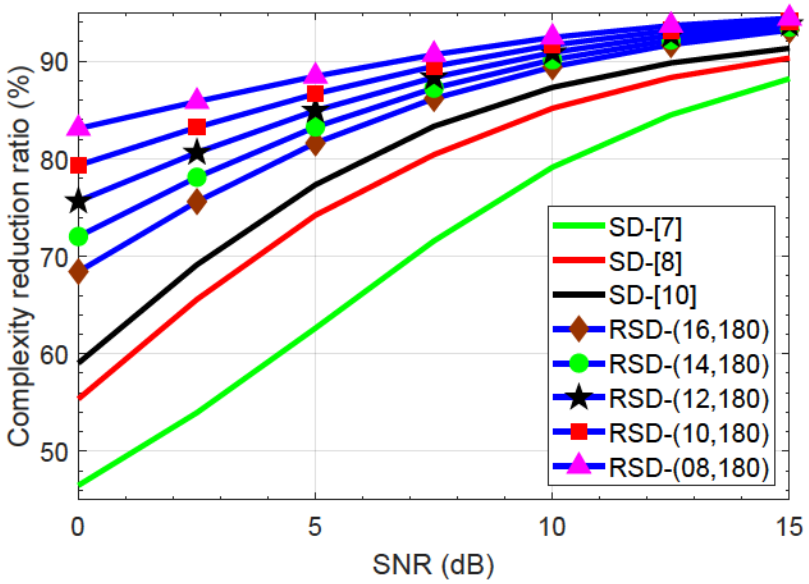

Fig. 5.7: Complexity reduction comparison for the 16-QAM and 16×16 SM-MIMO system.

References

[1] E. Basar, "Index modulation techniques for 5G wireless networks," *IEEE Commun. Mag.,* vol. 54, no. 7, pp. 168–175, Jul. 2016.

[2] Z. Pan, J. Luo, J. Lei, L. Wen, and C. Tang, "Uplink spatial modulation SCMA system," *IEEE Commun. Lett.,* vol. 23, no. 1, pp. 184-187, Jan. 2019.

[3] I. Al-Nahhal, O. A. Dobre, E. Basar, and S. Ikki, "Low-cost uplink sparse code multiple access for spatial modulation," *IEEE Trans. Veh. Technol.*, vol. 68, no. 9, pp. 9313-9317, Jul. 2019.

[4] R. Mesleh, H. Haas, S. Sinanovic, C. W. Ahn, and S. Yun, "Spatial modulation," *IEEE Trans. Veh. Technol.,* vol. 57, no. 4, pp. 2228–2241, July 2008.

[5] M. Di Renzo, H. Haas, and P. M. Grant, "Spatial modulation for multiple-antenna wireless systems: A survey," *IEEE Commun. Mag.*, vol. 49, no. 12, pp. 182–191, Dec. 2011.

[6] E. Basar, U. Aygolu, E. Panayırcı, and H. V. Poor, "Performance of spatial modulation in the presence of channel estimation errors," *IEEE Commun. Lett.,* vol. 16, no. 2, pp. 176–179, Feb. 2012.

[7] A. Younis, S. Sinanovic, M. Di Renzo, R. Mesleh, and H. Haas, "Generalised sphere decoding for spatial modulation," *IEEE Trans. Commun.,* vol. 61, no. 7, pp. 2805–2815, July 2013.

[8] I. Al-Nahhal, O. A. Dobre, and S. Ikki, "Quadrature spatial modulation decoding complexity: Study and reduction," *IEEE Wireless Commun. Lett.,* vol. 6, pp. 378-381, Jun. 2017.

[9] I. Al-Nahhal, O. A. Dobre, and S. Ikki, "Low complexity decoders for spatial and quadrature spatial modulations," in *Proc. IEEE VTC Spring*, Jun. 2018, pp. 1–5.

[10] I. Al-Nahhal, E. Basar, O. A. Dobre, and S. Ikki, "Optimum low-complexity decoder for spatial modulation," *IEEE J. Sel. Areas Commun.*, vol. 37, no. 9, pp. 2001-2013, Jul. 2019.

[11] Q. Tang, Y. Xiao, P. Yang, Q. Yu, and S. Li, "A new low-complexity near-ml detection algorithm for spatial modulation," *IEEE Wireless Commun. Lett.,* vol. 2, no. 1, pp. 90–93, Feb. 2013.

[12] L. Xiao, P. Yang, S. Fan, S. Li, L. Song, and Y. Xiao, "Low-complexity signal detection for large-scale quadrature spatial modulation systems," *IEEE Commun. Lett.,* vol. 20, pp. 2173-2176, Nov. 2016.

[13] R. Mesleh, S. S. Ikki, and H. M. Aggoune, "Quadrature spatial modulation," *IEEE Trans. Veh. Technol.*, vol. 64, pp. 2738–2742, Jun. 2015.

[14] J. Proakis, *Digital Communications Systems Engineering*, 4th ed. McGraw-Hill, New Yourk, 2000.

[15] P. C. Sofotasios, S. Muhaidat, G. K. Karagiannidis, and B. S. Sharif, "Solutions to integrals involving the Marcum Q-function and applications," *IEEE Signal Process. Lett.*, vol. 22, no. 10, pp. 1752–1756, Oct. 2015.

[16] M. Abramowitz and I. A. Stegun, *Handbook of Mathematical Functions with Formulas, Graphs, and Mathematical Tables*, 9th ed. Dover Publications, New York, 1972.

Chapter 6

Low-Cost Uplink Sparse Code Multiple Access for Spatial Modulation

6.1 Abstract

Spatial modulation (SM)-sparse code multiple access (SCMA) systems provide high spectral efficiency (SE) at the expense of using a high number of transmit antennas. To overcome this drawback, this chapter proposes a novel SM-SCMA system operating in uplink transmission, referred to as rotational generalized SM-SCMA (RGSM-SCMA). For the proposed system, the following are introduced: a) transmitter design and its formulation, b) maximum likelihood and maximum a posteriori probability decoders, and c) practical low-complexity message passing algorithm and its complexity analysis. Simulation results and complexity analysis show that the proposed RGSM-SCMA system delivers the same SE with significant savings in the number of transmit antennas, at the expense of close bit error rate and a negligible increase in the decoding complexity, when compared with SM-SCMA.

6.2 Introduction

Sparse code multiple access (SCMA) is a promising non-orthogonal multiple access (NOMA) approach for 5G wireless networks [1]-[3] that has been introduced in [4]. SCMA assigns unique multi-carrier sparse codes to each user to access the medium [5]. The sparsity property of codes enables the application of the message passing algorithm (MPA) at the receiver, to provide near maximum likelihood (ML) bit error rate (BER) performance with lower decoding complexity [6]. The number of interfered users for each sub-carrier is also reduced, allowing more users to be overloaded, hence increasing the spectral efficiency (SE) of the system.

Spatial modulation (SM) is another promising technique that provides high SE with low-complexity signal detection [7], [8]. It increases the SE by assigning part of the input data stream, named spatial symbol, to activate an antenna to transmit the modulation symbol. In [9], generalized SM (GSM) is proposed to overcome the limitation of the high number of transmit antennas required in the SM system.

Recently, for further SE improvement, SM and NOMA have been jointly considered [10]-[12]. Power-domain NOMA, low-density signature, and SCMA have been explored for SM in [10], [11], and [12], respectively. Such systems require an integer power of two transmit antennas to deliver spatial symbols, which comes to be infeasible for higher rate transmission.

This chapter proposes a novel uplink SM system, referred to as rotational GSM (RGSM)-SCMA, which overcomes the previously mentioned drawback of the existing SM-NOMA systems. The models of the proposed RGSM-SCMA transmitter and receiver for the uplink scenario are introduced. ML and maximum *a posteriori* probability (MAP) decoders are provided as theoretical receivers. Additionally, the iterative MPA decoder is presented and analyzed to provide a practical low-complexity detection. The proposed RGSM-SCMA

system enjoys a high SE transmission as the SM-SCMA system with a significant reduction in the number of transmit antennas, which leads to saving resources that can then be used for channel estimation. It is shown that the MPA decoder for the proposed RGSM-SCMA system attains a close BER performance to the MPA of the SM-SCMA system, with nearly the same complexity.

6.3 Related Work and Motivation

In a single-user SM system, the input data stream is transmitted as a combination of spatial symbols and modulated symbols. At the receiver side, the decoder estimates both the spatial and modulated symbols by performing an exhaustive search or by using one of the low-complexity decoding algorithms, such as those in [13]-[15]. For instance, assume that an SM system is equipped with four transmit antennas (i.e., four spatial symbols) and two modulated symbols (i.e., binary phase shift keying). Thus, this system can deliver 3-bits at a time; 2-bits spatial symbol (i.e., $\log_2$(number of transmit antennas)-bits which corresponding to each of the four antennas) and 1-bit modulated symbol. As seen from this example, the number of transmit antenna must be a power of two, which increases exponentially as the SE increases.

For a multi-user SM system, the SCMA technique is used to organize the accessing of the users to the medium. This system is known as SM-SCMA. The SM-SCMA system enjoys a high SE with good BER performance, which is suitable for the future generations of the wireless networks. However, the use of high number of transmit antennas is still required.

In this chapter, I propose a solution to this problem by activating more than one antenna at a time to deliver the same SE of SM-SCMA with a much lower number of transmit antennas. In addition, rotational angles are used to provide a close BER performance to the SM-SCMA.

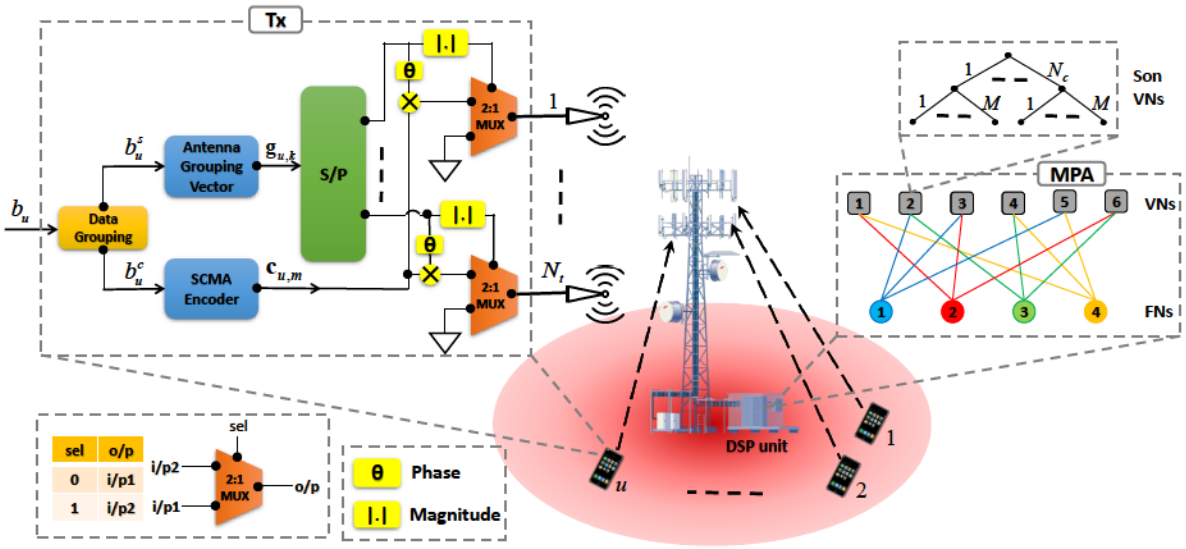

Fig. 6.1: Uplink RGSM-SCMA block diagram for the u-th user.

6.4 RGSM-SCMA System Model

In this section, the RGSM-SCMA system is introduced. Assume that R orthogonal resource elements (OREs), e.g., subcarriers, are overloaded with U users (i.e., $U > R$); each user has a unique sparse codebook, $\mathbf{C}_u \in \mathbb{C}^{R\times M}$, $u = 1, \ldots, U$, which contains M codewords, $\mathbf{c}_{u,m} \in \mathbb{C}^{R\times 1}$, $m = 1, \ldots, M$. $\mathbf{c}_{u,m}$ has d_v non-zero codeword elements in the same positions for each codebook, and vary from one codebook to another. The number of the overlapped users per ORE, d_f, is fixed for $\forall R$. The SE for the u-th user is $\eta_u = \eta_u^s + \eta_u^c$ bit per channel use (bpcu), where η_u^s and η_u^c denote the spatial and code spectral efficiencies, respectively.

Consider that N_t and M are the number of transmit antennas used to deliver η_u^s bpcu and the number of codewords used to deliver η_u^c bpcu, respectively, for each user. It is assumed that the system parameters for all users are the same (i.e., same N_t, SEs and M). In the RGSM-SCMA system, $\eta_u^s = \log_2(N_c)$ bpcu, where $N_c = 2^{n_c}$ antenna combinations, $n_c = \left\lfloor \log_2 \begin{pmatrix} N_t \\ N_a \end{pmatrix} \right\rfloor$, with $\lfloor \cdot \rfloor$ as the floor operation, and $N_a < N_t$ is the number of active antennas at a time, while $\eta_u^c = \log_2(M)$ bpcu.

Fig. 6.1 shows the uplink scenario of the RGSM-SCMA system for the u-th user; the

TABLE 6.1: The RGSM-SCMA antenna grouping vector lookup table for $N_t = 5$, $N_a = 2$, $N_c = 8$, and $\eta_u^s = 3$ bpcu.

$\mathbf{b}_u^s$	k	$\mathbf{g}_{u.k}$
000	1	$[\ 1 \quad 0 \quad 1 \quad 0 \quad 0\ ]$
001	2	$[\ e^{-j\frac{2\pi}{3}} \quad 0 \quad 0 \quad 1 \quad 0\ ]$
010	3	$[\ e^{-j\frac{4\pi}{3}} \quad 0 \quad 0 \quad 0 \quad 1\ ]$
011	4	$[\ 0 \quad 1 \quad e^{-j\frac{\pi}{2}} \quad 0 \quad 0\ ]$
100	5	$[\ 0 \quad e^{-j\frac{2\pi}{3}} \quad 0 \quad e^{-j\frac{2\pi}{3}} \quad 0\ ]$
101	6	$[\ 0 \quad e^{-j\frac{4\pi}{3}} \quad 0 \quad 0 \quad e^{-j\frac{2\pi}{3}}\ ]$
110	7	$[\ 0 \quad 0 \quad e^{-j\pi} \quad e^{-j\frac{4\pi}{3}} \quad 0\ ]$
111	8	$[\ 0 \quad 0 \quad e^{-j\frac{3\pi}{2}} \quad 0 \quad e^{-j\frac{4\pi}{3}}\ ]$

input $\mathbf{b}_u \in \mathbb{B}^{\eta_u}$ bits for the u-th user is divided into two parts: the first $\mathbf{b}_u^s \in \mathbb{B}^{\eta_u^s}$ bits represent the spatial symbol, while the last $\mathbf{b}_u^c \in \mathbb{B}^{\eta_u^c}$ bits represent the code symbol. The SCMA encoder block maps the $\mathbf{b}_u^c$ bits to its corresponding codeword $\mathbf{c}_{u,m}$ and delivers it to the input of all transmit antenna multiplexers. The antenna grouping vector block chooses the antenna grouping vector, $\mathbf{g}_{u,k} \in \mathbb{C}^{1\times N_t}$, $k \in \{1, \ldots, N_c\}$, according to the value of $\mathbf{b}_u^s$ from a predetermined lookup table (Table 6.1 is an example lookup table with $N_t = 5$, $N_a = 2$, $N_c = 8$, and $\mathbf{b}_u^s = 3$ bpcu). It should be noted that $\mathbf{g}_{u,k}$ has N_a non-zero elements that correspond to the N_a active antennas. The serial-to-parallel (S/P) block distributes the zero and non-zero elements of $\mathbf{g}_{u,k}$ at the same time, to the next stage. The magnitude of $\mathbf{g}_{u,k}$, $|\mathbf{g}_{u,k}| \in \mathbb{R}^{1\times N_t}$, is applied to the multiplexers' selector pins, which allow the antennas corresponding to the non-zero elements to transmit $\mathbf{c}_{u,m}$ rotated with the associated rotation angle of $\mathbf{g}_{u,k}$. To ensure maximum distance between the successive angles, they should be equally spaced for each antenna. Thus, the rotation angles of the n_t-th antenna are

$$\theta_{d,n_t} = \frac{-2\,(d-1)\,\pi}{a_{n_t}}, \quad n_t = 1, \ldots, N_t, \quad d = 1, \ldots, a_{n_t}, \tag{6.1}$$

where θ_{d,n_t} denotes the rotation angle of the d-th occurrence of the n_t-th antenna, and a_{n_t} is the number of times that the n_t-th antenna is activated for $\forall k$. For instance, in Table 6.1, the

third antenna (i.e., $n_t = 3$) is activated 4 times (i.e., $a_3 = 4$) at $k = 1,\ 4,\ 7$ and 8. Then, $\theta_{1,3}$, $\theta_{2,3}$, $\theta_{3,3}$ and $\theta_{4,3}$ equal to 0, $\frac{-\pi}{2}$, $-\pi$ and $\frac{-3\pi}{2}$, respectively.

At the receiver side, the noisy received signal for each ORE at the n-th receive antenna, y_n^r, is

$$y_n^r = \sum_{u \in \Lambda_r} \left(\mathbf{h}_{u,n}^r \mathbf{g}_{u,k}^{\mathrm{T}} c_{u,m}^r \right) + n_n^r, \tag{6.2}$$

where $\mathbf{h}_{u,n}^r \in \mathbb{C}^{1 \times N_t}$ denotes the Rayleigh fading channel between the N_t transmit antennas and n-th receive antenna of the u-th user for the r-th ORE, $c_{u,m}^r$ represents the r-th element of the m-th codeword for user u, $n_n^r \sim \mathcal{N}(0, \sigma^2)$ is the Gaussian noise at the r-th ORE of the n-th receive antenna with zero-mean and a variance of σ^2, and Λ_r is the set of indices of the users that share the r-th ORE. The received signals vector, $\mathbf{y}_n$, for all OREs at the n-th receive antenna is

$$\mathbf{y}_n = \sum_{u=1}^{U} \left(\mathrm{diag}\left(\mathbf{h}_{u,n} \mathbf{g}_{u,k}^{\mathrm{T}} \right) \mathbf{c}_{u,m} \right) + \mathbf{n}_n, \tag{6.3}$$

where $\mathbf{y}_n \in \mathbb{C}^{R \times 1} = \left[y_n^1, \ldots, y_n^R \right]^{\mathrm{T}}$, $\mathbf{h}_{u,n} \in \mathbb{C}^{R \times N_t} = \left[\mathbf{h}_{u,n}^{1T}, \ldots, \mathbf{h}_{u,n}^{RT} \right]^{\mathrm{T}}$, $\mathbf{n}_n \in \mathbb{C}^{R \times 1} = \left[n_n^1 \ldots n_n^R \right]^{\mathrm{T}}$, and $\mathrm{diag}\left(\mathbf{h}_{u,n} \mathbf{g}_{u,k}^{\mathrm{T}} \right) \in \mathbb{C}^{R \times R}$ is a diagonal matrix whose r-th diagonal element is $\mathbf{h}_{u,n}^r \mathbf{g}_{u,k}^{\mathrm{T}}$.

6.5 RGSM-SCMA Signal Detection

In this section, the formulation of three decoders for the proposed RGSM-SCMA system is deduced, which are ML, MAP, and MPA decoders.

6.5.1 ML Decoder

The ML decoder performs an exhaustive search for all $(N_c M)^U$ possibilities to provide the optimum BER performance. The ML solution for N_r receive antennas is

$$\left\{\hat{\mathbf{C}}, \hat{\mathbf{G}}\right\} = \underset{\substack{j \in N_c^U \\ l \in M^U}}{\arg\min} \left\{ \sum_{n=1}^{N_r} \left\| \mathbf{y}_n - \sum_{u=1}^{U} \left(\operatorname{diag}\left(\mathbf{h}_{u,n} \mathbf{g}_{u,k(j)}^{\mathrm{T}} \right) \mathbf{c}_{u,m(l)} \right) \right\|^2 \right\}. \tag{6.4}$$

Here, $\hat{\mathbf{C}} \in \mathbb{C}^{R \times U} = [\hat{\mathbf{c}}_{1,m} \dots \hat{\mathbf{c}}_{U,m}]$ denotes the estimated transmitted codewords for all users, with $\hat{\mathbf{c}}_{u,m}$ as the estimated transmitted codeword for the u-th user, and $m(l)$ represents the value of $m \in \{1, \dots, M\}$ at the l-th antenna combination. $\hat{\mathbf{G}} \in \mathbb{C}^{U \times N_t} = [\hat{\mathbf{g}}_{1,k} \dots \hat{\mathbf{g}}_{U,k}]$ denotes the estimated grouping vectors for all users, with $\hat{\mathbf{g}}_{u,k}$ as the estimated grouping vector for the u-th user, and $k(j)$ represents the value of $k \in \{1, \dots, N_c\}$ at the j-th antenna combination.

6.5.2 MAP Decoder

Unlike the ML decoder, the MAP decoder estimates the pair of transmitted codeword and grouping vector, $\{\hat{\mathbf{c}}_{u,m}, \hat{\mathbf{g}}_{u,k}\}$, for each user one-by-one by maximizing *a posteriori* probability of this pair given the received signal as

$$\{\hat{\mathbf{c}}_{u,m}, \hat{\mathbf{g}}_{u,k}\} = \underset{\substack{\hat{\mathbf{c}}_{u,m} \in \mathbf{C}_u \\ \hat{\mathbf{g}}_{u,k} \in \mathbf{G}_u}}{\arg\max} \{P(\{\hat{\mathbf{c}}_{u,m}, \hat{\mathbf{g}}_{u,k}\} | \mathbf{y}_n)\}$$

$$= \underset{\substack{\hat{\mathbf{c}}_{u,m} \in \mathbf{C}_u \\ \hat{\mathbf{g}}_{u,k} \in \mathbf{G}_u}}{\arg\max} \left\{ P\left(\{\hat{\mathbf{c}}_{u,m}, \hat{\mathbf{g}}_{u,k}\}\right) P\left(\mathbf{y}_n | \{\hat{\mathbf{c}}_{u,m}, \hat{\mathbf{g}}_{u,k}\}\right) \right\}$$

$$= \underset{\substack{\hat{\mathbf{c}}_{u,m} \in \mathbf{C}_u \\ \hat{\mathbf{g}}_{u,k} \in \mathbf{G}_u}}{\arg\max} \Bigg\{ \sum_{\exists \setminus \{\hat{\mathbf{c}}_{u,m}, \hat{\mathbf{g}}_{u,k}\} \in \Xi \setminus \{\mathbf{C}_u, \mathbf{G}_u\}} P\left(\{\hat{\mathbf{c}}_{u,m}, \hat{\mathbf{g}}_{u,k}\}, \exists \setminus \{\hat{\mathbf{c}}_{u,m}, \hat{\mathbf{g}}_{u,k}\}\right)$$

$$\times P\left(\mathbf{y}_n | \{\hat{\mathbf{c}}_{u,m}, \hat{\mathbf{g}}_{u,k}\}, \exists \setminus \{\hat{\mathbf{c}}_{u,m}, \hat{\mathbf{g}}_{u,k}\}\right) \Bigg\}, \tag{6.5}$$

where $\exists = [\{\hat{\mathbf{c}}_{1,m}, \hat{\mathbf{g}}_{1,k}\}, \ldots, \{\hat{\mathbf{c}}_{U,m}, \hat{\mathbf{g}}_{U,k}\}]$ represents one possible combination of the transmitted set of codewords and grouping vectors for all U users, Ξ is the set containing all $(N_c M)^U$ possibilities of $\exists$, $\exists \setminus \{\hat{\mathbf{c}}_{u,m}, \hat{\mathbf{g}}_{u,k}\}$ denotes $\exists$ except the set $\{\hat{\mathbf{c}}_{u,m}, \hat{\mathbf{g}}_{u,k}\}$, and $\Xi \setminus \{\mathbf{C}_u, \mathbf{G}_u\}$ denotes Ξ except $\{\mathbf{C}_u, \mathbf{G}_u\}$. Note that the total probability theorem is applied to obtain the last line of (6.5). Since all elements of $\mathbf{y}_n$ are independent for all OREs and N_r receive antennas, the conditional probability in the last term of (6.5) becomes

$$P\left(\mathbf{y}_n | \{\hat{\mathbf{c}}_{u,m}, \hat{\mathbf{g}}_{u,k}\}, \exists \setminus \{\hat{\mathbf{c}}_{u,m}, \hat{\mathbf{g}}_{u,k}\}\right) = \prod_{n=1}^{N_r} \prod_{r \in \Omega_u} P\left(\mathbf{y}_n | \exists(r)\right), \tag{6.6}$$

where Ω_u is the set of indices of the d_v non-zero OREs for the u-th user, $\exists(r)$ denotes one possible set of transmitted codewords and grouping vectors at the r-th ORE for the d_f users that share the r-th ORE, and

$$P\left(\mathbf{y}_n | \exists(r)\right) = \frac{1}{\sqrt{2\pi}\sigma} \exp\left(- \frac{\left| y_n^r - \sum_{u \in \Lambda_r} \left(\mathbf{h}_{u,n}^r \mathbf{g}_{u,k}^{\mathrm{T}} c_{u,m}^r \right) \right|^2}{2\sigma^2} \right). \tag{6.7}$$

6.5.3 MPA Decoder

The MPA decoder provides an approximation to the MAP detector using the factor graph method, shown in Fig. 6.1. In the factor graph, the OREs and served users are represented as function nodes (FNs) and variable nodes (VNs), respectively. For each FN, all VNs that share this FN are connected. Note that each VN has $N_c M$ son VNs. The idea of the MPA is to iteratively update the probability of passing the messages from FNs to VNs and vice versa. After T iterations, the MPA stops and detects the message which corresponds to the maximum joint probability. Note that the conventional MPA of the proposed RGSM-SCMA is modified to jointly estimate the antenna grouping vector and transmitted codeword.

To formulate the MPA, assume that $\mathcal{P}^{(t)}_{f_r \to v_u}(\{c^r_{u,m}, \mathrm{g}_{u,k}\})$ and $\mathcal{P}^{(t)}_{v_u \to f_r}(\{c^r_{u,m}, \mathrm{g}_{u,k}\})$ is the probability of passing the message $\{c^r_{u,m}, \mathrm{g}_{u,k}\}$ from the r-th FN to the u-th VN and from the u-th VN to the r-th FN, respectively, at the t-th iteration, $t = 1, \ldots, T$. First, all messages sent from VNs to FNs are assumed equiprobable at the first iteration; i.e.,

$$\mathcal{P}^{(0)}_{v_u \to f_r}\left(\{c^r_{u,m}, \mathrm{g}_{u,k}\}\right) = \frac{1}{N_c M}, \quad \forall u,\ \forall r,\ \forall m,\ \forall k. \tag{6.8}$$

Now, $\mathcal{P}^{(t+1)}_{f_r \to v_u}(\{c^r_{u,m}, \mathrm{g}_{u,k}\})$ can be written as

$$\mathcal{P}^{(t+1)}_{f_r \to v_u}\left(\{c^r_{u,m}, \mathrm{g}_{u,k}\}\right) = \sum_{\exists(i), i \in \Lambda_r \setminus u} \left\{ \prod_{n=1}^{N_r} \left(P\left(\mathrm{y}_n | \exists(i), \exists(u) = \{c^r_{u,m}, \mathrm{g}_{u,k}\}\right)\right) \right.$$

$$\left. \times \prod_{i \in \Lambda_r \setminus u} \mathcal{P}^{(t)}_{v_i \to f_r}\left(\exists(i)\right) \right\}, \quad \forall m,\ \forall k,\ \forall r,\ u \in \Lambda_r, \tag{6.9}$$

where $\Lambda_r \setminus u$ denotes Λ_r except the u-th user, and $P\left(\mathrm{y}_n | \exists(i), \exists(u) = \{c^r_{u,m}, \mathrm{g}_{u,k}\}\right)$ is given in (6.7). Then, the probability of passing the messages from VNs to FNs is updated as

$$\mathcal{P}_{v_u \to f_r}^{(t+1)} \left(\{ c_{u,m}^r, \mathbf{g}_{u,k} \} \right) = \gamma_{u,r}^{(t+1)} \prod_{j \in \Omega_u \backslash r} \mathcal{P}_{f_j \to v_u}^{(t+1)} \left(\{ c_{u,m}^r, \mathbf{g}_{u,k} \} \right), \quad \forall m, \ \forall k, \ \forall u, \ r \in \Omega_u, \tag{6.10}$$

where $\Omega_u \backslash r$ denotes Ω_u except the r-th ORE, and $\gamma_{u,r}^{(t+1)}$ is the normalization factor, which is given by

$$\gamma_{u,r}^{(t+1)} = \left(\sum_{m=1}^{M} \sum_{k=1}^{N_c} \mathcal{P}_{v_u \to f_r}^{(t)} \left(\{ c_{u,m}^r, \mathbf{g}_{u,k} \} \right) \right)^{-1}. \tag{6.11}$$

After T iterations, the estimated transmitted codeword and grouping vector are obtained as

$$\{ \hat{\mathbf{c}}_{u,m}, \hat{\mathbf{g}}_{u,k} \} = \underset{\substack{m=1,\ldots,M \\ k=1,\ldots,N_c}}{\arg\max} \prod_{j \in \Omega_u} \mathcal{P}_{f_j \to v_u}^{(T)} \left(\{ \mathbf{c}_{u,m}, \mathbf{g}_{u,k} \} \right), \ \forall u. \tag{6.12}$$

6.5.4 MPA Complexity Analysis

In this subsection, the computational complexity of the MPA decoders for the SM-SCMA and RGSM-SCMA systems is deduced in terms of real additions and multiplications. Table 6.2 shows the complexity summary, calculated based on (6.8)-(6.12) and the factor graphs of both systems. At the same SE, it is shown from Table 6.2 that there is a negligible increase in the number of real multiplications and additions of the RGSM-SCMA by $4Ud_vN_rN_cN_a$ and $2Ud_vN_rN_c\left(2N_a-1\right)$, respectively. This increase is a result of combining the channel entries by the antenna grouping vectors before performing the MPA decoder, and is independent of the number of iterations. Thus, at the same SE, the decoding complexity of both systems is almost similar.

TABLE 6.2: The real operations of the MPA decoders for the SM-SCMA and RGSM-SCMA systems.

	SM-SCMA	RGSM-SCMA
Additions	$Rd_f \left(N_t M\right)^{d_f} \left(2N_r(2d_f+1)-1\right)$ $+TRd_f \left(\left(N_t M\right)^{d_f}-1\right)$	$Rd_f \left(N_c M\right)^{d_f} \left(2N_r(2d_f+1)-1\right)$ $+TRd_f \left(\left(N_c M\right)^{d_f}-1\right)$ $+2Ud_v N_r N_c \left(2N_a-1\right)$
Multiplications	$Rd_f \left(N_t M\right)^{d_f}$ $\times \left(2N_r(2d_f+1)+Td_f+1\right)$ $+N_t M \left(d_v-1\right)\left(TRd_f+U\right)$	$Rd_f \left(N_c M\right)^{d_f}$ $\times \left(2N_r(2d_f+1)+Td_f+1\right)$ $+N_c M \left(d_v-1\right)\left(TRd_f+U\right)$ $+4Ud_v N_r N_c N_a$

6.6 Simulation Results

In this section, simulation is used to study the BER performance of the proposed RGSM-SCMA system, additionally in comparison with the SM-SCMA [12]. The effect of the rotation angles in (6.1) is shown, and I refer to the zero rotation angles version of the RGSM-SCMA as GSM-SCMA. The MPA decoder is considered for all systems. Furthermore, the Rayleigh fading channel is assumed to be perfectly known at the receiver. The required number of transmit antennas and decoding complexity comparisons between the proposed RGSM-SCMA and SM-SCMA are also provided. The system parameters for all systems are chosen as follows: $U = 6$, $R = 4$ and $M = 4$.

Fig. 6.2 shows the BER performance comparison for $\eta_u^s = 3$ bpcu ($N_t = 8$ and 5 for SM-SCMA and RGSM-SCMA, respectively), $N_a = 2$ and $T = 2$ in case of $N_r = 1$, 2, and 4. As shown in this figure, the BER performance is almost the same in the case of $N_r = 1$ and 2. In the case of high signal-to-noise ratio (SNR) for $N_r = 4$, the proposed RGSM-SCMA provides a better BER performance than the GSM-SCMA. Thus, using the rotation angles in (6.1) for the proposed RGSM-SCMA degrades the BER performance by only 0.6 dB instead of 1.2 dB SNR as in GSM-SCMA, when compared with SM-SCMA.

Fig. 6.3 shows the extra complexity (ExCo) of the RGSM-SCMA over SM-SCMA mentioned in Table 6.2 and given by: ExCo = (RGSM operations - SM operations) / SM

operations, where operations can be either additions or multiplications. It can be seen from Fig. 6.3 that the ExCo is negligible (less than 0.05%) for both additions and multiplications, and decreases when T or η_u^s increase.

The RGSM-SCMA system provides significant savings in the number of transmit antennas, N_t, required to deliver the same η_u^s of the SM-SCMA, as shown in Fig. 6.4. Note that $N_a = \{2, 2, 3, 3, 4, 4, 4, 5, 5\}$ is used to achieve $\eta_u^s = 2 : 10$ bpcu. The RGSM-SCMA saves more in terms of N_t when η_u^s increases. For example, to deliver $\eta_u^s = 7$ bpcu, the SM-SCMA requires 128 transmit antennas, while the RGSM-SCMA requires only 10 antennas.

Finally, the RGSM-SCMA provides a significant reduction in the number of transmit antennas with almost the same decoding complexity and a very slight deterioration in the BER performance to deliver the same SE of the SM-SCMA.

6.7 Conclusion

A low-cost SM-SCMA system has been proposed, which utilizes a reduced number of transmit antennas, referred to as RGSM-SCMA. The transmitter design, as well as the ML and MAP decoders have been introduced. Furthermore, the low-complexity MPA decoder has been revised and analyzed for the proposed RGSM-SCMA system. This delivers the same SE as SM-SCMA with a much lower number of required antennas, at the expense of less than 0.05% increase in the decoding complexity and up to 0.6 dB SNR degradation in the BER performance.

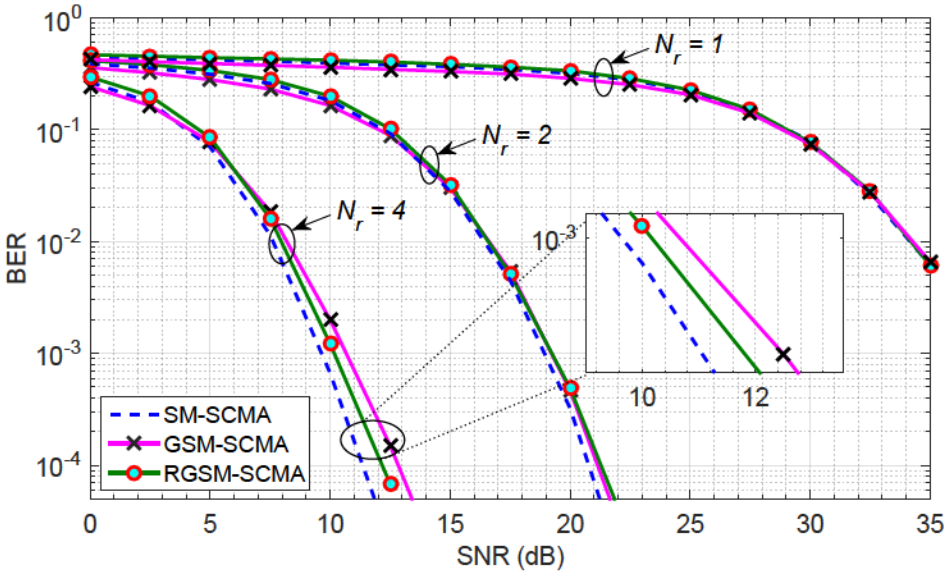

Fig. 6.2: BER performance comparison.

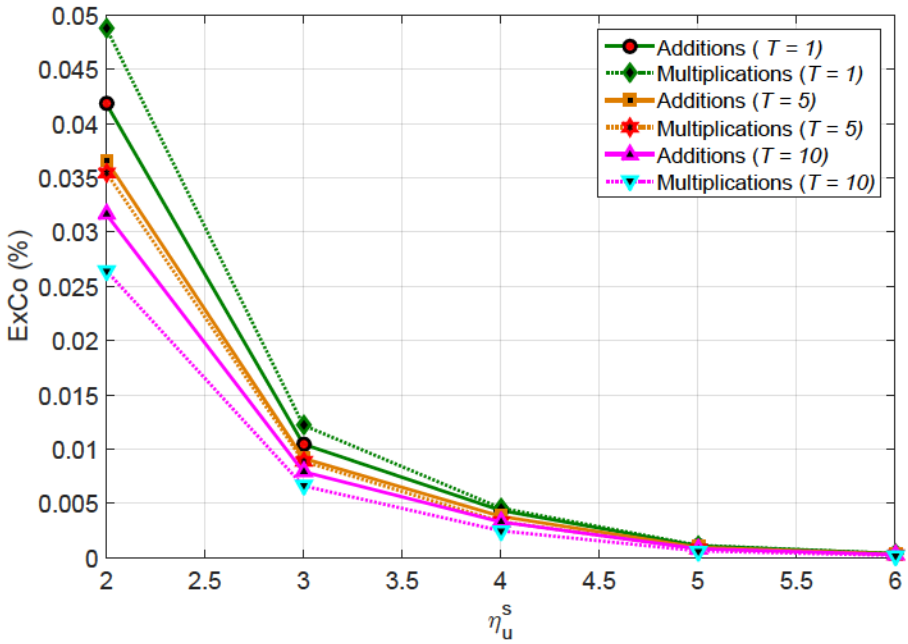

Fig. 6.3: Extra complexity comparison between SM-SCMA and RGSM-SCMA.

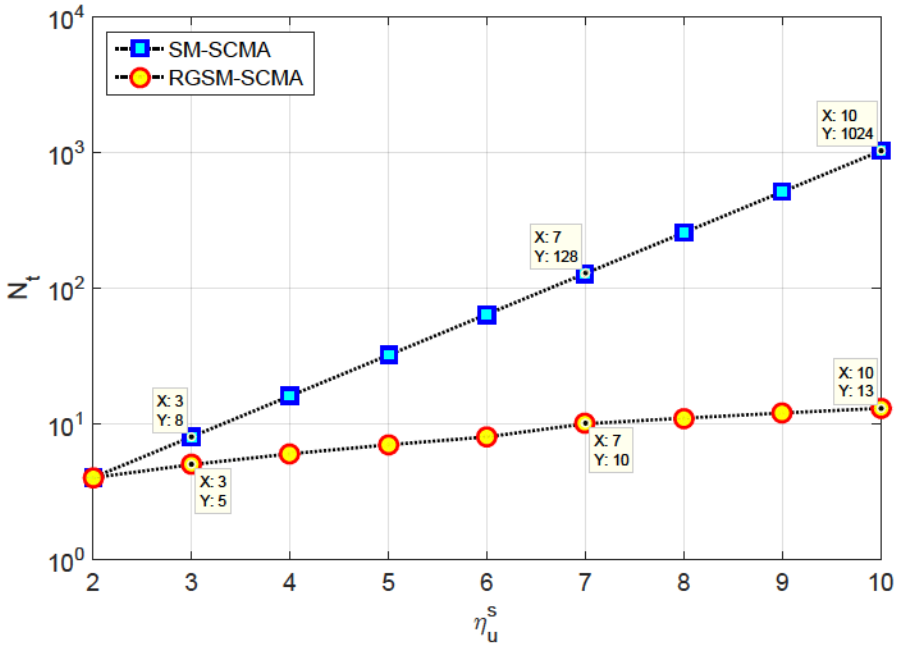

Fig. 6.4: N_t comparison between SM-SCMA and RGSM-SCMA.

References

[1] M. Mohammadkarimi, M. A. Raza, and O. A. Dobre, "Signature-based nonorthogonal massive multiple access for future wireless networks: Uplink massive connectivity for machine-type communications," *IEEE Veh. Technol. Mag.*, vol. 13, no. 4, pp. 40–50, Dec. 2018.

[2] S. M. R. Islam, N. Avazov, O. A. Dobre, and K. S. Kwak, "Power-domain non-orthogonal multiple access (NOMA) in 5G systems: Potentials and challenges," *IEEE Commun. Surv. Tuts.*, vol. 19, no. 2, pp. 721-742, Oct. 2016.

[3] Z. Ding et al., "A survey on non-orthogonal multiple access for 5G networks: Research challenges and future trends," *IEEE J. Sel. Areas Commun.*, vol. 35, no. 10, pp. 2181 –2195, Oct. 2017.

[4] H. Nikopour and H. Baligh, "Sparse code multiple access," in *Proc. IEEE Int. Symposium on Personal Indoor and Mobile Radio Commun. (PIMRC)*, Sep. 2013, pp. 332–336.

[5] M. Taherzadeh et al., "SCMA codebook design," in *Proc. IEEE Veh. Technol. Conf. (VTC Fall)*, Sep. 2014, pp. 1–5.

[6] H. Mu, Z. Ma, M. Alhaji, P. Fan, and D. Chen, "A fixed low complexity message pass algorithm detector for up-link SCMA system," *IEEE Wireless Commun. Lett.,* vol. 4, no. 6, pp. 585–588, Dec. 2015.

[7] R. Y. Mesleh et al., "Spatial modulation," *IEEE Trans. Veh. Technol.*, vol. 57, no. 4, pp. 2228–2241, Jul. 2008.

[8] E. Basar, "Index modulation techniques for 5G wireless networks," *IEEE Commun. Mag.,* vol. 54, no. 7, pp. 168–175, Jul. 2016.

[9] A. Younis, N. Serafimovski, R. Mesleh, and H. Haas, "Generalised spatial modulation," in *Proc. Forty Fourth Asilomar Conf. Signals, Syst., Comput. (ASILOMAR)*, Nov. 2010, pp. 1498–1502.

[10] C. Zhong, X. Hu, X. Chen, D. W. Ng, and Z. Zhang, "Spatial modulation assisted multi-antenna non-orthogonal multiple access", *IEEE Wireless Commun. Lett.,* vol. 25, no. 2, pp. 61-67, Apr. 2018.

[11] Y. Liu, L. L. Yang, and L. Hanzo, "Spatial modulation aided sparse code division multiple access," *IEEE Trans. Wireless Commun.*, vol. 17, no. 3, pp. 1474–1487, Mar. 2018.

[12] Z. Pan, J. Luo, J. Lei, L. Wen, and C. Tang, "Uplink spatial modulation SCMA system," *IEEE Commun. Lett.,* vol. 23, no. 1, pp. 184-187, Jan. 2019.

[13] I. Al-Nahhal, O. A. Dobre, and S. Ikki, "Quadrature spatial modulation decoding complexity: Study and reduction," *IEEE Wireless Commun. Lett.,* vol. 6, pp. 378-381, Jun. 2017.

[14] I. Al-Nahhal, O. A. Dobre, and S. Ikki, "Low complexity decoders for spatial and quadrature spatial modulations," in *Proc. IEEE Veh. Technol. Conf. (VTC-Spring)*, 2018, pp. 1–5.

[15] I. Al-Nahhal, E. Basar, O. A. Dobre, and S. Ikki, "Optimum low-complexity decoder for spatial modulation," *IEEE J. Sel. Areas Commun.*, vol. 37, no. 9, pp. 2001-2013, Jul. 2019.

Chapter 7

On the Complexity Reduction of Uplink Sparse Code Multiple Access for Spatial Modulation

7.1 Abstract

Multi-user spatial modulation (SM) assisted by sparse code multiple access (SCMA) has been recently proposed to provide high spectral efficiency transmission. The message passing algorithm (MPA) is employed to detect the transmitted signals, which suffers from high decoding complexity in practical implementations. In this chapter, three low-complexity decoding algorithms are proposed for the SM-SCMA system. The first algorithm is referred to as successive user detection (SUD), while the second algorithm is the modified version of SUD, namely modified SUD (MSUD). Then, for the first time, the tree-search of the SM-SCMA system is constructed. Based on that tree-search, another variant of the sphere decoder (SD) algorithm is proposed for the SM-SCMA system, referred to as fixed-complexity SD (FCSD). SUD provides the lowest decoding complexity that can be achieved

at the expense of bit-error-rate (BER) performance. Further, MSUD slightly increases the decoding complexity of SUD with a significant improvement in BER performance. Finally, FCSD provides a near-optimum BER performance with a considerable reduction of the decoding complexity compared to the MPA decoder. The FCSD algorithm also supports parallel hardware implementation and strikes a trade-off between decoding complexity and BER performance. The proposed algorithms provide flexible design choices for practical implementation based on system design demands. The complexity analysis and Monte-Carlo simulations of the BER performance are provided for the proposed algorithms.

7.2 Introduction

Non-orthogonal multiple access (NOMA) has been recognized as a promising technique for future wireless networks, and has received considerable attention in recent years [1]-[2]. NOMA is composed of two types: power-domain and code-domain. The power and code orthogonality constraints are relaxed for multiple-user access to improve the spectral efficiency and increase the number of served users for power-domain and code-domain NOMA, respectively [3]-[5]. In this chapter, sparse code multiple access (SCMA) code-domain NOMA is considered, which was firstly proposed in [6]. In the SCMA scheme, a unique multidimensional codebook is assigned to each user to share the medium with the other users. The SCMA codebooks are sparse (i.e., contain zeros) and carefully designed to provide a good performance [7]-[9]. The sparsity property of the SCMA codebooks makes it feasible to employ the iterative message passing algorithm (MPA) to provide near maximum-likelihood (ML) bit-error-rate (BER) performance at low-complexity detection [10]. The complexity of the MPA is still high for practical implementations; several algorithms have been proposed to tackle this problem [11]-[15]. In [11], the authors proposed a reduced-complexity version of the MPA decoder, whereas the authors in [12]-[15] adopted the

concept of the sphere decoder (SD) to reduce the complexity of the SCMA signal detection.

On the other hand, spatial modulation (SM) is a promising technology for single-user communications, which overcomes the inter-channel-interference problem present in multiple-input multiple-output (MIMO) schemes [16]-[19]. The SM system employs the index of the active antenna to deliver additional information supplementary to the modulated quadrature amplitude modulation (QAM)/phase-shift-keying (PSK) symbol that can be transmitted from that active antenna [16]. At the receiver side, the ML jointly detects the active transmit antenna as well as the transmitted QAM/PSK symbol by implementing an exhaustive search that leads to high decoding complexity. The algorithms in [20]-[25] have been proposed based on the SD and tree-search concepts to significantly reduce the decoding complexity while retaining the same BER performance of the ML decoder.

Recently, the multi-user SM has been assisted by SCMA (SM-SCMA) to provide a high spectral efficiency transmission [26]-[28]. The SM-SCMA system requires a high number of transmit antennas to provide high spectral efficiency for all users. To effectively tackle this problem, the rotational generalized SM (RGSM)-SCMA has been proposed in [29]. In the RGSM-SCMA system, the same spectral efficiency of the SM-SCMA can be achieved using a significantly reduced number of transmit antennas at the expense of almost negligible changes to BER performance and decoding complexity, when compared with the SM-SCMA system. For the SM-SCMA and RGSM-SCMA systems, the iterative MPA decoder has been proposed to detect the transmitted signal [28], [29]. The MPA decoder iteratively updates the users message probabilities until achieving the maximum number of iterations; this leads to an increase in the decoding complexity of both systems. To the best of the authors' knowledge, low-complexity algorithms for the SM-SCMA and RGSM-SCMA systems are yet to be proposed.

In this chapter, three low-complexity decoding algorithms for the SM-SCMA system are proposed, which can also be directly applied for the RGSM-SCMA system. The first

algorithm is termed successive user detection (SUD). It detects the users messages that share the first orthogonal resource element (ORE), then by using those detected users messages, it successively detects the users messages that share the next OREs. The SUD algorithm detects the user message using only one of the available OREs that carry the signal of that user. The proposed SUD algorithm is considered to be the lower bound of the decoding complexity for the SM-SCMA and RGSM-SCMA systems at the expense of the BER performance. By exploiting all available OREs for each user with some iterative procedure, the modified SUD (MSUD) provides a considerable improvement in the BER performance at the expense of a small increase in the decoding complexity.

The SD and tree-search concepts are carefully designed for the SM-SCMA, referred to as a fixed-complexity SD (FCSD) algorithm. The FCSD algorithm provides almost the same BER performance as that of MPA with a significant reduction in the decoding complexity. The proposed FCSD has a fixed decoding complexity for all values for signal-to-noise ratio (SNR), as well as for its feasibility of parallel hardware implementation, which is proper for practical applications [30], [33]. Besides, the FCSD algorithm provides a favorable trade-off between the decoding complexity and BER performance, which fits a wide range of practical applications. In summary, each of the three proposed algorithms enjoys different advantages that can fit a wide range of system specifications. The complexity analysis in terms of the number of real additions and multiplications is derived. The Monte-Carlo simulations for the BER performance of the proposed algorithms are provided to support the chapter findings.

The rest of the chapter[1] is organized as follows: In Section 7.3, the system model of the SM-SCMA transmitter and receiver is summarized. In Section 7.4, the proposed decoding algorithms for the SM-SCMA system are introduced. In Section 7.5, the complexity analysis

[1]Notations: Boldface lowercase and uppercase letters represent vectors and matrices, respectively. $\mathcal{CN}$ denotes a complex-valued normal random variable. diag$(\cdot)$ converts a vector into a diagonal matrix with diagonal elements that are the same as the original vector elements. $\|\cdot\|$ denotes the Euclidean norm. card $\{\cdot\}$ is the is the cardinality of a set that refers to the number of elements in that set. $[\cdot]^{\mathrm{T}}$ denotes the matrix or vector transpose. $\mathbb{E}\{\cdot\}$ denotes the expectation operation. $\mathcal{P}(\cdot)$ is the probability of an event. $f(\cdot)$ denotes the probability density function (pdf) of a random variable. ϕ is the empty set.

of the proposed decoding algorithms are derived in terms of the number of real additions and multiplications. The simulation results and conclusions are provided in Sections 7.6 and 7.7, respectively.

7.3 System Model

In this section, the transmitter and receiver of the SM-SCMA system are discussed. Assume that U users are sharing R OREs, where $U > R$. Each of these users has an unparalleled multidimensional codebook, $\mathbf{C}^u \in \mathbb{C}^{R \times M}$, $u = 1, \ldots, U$, with $\mathbf{c}_m^u \in \mathbb{C}^{R \times 1}$, $m = 1, \ldots, M$ as codewords within the codebook and M as the number of codewords. Since $\mathbf{c}_m^u$ is sparse, the number of non-zero elements for each codeword is denoted by d_v, whereas the number of zero elements is $R - d_v$. It should be noted that the positions of zero and non-zero elements are fixed for a codebook (i.e., for a user), and vary from codebook to another to provide a fixed number of overlapped users per ORE of $\forall R$. In this chapter, the number of overlapped users per ORE is denoted by d_f.

7.3.1 Transmitted and Received Signal

Consider an $N_r \times N_t$ MIMO system for each user, where N_t and N_r represent the number of transmit and receive antennas, respectively. For the u-th user in the SM-SCMA transmitter, the first $\log_2(N_t)$ of the input bits select the transmit antenna to be activated, while the remaining $\log_2(M)$ bits are mapped to choose a corresponding codebook, $\mathbf{c}_m^u$, to be transmitted from that active antenna. Hence, the spectral efficiency of the u-th user is given by

$$\eta_u = \log_2(N_t) + \log_2(M), \tag{7.1}$$

where η_u is the spectral efficiency of the u-th user that is measured in bit per channel use

(bpcu). It should be noted that the total system spectral efficiency for all users is $U\eta_u$ bpcu.

At the receiver, the noisy received signal at the n_r-th receive antenna of the r-th ORE, y_n^r, is

$$y_{n_r}^r = \sum_{u \in \Lambda_r} \left(h_{n_r, n_t^u}^{r,u} c_m^{r,u} \right) + n_{n_r}^r, \quad r = 1, \ldots, R, \tag{7.2}$$

where $h_{n_r, n_t^u}^{r,u}$ represents the Rayleigh fading channel coefficient between the n_r-th $\in \{1, \ldots, N_r\}$ receive antenna and n_t^u-th $\in \{1, \ldots, N_t\}$ transmit antenna of the u-th user for the r-th ORE, $c_m^{r,u}$ is the non-zero r-th element for the m-th codeword of the u-th user. Here, Λ_r denotes the set of users indices that share the r-th ORE, and $n_{n_r}^r \sim \mathcal{CN}(0, \sigma^2)$ is the complex additive white Gaussian noise (AWGN) with zero-mean and a variance of σ^2 for the r-th ORE at the n_r-th receive antenna.

For all OREs, the received signal at the n_r-th receive antenna, $\mathbf{y}_{n_r} \in \mathbb{C}^{R \times 1} = [y_{n_r}^1, \ldots, y_{n_r}^R]^{\mathrm{T}}$, is given by

$$\mathbf{y}_{n_r} = \sum_{u=1}^{U} \left(\mathrm{diag} \left(\mathbf{h}_{n_r, n_t^u}^u \right) \mathbf{c}_m^u \right) + \mathbf{n}_{n_r}, \tag{7.3}$$

where $\mathbf{h}_{n_r, n_t^u}^u \in \mathbb{C}^{R \times 1} = [h_{n_r, n_t^u}^{1,u}, \ldots, h_{n_r, n_t^u}^{R,u}]^{\mathrm{T}}$ is the Rayleigh fading channel vector between the n_r-th receive antenna and n_t^u-th transmit antenna of the u-th user, and $\mathbf{n}_{n_r} \in \mathbb{C}^{R \times 1} = [n_{n_r}^1 \ldots n_{n_r}^R]^{\mathrm{T}}$ is the AWGN vector.

It is worth noting that the relationship between the position of zero/non-zero elements of users codebooks and OREs can be described by a binary indicator matrix, F. In the indicator matrix, the number of rows and columns represents the number of OREs and number of users, respectively. Moreover, the ones in F show the position of non-zero elements of the user codebooks. In this chapter, six users overloaded over four OREs (i.e., $U = 6$ and $R = 4$) are considered, with F given by [6], [29]:

$$F = \begin{bmatrix} 0 & 1 & 1 & 0 & 1 & 0 \\ 1 & 0 & 1 & 0 & 0 & 1 \\ 0 & 1 & 0 & 1 & 0 & 1 \\ 1 & 0 & 0 & 1 & 1 & 0 \end{bmatrix}. \tag{7.4}$$

As seen from (7.4), $d_v = 2$ for all users and $d_f = 3$ for all OREs. A useful representation for the indicator matrix is

$$\Lambda_r = \{\Lambda_r(1), \ldots, \Lambda_r(d_f)\}, \tag{7.5}$$

where $\Lambda_r(1)$ denotes the index of the first user that shares the r-th ORE, and card$\{\Lambda_r\} = d_f$. Thus, F in (7.4) yields

$$\Lambda_1 = \{\Lambda_1(1), \Lambda_1(2), \Lambda_1(3)\} = \{2, 3, 5\}, \tag{7.6a}$$

$$\Lambda_2 = \{\Lambda_2(1), \Lambda_2(2), \Lambda_2(3)\} = \{1, 3, 6\}, \tag{7.6b}$$

$$\Lambda_3 = \{\Lambda_3(1), \Lambda_3(2), \Lambda_3(3)\} = \{2, 4, 6\}, \tag{7.6c}$$

$$\Lambda_4 = \{\Lambda_4(1), \Lambda_4(2), \Lambda_4(3)\} = \{1, 4, 5\}. \tag{7.6d}$$

7.3.2 Signal Detection

At the receiver side, the decoder task is to estimate the activated transmit antenna and the mapped codeword for each user (i.e., user message). In this subsection, the ML and MPA decoders are discussed.

7.3.2.1 ML Decoder

The ML decoder jointly performs an exhaustive search for all possible combinations between the transmit antennas and codewords for all users (i.e., $(N_t M)^U$ possible combinations). Although the ML provides the optimum BER performance, it has an impractically high decoding complexity. The mathematical formulation of the ML decoder is given by

$$\left\{\hat{\mathbf{C}}, \hat{\mathbf{j}}\right\} = \underset{\substack{j=1,\ldots,N_t^U \\ l=1,\ldots,M^U}}{\arg\min} \left\{ \sum_{n_r=1}^{N_r} \left\| \mathbf{y}_{n_r} - \sum_{u=1}^{U} \left(\text{diag}\left(\mathbf{h}^u_{n_r, n_t^u(j)} \right) \mathbf{c}^u_{m(l)} \right) \right\|^2 \right\}, \tag{7.7}$$

where $\hat{\mathbf{j}} = \{\hat{n_t}^1, \ldots, \hat{n_t}^U\}$ denotes the set of indices of the estimated active transmit antenna for all U users, with $\hat{n_t}^u$ as the estimated index of the active transmit antenna for the u-th user, $n_t^u(j)$ is the active transmit antenna index of the u-th user that corresponds to the j-th antenna combinations (out of $(N_t)^U$ combinations) of all U users, $\hat{\mathbf{C}} \in \mathbb{C}^{R \times U} = [\hat{\mathbf{c}}_m^1 \ldots \hat{\mathbf{c}}_m^U]$ represents the estimated transmitted codewords of the U users, with $\hat{\mathbf{c}}_m^u$ as the estimated transmitted codeword of the u-th user, and $m(l)$ is the m-th codeword of the u-th user that corresponds to the l-th codeword combinations (out of $(M)^U$ combinations) of all U users.

7.3.2.2 MPA Decoder

The MPA is an alternative practical decoder to the ML decoder. It iteratively updates the probability of users messages between the function nodes (FNs) that represent the number of OREs, and the variable nodes (VNs) that represents the number of users. It is worth noting that each of the FNs is connected with all VNs that share the same FN based on indicator matrix in (7.4) to form what is called a factor graph. The factor graph of the MPA decoder used in this chapter is shown in Fig. 7.1 for $U = 6$, $R = 4$ and F, which is given from (7.4).

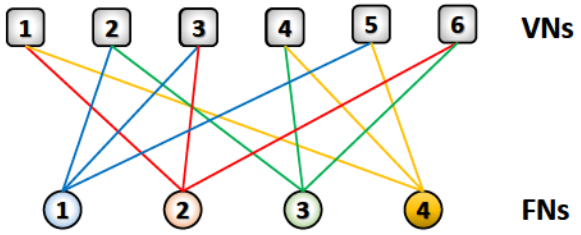

Fig. 7.1: MPA factor graph of the SM-SCMA for $U = 6$ and $R = 4$.

It is assumed that the probability of passing the u-th message, $\{c_m^{r,u}, n_t^u\}$, from the u-th VN to the r-th FN and vice versa at the k-th iteration (out of K iterations) is $\mathcal{P}_{v_u \to f_r}^{(k)}(\{c_m^{r,u}, n_t^u\})$ and $\mathcal{P}_{f_r \to v_u}^{(k)}(\{c_m^{r,u}, n_t^u\})$, respectively. Initially, all users messages passing from the VNs to FNs are equiprobable, i.e.,

$$\mathcal{P}_{v_u \to f_r}^{(0)}(\{c_m^{r,u}, n_t^u\}) = \frac{1}{N_t M}, \quad \forall u, \ \forall r, \ \forall m. \tag{7.8}$$

The mathematical formulation of updating the messages at the $(k+1)$-th iteration of the MPA decoder is given by [28], [29]:

$$\mathcal{P}_{f_r \to v_u}^{(k+1)}(\{c_m^{r,u}, n_t^u\}) = \sum_{\psi(i), i \in \Lambda_r \backslash u} \left\{ \prod_{n_r=1}^{N_r} \left(\mathcal{P}\left(\mathbf{y}_{n_r} | \psi(i), \psi(u) = \{c_m^{r,u}, n_t^u\}\right)\right) \right.$$

$$\left. \times \prod_{i \in \Lambda_r \backslash u} \mathcal{P}_{v_i \to f_r}^{(k)}(\psi(i)) \right\}, \quad \forall m, \ \forall r, \ u \in \Lambda_r, \tag{7.9}$$

where $\Lambda_r \backslash u$ represents Λ_r in (7.5) except the u-th user and $\psi(.)$ represents the message of a user. The conditional probability in (7.9) is given by

$$\mathcal{P}\left(\mathbf{y}_{n_r} | \psi^r\right) = \frac{1}{\sqrt{2\pi}\sigma} \exp\left(- \frac{\left| y_{n_r}^r - \sum_{u \in \Lambda_r} \left(h_{n_r, n_t^u}^{r,u} c_m^{r,u} \right) \right|^2}{2\sigma^2} \right), \tag{7.10}$$

where ψ^r represents the possible messages of all users that share the r-th ORE.

Now, $\mathcal{P}_{v_u \to f_r}^{(k+1)}(\{c_m^{r,u}, n_t^u\})$ can be calculated as

$$\mathcal{P}^{(k+1)}_{v_u \to f_r}\left(\{c^{r,u}_m, n^u_t\}\right) = \gamma^{(k+1)}_{u,r} \prod_{j \in \Omega_u \backslash r} \mathcal{P}^{(k+1)}_{f_r \to v_u}\left(\{c^{r,u}_m, n^u_t\}\right), \quad \forall m,\ \forall u,\ r \in \Omega_u, \tag{7.11}$$

where Ω_u denotes the set of ORE indices that correspond to d_v non-zero positions for the u-th user, $\Omega_u \backslash r$ represents the set Ω_u except the r-th ORE, and $\gamma^{(k+1)}_{u,r}$ is

$$\gamma^{(k+1)}_{u,r} = \left(\sum_{m=1}^{M} \sum_{n_t=1}^{N_t} \mathcal{P}^{(k)}_{v_u \to f_r}\left(\{c^{r,u}_m, n^u_t\}\right) \right)^{-1}. \tag{7.12}$$

After the MPA completes K iterations, the estimated message of the u-th user can be calculated by

$$\begin{aligned} \{\hat{\mathbf{c}}^u_m, \hat{n_t}^u\}^{(K)} = \ & \arg\max \prod_{j \in \Omega_u} \mathcal{P}^{(K)}_{f_j \to v_u}\left(\{c^{r,u}_m, n^u_t\}\right), \ \forall u. \\ & m = 1, \ldots, M \\ & n_t = 1, \ldots, N_t \end{aligned} \tag{7.13}$$

The set of all estimated users messages using the MPA in (7.13), $\hat{\Theta}_{\text{MPA}}$, can be given as

$$\hat{\Theta}_{\text{MPA}} = \left\{ \{\hat{\mathbf{c}}^1_m, \hat{n_t}^1\}^{(K)}, \ldots, \{\hat{\mathbf{c}}^U_m, \hat{n_t}^U\}^{(K)} \right\}. \tag{7.14}$$

7.4 The Proposed Decoding Algorithms

In this section, the three proposed decoding algorithms are introduced. The first two algorithms focus on decoding the signal with very low complexity and acceptable BER performance. The third proposed algorithm employs the SD concept to provide a near-optimum BER performance with low-decoding complexity in addition to other advantages, such as the feasibility of parallel hardware implementation and the flexible trade-off between decoding complexity and BER performance.

7.4.1 The SUD Algorithm

The SUD algorithm provides the lowest decoding complexity among the proposed algorithms at the expense of BER performance. First, the SUD algorithm performs an exhaustive search for all combinations of the users messages that share the first ORE. It starts with the OREs with highest energy, E^r, based on the following

$$E^r = \sum_{u \in \Lambda_r} \sum_{n_r=1}^{N_r} \left| h^{r,u}_{n_r,n_t^u} \right|^2, \qquad r = 1, \ldots, R. \tag{7.15}$$

Then, these estimated users messages are employed to estimate the messages of other users that share the next OREs. Sequentially, the SUD algorithm estimates the undetected users messages until they are all estimated based on the descending order of E^r in (7.15) for $\forall R$.

The mathematical formulation of the SUD algorithm is given by

$$\left\{ \hat{\mathrm{C}}^r, \hat{\mathbf{j}}^r \right\} = \underset{\substack{j = 1, \ldots, N_t^{\grave{U}^r} \\ l = 1, \ldots, M^{\grave{U}^r}}}{\arg\min} \left\{ \sum_{n_r=1}^{N_r} \left| y^r_{n_r} - \underbrace{\sum_{u \in \grave{\Lambda}_r} h^{r,u}_{n_r,\hat{n}_t^u} c^{r,u}_{\hat{m}}}_{\text{Term 1}} - \underbrace{\sum_{u \in \Lambda_r \backslash \grave{\Lambda}_r} h^{r,u}_{n_r,n_t^u(j)} c^{r,u}_{m(l)}}_{\text{Term 2}} \right|^2 \right\}, \tag{7.16}$$

$$1 \leq r \leq R,$$

where $\grave{\Lambda}_r$ is the set of users indices that share the r-th ORE in which their messages are already estimated previously, $\Lambda_r \backslash \grave{\Lambda}_r$ is Λ_r except $\grave{\Lambda}_r$ or it is the set of users indices that share the r-th ORE and their messages need to be estimated, $\grave{U}^r = \text{card}\{\Lambda_r \backslash \grave{\Lambda}_r\} \leq d_f$ is the number of users whose messages need to be estimated at the r-th ORE, $\hat{\mathbf{j}}^r$ represents the set of indices of the estimated active transmit antennas for all $\grave{U}^r$ users at the r-th ORE, and $\hat{\mathrm{C}}^r$ denotes the estimated transmitted codewords of the $\grave{U}^r$ users at the r-th ORE. Here, Term 1 and Term 2 represent the users messages that have already been estimated from previous OREs and that need to be estimated at the r-th ORE, respectively. It is worth

noting that Term 1 equals zero at the first ORE used by the SUD algorithm (i.e., $\grave{\lambda}_1 = \phi$). After estimating all users messages from certain OREs, the set of complete estimated users messages using the SUD algorithm in (7.16), $\hat{\Theta}_{\text{SUD}}$, can be written as

$$\hat{\Theta}_{\text{SUD}} = \left\{ \left\{ \hat{\mathbf{c}}_m^1, \hat{n_t}^1 \right\}, \ldots, \left\{ \hat{\mathbf{c}}_m^U, \hat{n_t}^U \right\} \right\}. \tag{7.17}$$

Consequently, the SUD algorithm detects users messages using a single ORE. Then, these detected messages are used as given messages to detect the others that share the rest of the $d_v - 1$ OREs. It should be noted that the SUD algorithm may not use all received signals on OREs if all users messages are already estimated using certain OREs. The SUD algorithm is summarized in Algorithm 7.1.

7.4.2 The MSUD Algorithm

As mentioned in the SUD algorithm, the user message is detected using a single ORE; however, the $(d_v - 1)$ non-zero OREs for each user are not included in the decoding process with the aim of reducing the decoding complexity. This leads to a significant deterioration in the BER performance (i.e., losing the diversity gain). The MSUD is an iterative algorithm that estimates the user message by considering only one user message unknown at a time. In contrast, the rest of the users messages are considered to be known from the previous iteration. Moreover, the MSUD algorithm considers the received signals from all d_v non-zero OREs for each user in the detection process to improve the BER performance. It is important to mention that the initial values of the users messages used in the MSUD algorithm are estimated using the SUD algorithm. In other words, the MSUD algorithm performs the SUD algorithm first. Then, K iterations are performed to improve the BER performance.

To formulate the MSUD algorithm, user messages are first estimated from the SUD algorithm (i.e., $\hat{\Theta}_{\text{SUD}}$, in (7.17)) and are subsequently used as input to/initialization of the

Algorithm 7.1 The proposed SUD algorithm pseudo-code.

- **Store** codebooks for all users;
- **Input** channel matrices for all users;
- **Define** $\hat{\Theta}_{\text{SUD}}$ and Λ as the set of estimated users messages and set of users indices corresponding to the estimated messages in $\hat{\Theta}_{\text{SUD}}$, respectively;
- **Initialize** $\hat{\Theta}_{\text{SUD}} = \{\cdot\}$ and $\Lambda = \{\cdot\}$;
- **Order** the OREs which should be visited based on (7.15);

While $r \leq R$, ***do***
  Set $\grave{\Lambda}_r \leftarrow \{\Lambda \cap \Lambda_r\}$;
  Assign $\bar{y}^r_{n_r} \leftarrow y^r_{n_r} - \sum_{u \in \grave{\Lambda}_r} h^{r,u}_{n_r,\hat{n}^u_t} c^{r,u}_{\hat{m}}$;
  Find $\{\hat{\mathbf{C}}^r, \hat{\mathbf{j}}^r\}$ that solves the following:
  $\arg\min\limits_{j\,\&\,l} \{\sum_{n_r=1}^{N_r} |\bar{y}^r_{n_r} - \sum_{u \in \Lambda_r \backslash \grave{\Lambda}_r} h^{r,u}_{n_r,n^u_t(j)} c^{r,u}_{m(l)}|^2\}$
  s.t. $j = 1, \ldots, N_t^{\grave{U}^r}$ and $l = 1, \ldots, M^{\grave{U}^r}$;
  Update $\hat{\Theta}_{\text{SUD}}$ based on $\{\hat{\mathbf{C}}^r, \hat{\mathbf{j}}^r\}$;
  Update Λ based on $\hat{\Theta}_{\text{SUD}}$;
  if card$\{\Lambda\} == U$
    break and end the algorithm;
  end if
  Set $r \leftarrow r + 1$;
end While

- **Output** $\hat{\Theta}_{\text{SUD}}$.

iteration stage of the MSUD algorithm. At the $(k+1)$-th iteration, the estimated u-th user message, $\{\hat{\mathbf{c}}^u_m, \hat{n_t}^u\}^{(k+1)}$, is given by

$$\{\hat{\mathbf{c}}^u_m, \hat{n_t}^u\}^{(k+1)} = \underset{\substack{j=1,\ldots,N_t \\ l=1,\ldots,M}}{\arg\min} \left\{ \sum_{r \in \Omega_u} \sum_{n_r=1}^{N_r} \left| y^r_{n_r} - \underbrace{\sum_{\grave{u} \in \Lambda_r \backslash u} \left\{ h^{r,\grave{u}}_{n_r,\hat{n}^{\grave{u}}_t} c^{r,\grave{u}}_{\hat{m}} \right\}^{(k)}}_{\text{Term 3}} - \underbrace{h^{r,u}_{n_r,n^u_t(j)} c^{r,u}_{m(j)}}_{\text{Term 4}} \right|^2 \right\},$$

$$u = 1, \ldots, U, \tag{7.18}$$

where Term 3 and Term 4 represent the given estimated users messages that share the same ORE with the u-th user and the desired user message of the u-th user to be estimated, respectively. The MSUD algorithm uses all d_v non-zero OREs for each user in the detection, which can be seen from $\sum_{r\in\Omega_u}$ in (7.18). The estimation process using (7.18) is performed for all U users for each iteration. After K iterations, the set of estimated messages for all U users, $\hat{\Theta}_{\text{MSUD}}$, is

$$\hat{\Theta}_{\text{MSUD}} = \left\{ \{\hat{\mathbf{c}}_m^1, \hat{n_t}^1\}^{(K)}, \ldots, \{\hat{\mathbf{c}}_m^U, \hat{n_t}^U\}^{(K)} \right\}. \tag{7.19}$$

Algorithm 7.2 shows the summary of the MSUD algorithm.

7.4.3 The FCSD Algorithm

The MPA decoder has a limited support to the parallel hardware implementation, where all users messages are detected together after iterative sequential stages, as seen from (7.9), (7.11) and (7.13). In practice, this kind of hardware implementation is not preferable. Besides, the MPA decoder provides a limited trade-off between decoding complexity and BER performance, which limits its practicality for applications with specific requirements.

The FCSD algorithm supports the parallel hardware implementation and also provides a flexible trade-off between decoding complexity and BER performance. To clearly understand the concept of the FCSD algorithm, a tree-search for the SM-SCMA should be constructed first.

7.4.3.1 SM-SCMA Tree-search

The ML decoder of the SM-SCMA in (7.7) can be represented as a multi-level tree-search, as in Fig. 7.2. Each of the tree-search levels corresponds to an ORE (i.e., the number of levels equals R). At each level, there is a certain number of nodes representing the distance

Algorithm 7.2 The proposed MSUD algorithm pseudo-code.

- **Store** codebooks for all users;
- **Input** channel matrices for all users;
- **Perform** Algorithm 7.1 to obtain $\hat{\Theta}_{\text{SUD}}$;
- **Initialize** $\hat{\Theta}_{\text{MSUD}} = \hat{\Theta}_{\text{SUD}}$;

1: ***For*** $k = 1 : K$, ***do***
2: ***For*** $u = 1 : U$, ***do***
3: **Assign** $\bar{y}_{n_r}^r \leftarrow y_{n_r}^r - \sum_{\grave{u} \in \Lambda_r \setminus u} \left\{ h_{n_r, \hat{n}_t^{\grave{u}}}^{r,\grave{u}} c_{\hat{m}}^{r,\grave{u}} \right\}^k$;
4: **Find** $\{\hat{\mathrm{c}}_m^u, \hat{n_t}^u\}^{(k)}$ that solves the following:
$\arg\min_{j \,\&\, l} \{ \sum_{r \in \Omega_u} \sum_{n_r=1}^{N_r} |\bar{y}_{n_r}^r - h_{n_r, n_t^u(j)}^{r,u} c_{m(j)}^{r,u}|^2 \}$
s.t. $j = 1, \ldots, N_t$ and $l = 1, \ldots, M$;
5: **Update** $\hat{\Theta}_{\text{MSUD}}$ based on $\{\hat{\mathrm{c}}_m^u, \hat{n_t}^u\}^{(k)}$;
6: ***end For***
7: ***end For***

- **Output** $\hat{\Theta}_{\text{MSUD}}$.

metric between the received signal at the r-th ORE and possible combinations of the users messages that share this ORE. Each node at the r-th level is expanded into child nodes at the next level.

The mathematical formulation of the i-th node at the r-th level, d_i^r, is

$$d_i^r = d_i^{r-1} + e_i^r, \quad r = 1, \ldots, R, \tag{7.20}$$

where d_i^{r-1} is the mother node of d_i^r and e_i^r is given by

$$e_i^r = \sum_{n_r=1}^{N_r} \left| y_{n_r}^r - \sum_{u \in \grave{\Lambda}_r} h_{n_r, \hat{n}_t^u}^{r,u} c_{\hat{m}}^{r,u} - \sum_{u \in \Lambda_r \setminus \grave{\Lambda}_r} h_{n_r, n_t^u(i)}^{r,u} c_{m(i)}^{r,u} \right|^2. \tag{7.21}$$

At the first level (i.e., $r = 1$), $d_i^0 = 0$ in calculating d_i^1 and $i = 1, \ldots, (MN_t)^{d_f}$. From (7.20) and (7.21), it should be noted that a node is an accumulation of the distance metric

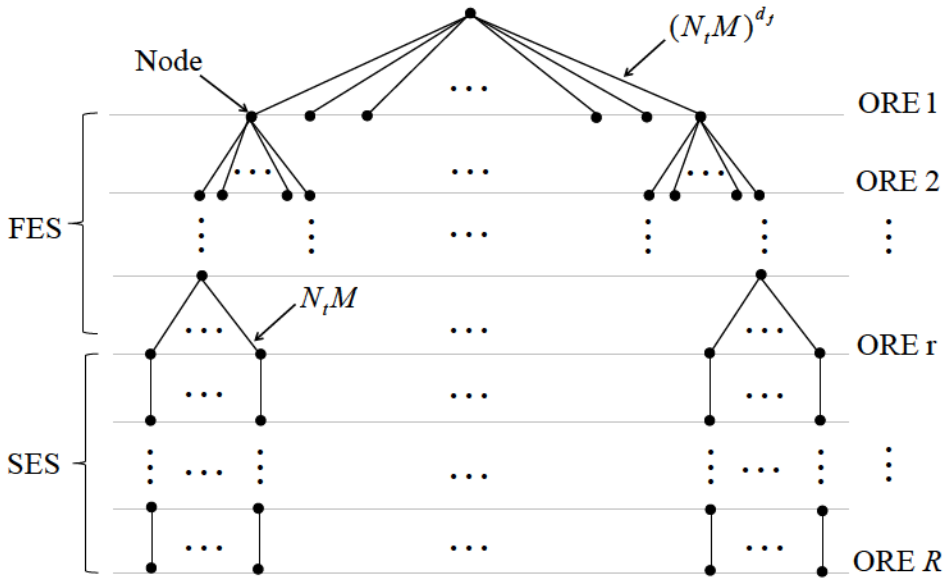

Fig. 7.2: The proposed tree-search for the SM-SCMA system.

of all preceding nodes in the same branch and that the value of e_i^r increases as r increases, respectively.

Unlike the construction of the SM tree-search [25] and MIMO tree-search [31]-[33], the number of expanded nodes for each mother node of the SM-SCMA tree-search, as seen in Fig. 7.2 gradually reduces across the OREs, reaching a limit of one. Consequently, the SM-SCMA tree-search consists of two stages. The upper stage in which each of the mother nodes is fully expanded to multiple child nodes, is referred to as fully expanded stage (FES). The lower stage is called single expanded stage (SES), in which each of the mother nodes is expanded to only one node. Typically, each level of FES has at least one or more users messages that have not been estimated from the previous OREs; the number of these users messages gradually decreases as the ORE increases,

$$d_f \geq \grave{U}^2 \geq \cdots \geq \grave{U}^r > 1, \quad r \in \text{FES}. \tag{7.22}$$

It is worth noting that the number of nodes at the first level is $(N_tM)^{d_f}$ since there are d_f users sharing ORE 1 and no users messages have been estimated previously.

7.4.3.2 The FCSD Algorithm

In the tree-search provided in Fig. 7.2, the ML solution in (7.7) (close to the MPA solution) can be achieved by visiting all nodes, which is extremely high in terms of decoding complexity. The basic concept of the FCSD algorithm is to reduce the decoding complexity of the SM-SCMA system by reducing the search space inside the tree-search based on a predetermined pruned radius (i.e., threshold). For that, at each level, the nodes that have values smaller than a certain threshold (i.e., pruned radius) are the only ones which are expanded at the next level. It is worth noting that the tree-search levels of Fig. 7.2 can be ordered based on (7.15) before performing the FCSD algorithm.

Let us consider that the pruned radius is denoted by $\boldsymbol{\gamma} \in \mathbb{R}^{R-1} = [\gamma_1 \dots \gamma_r \dots \gamma_{R-1}]$ and keeps $[\rho_1 \dots \rho_r \dots \rho_{R-1}]$ survived nodes, where γ_r is the pruned radius and ρ_r is the number of survived nodes at the r-th level. At the final level (i.e., the R-th level), the minimum node is chosen to be the solution of the algorithm. Consequently, ρ_r for the upper $R-1$ levels is given by

$$\rho_r = \left\{ d_i^r \leq \gamma_r | i = 1, \dots, \rho_{r-1}(N_t M)^{\grave{U}^r} \right\}, \quad 0 \leq \grave{U}^r \leq d_f, \quad 1 \leq r \leq R-1, \tag{7.23}$$

where $\grave{U}^r = 0$ at $r \in$ SES, $0 < \grave{U}^r \leq d_f$ at $r \in$ FES, and $\rho_0 = 1$ at the first ORE (i.e., $r = 1$). At the last level (i.e., $r = R$), the number of nodes is ρ_{R-1}, since there are only ρ_{R-1} survived nodes from the $R-1$-th level. Thus, the FCSD algorithm declares the argument of the minimum node at the last level as the solution, which can be represented as

$$\left\{ \hat{\mathbf{C}}, \hat{\mathbf{j}} \right\} = \underset{i = 1, \dots, \rho_{R-1}}{\arg\min} \left\{ d_i^R \right\}. \tag{7.24}$$

It is worth noting that a higher value of the pruned radius may lead to expanding

Algorithm 7.3 The proposed FCSD algorithm pseudo-code.

- **Store** codebooks for all users.
- **Input** channel matrices for all users.
- **Input** $\boldsymbol{\rho} = [\rho_1 \dots \rho_r \dots \rho_{R-1}] \in \mathbb{R}^{R-1}$;
- **Order** the OREs which should be visited based on (7.15);
- **Assign** ∇^r as an empty vector that contains the distance metric nodes at the r-th level;
- **Define** ℓ^r as the total number of nodes in the r-th level;

1: ***While*** $r \leq R-1$, ***do***
2: ***For*** $i = 1 : \ell^r$, ***do***
3: **Compute** d_i^r from (7.20) and (7.21);
4: **Store** d_i^r in ∇^r;
5: ***end For***
6: **Keep** the smallest ρ_r nodes from ∇^r;
7: **Expand** the survived ρ_r nodes from ***Line #6*** into ∇^{r+1};
8: **Set** $r \leftarrow r+1$;
9: ***end While***
10: **Find** the minimum node in ∇^R;

- **Output** $\hat{\Theta}_{\text{FCSD}}$ as the messages corresponding to the argument of the minimum node in ***Line #10***.

unnecessary nodes, which increases the decoding complexity. On the other hand, a smaller value of the pruned radius may cause an early dropping of the optimum solution, which deteriorates the BER performance. Thus, the appropriate choice of the pruned radius is a crucial process in the FCSD algorithm. For more clarifications, the accumulated node, d_i^r, in (7.20) is a non-central chi-squared random variable with $2rN_r$ degrees of freedom and its pdf is given by [34, (Ch. 2)]

$$f_{d_i^r}(d_i^r) = \frac{1}{\sigma^2}\left(\frac{d_i^r}{\alpha_{r,i}^2}\right)^{(rN_r-1)/2} \exp\left(-\frac{\alpha_{r,i}^2 + d_i^r}{\sigma^2}\right) I_{rN_r-1}\left(\frac{\sqrt{d_i^r\,\alpha_{r,i}^2}}{\sigma_n^2/2}\right), \tag{7.25}$$

where $I_{rN_r-1}(\centerdot)$ is the first kind modified Bessel function with order $(rN_r - 1)$ and the non-centrality parameter $\alpha_{r,i}^2$ is

$$\alpha_{r,i}^2 = \sum_{n_r=1}^{N_r} \sum_{\bar{r}=1}^{r} \left| \sum_{u \in \Lambda_{\bar{r}}} \left(h_{n_r,n_t^u}^{\bar{r},u} c_m^{\bar{r},u} \right) - \sum_{u \in \grave{\Lambda}_{\bar{r}}} h_{n_r,\hat{n}_t^u}^{\bar{r},u} c_{\hat{m}}^{\bar{r},u} - \sum_{u \in \Lambda_{\bar{r}} \setminus \grave{\Lambda}_{\bar{r}}} h_{n_r,n_t^u(i)}^{\bar{r},u} c_{m(i)}^{\bar{r},u} \right|^2 . \tag{7.26}$$

Since d_i^r has an even degrees of freedom value, the probability of not dropping the optimum solution early, $d_i^r|_{\text{opt}}$, can be calculated as [34, (Ch. 2)]

$$\mathcal{P}\left(d_i^r|_{\text{opt}} \leq \gamma_r\right) = 1 - Q_{rN_r}\left(\frac{\alpha_{r,i}}{\sigma/\sqrt{2}}, \frac{\sqrt{\gamma_r}}{\sigma/\sqrt{2}}\right), \tag{7.27}$$

where $Q_{rN_r}(\centerdot,\centerdot)$ is the generalized Marcum function of order rN_r. As seen from (7.27), by increasing the value of γ_r, the value of $\mathcal{P}(d_i^r|_{\text{opt}} \leq \gamma_r)$ becomes closer to unity.

In the FCSD algorithm, the value of γ_r is empirically selected to choose a fixed number of nodes from each level to increase the probability of including the optimal solution based on (7.27). Accordingly, at each level, the value of ρ_r in the FCSD algorithm is fixed for $1 \leq r \leq R-1$. Finally, the FCSD algorithm selects the minimum node among all expanded nodes at the last level to be declared as a solution. Thus, the set of estimated messages for all U users, $\hat{\Theta}_{\text{FCSD}}$, is

$$\hat{\Theta}_{\text{FCSD}} = \left\{ \{\hat{\mathbf{c}}_m^1, \hat{n_t}^1\}^{(R)}, \ldots, \{\hat{\mathbf{c}}_m^U, \hat{n_t}^U\}^{(R)} \right\}, \tag{7.28}$$

where $\{\hat{\mathbf{c}}_m^u, \hat{n_t}^u\}^{(R)}$ is the estimated message of the u-th user corresponding to the minimum node at the R-th level. Algorithm 7.3 summarizes the procedure of the FCSD algorithm.

7.5 Complexity Analysis

In this section, the decoding complexities of the conventional MPA and the proposed algorithms for the SM-SCMA system are discussed. In this chapter, the decoding complexity is measured by the number of real additions and multiplications required to perform a particular algorithm. For the conventional MPA decoder of the SM-SCMA system, the required number of real additions and multiplications, $\text{Add}^{(\text{MPA})}$ and $\text{Mul}^{(\text{MPA})}$, respectively, are given by [29]

$$\text{Add}^{(\text{MPA})} = Rd_f \left(N_t M\right)^{d_f} \left(2N_r(2d_f+1)-1\right) + KRd_f \left(\left(N_t M\right)^{d_f} - 1\right), \tag{7.29}$$

and

$$\text{Mul}^{(\text{MPA})} = Rd_f \left(N_t M\right)^{d_f} \left(2N_r(2d_f+1) + Kd_f + 1\right) + N_t M \left(d_v - 1\right)\left(KRd_f + U\right). \tag{7.30}$$

7.5.1 The SUD Algorithm

In the SUD algorithm, the cost of (7.15) is $R(2N_r d_f - 1)$ real additions and $2RN_r d_f$ real multiplications. The cost of one possible combination of j and l in (7.16) for N_r receive antennas is $N_r(4d_f+2)-1$ real additions and $N_r(4d_f+2)$ real multiplications. The number of possible combinations between j and l in (7.16) varies from one ORE to another based on the system indicator matrix. Thus, the required number of real additions and multiplications, $\text{Add}^{(\text{SUD})}$ and $\text{Mul}^{(\text{SUD})}$, respectively, of the SUD algorithm can be written as

$$\text{Add}^{(\text{SUD})} = R\left(2N_r d_f - 1\right) + \left(N_r\left(4d_f + 2\right) - 1\right) \sum_{\substack{r=1 \\ \grave{U}^r \neq 0}}^{R} \left(MN_t\right)^{\grave{U}^r}, \tag{7.31}$$

and

$$\text{Mul}^{(\text{SUD})} = 2RN_r d_f + N_r\left(4d_f + 2\right) \sum_{\substack{r=1 \\ \grave{U}^r \neq 0}}^{R} \left(MN_t\right)^{\grave{U}^r}. \tag{7.32}$$

The summation term in (7.31) and (7.32) depends on the indicator matrix of the system.[2]

7.5.2 The MSUD Algorithm

The MSUD algorithm iteratively updates the estimated users messages of the SUD algorithm at an extra cost of $KUMN_t(N_r(4d_f + 2) - 1)$ and $KUMN_tN_r(4d_f + 2)$ real additions and multiplications, respectively. Thus, the required number of real additions and multiplications, $\text{Add}^{(\text{MSUD})}$ and $\text{Mul}^{(\text{MSUD})}$, respectively, of the MSUD algorithm are given by[2]

$$\text{Add}^{(\text{SUD})} = R\left(2N_r d_f - 1\right) + \left(N_r\left(4d_f + 2\right) - 1\right) \left(KUMN_t + \sum_{\substack{r=1 \\ \grave{U}^r \neq 0}}^{R} \left(MN_t\right)^{\grave{U}^r} \right), \tag{7.33}$$

and

[2]In this chapter, the system in (7.6) is considered. Consequently, the result of the summation term in (7.31) and (7.32) becomes $(MN_t)^3 + (MN_t)^2 + (MN_t)^1$.

$$\text{Mul}^{(\text{SUD})} = 2RN_r d_f + N_r\left(4d_f+2\right)\left(KUMN_t + \sum_{\substack{r=1 \\ \grave{U}^r \neq 0}}^{R} \left(MN_t\right)^{\grave{U}^r}\right). \tag{7.34}$$

7.5.3 The FCSD Algorithm

The FCSD algorithm visits $(MN_t)^{d_f}$ nodes at the first tree-search level, where each node costs $(N_r(4d_f+2)-R-2)$ and $N_r(4d_f+2)$ real additions and multiplications, respectively. Then, for the rest of $R-1$ levels, the FCSD algorithm visits a fixed number of nodes at each level according to ρ_r. Thus, the required number of real additions and multiplications, $\text{Add}^{(\text{FCSD})}$ and $\text{Mul}^{(\text{FCSD})}$, respectively, of the FCSD algorithm are given by

$$\text{Add}^{(\text{FCSD})} = R\left(2N_r d_f - 1\right) + \left(N_r\left(4d_f+2\right) - R - 2\right)\left(\left(MN_t\right)^{d_f} + \sum_{r=2}^{R} \rho_{r-1}\left(MN_t\right)^{\grave{U}^r}\right), \tag{7.35}$$

and

$$\text{Mul}^{(\text{FCSD})} = 2RN_r d_f + N_r\left(4d_f+2\right)\left(\left(MN_t\right)^{d_f} + \sum_{r=2}^{R} \rho_{r-1}\left(MN_t\right)^{\grave{U}^r}\right). \tag{7.36}$$

7.6 Simulation Results and Discussions

In this section, the proposed decoding algorithms and conventional MPA decoder in [28] are assessed using Monte-Carlo simulations for the SM-SCMA system. The assessment

includes the study of parameters sensitivity for the proposed algorithms, BER performance and decoding complexity comparisons. The Rayleigh fading channel coefficients between the transmit and receive antennas for all users are assumed to be perfectly known at the receiver side. An SM-SCMA system of six users that share four OREs based on (7.4) or (7.6) is considered for the assessment (i.e., $U = 6$, $R = 4$, $d_f = 3$ and $d_v = 2$). Two user spectral efficiencies based on (7.1) are considered in the results: $\eta_u = 3$ bpcu ($N_t = 4$ and $M = 2$) and $\eta_u = 4$ bpcu ($N_t = 4$ and $M = 4$), and the M-QAM scheme is used in the simulations.

Three MIMO scenarios are studied for each user spectral efficiency: under-determined MIMO system (e.g., $N_r = 2$), determined MIMO system (e.g., $N_r = 4$) and over-determined MIMO system (e.g., $N_r = 6$). Thus, there are six scenarios within the scope of this chapter (i.e., three MIMO scenarios for each of the two user spectral efficiencies). It is worth noting that the BER performance of the conventional MPA decoder for the SM-SCMA converges after five iterations (i.e., $K = 5$) for the considered six scenarios. The following simulation results are obtained by running at least 10^5 independent realizations.

7.6.1 Parameters Sensitivity

In this subsection, the effect of some parameters used with the proposed algorithms is studied. First, the convergence behavior of the BER performance for the proposed MSUD algorithm is provided. Finally, the sensitivity of choosing γ_r (or ρ_r) across the tree-search level for the proposed FCSD algorithm is included.

Convergence of the MSUD Algorithm

As mentioned in Section 7.4, the proposed MSUD algorithm is iterative. Thus, after a certain number of iterations, the MSUD algorithm no longer improves the BER performance, a

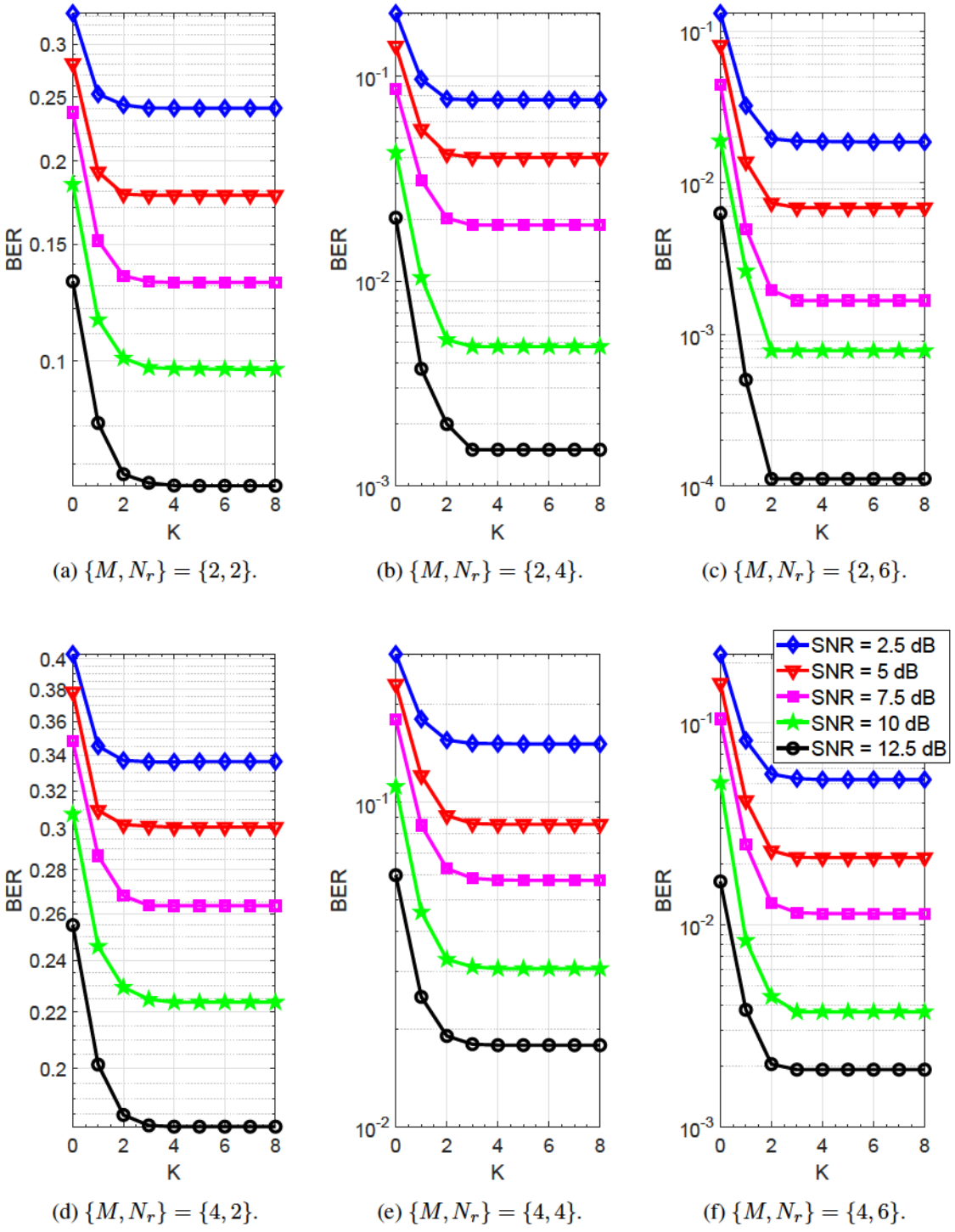

(a) $\{M, N_r\} = \{2, 2\}$. (b) $\{M, N_r\} = \{2, 4\}$. (c) $\{M, N_r\} = \{2, 6\}$.

(d) $\{M, N_r\} = \{4, 2\}$. (e) $\{M, N_r\} = \{4, 4\}$. (f) $\{M, N_r\} = \{4, 6\}$.

Fig. 7.3: Convergence of the proposed MSUD decoder for $N_r \times 4$ MIMO SM-SCMA system.

point called the convergence of the MSUD algorithm. In Fig. 7.3, the convergence of the proposed MSUD algorithm is depicted for all six scenarios. For different SNR values (e.g., 2.5, 5, 7.5, 10 and 12.5 dB), the BER performance of the MSUD algorithm is evaluated for a different number of iterations, K. As seen in Fig. 7.3, the BER performance converges to a particular value after four iterations (i.e., $K = 4$) for all six scenarios. Consequently, the proposed MSUD algorithm requires a few numbers of iterations to converge.

Pruned Radius Sensitivity of the FCSD Algorithm

As seen from (7.27), as γ_r increases, the probability of not missing the optimal solution (i.e., MPA solution) increases. The question that arises is which level has a significant effect on the probability in (7.27). To answer this question, let us define the number of misses (NoM) as the number of times that the FCSD algorithm misses the MPA solution. The NoM can be used as an indicator to study the effect of selecting γ_r at each level, taking into account that a small value of the NoM is a good indicator and vice versa. Thus, the NoM can be formulated as

$$\text{NoM} = \mathbb{E}\left\{\sum_{u=1}^{U} \mathcal{P}\left(\{\hat{\mathbf{c}}_m^u, \hat{n_t}^u\}\,|_{\text{FCSD}} \neq \{\hat{\mathbf{c}}_m^u, \hat{n_t}^u\}\,|_{\text{MPA}}\right)\right\}, \tag{7.37}$$

where $\mathcal{P}(\boldsymbol{.})$ in (7.37) equals 1 or 0 when the estimated messages of the u-th user using the FCSD and MPA decoders are different or the same, respectively.

To study the effect of γ_r, the FCSD algorithm with $[\rho_1 \quad \rho_2 \quad \rho_3] = [15 \quad 15 \quad 15]$ is considered to be the baseline of this study for the three MIMO scenarios of $\eta_u = 3$ bpcu. As depicted in Fig. 7.4, the increase of ρ_2 to 50 when ρ_1 is kept 15 provides a significant improvement in the NoM compared to the increase of survived nodes in the first level (i.e., $\rho_1 = 15$ and $\rho_2 = 50$ is better than $\rho_1 = 50$ and $\rho_2 = 15$). It should be noted that ρ_3 can not be greater than ρ_2 since both belong to SES. Therefore, to study the sensitivity between ρ_1

and ρ_3, let us consider $[\rho_1 \quad \rho_2 \quad \rho_3] = [15 \quad 50 \quad 15]$ as the baseline for that comparison. As shown in Fig. 7.4, the third level provides a noticeable improvement in NoM when extra nodes are considered at that level instead of the first level. Consequently, increasing the number of survived nodes at the SES levels is more effective than at the FES levels. By taking an in-depth look at Fig. 7.4, one can observe that the increase in the number of survived nodes at the second level provides better NoM improvements, compared to the increase in the number of survived nodes at any other level. The reason is that only part of users share the upper levels of FES; thus, the distance metric nodes at these levels do not represent all users. On the other hand, the nodes at lower levels include the distance metrics of all users, which significantly affects the BER performance.

Fig. 7.5 shows the sensitivity of ρ_r in terms of NoM for $\eta_u = 4$ bpcu. In these scenarios, the FCSD algorithm with $[\rho_1 \quad \rho_2 \quad \rho_3] = [30 \quad 30 \quad 30]$ is considered. As discussed for $\eta_u = 3$ bpcu, ρ_2 provides significant improvements in the NoM. On the other hand, ρ_1 and ρ_3 provide almost the same improvements for the three scenarios depicted in Fig. 7.5. In other words, there is no preference for increasing the number of survived nodes at these two levels from the NoM perspective. However, it is preferable to increase ρ_3 rather than ρ_1 from the decoding complexity point of view, as seen from (7.35) and (7.36). This means that increasing ρ_3 results in a lower increase in the decoding complexity compared with the increase of ρ_1.

Finally, increasing the number of survived nodes at the lower tree-search levels has a better effect on the BER performance or/and decoding complexity. It is worth noting that the number of survived nodes at the first levels should be empirically chosen to avoid the early dropping of the MPA solution. Empirically, the FCSD algorithm with $[35 \quad 70 \quad 50]$ and $[110 \quad 320 \quad 300]$ provides near MPA BER performances (i.e., NoM close to zero) for $\eta_u = 3$ bpcu and $\eta_u = 4$ bpcu, respectively.

7.6.2 BER Performance Assessment

In this subsection, the BER performance of the proposed decoders is compared with the conventional MPA versus different values of SNR for all six scenarios. The proposed MSUD algorithm and conventional MPA converges at four and five iterations, respectively (i.e., $K = 4$ for MSUD and $K = 5$ for MPA). Moreover, $K = 1$ is provided for the MSUD and MPA to highlight the improvement in the BER performance when using the value of K at the convergence for both algorithms.

Figs. 7.6, 7.7 and 7.8 depict the BER performance of the proposed and MPA decoders for $\eta_u = 3$ bpcu in different three MIMO scenarios (i.e., $N_r = 2$, 4 and 6). As mentioned in Subsection 7.6.1 and as seen from this figure, the proposed FCSD algorithm with $[\rho_1 \quad \rho_2 \quad \rho_3] = [35 \quad 70 \quad 50]$ provides a very similar BER performance as MPA. The FCSD algorithm with $[\rho_1 \quad \rho_2 \quad \rho_3] = [5 \quad 10 \quad 8]$ is depicted in these figures to show that the FCSD can provide a flexible trade-off between the BER performance and decoding complexity. It is also shown that the proposed SUD provides an acceptable BER performance with a considerable degradation in the BER performance of the MPA. The MSUD with $K = 1$ and $K = 4$ both provide a considerable improvement in the SUD BER performance.

Figs. 7.9, 7.10 and 7.11 show the BER performance of the proposed and MPA decoders for $\eta_u = 4$ bpcu in three different MIMO scenarios (i.e., $N_r = 2$, 4 and 6). Here, the value of $[\rho_1 \quad \rho_2 \quad \rho_3]$ of the proposed FCSD algorithm is modified to be $[110 \quad 320 \quad 300]$ to provide a very similar BER performance as MPA. Same as the findings of Figs. 7.6, 7.7 and 7.8, the SUD algorithm yields an acceptable BER performance, while the MSUD algorithm significantly improves the BER performance of the SUD algorithm, as seen in Figs. 7.9, 7.10 and 7.11.

7.6.3 Decoding Complexity Assessment

In this subsection, the decoding complexity of the proposed and MPA decoders are compared in terms of the required number of real additions and multiplications, based on the deduced equations mentioned in Section 7.5.

Figs. 7.12 and 7.13 show the required number of real additions and multiplications, respectively, for $\eta_u = 3$ bpcu for the three MIMO scenarios. On the other hand, Figs. 7.14 and 7.15 depict the required number of real additions and multiplications, respectively, for $\eta_u = 4$ bpcu for the three MIMO scenarios (i.e., $N_r = 2$, 4 and 6). It can be inferred from all these figures that the proposed SUD algorithm provides the lowest decoding complexity and is significantly low when compared with the MPA and FCSD algorithms. The proposed MSUD algorithm slightly increases the decoding complexity compared with the SUD algorithm; however, its decoding complexity is still very low when compared with the MPA. Finally, although the complexity of the FCSD algorithm is higher when compared with the SUD and MSUD algorithms, it is still significantly lower when compared with MPA.

7.7 Conclusions

This chapter proposes three different low-complexity decoding algorithms for the SM-SCMA system. The proposed SUD algorithm is a non-iterative algorithm that provides a benchmark for the decoding complexity at the expense of the BER performance which is still acceptable for some practical applications. The degradation of its BER performance comes from using only some of the available OREs in estimating the users messages. The proposed MSUD algorithm is an iterative algorithm that considerably improves the BER performance of the SUD algorithm, with the cost of a slight increase in the decoding complexity. The MSUD algorithm uses all available OREs to decode the users messages. The proposed FCSD algorithm provides a close BER performance as MPA with a considerable reduction

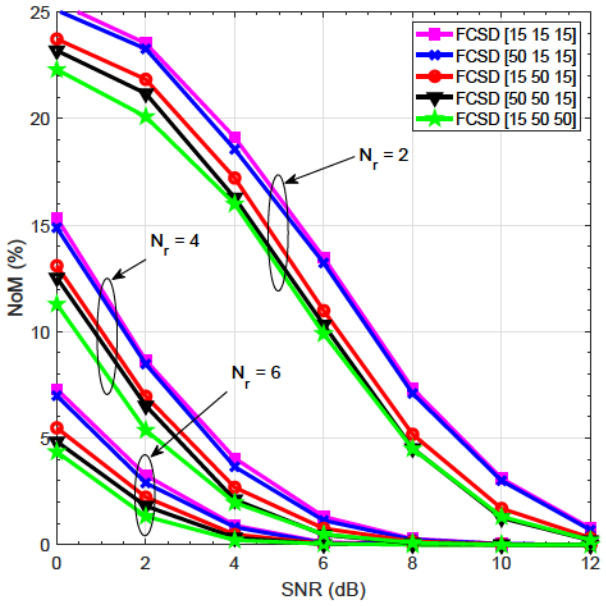

Fig. 7.4: NoM of different values of ρ_r for $\eta_u = 3$ bpcu.

in the decoding complexity. Moreover, the FCSD provides a flexible trade-off between the BER performance and decoding complexity. Unlike the MPA, the proposed FCSD algorithm supports parallel hardware implementation. These proposed algorithms can fit a wide range of practical applications with specific requirements for both operation and hardware implementation. The mathematical formulation, complexity analysis for all proposed algorithms, and simulation results are provided to support these findings.

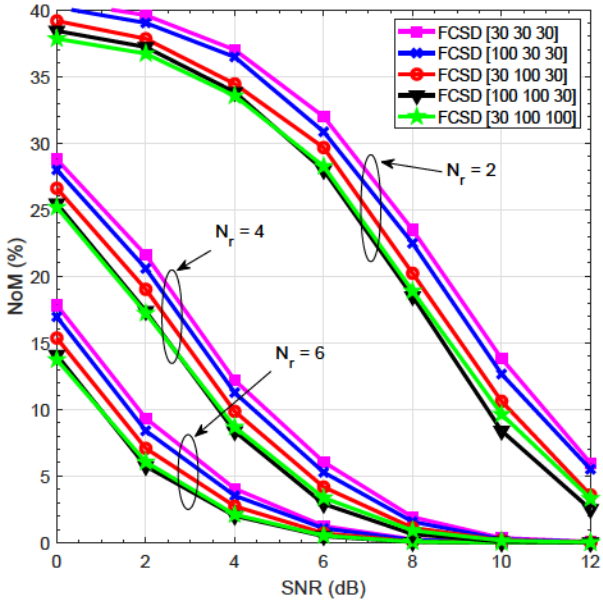

Fig. 7.5: NoM of different values of ρ_r for $\eta_u = 4$ bpcu.

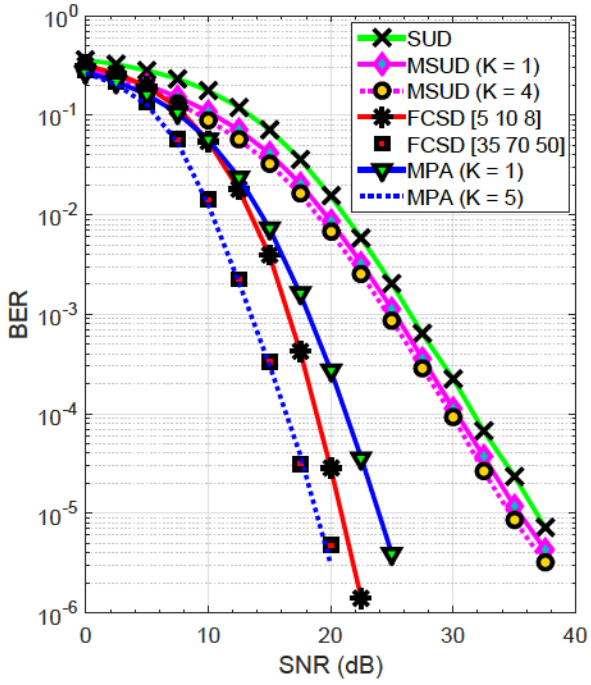

Fig. 7.6: BER performance comparison of 2×4 MIMO with $M = 2$ (i.e., $\eta_u = 3$ bpcu).

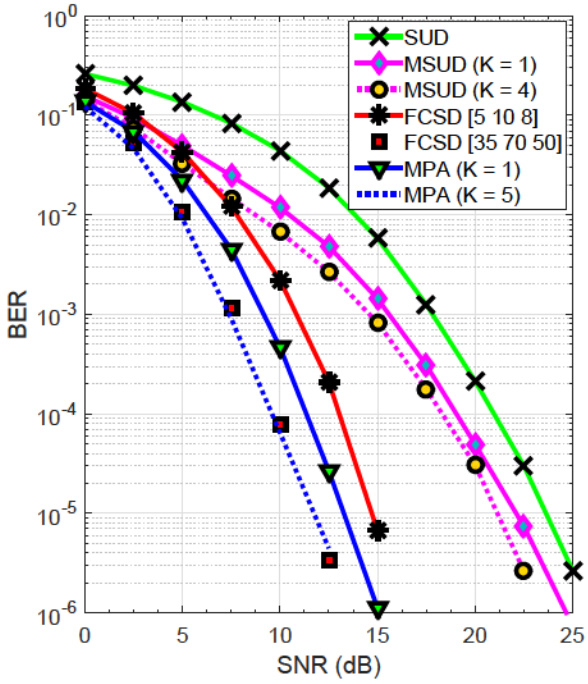

Fig. 7.7: BER performance comparison of 4×4 MIMO with $M = 2$ (i.e., $\eta_u = 3$ bpcu).

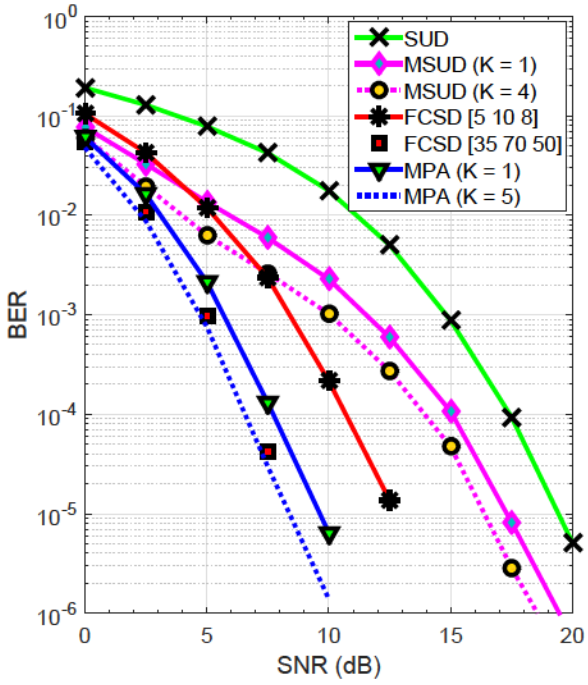

Fig. 7.8: BER performance comparison of 6×4 MIMO with $M = 2$ (i.e., $\eta_u = 3$ bpcu).

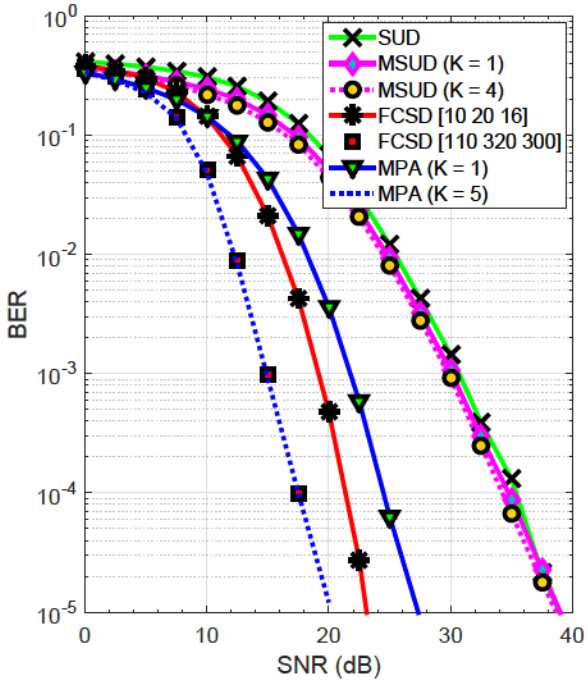

Fig. 7.9: BER performance comparison of 2×4 MIMO with $M = 4$ (i.e., $\eta_u = 4$ bpcu).

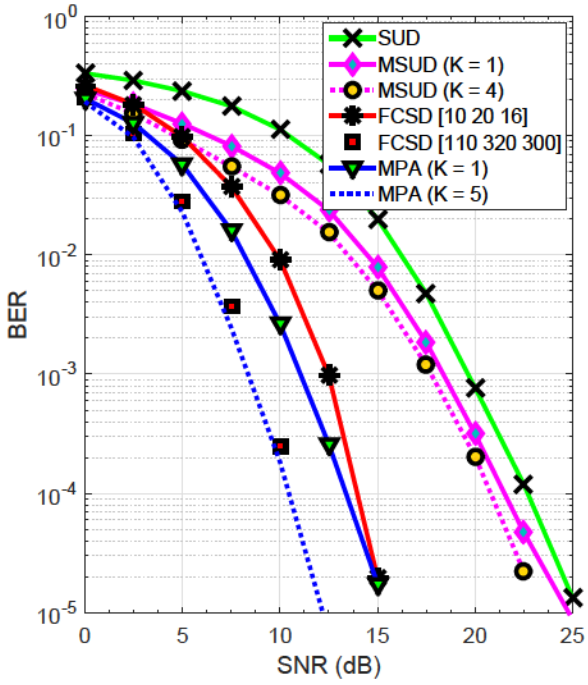

Fig. 7.10: BER performance comparison of 4×4 MIMO with $M = 4$ (i.e., $\eta_u = 4$ bpcu).

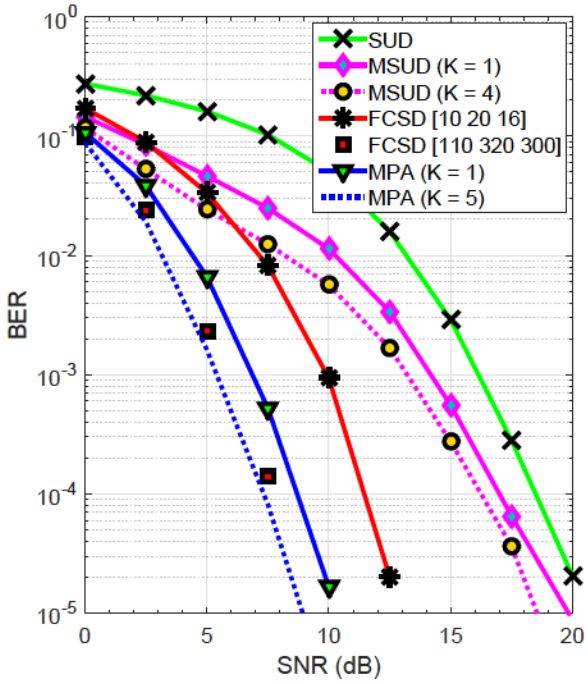

Fig. 7.11: BER performance comparison of 6×4 MIMO with $M = 4$ (i.e., $\eta_u = 4$ bpcu).

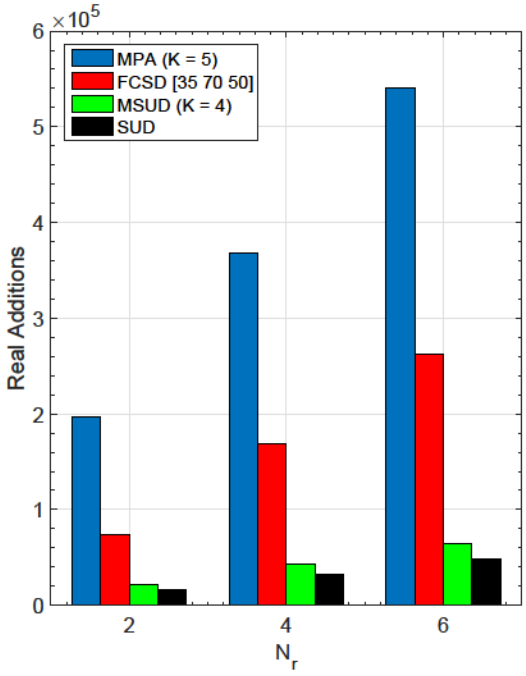

Fig. 7.12: Real additions comparison of different SM-SCMA decoders for $\eta_u = 3$ bpcu.

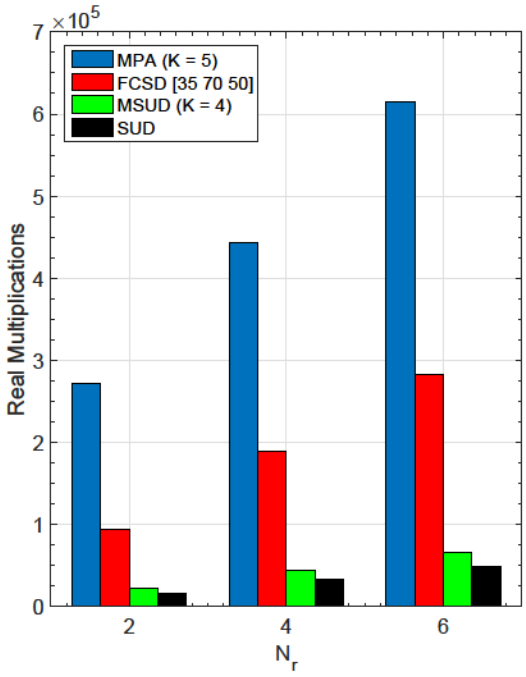

Fig. 7.13: Real multiplications comparison of different SM-SCMA decoders for $\eta_u = 3$ bpcu.

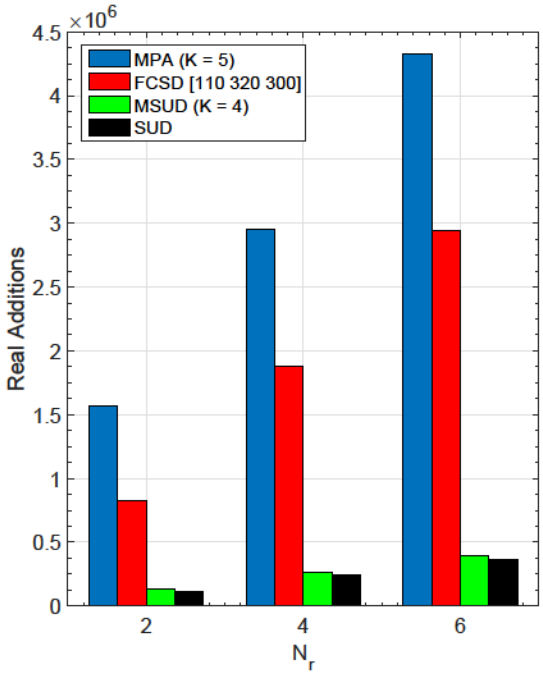

Fig. 7.14: Real additions comparison of different SM-SCMA decoders for $\eta_u = 4$ bpcu.

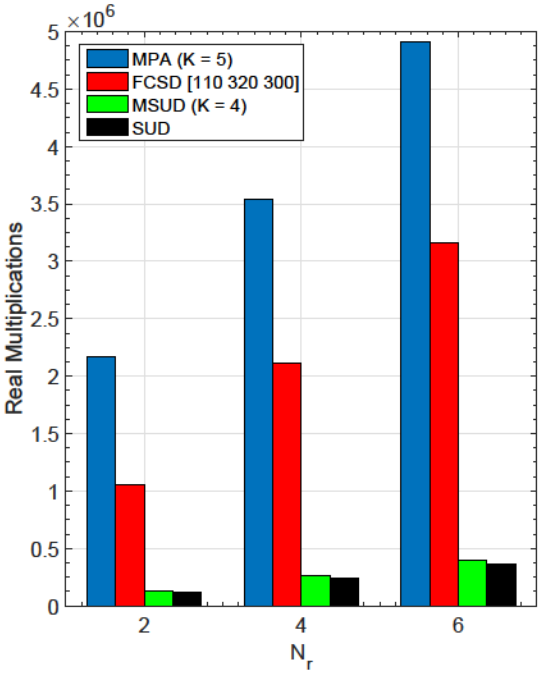

Fig. 7.15: Real multiplications comparison of different SM-SCMA decoders for $\eta_u = 4$ bpcu.

References

[1] W. Shin, M. Vaezi, B. Lee, D. J. Love, J. Lee, and H. V. Poor, "Non-orthogonal multiple access in multi-cell networks: Theory, performance, and practical challenges," *IEEE Commun. Mag.*, vol. 55, no. 10, pp. 176–183, Oct. 2017.

[2] A. Yadav and O. A. Dobre, "All technologies work together for good: A glance at future mobile networks," in *IEEE Wireless Commun.*, vol. 25, no. 4, pp. 10-16, Aug. 2018.

[3] M. Mohammadkarimi, M. A. Raza, and O. A. Dobre, "Signature-based nonorthogonal massive multiple access for future wireless networks: Uplink massive connectivity for machine-type communications," *IEEE Veh. Technol. Mag.*, vol. 13, no. 4, pp. 40–50, Dec. 2018.

[4] S. M. R. Islam, N. Avazov, O. A. Dobre, and K. S. Kwak, "Power-domain non-orthogonal multiple access (NOMA) in 5G systems: Potentials and challenges," *IEEE Commun. Surv. Tuts.*, vol. 19, no. 2, pp. 721-742, Oct. 2016.

[5] Z. Ding, X. Lei, G. K. Karagiannidis, R. Schober, J. Yuan, and V. Bhargava, "A survey on non-orthogonal multiple access for 5G networks: Research challenges and future trends," *IEEE J. Sel. Areas Commun.*, vol. 35, no. 10, pp. 2181 –2195, Oct. 2017.

[6] H. Nikopour and H. Baligh, "Sparse code multiple access," in *Proc. IEEE Int. Symposium on Personal Indoor and Mobile Radio Commun. (PIMRC)*, Sep. 2013, pp. 332–336.

[7] M. Taherzadeh, H. Nikopour, A. Bayesteh, and H. Baligh, "SCMA codebook design," in *Proc. IEEE Veh. Technol. Conf. (VTC Fall)*, Sep. 2014, pp. 1–5.

[8] D. Cai, P. Fan, X. Lei, Y. Liu, and D. Chen, "Multi-dimensional SCMA codebook design based on constellation rotation and interleaving," in *Proc. IEEE Veh. Technol. Conf. (VTC Spring)*, May 2016, pp. 1–5.

[9] M. Vameghestahbanati, I. D. Marsland, R. H. Gohary, and H. Yanikomeroglu, "Multi-dimensional constellations for uplink SCMA systems - A comparative study," *arXiv*, Apr. 2018. [Online]. Available: http://arxiv.org/abs/1804.05814.

[10] H. Mu, Z. Ma, M. Alhaji, P. Fan, and D. Chen, "A fixed low complexity message pass algorithm detector for up-link SCMA system," *IEEE Wireless Commun. Lett.,* vol. 4, no. 6, pp. 585–588, Dec. 2015.

[11] L. Yang, Y. Liu, and Y. Siu, "Low complexity message passing algorithm for SCMA system," *IEEE Commun. Lett.*, vol. 20, no. 12, pp. 2466–2469, Dec. 2016.

[12] J. Dai, K. Niu, C. Dong, and J. Lin, "Improved message passing algorithms for sparse code multiple access," *IEEE Trans. Veh. Technol.*, vol. 66, no. 11, pp. 9986–9999, Nov. 2017.

[13] L. Yang, X. Ma, and Y. Siu, "Low complexity MPA detector based on sphere decoding for SCMA," *IEEE Commun. Lett.*, vol. 21, no. 8, pp. 1855–1858, Aug. 2017.

[14] M. Vameghestahbanati, E. Bedeer, I. Marsland, R. H. Gohary, and H. Yanikomeroglu, "Enabling sphere decoding for SCMA," *IEEE Commun. Lett.*, vol. 21, no. 12, pp. 2750–2753, Dec. 2017.

[15] L. Li, J. Wen, X. Tang, and C. Tellambura, "Modified sphere decoding for sparse code multiple access," *IEEE Commun. Lett.*, vol. 22, no. 8, pp. 1544–1547, Aug. 2018.

[16] R. Y. Mesleh, H. Haas, S. Sinanovic, C. W. Ahn, and S. Yun, "Spatial modulation," *IEEE Trans. Veh. Technol.*, vol. 57, no. 4, pp. 2228–2241, Jul. 2008.

[17] A. Younis, N. Serafimovski, R. Mesleh, and H. Haas, "Generalised spatial modulation," in *Proc. Forty Fourth Asilomar Conf. Signals, Syst., Comput. (ASILOMAR)*, Nov. 2010, pp. 1498–1502.

[18] M. Renzo, H. Haas, A. Ghrayeb, S. Sugiura, and L. Hanzo, "Spatial modulation for generalized MIMO: Challenges, opportunities and implementation," *Proc. IEEE*, vol. 102, no. 1, pp. 56–103, Jan. 2014.

[19] E. Basar, "Index modulation techniques for 5G wireless networks," *IEEE Commun. Mag.,* vol. 54, no. 7, pp. 168–175, Jul. 2016.

[20] A. Younis, R. Mesleh, H. Haas, and P. M. Grant, "Reduced complexity sphere decoder for spatial modulation detection receivers," in *Proc. IEEE GLOBECOM*, 2010, pp. 1–5.

[21] A. Younis, M. Di Renzo, R. Mesleh, and H. Haas, "Sphere decoding for spatial modulation," in *Proc. 2011 IEEE Int. Conf. Commun.*, pp. 1–6.

[22] A. Younis, S. Sinanovic, M. Di Renzo, R. Mesleh, and H. Haas, "Generalised sphere decoding for spatial modulation," *IEEE Trans. Commun.*, vol. 61, no. 7, pp. 2805–2815, July 2013.

[23] I. Al-Nahhal, O. A. Dobre, and S. Ikki, "Quadrature spatial modulation decoding complexity: Study and reduction," *IEEE Wireless Commun. Lett.,* vol. 6, pp. 378-381, Jun. 2017.

[24] I. Al-Nahhal, O. A. Dobre, and S. Ikki, "Low complexity decoders for spatial and quadrature spatial modulations," in *Proc. IEEE Veh. Technol. Conf. (VTC-Spring)*, 2018, pp. 1–5.

[25] I. Al-Nahhal, E. Basar, O. A. Dobre, and S. Ikki, "Optimum low-complexity decoder for spatial modulation," *IEEE J. Sel. Areas Commun.*, vol. 37, no. 9, pp. 2001-2013, Jul. 2019.

[26] C. Zhong, X. Hu, X. Chen, D. W. Ng, and Z. Zhang, "Spatial modulation assisted multi-antenna non-orthogonal multiple access," *IEEE Wireless Commun. Lett.,* vol. 25, no. 2, pp. 61-67, Apr. 2018.

[27] Y. Liu, L. L. Yang, and L. Hanzo, "Spatial modulation aided sparse code division multiple access," *IEEE Trans. Wireless Commun.*, vol. 17, no. 3, pp. 1474–1487, Mar. 2018.

[28] Z. Pan, J. Luo, J. Lei, L. Wen, and C. Tang, "Uplink spatial modulation SCMA system," *IEEE Commun. Lett.,* vol. 23, no. 1, pp. 184-187, Jan. 2019.

[29] I. Al-Nahhal, O. A. Dobre, E. Basar, and S. Ikki, "Low-cost uplink sparse code multiple access for spatial modulation," *IEEE Trans. Veh. Technol.*, vol. 68, no. 9, pp. 9313-9317, Jul. 2019.

[30] L. G. Barbero and J. S. Thompson, "Fixing the complexity of the sphere decoder for MIMO detection," *IEEE Trans. Wireless Commun.,* vol. 7, pp. 2131–2142, Jun. 2008.

[31] I. Al-Nahhal, A. Emran, H. Kasem, A. B. Abd El-Rahman, O. Muta, and H. Furukawa, "Flexible fractional K-best sphere decoding for uncoded MIMO channels," *IEICE Communications Express*, vol., 4, pp. 20-25, Jan. 2015.

[32] I. Al-Nahhal, M. Alghoniemy, A. B. Abd El-Rahman, Z. Kawasaki, "Modified zero forcing decoder for ill-conditioned channels" in *Proc.* IFIP Wireless Days (WD), Nov 2013, pp. 1–3.

[33] I. Al-Nahhal, M. Alghoniemy, O. Muta, and A. B. A. El-Rahman, "Reduced complexity k-best sphere decoding algorithms for ill-conditioned MIMO channels," in *Proc. IEEE Annu. Consum. Commun. Netw. Conf.*, pp. 183-187, Jan. 2016.

[34] J. Proakis, *Digital Communications*, 4th ed. New York, NY, USA: McGraw-Hill, 2000.

Chapter 8

Conclusions and Potential Directions of Future Investigation

In this final chapter, I summarize the contributions presented in this thesis and discuss several potential future directions of investigation.

8.1 Conclusions

In this work, the focus was on designing efficient schemes for future wireless technologies, such as SM and QSM in single-user, and SM-SCMA in multi-user scenarios. Most of the proposed designs provide the optimum BER performance. In Chapter 2, a low-complexity decoding algorithm for square QSM single-user MIMO was proposed, which significantly reduces the decoding complexity of the ML decoder with no loss in the optimal BER performance. A further reduction in the decoding complexity with optimum BER performance was proposed in Chapter 3 for general QSM and SM single-user MIMO system. Chapter 4 provided further analysis of the algorithm proposed in Chapter 3 in terms of expected decoding complexity and the behavior of the algorithm for perfect and imperfect channel

state information at the receiver side. Furthermore, a novel reliable algorithm to decode single-user SM transmitted messages was proposed in Chapter 5. The BER performance and complexity of the proposed algorithm were theoretically derived. The proposed algorithm provides a significant reduction in the decoding complexity compared to ML, without sacrificing the BER performance. Moreover, a flexible trade-off between the BER performance and complexity was presented to demonstrate the reliability of the proposed algorithm.

A low-cost multi-user SM MIMO system was proposed in Chapter 6 with the aid of the SCMA technique. This proposed system requires a smaller number of the transmit antenna with almost no additional detriments to the BER performance or decoding complexity when compared with the conventional SM-SCMA. Moreover, three low-complexity decoding algorithms were proposed in Chapter 7 for the SM-SCMA system. The first algorithm can be considered the benchmark for the decoding complexity at the expense of the BER performance, which is still acceptable for some practical applications. The second algorithm improves the BER performance of the first algorithm with the added cost of slightly increased decoding complexity. Finally, the third algorithm not only provides the optimal BER performance with a significant reduction in the decoding complexity, but also provides a flexible trade-off between BER and complexity. These algorithms can fit a wide range of practical applications with specific requirements for both operation and hardware implementation. The mathematical formulation, complexity analysis for all proposed algorithms, and simulation results were provided to support these findings.

8.2 Potential Directions of Future Investigation

The work presented in this thesis opens the door for future investigations, among which I list the following:

- Machine learning methods can be applied to the single-user SM-MIMO system. Neural

networks should be a suitable option, as they can approximate any function when the dataset size is sufficiently large. The number of layers and neurons for each layer should be investigated according to the given problem, such as system size and target BER performance.

- Since the multi-user SM-SCMA system is a promising technique proposed very recently, more investigations should be performed on it, such as evaluating the system under diverse transmission environments.

- Novel schemes may be proposed for the SM-SCMA system to enhance the functionality of the transmitter and/or receiver.

- Low-complexity receivers may be explored for the SM-SCMA system for further reduction in the decoding complexity, while taking into account the BER performance.

- Machine learning models may be studied for the SM-SCMA system to reduce its decoding complexity.

In conclusion, more investigations can be done regarding reducing the decoding complexity of the SM-MIMO and SM-SCMA systems. The neural network approach should be one of the avenues to be considered in these investigations.

References

Chapter 1

[1] A. Kaye and D. George, “Transmission of multiplexed PAM signals over multiple channel and diversity systems," *IEEE Transactions on Communication Technology*, vol. 18, no. 5, pp. 520-526, Oct. 1970.

[2] J. Mietzner, R. Schober, L. Lampe, W. H. Gerstacker, and P. A. Hoher, “Multiple–antenna techniques for wireless communications – A comprehensive literature survey”, *IEEE Commun. Surveys Tuts.*, vol. 11, no. 2, pp. 87–105, 2nd quarter 2009.

[3] M. A. Albreem, M. Juntti, and S. Shahabuddin, “Massive MIMO Detection Techniques: A Survey,” *IEEE Commun. Surveys Tuts.*, vol. 21, no. 4, pp. 3109-3132, 4th quarter 2019.

[4] M. D. Renzo, H. Haas, and P. M. Grant, “Spatial modulation for multiple-antenna wireless systems: A survey,” *IEEE Commun. Mag.*, vol. 49, no. 12, pp. 182-191, Dec. 2011.

[5] M. Renzo, H. Haas, A. Ghrayeb, S. Sugiura, and L. Hanzo, “Spatial modulation for generalized MIMO: Challenges, opportunities and implementation,” *Proc. IEEE*, vol. 102, no. 1, pp. 56–103, Jan. 2014.

[6] T. Mao, Q. Wang, Z. Wang, and S. Chen, “Novel index modulation techniques:

A survey," *IEEE Commun. Surveys Tuts.*, vol. 21, no. 1, pp. 315-348, 1st quarter 2019.

[7] M. Wen et al., "A survey on spatial modulation in emerging wireless systems: Research progresses and applications," *IEEE J. Sel. Areas Commun.*, vol. 37, no. 9, pp. 1949-1972, Sep. 2019.

[8] R. Mesleh, H. Haas, S. Sinanovic, C. W. Ahn, and S. Yun, "Spatial modulation," *IEEE Trans. Veh. Technol.*, vol. 57, no. 4, pp. 2228–2241, July 2008.

[9] R. Mesleh, S. S. Ikki, and H. M. Aggoune, "Quadrature spatial modulation," *IEEE Trans. Veh. Technol.*, vol. 64, pp. 2738–2742, Jun. 2015.

[10] W. Shin, M. Vaezi, B. Lee, D. J. Love, J. Lee, and H. V. Poor, "Non-orthogonal multiple access in multi-cell networks: Theory, performance, and practical challenges," *IEEE Commun. Mag.*, vol. 55, no. 10, pp. 176–183, Oct. 2017.

[11] H. Nikopour and H. Baligh, "Sparse code multiple access," in *Proc. IEEE Int. Symposium on Personal Indoor and Mobile Radio Commun. (PIMRC)*, Sep. 2013, pp. 332–336.

[12] M. Taherzadeh, H. Nikopour, A. Bayesteh, and H. Baligh, "SCMA codebook design," in *Proc. IEEE Veh. Technol. Conf. (VTC Fall)*, Sep. 2014, pp. 1–5.

[13] Y. Liu, L. L. Yang, and L. Hanzo, "Spatial modulation aided sparse code division multiple access," *IEEE Trans. Wireless Commun.*, vol. 17, no. 3, pp. 1474–1487, Mar. 2018.

[14] Z. Pan, J. Luo, J. Lei, L. Wen, and C. Tang, "Uplink spatial modulation SCMA system," *IEEE Commun. Lett.,* vol. 23, no. 1, pp. 184-187, Jan. 2019.

[15] S. Rangan, T. S. Rappaport, and E. Erkip, "Millimeter-wave cellular wireless networks: Potentials and challenges," *Proc. IEEE*, vol. 102, no. 3, pp. 366–385, Mar. 2014.

[16] W. Wu, N. Zhang, N. Cheng, Y. Tang, K. Aldubaikhy, and X. Shen, "Beef up

mmWave dense cellular networks with D2D-assisted cooperative edge caching," *IEEE Trans. Veh. Technol.*, vol. 68, no. 4, pp. 3890-3904, Apr. 2019.

[17] N. Ishikawa, R. Rajashekar, S. Sugiura, and L. Hanzo, "Generalized spatial modulation-based reduced-RF-chain millimeter-wave communications," *IEEE Trans. Veh. Technol.*, vol. 66, no. 1, pp. 879–883, Jan. 2017.

[18] P. Liu and A. Springer, "Space shift keying for LOS communication at mmWave frequencies," *IEEE Wireless Commun. Lett.,* vol. 4, no. 2, pp. 121–124, Apr. 2015.

[19] P. Liu, M. D. Renzo, and A. Springer, "Line-of-sight spatial modulation for indoor mmWave communication at 60 GHz," *IEEE Trans. Wireless Commun.*, vol. 15, no. 11, pp. 7373–7389, Nov. 2016.

[20] P. Liu, J. Blumenstein, N. S. Perovi, M. D. Renzo, and A. Springer, "Performance of generalized spatial modulation MIMO over measured 60GHz indoor channels," *IEEE Trans. Commun.*, vol. 66, no. 1, pp. 133– 148, Jan. 2018.

[21] A. Younis, N. Abuzgaia, R. Mesleh, and H. Haas, "Quadrature spatial modulation for 5G outdoor millimeterwave communications: Capacity analysis," *IEEE Trans. Wireless Commun.*, vol. 16, no. 5, pp. 2882–2890, May 2017.

[22] D. Karunatilaka, F. Zafar, V. Kalavally, and R. Parthiban, "LED based indoor visible light communications: State of the art," *IEEE Commun. Surveys Tuts.*, vol. 17, no. 3, pp. 1649–1678, Third Quarter 2015.

[23] W. O. Popoola, "Impact of VLC on light emission quality of white LEDs," *J. Lightw. Technol.*, vol. 34, no. 10, pp. 2526–2532, May 2016.

[24] C. R. Kumar and R. K. Jeyachitra, "Power efficient generalized spatial modulation MIMO for indoor visible light communications," *IEEE Photon. Technol. Lett.*, vol. 29, no. 11, pp. 921–924, Jun. 2017.

[25] W. O. Popoola and H. Haas, "Demonstration of the merit and limitation of

generalised space shift keying for indoor visible light communications," *J. Lightw. Technol.*, vol. 32, no. 10, pp. 1960–1965, May 2014.

[26] K. Xu, H. Yu, and Y. Zhu, "Channel-adapted spatial modulation for massive MIMO visible light communications," *IEEE Photon. Technol. Lett.*, vol. 28, no. 23, pp. 2693–2696, Dec. 2016.

[27] T. Wang, F. Yang, L. Cheng, and J. Song, "Spectral-efficient generalized spatial modulation based hybrid dimming scheme with LACO-OFDM in VLC," *IEEE Access*, vol. 6, pp. 41 153–41 162, 2018.

[28] J. Wang, J. Zhu, S. Lin, and J. Wang, "Adaptive spatial modulation based visible light communications: SER analysis and optimization," *IEEE Photon. J.*, vol. 10, no. 3, pp. 1–14, Jun. 2018.

[29] A. Yesilkaya, E. Basar, F. Miramirkhani, E. Panayirci, M. Uysal, and H. Haas, "Optical MIMO-OFDM with generalized LED index modulation," *IEEE Trans. Commun.*, vol. 65, no. 8, pp. 3429–3441, Aug. 2017.

[30] J. G. Andrews, S. Buzzi, W. Choi, S. V. Hanly, A. Lozano, A. C. Soong, and J. C. Zhang, "What will 5g be?" *IEEE J. Sel. Areas Commun.*, vol. 32, pp. 1065–1082, Jun. 2014.

[31] P. Yang, M. Di Renzo, Y. Xiao, S. Li, and L. Hanzo, "Design guidelines for spatial modulation," *IEEE Commun. Surveys Tuts.*, vol. 17, pp. 6–26, 1st Quart. 2015.

[32] I. Al-Nahhal, O. A. Dobre, and S. Ikki, "Quadrature spatial modulation decoding complexity: Study and reduction," *IEEE Wireless Commun. Lett.,* vol. 6, pp. 378-381, Jun. 2017.

[33] I. Al-Nahhal, O. A. Dobre, and S. Ikki, "Low complexity decoders for spatial and quadrature spatial modulations," in *Proc. IEEE Veh. Technol. Conf. (VTC-Spring)*, 2018, pp. 1–5.

[34] I. Al-Nahhal, E. Basar, O. A. Dobre, and S. Ikki, "Optimum low-complexity decoder for spatial modulation," *IEEE J. Sel. Areas Commun.*, vol. 37, no. 9, pp. 2001-2013, Jul. 2019.

[35] I. Al-Nahhal, O. A. Dobre, and S. Ikki, "Reliable detection for spatial modulation systems," arXiv preprint arXiv:2006.05084.

[36] I. Al-Nahhal, O. A. Dobre, E. Basar, and S. Ikki, "Low-cost uplink sparse code multiple access for spatial modulation," *IEEE Trans. Veh. Technol.*, vol. 68, no. 9, pp. 9313-9317, Jul. 2019.

[37] I. Al-Nahhal, O. A. Dobre, and S. Ikki, "On the complexity reduction of uplink sparse code multiple access for spatial modulation," accepted, *IEEE Trans. Commun., Aug. 2020. doi: 10.1109/TCOMM.2020.3018184.*

Chapter 2

[1] J. G. Andrews, S. Buzzi, W. Choi, S. V. Hanly, A. Lozano, A. C. Soong, and J. C. Zhang, "What will 5g be?" *IEEE J. Sel. Areas Commun.*, vol. 32, pp. 1065–1082, Jun. 2014.

[2] R. Mesleh, S. S. Ikki, and H. M. Aggoune, "Quadrature spatial modulation," *IEEE Trans. Veh. Technol.*, vol. 64, pp. 2738–2742, Jun. 2015.

[3] R. Y. Mesleh, H. Haas, S. Sinanovic, C. W. Ahn, and S. Yun, "Spatial modulation," *IEEE Trans. Veh. Technol.*, vol. 57, pp. 2228–2241, Jul. 2008.

[4] A. Younis, R. Mesleh, H. Haas, and P. M. Grant, "Reduced complexity sphere decoder for spatial modulation detection receivers," in *Proc. IEEE GLOBECOM*, 2010, pp. 1–5.

[5] A. Younis, S. Sinanovic, M. Di Renzo, R. Mesleh, and H. Haas, "Generalised sphere decoding for spatial modulation," *IEEE Trans. Commun.*, vol. 61, pp.

2805–2815, Jul. 2013.

[6] Q. Tang, Y. Xiao, P. Yang, Q. Yu, and S. Li, "A new low-complexity near-ml detection algorithm for spatial modulation," *IEEE Wireless Commun. Lett.*, vol. 2, pp. 90–93, Feb. 2013.

[7] P. Yang, M. Di Renzo, Y. Xiao, S. Li, and L. Hanzo, "Design guidelines for spatial modulation," *IEEE Commun. Surveys Tuts.*, vol. 17, pp. 6–26, 1st Quart. 2015.

[8] E. Viterbo and J. Boutros, "A universal lattice code decoder for fading channels," *IEEE Trans. Inf. Theory*, vol. 45, pp. 1639–1642, Jul. 1999.

[9] F. Bellili, R. Meftehi, S. Affes, and A. Stéphenne, "Maximum likelihood snr estimation of linearly-modulated signals over time-varying flat-fading simo channels," *IEEE Trans. Signal Process.*, vol. 63, pp. 441–456, Jan. 2015.

[10] L. Xiao, P. Yang, S. Fan, S. Li, L. Song, and Y. Xiao, "Low-complexity signal detection for large-scale quadrature spatial modulation systems," *IEEE Commun. Letters*, vol. 20, pp. 2173-2176, Nov. 2016.

[11] B. Hassibi and H. Vikalo, "On the sphere-decoding algorithm I. Expected complexity," *IEEE Trans. Signal Process.*, vol. 53, pp. 2806–2818, Aug. 2005.

[12] J. Proakis, *Digital Communications Systems Engineering*, 4th ed. McGraw-Hill, 2000.

[13] A. Leon-Garcia, *Probability, Statistics, and Random Processes for Electrical Engineering*, 3rd ed. Pearson/Prentice Hall Upper Saddle River, NJ, 2008.

Chapter 3

[1] J. G. Andrews, S. Buzzi, W. Choi, S. V. Hanly, A. Lozano, A. C. Soong, and J. C. Zhang, "What will 5g be?," *IEEE J. Sel. Areas Commun.*, vol. 32, pp.

1065–1082, Jun. 2014.

[2] R. Y. Mesleh, H. Haas, S. Sinanovic, C. W. Ahn, and S. Yun, "Spatial modulation," *IEEE Trans. Veh. Technol.*, vol. 57, pp. 2228–2241, Jul. 2008.

[3] R. Mesleh, S. S. Ikki, and H. M. Aggoune, "Quadrature spatial modulation," *IEEE Trans. Veh. Technol.*, vol. 64, pp. 2738–2742, Jun. 2015.

[4] A. Younis, R. Mesleh, H. Haas, and P. M. Grant, "Reduced complexity sphere decoder for spatial modulation detection receivers," in *Proc. IEEE GLOBECOM*, 2010, pp. 1–5.

[5] A. Younis, S. Sinanovic, M. Di Renzo, R. Mesleh, and H. Haas, "Generalised sphere decoding for spatial modulation," *IEEE Trans. Commun.*, vol. 61, pp. 2805–2815, Jul. 2013.

[6] Q. Tang, Y. Xiao, P. Yang, Q. Yu, and S. Li, "A new low-complexity near-ml detection algorithm for spatial modulation," *IEEE Wireless Commun. Lett.*, vol. 2, pp. 90–93, Feb. 2013.

[7] L. Xiao, P. Yang, S. Fan, S. Li, L. Song, and Y. Xiao, "Low-complexity signal detection for large-scale quadrature spatial modulation systems," *IEEE Commun. Lett.*, vol. 20, pp. 2173-2176, Nov. 2016.

[8] I. Al-Nahhal, O. A. Dobre, and S. Ikki, "Quadrature spatial modulation decoding complexity: Study and reduction," *IEEE Wireless Commun. Lett.*, vol. 6, pp. 378-381, Jun. 2017.

[9] E. Viterbo and J. Boutros, "A universal lattice code decoder for fading channels," *IEEE Trans. Inf. Theory*, vol. 45, pp. 1639–1642, Jul. 1999.

[10] F. Bellili, R. Meftehi, S. Affes, and A. Stéphenne, "Maximum likelihood snr estimation of linearly-modulated signals over time-varying flat-fading simo channels," *IEEE Trans. Signal Process.*, vol. 63, pp. 441–456, Jan. 2015.

[11] J. Proakis, *Digital Communications Systems Engineering*, 4th ed. New York,

NY, USA: McGraw-Hill, 2000.

Chapter 4

[1] I. Al-Nahhal, O. A. Dobre, and S. Ikki, "Low complexity decoders for spatial and quadrature spatial modulations," in *Proc. IEEE Veh. Technol. Conf. (VTC-Spring)*, 2018, pp. 1–5.

[2] E. Telatar, "Capacity of multi-antenna Gaussian channels," *European Trans. Telecommun.*, vol. 10, no. 6, pp. 585–595, Nov.-Dec. 1999.

[3] C.-X. Wang et al., "Cellular architecture and key technologies for 5G wireless communication networks," *IEEE Commun. Mag.*, vol. 52, no. 2, pp. 122–130, Feb. 2014.

[4] M. Renzo, H. Haas, A. Ghrayeb, S. Sugiura, and L. Hanzo, "Spatial modulation for generalized MIMO: Challenges, opportunities and implementation," *Proc. IEEE*, vol. 102, no. 1, pp. 56–103, Jan. 2014.

[5] E. Basar, "Index modulation techniques for 5G wireless networks," *IEEE Commun. Mag.*, vol. 54, no. 7, pp. 168–175, Jul. 2016.

[6] R. Mesleh, H. Haas, S. Sinanovic, C. W. Ahn, and S. Yun, "Spatial modulation," *IEEE Trans. Veh. Technol.*, vol. 57, no. 4, pp. 2228–2241, July 2008.

[7] J. Jeganathan, A. Ghrayeb, and L. Szczecinski, "Spatial modulation: Optimal detection and performance analysis," *IEEE Commun. Lett.*, vol. 12, no. 8, pp. 545–547, Aug. 2008.

[8] E. Basar, Ü. Aygölü, E. Panayırcı, and H. V. Poor, "Space-time block coded spatial modulation," *IEEE Trans. Commun.*, vol. 59, no. 3, pp. 823–832, Mar. 2011.

[9] M. Di Renzo, H. Haas, and P. M. Grant, "Spatial modulation for multiple-

antenna wireless systems: A survey," *IEEE Commun. Mag.*, vol. 49, no. 12, pp. 182–191, Dec. 2011.

[10] J. G. Andrews, S. Buzzi, W. Choi, S. V. Hanly, A. Lozano, A. C. Soong, and J. C. Zhang, "What will 5G be?" *IEEE J. Sel. Areas Commun.*, vol. 32, no. 6, pp. 1065–1082, Jun. 2014.

[11] A. Younis, R. Mesleh, H. Haas, and P. M. Grant, "Reduced complexity sphere decoder for spatial modulation detection receivers," in *Proc. IEEE GLOBECOM*, 2010, pp. 1–5.

[12] A. Younis, M. Di Renzo, R. Mesleh, and H. Haas, "Sphere decoding for spatial modulation," in *Proc. 2011 IEEE Int. Conf. Commun.*, pp. 1–6.

[13] A. Younis, S. Sinanovic, M. Di Renzo, R. Mesleh, and H. Haas, "Generalised sphere decoding for spatial modulation," *IEEE Trans. Commun.*, vol. 61, no. 7, pp. 2805–2815, July 2013.

[14] Q. Tang, Y. Xiao, P. Yang, Q. Yu, and S. Li, "A new low-complexity near-ml detection algorithm for spatial modulation," *IEEE Wireless Commun. Lett.*, vol. 2, no. 1, pp. 90–93, Feb. 2013.

[15] L. Xiao, P. Yang, S. Fan, S. Li, L. Song, and Y. Xiao, "Low-complexity signal detection for large-scale quadrature spatial modulation systems," *IEEE Commun. Lett.*, vol. 20, pp. 2173-2176, Nov. 2016.

[16] I. Al-Nahhal, O. A. Dobre, and S. Ikki, "Quadrature spatial modulation decoding complexity: Study and reduction," *IEEE Wireless Commun. Lett.*, vol. 6, pp. 378-381, Jun. 2017.

[17] X. Zhang, Y. Zhang, C. Liu, and H. Jia, "Low-complexity detection algorithms for spatial modulation MIMO systems," *Hindawi Journal of Electrical and Computer Engineering*, doi:10.1155/2018/4034625, 2018.

[18] P. Yang, M. Di Renzo, Y. Xiao, S. Li, and L. Hanzo, "Design guidelines for

spatial modulation," *IEEE Commun. Surveys Tuts.*, vol. 17, pp. 6–26, 1st Quart. 2015.

[19] E. Viterbo and J. Boutros, "A universal lattice code decoder for fading channels," *IEEE Trans. Inf. Theory*, vol. 45, no. 5, pp. 1639–1642, Jul. 1999.

[20] B. Hassibi and H. Vikalo, "On the sphere-decoding algorithm I. Expected complexity," *IEEE Trans. Signal Process.*, vol. 53, no. 8, pp. 2806–2818, Aug. 2005.

[21] A. Das and B. D. Rao, "SNR and noise variance estimation for MIMO systems," *IEEE Trans. Signal Process.*, vol. 60, no. 8, pp. 3929–3941, Aug. 2012.

[22] F. Bellili, R. Meftehi, S. Affes, and A. Stéphenne, "Maximum likelihood snr estimation of linearly-modulated signals over time-varying flat-fading simo channels," *IEEE Trans. Signal Process.*, vol. 63, no. 2, pp. 441–456, Jan. 2015.

[23] J. Proakis, *Digital Communications Systems Engineering*, 4th ed. McGraw-Hill, New Yourk, 2000.

[24] P. C. Sofotasios, S. Muhaidat, G. K. Karagiannidis, and B. S. Sharif, "Solutions to integrals involving the Marcum Q-function and applications," *IEEE Signal Process. Lett.*, vol. 22, no. 10, pp. 1752–1756, Oct. 2015.

[25] Y. A. Brychkov, *Handbook of Special Functions: Derivatives, Integrals, Series and other Formulas*, CRC, Florida, USA, 2008.

[26] J. Wu and C. Xiao, "Optimal diversity combining based on linear estimation of Rician fading channels," *IEEE Trans. Commun.*, vol. 56, no. 10, pp. 1612–1615, Oct. 2008.

[27] E. Basar, Ü. Aygölü, E. Panayırcı, and H. V. Poor, "Performance of spatial modulation in the presence of channel estimation errors," *IEEE Commun. Lett.*, vol. 16, no. 2, pp. 176–179, Feb. 2012.

[28] A. Leon-Garcia, *Probability, Statistics, and Random Processes for Electrical*

Engineering, 3rd ed. Pearson/Prentice Hall Upper Saddle River, NJ, 2008.

[29] V. Tarokh, A. Naguib, N. Seshadri, and A. Calderbank, "Space-time codes for high data rate wireless communication: performance criteria in the presence of channel estimation errors, mobility, and multiple paths," *IEEE Trans. Commun.*, vol. 47, no. 2, pp. 199–207, Feb. 1999.

[30] M. Biguesh and A. B. Gershman, "MIMO channel estimation: Optimal training and tradeoffs between estimation techniques," in *Proc. ICC*, Paris, France, June 2004, vol. 5, pp. 2658-2662.

[31] M. Biguesh, and A. B. Gershman, "Training based MIMO channel estimation: A study of estimator tradeoffs and optimal training signals," *IEEE Trans. Signal Process.*, vol. 54, pp. 884-893, Mar. 2006.

[32] W. Liu, N. Wang, M. Jin, and H. Xu, "Denoising detection for the generalized spatial modulation system using sparse property," *IEEE Commun. Lett.*, vol. 18, no. 1, pp. 22–25, Jan. 2014.

[33] L. Xiao et al., "Compressive sensing assisted spatial multiplexing aided spatial modulation," *IEEE Trans. Wireless Commun.*, vol. 17, no. 2, pp. 794–807, Feb. 2018.

[34] C. Wang, P. Cheng, Z. Chen, J. A. Zhang, Y. Xiao, and L. Gui, "Near ML low-complexity detection for generalized spatial modulation," *IEEE Commun. Lett.*, vol. 20, no. 3, pp. 618–621, Mar. 2016.

[35] A. Younis, N. Serafimovski, R. Mesleh, and H. Haas, "Generalised spatial modulation," in *Proc. Forty Fourth Asilomar Conf. Signals, Syst., Comput. (ASILOMAR)*, Nov. 2010, pp. 1498–1502.

[36] R. Mesleh, S. S. Ikki, and H. M. Aggoune, "Quadrature spatial modulation," *IEEE Trans. Veh. Technol.*, vol. 64, no. 6, pp. 2738–2742, Jun. 2015.

Chapter 5

[1] E. Basar, "Index modulation techniques for 5G wireless networks," *IEEE Commun. Mag.,* vol. 54, no. 7, pp. 168–175, Jul. 2016.

[2] Z. Pan, J. Luo, J. Lei, L. Wen, and C. Tang, "Uplink spatial modulation SCMA system," *IEEE Commun. Lett.,* vol. 23, no. 1, pp. 184-187, Jan. 2019.

[3] I. Al-Nahhal, O. A. Dobre, E. Basar, and S. Ikki, "Low-cost uplink sparse code multiple access for spatial modulation," *IEEE Trans. Veh. Technol.*, vol. 68, no. 9, pp. 9313-9317, Jul. 2019.

[4] R. Mesleh, H. Haas, S. Sinanovic, C. W. Ahn, and S. Yun, "Spatial modulation," *IEEE Trans. Veh. Technol.,* vol. 57, no. 4, pp. 2228–2241, July 2008.

[5] M. Di Renzo, H. Haas, and P. M. Grant, "Spatial modulation for multiple-antenna wireless systems: A survey," *IEEE Commun. Mag.*, vol. 49, no. 12, pp. 182–191, Dec. 2011.

[6] E. Basar, U. Aygolu, E. Panayırcı, and H. V. Poor, "Performance of spatial modulation in the presence of channel estimation errors," *IEEE Commun. Lett.,* vol. 16, no. 2, pp. 176–179, Feb. 2012.

[7] A. Younis, S. Sinanovic, M. Di Renzo, R. Mesleh, and H. Haas, "Generalised sphere decoding for spatial modulation," *IEEE Trans. Commun.,* vol. 61, no. 7, pp. 2805–2815, July 2013.

[8] I. Al-Nahhal, O. A. Dobre, and S. Ikki, "Quadrature spatial modulation decoding complexity: Study and reduction," *IEEE Wireless Commun. Lett.,* vol. 6, pp. 378-381, Jun. 2017.

[9] I. Al-Nahhal, O. A. Dobre, and S. Ikki, "Low complexity decoders for spatial and quadrature spatial modulations," in *Proc. IEEE VTC Spring*, Jun. 2018, pp. 1–5.

[10] I. Al-Nahhal, E. Basar, O. A. Dobre, and S. Ikki, "Optimum low-complexity decoder for spatial modulation," *IEEE J. Sel. Areas Commun.*, vol. 37, no. 9, pp. 2001-2013, Jul. 2019.

[11] Q. Tang, Y. Xiao, P. Yang, Q. Yu, and S. Li, "A new low-complexity near-ml detection algorithm for spatial modulation," *IEEE Wireless Commun. Lett.,* vol. 2, no. 1, pp. 90–93, Feb. 2013.

[12] L. Xiao, P. Yang, S. Fan, S. Li, L. Song, and Y. Xiao, "Low-complexity signal detection for large-scale quadrature spatial modulation systems," *IEEE Commun. Lett.,* vol. 20, pp. 2173-2176, Nov. 2016.

[13] R. Mesleh, S. S. Ikki, and H. M. Aggoune, "Quadrature spatial modulation," *IEEE Trans. Veh. Technol.*, vol. 64, pp. 2738–2742, Jun. 2015.

[14] J. Proakis, *Digital Communications Systems Engineering*, 4th ed. McGraw-Hill, New Yourk, 2000.

[15] P. C. Sofotasios, S. Muhaidat, G. K. Karagiannidis, and B. S. Sharif, "Solutions to integrals involving the Marcum Q-function and applications," *IEEE Signal Process. Lett.*, vol. 22, no. 10, pp. 1752–1756, Oct. 2015.

[16] M. Abramowitz and I. A. Stegun, *Handbook of Mathematical Functions with Formulas, Graphs, and Mathematical Tables*, 9th ed. Dover Publications, New York, 1972.

Chapter 6

[1] M. Mohammadkarimi, M. A. Raza, and O. A. Dobre, "Signature-based nonorthogonal massive multiple access for future wireless networks: Uplink massive connectivity for machine-type communications," *IEEE Veh. Technol. Mag.*, vol. 13, no. 4, pp. 40–50, Dec. 2018.

[2] S. M. R. Islam, N. Avazov, O. A. Dobre, and K. S. Kwak, "Power-domain non-orthogonal multiple access (NOMA) in 5G systems: Potentials and challenges," *IEEE Commun. Surv. Tuts.*, vol. 19, no. 2, pp. 721-742, Oct. 2016.

[3] Z. Ding et al., "A survey on non-orthogonal multiple access for 5G networks: Research challenges and future trends," *IEEE J. Sel. Areas Commun.*, vol. 35, no. 10, pp. 2181 –2195, Oct. 2017.

[4] H. Nikopour and H. Baligh, "Sparse code multiple access," in *Proc. IEEE Int. Symposium on Personal Indoor and Mobile Radio Commun. (PIMRC)*, Sep. 2013, pp. 332–336.

[5] M. Taherzadeh et al., "SCMA codebook design," in *Proc. IEEE Veh. Technol. Conf. (VTC Fall)*, Sep. 2014, pp. 1–5.

[6] H. Mu, Z. Ma, M. Alhaji, P. Fan, and D. Chen, "A fixed low complexity message pass algorithm detector for up-link SCMA system," *IEEE Wireless Commun. Lett.,* vol. 4, no. 6, pp. 585–588, Dec. 2015.

[7] R. Y. Mesleh et al., "Spatial modulation," *IEEE Trans. Veh. Technol.*, vol. 57, no. 4, pp. 2228–2241, Jul. 2008.

[8] E. Basar, "Index modulation techniques for 5G wireless networks," *IEEE Commun. Mag.,* vol. 54, no. 7, pp. 168–175, Jul. 2016.

[9] A. Younis, N. Serafimovski, R. Mesleh, and H. Haas, "Generalised spatial modulation," in *Proc. Forty Fourth Asilomar Conf. Signals, Syst., Comput. (ASILOMAR)*, Nov. 2010, pp. 1498–1502.

[10] C. Zhong, X. Hu, X. Chen, D. W. Ng, and Z. Zhang, "Spatial modulation assisted multi-antenna non-orthogonal multiple access", *IEEE Wireless Commun. Lett.,* vol. 25, no. 2, pp. 61-67, Apr. 2018.

[11] Y. Liu, L. L. Yang, and L. Hanzo, "Spatial modulation aided sparse code division multiple access," *IEEE Trans. Wireless Commun.*, vol. 17, no. 3, pp.

1474–1487, Mar. 2018.

[12] Z. Pan, J. Luo, J. Lei, L. Wen, and C. Tang, "Uplink spatial modulation SCMA system," *IEEE Commun. Lett.,* vol. 23, no. 1, pp. 184-187, Jan. 2019.

[13] I. Al-Nahhal, O. A. Dobre, and S. Ikki, "Quadrature spatial modulation decoding complexity: Study and reduction," *IEEE Wireless Commun. Lett.,* vol. 6, pp. 378-381, Jun. 2017.

[14] I. Al-Nahhal, O. A. Dobre, and S. Ikki, "Low complexity decoders for spatial and quadrature spatial modulations," in *Proc. IEEE Veh. Technol. Conf. (VTC-Spring)*, 2018, pp. 1–5.

[15] I. Al-Nahhal, E. Basar, O. A. Dobre, and S. Ikki, "Optimum low-complexity decoder for spatial modulation," *IEEE J. Sel. Areas Commun.*, vol. 37, no. 9, pp. 2001-2013, Jul. 2019.

Chapter 7

[1] W. Shin, M. Vaezi, B. Lee, D. J. Love, J. Lee, and H. V. Poor, "Non-orthogonal multiple access in multi-cell networks: Theory, performance, and practical challenges," *IEEE Commun. Mag.*, vol. 55, no. 10, pp. 176–183, Oct. 2017.

[2] A. Yadav and O. A. Dobre, "All technologies work together for good: A glance at future mobile networks," in *IEEE Wireless Commun.*, vol. 25, no. 4, pp. 10-16, Aug. 2018.

[3] M. Mohammadkarimi, M. A. Raza, and O. A. Dobre, "Signature-based nonorthogonal massive multiple access for future wireless networks: Uplink massive connectivity for machine-type communications," *IEEE Veh. Technol. Mag.*, vol. 13, no. 4, pp. 40–50, Dec. 2018.

[4] S. M. R. Islam, N. Avazov, O. A. Dobre, and K. S. Kwak, "Power-domain non-

orthogonal multiple access (NOMA) in 5G systems: Potentials and challenges," *IEEE Commun. Surv. Tuts.*, vol. 19, no. 2, pp. 721-742, Oct. 2016.

[5] Z. Ding, X. Lei, G. K. Karagiannidis, R. Schober, J. Yuan, and V. Bhargava, "A survey on non-orthogonal multiple access for 5G networks: Research challenges and future trends," *IEEE J. Sel. Areas Commun.*, vol. 35, no. 10, pp. 2181 –2195, Oct. 2017.

[6] H. Nikopour and H. Baligh, "Sparse code multiple access," in *Proc. IEEE Int. Symposium on Personal Indoor and Mobile Radio Commun. (PIMRC)*, Sep. 2013, pp. 332–336.

[7] M. Taherzadeh, H. Nikopour, A. Bayesteh, and H. Baligh, "SCMA codebook design," in *Proc. IEEE Veh. Technol. Conf. (VTC Fall)*, Sep. 2014, pp. 1–5.

[8] D. Cai, P. Fan, X. Lei, Y. Liu, and D. Chen, "Multi-dimensional SCMA codebook design based on constellation rotation and interleaving," in *Proc. IEEE Veh. Technol. Conf. (VTC Spring)*, May 2016, pp. 1–5.

[9] M. Vameghestahbanati, I. D. Marsland, R. H. Gohary, and H. Yanikomeroglu, "Multidimensional constellations for uplink SCMA systems - A comparative study," *arXiv*, Apr. 2018. [Online]. Available: http://arxiv.org/abs/1804.05814.

[10] H. Mu, Z. Ma, M. Alhaji, P. Fan, and D. Chen, "A fixed low complexity message pass algorithm detector for up-link SCMA system," *IEEE Wireless Commun. Lett.,* vol. 4, no. 6, pp. 585–588, Dec. 2015.

[11] L. Yang, Y. Liu, and Y. Siu, "Low complexity message passing algorithm for SCMA system," *IEEE Commun. Lett.*, vol. 20, no. 12, pp. 2466–2469, Dec. 2016.

[12] J. Dai, K. Niu, C. Dong, and J. Lin, "Improved message passing algorithms for sparse code multiple access," *IEEE Trans. Veh. Technol.*, vol. 66, no. 11, pp. 9986–9999, Nov. 2017.

[13] L. Yang, X. Ma, and Y. Siu, "Low complexity MPA detector based on sphere decoding for SCMA," *IEEE Commun. Lett.*, vol. 21, no. 8, pp. 1855–1858, Aug. 2017.

[14] M. Vameghestahbanati, E. Bedeer, I. Marsland, R. H. Gohary, and H. Yanikomeroglu, "Enabling sphere decoding for SCMA," *IEEE Commun. Lett.*, vol. 21, no. 12, pp. 2750–2753, Dec. 2017.

[15] L. Li, J. Wen, X. Tang, and C. Tellambura, "Modified sphere decoding for sparse code multiple access," *IEEE Commun. Lett.*, vol. 22, no. 8, pp. 1544–1547, Aug. 2018.

[16] R. Y. Mesleh, H. Haas, S. Sinanovic, C. W. Ahn, and S. Yun, "Spatial modulation," *IEEE Trans. Veh. Technol.*, vol. 57, no. 4, pp. 2228–2241, Jul. 2008.

[17] A. Younis, N. Serafimovski, R. Mesleh, and H. Haas, "Generalised spatial modulation," in *Proc. Forty Fourth Asilomar Conf. Signals, Syst., Comput. (ASILOMAR)*, Nov. 2010, pp. 1498–1502.

[18] M. Renzo, H. Haas, A. Ghrayeb, S. Sugiura, and L. Hanzo, "Spatial modulation for generalized MIMO: Challenges, opportunities and implementation," *Proc. IEEE*, vol. 102, no. 1, pp. 56–103, Jan. 2014.

[19] E. Basar, "Index modulation techniques for 5G wireless networks," *IEEE Commun. Mag.,* vol. 54, no. 7, pp. 168–175, Jul. 2016.

[20] A. Younis, R. Mesleh, H. Haas, and P. M. Grant, "Reduced complexity sphere decoder for spatial modulation detection receivers," in *Proc. IEEE GLOBECOM*, 2010, pp. 1–5.

[21] A. Younis, M. Di Renzo, R. Mesleh, and H. Haas, "Sphere decoding for spatial modulation," in *Proc. 2011 IEEE Int. Conf. Commun.*, pp. 1–6.

[22] A. Younis, S. Sinanovic, M. Di Renzo, R. Mesleh, and H. Haas, "Generalised

sphere decoding for spatial modulation," *IEEE Trans. Commun.*, vol. 61, no. 7, pp. 2805–2815, July 2013.

[23] I. Al-Nahhal, O. A. Dobre, and S. Ikki, "Quadrature spatial modulation decoding complexity: Study and reduction," *IEEE Wireless Commun. Lett.,* vol. 6, pp. 378-381, Jun. 2017.

[24] I. Al-Nahhal, O. A. Dobre, and S. Ikki, "Low complexity decoders for spatial and quadrature spatial modulations," in *Proc. IEEE Veh. Technol. Conf. (VTC-Spring)*, 2018, pp. 1–5.

[25] I. Al-Nahhal, E. Basar, O. A. Dobre, and S. Ikki, "Optimum low-complexity decoder for spatial modulation," *IEEE J. Sel. Areas Commun.*, vol. 37, no. 9, pp. 2001-2013, Jul. 2019.

[26] C. Zhong, X. Hu, X. Chen, D. W. Ng, and Z. Zhang, "Spatial modulation assisted multi-antenna non-orthogonal multiple access," *IEEE Wireless Commun. Lett.,* vol. 25, no. 2, pp. 61-67, Apr. 2018.

[27] Y. Liu, L. L. Yang, and L. Hanzo, "Spatial modulation aided sparse code division multiple access," *IEEE Trans. Wireless Commun.*, vol. 17, no. 3, pp. 1474–1487, Mar. 2018.

[28] Z. Pan, J. Luo, J. Lei, L. Wen, and C. Tang, "Uplink spatial modulation SCMA system," *IEEE Commun. Lett.,* vol. 23, no. 1, pp. 184-187, Jan. 2019.

[29] I. Al-Nahhal, O. A. Dobre, E. Basar, and S. Ikki, "Low-cost uplink sparse code multiple access for spatial modulation," *IEEE Trans. Veh. Technol.*, vol. 68, no. 9, pp. 9313-9317, Jul. 2019.

[30] L. G. Barbero and J. S. Thompson, "Fixing the complexity of the sphere decoder for MIMO detection," *IEEE Trans. Wireless Commun.,* vol. 7, pp. 2131–2142, Jun. 2008.

[31] I. Al-Nahhal, A. Emran, H. Kasem, A. B. Abd El-Rahman, O. Muta, and H.

Furukawa, “Flexible fractional K-best sphere decoding for uncoded MIMO channels,” *IEICE Communications Express*, vol., 4, pp. 20-25, Jan. 2015.

[32] I. Al-Nahhal, M. Alghoniemy, A. B. Abd El-Rahman, Z. Kawasaki, “Modified zero forcing decoder for ill-conditioned channels” in *Proc.* IFIP Wireless Days (WD), Nov 2013, pp. 1–3.

[33] I. Al-Nahhal, M. Alghoniemy, O. Muta, and A. B. A. El-Rahman, “Reduced complexity k-best sphere decoding algorithms for ill-conditioned MIMO channels,” in *Proc. IEEE Annu. Consum. Commun. Netw. Conf.*, pp. 183-187, Jan. 2016.

[34] J. Proakis, *Digital Communications*, 4th ed. New York, NY, USA: McGraw-Hill, 2000.